

DEVELOPMENT OF NOVEL ELECTRODE/ELECTROLYTE SYSTEMS FOR A  
LI-ION CELL WITH HIGHER ENERGY DENSITY AND LONGER LIFETIME

by

Lin Ma

Submitted in partial fulfilment of the requirements  
for the degree of Doctor of Philosophy

at

Dalhousie University  
Halifax, Nova Scotia  
August 2018

© Copyright by Lin Ma, 2018

致 爸爸，妈妈及所有我爱和爱我的人  
以及偶像林俊杰

## TABLE OF CONTENTS

LIST OF TABLES .....	ix
LIST OF FIGURES .....	x
ABSTRACT .....	xvii
LIST OF ABBREVIATIONS AND SYMBOLS USED.....	xviii
ACKNOWLEDGMENTS .....	xxii
CHAPTER 1 INTRODUCTION .....	1
1.1 Motivation.....	1
1.2 Basic configuration of a Li-ion cell .....	3
1.3 Positive electrode materials .....	5
1.4 Negative electrode materials.....	6
1.5 Electrolyte systems .....	7
CHAPTER 2 ELECTRODE/ELECTROLYTE INTERPHASE: WAYS TO CHANGE ITS CHEMISTRY .....	10
2.1 Solid electrolyte interphase.....	10
2.1.1 Negative electrode/electrolyte interphase .....	10
2.1.2 Positive electrode/electrolyte interphase.....	13
2.2 Electrolyte additives.....	15
2.2.1 Electrolyte additives for the graphite negative electrode.....	16
2.2.2 Electrolyte additives for the silicon-containing negative electrode.....	18
2.2.3 Electrolyte additives for the positive electrode.....	19
2.3 Introduction of coatings on the electrode materials.....	21
2.3.1 Surface coatings on the positive electrode.....	21
2.3.2 Surface coatings on the negative electrode .....	23

CHAPTER 3	EXPERIMENTAL TECHNIQUES .....	25
3.1	Cell chemistry and preparation .....	25
3.1.1	Cell chemistry .....	25
3.1.2	Cell preparation.....	31
3.1.3	Electrolyte chemicals .....	32
3.2	Storage testing.....	34
3.3	Gas chromatography (GC).....	36
3.4	Mass spectrometry (MS).....	38
3.5	Ultra-high precision coulometry (UHPC).....	40
3.6	Gas evolution .....	43
3.7	Electrochemical impedance spectroscopy (EIS).....	45
3.8	Differential voltage analysis .....	49
CHAPTER 4	A GUIDE TO ETHYLENE CARBONATE-FREE ELECTROLYTE MAKING FOR LI-ION CELLS .....	52
4.1	Experimental .....	53
4.1.1	The preparation of pouch cells.....	53
4.1.2	EIS testing .....	53
4.1.3	Charge-discharge cycling testing .....	54
4.1.4	Storage testing.....	54
4.1.5	GC-MS testing .....	54
4.1.6	UHPC testing .....	55
4.2	Results and discussion .....	55
4.2.1	The effect of electrolyte additives in EC-free electrolytes on Li-ion cell performance.....	55
4.2.2	Storage and cycling tests.....	60

4.2.3 Cell failure mechanism analysis .....	63
4.2.4 Prediction of cell lifetime at a lower upper cut-off voltage .....	72
4.2.5 The disadvantages of EC-free electrolyte systems .....	77
4.3 Conclusions for Chapter 4 .....	82
<b>CHAPTER 5 LITHIUM DIFLUOROPHOSPHATE AS AN ELECTROLYTE</b>	
<b>ADDITIVE IN Li[Ni<sub>0.5</sub>Mn<sub>0.3</sub>Co<sub>0.2</sub>]O<sub>2</sub>/GRAPHITE POUCH CELLS .....</b>	
5.1 Experimental .....	86
5.1.1 The preparation of pouch cells .....	86
5.1.2 EIS testing .....	86
5.1.3 Charge-discharge cycling tests .....	86
5.1.4 Storage testing .....	87
5.1.5 Solution nuclear magnetic resonance (SNMR) tests .....	87
5.1.6 XPS for surface analysis .....	88
5.1.7 Isothermal microcalorimetry tests .....	89
5.1.8 UHPC tests .....	90
5.1.9 Frequency response analyzer (FRA) tests .....	90
5.2 Results and Discussion .....	91
5.2.1 The effect of LiPO <sub>2</sub> F <sub>2</sub> in EC-free electrolyte on cell formation .....	91
5.2.2 The effect of LiPO <sub>2</sub> F <sub>2</sub> in EC-based electrolyte on cell formation .....	93
5.2.3 The effect of LiPO <sub>2</sub> F <sub>2</sub> on storage testing .....	99
5.2.4 The effect of LiPO <sub>2</sub> F <sub>2</sub> on cell lifetime .....	101
5.2.5 The effect of LiPO <sub>2</sub> F <sub>2</sub> on gas evolution at high voltage .....	103

5.2.6 The effect of $\text{LiPO}_2\text{F}_2$ at fast charge rate .....	105
5.2.7 The effect of $\text{LiPO}_2\text{F}_2$ on impedance growth during cycling.....	106
5.2.8 The effect of $\text{LiPO}_2\text{F}_2$ on heat flow .....	108
5.3 Conclusions for Chapter 5 .....	110
<b>CHAPTER 6 COMBINATIONS OF LITHIUM DIFLUOROPHOSPHATE AND OTHER ELECTROLYTE ADDITIVES IN <math>\text{Li}[\text{Ni}_{0.5}\text{Mn}_{0.3}\text{Co}_{0.2}]\text{O}_2/\text{GRAPHITE POUCH CELLS}</math>.....</b>	<b>113</b>
6.1 Experimental.....	114
6.1.1 The preparation of pouch cells.....	114
6.1.2 EIS testing .....	115
6.1.3 Charge-discharge cycling tests.....	115
6.1.4 Storage testing.....	116
6.1.5 XPS for surface analysis .....	116
6.1.6 Isothermal microcalorimetry tests.....	116
6.1.7 UHPC tests.....	116
6.1.8 Automated EIS measurements during charge-discharge cycling.....	116
6.2 Results and discussion .....	117
6.2.1 The effect of $\text{LiPO}_2\text{F}_2$ -containing electrolyte additive combinations on storage testing.....	117
6.2.2 The effect of $\text{LiPO}_2\text{F}_2$ -containing electrolyte additive combinations on electrode surface chemistry, cell heat flow and cell lifetime.....	118
6.2.3 The effect of $\text{LiPO}_2\text{F}_2$ -containing electrolyte additive combinations on impedance growth during cycling .....	127
6.3 Conclusions for Chapter 6 .....	132

CHAPTER 7	IMPACT OF A SURFACE COATING ON $\text{Li}[\text{Ni}_{0.5}\text{Mn}_{0.3}\text{Co}_{0.2}]\text{O}_2$ ON LI-ION CELL PERFORMANCE.....	133
7.1	Experimental.....	134
7.1.1	The preparation of pouch cells and pouch bags.....	134
7.1.2	EIS testing .....	135
7.1.3	Charge-discharge cycling tests.....	135
7.1.4	Storage testing.....	136
7.1.5	XPS for surface analysis .....	136
7.1.6	UHPC tests.....	136
7.1.7	Accelerating rate calorimetry (ARC) experiments .....	136
7.1.8	Micro X-ray fluorescence (XRF) spectroscopy.....	137
7.1.9	Scanning electron microscopy (SEM) imaging.....	138
7.2	Results and discussion .....	138
7.2.1	The effect of surface coating on storage testing .....	138
7.2.2	The effect of surface coating on impedance growth and gas evolution.....	140
7.2.3	The effect of surface coating on cell lifetime .....	144
7.2.4	Cell failure mechanism analysis .....	150
7.2.5	The effect of surface coating on safety performance.....	159
7.2.6	The effect of surface coating on gas evolution at high voltage .....	159
7.3	Conclusions for Chapter 7 .....	167
CHAPTER 8	CONCLUSIONS .....	169
8.1	Conclusions.....	169
8.2	Future work.....	171

8.2.1 EC-free electrolyte systems .....	171
8.2.2 SC positive electrode materials.....	172
8.2.3 Electrode/electrolyte interactions.....	172
8.2.4 Coatings on positive electrode materials .....	173
8.2.5 Differences between SC and polycrystalline materials when Li metal is used as the negative electrode .....	174
8.2.6 Failure analysis on coated and uncoated SC NMC532/graphite pouch cells when superior electrolyte additives are used .....	175
REFERENCES .....	176
Appendix A .....	196
Appendix B .....	206



## LIST OF TABLES

Table 3.1 Electrode formulations used in the pouch cells of this thesis. ....	26
Table 3.2 Detailed information of electrolyte chemicals used this thesis. ....	33
Table 3.3 Basic electronic components and their calculated impedance. ....	46
Table 6.1 Atomic ratios of the elements on the surfaces of negative and positive electrodes cycled without additives, 1% $\text{LiPO}_2\text{F}_2$ , 1% $\text{LiPO}_2\text{F}_2$ + 2%FEC and 1% $\text{LiPO}_2\text{F}_2$ + 2%VC. ....	123

## LIST OF FIGURES

Figure 1.1 Schematic of a lithium-ion cell.....	4
Figure 1.2 Chemical structures of some solvents used in lithium-ion batteries. ....	8
Figure 1.3 Chemical structures of some common salts used in lithium-ion batteries .....	9
Figure 2.1 The reduction mechanism of EC on the graphite electrode.....	11
Figure 2.2 Possible mechanisms for the EMC trans-esterification reaction on the graphite electrode.....	12
Figure 2.3 The chemical structure of VC and its major reaction products on the graphite electrode during formation.....	13
Figure 2.4 The chemical structures of electrolyte additives used in this thesis .....	17
Figure 3.1 (a) STEM image of a fresh coated single crystal (SC) NMC532 particle. (b) EELS line scan profile of Ti.....	27
Figure 3.2 XPS spectra of Ti 2p peaks for coated and uncoated NMC532. ....	28
Figure 3.3 SEM images for fresh positive electrodes from the pouch cells used in this thesis. ....	29
Figure 3.4 Voltage vs. capacity for a coated SC NMC532/graphite pouch cell and its relevant reference curve.....	30
Figure 3.5 Voltage vs. capacity curve (a) and associated dQ/dV vs. voltage curve (b) for a NMC442/graphite cell during formation. ....	32
Figure 3.6 Voltage vs. state of charge curve for a LCO/graphite full cell, potential (vs. Li/Li <sup>+</sup> ) vs. state of charge curve for a graphite half cell and a LCO half cell, respectively. ....	35
Figure 3.7 A schematic of a GC.....	37
Figure 3.8 The chemical structure of 5% phenyl plus 95% dimethyl arylene siloxane....	38

Figure 3.9 A schematic of a mass spectrometer. ....	39
Figure 3.10 A schematic of an EI source. ....	40
Figure 3.11 A schematic of a quadrupole mass analyzer. ....	41
Figure 3.12 The UHPC test channels at Dalhousie University. ....	42
Figure 3.13 The <i>ex-situ</i> gas measurement set-up. ....	45
Figure 3.14 Schematic of a single active particle immersed in the electrolyte (a) and its corresponding simple equivalent circuit (b) and a simple equivalent circuit of a lithium-ion full cell. ....	48
Figure 3.15 Voltage vs. capacity for a fresh coated SC NMC532/graphite cell and its corresponding $dV/dQ$ vs. $Q$ curve. $dV/dQ$ vs. $Q$ for a fresh coated SC NMC532/lithium half cell, a fresh graphite/lithium half cell and calculated coated SC NMC532/graphite. ....	51
Figure 4.1 $dQ/dV$ vs. voltage for NMC442/graphite pouch cells with 1M LiPF <sub>6</sub> in EMC electrolyte or 1M LiPF <sub>6</sub> in EMC containing different amounts of “enablers” during formation. ....	56
Figure 4.2 Amount of enabler left (a) and % EMC trans-esterification (b) vs. initial enabler content in NMC442/graphite pouch cells that underwent their first full (formation) cycle between 2.8 – 4.4 V at 40°C, C/20 ....	59
Figure 4.3 Nyquist plots for NMC442/graphite pouch cells with 1M LiPF <sub>6</sub> in EMC electrolyte or 1M LiPF <sub>6</sub> in EMC with different enabler contents after formation....	61
Figure 4.4 Summary of voltage drop during 500 hour storage at 4.4 V and 40°C for NMC442/graphite pouch cells with 1M LiPF <sub>6</sub> in EMC electrolyte or 1M LiPF <sub>6</sub> in EMC with different enabler content. ....	63
Figure 4.5 Discharge capacity and cell polarization vs. cycle number for NMC442/graphite pouch cells with 1M LiPF <sub>6</sub> in EMC electrolyte or 1M LiPF <sub>6</sub> in EMC with different enabler content during long term CCCV cycling. ....	64
Figure 4.6 (a) Measured NMC442/graphite cell (after long term cycling shown in Figure 4.7) $V(Q)$ curves cycled at C/20 at 40°C. Extracted $V_p(Q)$ (b) and $V_n(Q)$ (c) curves, respectively, from the $dV/dQ$ analysis software. ....	67

Figure 4.7 Discharge capacity vs. cycle number for NMC442/graphite pouch cells with 1M LiPF <sub>6</sub> in EMC containing 3% FEC or 3% DiFEC during CCCV long term cycling. ....	68
Figure 4.8 Discharge capacity vs. cycle number for NMC442/graphite pouch cells with 1M LiPF <sub>6</sub> in EMC containing 1% VC, 1% MEC, 1% FEC and 1% DiFEC during CCCV long term cycling .....	69
Figure 4.9 A summary of the impedance results for NMC442/graphite pouch cells with 1M LiPF <sub>6</sub> in EMC with different enabler content as indicated after formation (40°C, C/20), after 500 h storage (4.4 V, 40°C) and after ~ 200 CCCV cycles (2.8 – 4.4 V, 40°C, C/2.5). ....	70
Figure 4.10 A summary of the gas volumes in NMC442/graphite pouch cells with 1M LiPF <sub>6</sub> in EMC electrolyte or 1M LiPF <sub>6</sub> in EMC with different enabler content as indicated. ....	71
Figure 4.11 Amount of enabler left and % EMC trans-esterification in NMC442/graphite pouch cells that underwent 500 h storage or ~ 200 CCCV cycles. ....	73
Figure 4.12 The typical measurables of a UHPC test .....	75
Figure 4.13 A summary of UHPC test results for NMC111/graphite and NMC442/graphite pouch cells filled with 1M LiPF <sub>6</sub> in EMC plus different concentrations of VC or FEC. ....	76
Figure 4.14 A summary of impedance results (a) and gas volumes (b) for NMC111/graphite or NMC442/graphite pouch cells with 1M LiPF <sub>6</sub> in EMC with different enabler content, as indicated, before and after UHPC cycling. ....	78
Figure 4.15 Discharge capacity versus cycle number for NMC111/graphite pouch cells with 1M LiPF <sub>6</sub> in the electrolytes indicated in the legend using different charge rates at 22°C. ....	79
Figure 4.16 In-situ gas measurement of NMC111/graphite pouch cells with EC-based electrolytes during cycling at different charge rates at 22°C. ....	80
Figure 4.17 In-situ gas measurement of NMC111/graphite pouch cells with EC-free electrolytes during cycling at different charge rates at 22°C. ....	81

Figure 4.18 Ionic conductivity of LiPF <sub>6</sub> /EC electrolytes measured at different temperatures .....	82
Figure 5.1 dQ/dV vs. voltage for NMC442/graphite pouch cells with different electrolytes during formation.....	92
Figure 5.2 % EMC trans-esterification vs. initial content of LiPO <sub>2</sub> F <sub>2</sub> in NMC442/graphite pouch cells that underwent their first full (formation) cycle between 2.8 – 4.4 V at 40°C, C/20. ....	93
Figure 5.3 dQ/dV vs. voltage for NMC532/graphite pouch cells with different electrolytes during formation at 40°C. ....	94
Figure 5.4 <sup>19</sup> F NMR spectra for control electrolyte or LiPO <sub>2</sub> F <sub>2</sub> containing electrolyte before and after formation. ....	96
Figure 5.5 Typical XPS core spectra for graphite electrodes and NMC532 electrodes, respectively, at 3.8 V after formation with different electrolytes as indicated. ....	98
Figure 5.6 Summary of voltage drop, volume change and charge transfer impedance during 500h storage at 4.4 V and 2.5 V. ....	100
Figure 5.7 A summary of UHPC test results for NMC532/graphite pouch cells filled with different electrolytes as indicated after 16 cycles between 3 V and various upper cut-off voltages (4.1, 4.2, 4.3, 4.4 V). ....	102
Figure 5.8 Normalized discharge capacity and cell polarization vs. cycle number for NMC532/graphite pouch cells during long term CCCV cycling.....	104
Figure 5.9 Voltage and gas volume of NMC532/graphite pouch cells as a function of time.. .....	105
Figure 5.10 Normalized discharge capacity and cell polarization vs. cycle number for NMC532/graphite pouch cells with different electrolytes at 20°C during rate capability testing. ....	107
Figure 5.11 The normalized discharge capacity and cell polarization as a function of cycle number for NMC532/graphite pouch cells with different electrolytes undergoing cycling tests and FRA measurements. ....	109

Figure 5.12 The parasitic heat flow of NMC532/graphite cells with different electrolytes as indicated.....	111
Figure 6.1 Chemical structures of the electrolyte additives used in this work.....	115
Figure 6.2 Summary of voltage drop and impedance change for NMC532/graphite pouch cells with different electrolytes stored at 60°C.....	118
Figure 6.3 A summary of UHPC testing results for NMC532/graphite pouch cells filled with different electrolytes during 16 cycles.....	120
Figure 6.4 Summary of impedance before and after 16 UHPC cycles between 3.0 and various upper cut-off voltages (4.2, 4.3, 4.4 V).....	121
Figure 6.5 Regions of the XPS spectra of negative and positive electrodes that underwent formation.....	124
Figure 6.6 The parasitic heat flow of NMC532/graphite cells with different electrolytes as indicated.....	125
Figure 6.7 The average parasitic heat flow during each cycle for cells shown in Figures 6.6. ....	126
Figure 6.8 Normalized discharge capacity and normalized cell polarization vs. cycle number for NMC532/graphite pouch cells with different electrolytes during long term CCCV cycling.....	128
Figure 6.9 The normalized discharge capacity and cell polarization as a function of cycle number for NMC532/graphite pouch cells with different electrolytes undergoing cycling tests and simultaneous EIS measurements.....	130
Figure 7.1 Summary of voltage drop at 4.4 V during 500h storage at 60°C for coated and uncoated SC NMC532/graphite pouch cells with different electrolytes.....	139
Figure 7.2 Summary of impedance change for coated and uncoated delithiated SC NMC532 before or during 500h storage testing. ....	141
Figure 7.3 Summary of impedance change for lithiated graphite.....	143

Figure 7.4 Gas evolution of pouch bags containing delithiated coated or uncoated SC NMC532 or lithiated graphite or full pouch cells during 500h storage testing at 60°C .....	145
Figure 7.5 A summary of UHPC testing results for coated and uncoated SC NMC532/graphite pouch cells .....	146
Figure 7.6 Summary of impedance change during 16 UHPC cycles.. .....	148
Figure 7.7 Normalized discharge capacity and cell polarization vs. cycle number for uncoated and coated SC NMC532/graphite pouch cells during long term CCCV cycling .....	149
Figure 7.8 Discharge capacity vs. cycle number for coated and uncoated SC NMC532/graphite pouch cells with 2% VC during CCCV long term cycling and their relevant dV/dQ vs. Q curves .....	152
Figure 7.9 SEM images of cross sections of positive electrodes taken from uncoated and coated SC NMC532/graphite pouch cells after formation or cycling.....	156
Figure 7.10 Regions of the XPS spectra of A) positive electrodes and B) negative electrodes that underwent formation or long term cycling in coated or uncoated SC NMC532/graphite pouch cells.....	158
Figure 7.11 Self-heating rate (SHR) vs. temperature for delithiated coated and uncoated SC NMC532 electrodes reacting with different electrolytes.....	160
Figure 7.12 Cell voltage as a function of time (a), and the gas volume of coated and uncoated SC NMC532/graphite pouch cells with different electrolytes as a function of time (b).....	162
Figure A1 Representative spectra showing the background subtraction procedure in the substrate (a), surface (b) and bulk (c) during EELS line scan testing.....	196
Figure A2 Nyquist plots for coated SC NMC532/graphite and uncoated SC NMC532/graphite pouch full cells or symmetric cells. The electrolyte used was 1.2M LiPF <sub>6</sub> EC/EMC 3/7. ....	197
Figure A3 Nyquist plots for coated SC NMC532/graphite and uncoated SC NMC532/graphite pouch full cells or symmetric cells. The electrolyte used was 1.2M LiPF <sub>6</sub> EC/EMC 3/7 plus 2% VC + 1% DTD.....	198

Figure A4 Nyquist plots for coated SC NMC532/graphite and uncoated SC NMC532/graphite pouch full cells or symmetric cells. The electrolyte used was 1.2M LiPF<sub>6</sub> EC/EMC 3/7 plus 1% LFO + 1% VC + 1% FEC..... 199

Figure A5 Nyquist plots for coated SC NMC532/graphite and uncoated SC NMC532/graphite pouch full cells or symmetric cells. The electrolyte used was 1.2M LiPF<sub>6</sub> EC/EMC 3/7 plus 2% PES + 1% DTD + 1% TTSPi (“PES211”)..... 200

Figure A6 Nyquist plots for coated SC NMC532/graphite and uncoated SC NMC532/graphite pouch full cells or symmetric cells. The electrolyte used was 1.2M LiPF<sub>6</sub> EC/EMC 3/7 plus 2% FEC + 1% DTD ..... 201

Figure A7 Nyquist plots for coated SC NMC532/graphite and uncoated SC NMC532/graphite pouch cells with 1.2M LiPF<sub>6</sub> EC/EMC 3/7 plus 2% VC before or after long term cycling..... 202

Figure A8 Voltage vs. time for coated and uncoated SC NMC532/graphite pouch cells with different electrolyte additives as indicated during storage testing (60°C, 500h)... 203

Figure A9 XRF images for (a) fresh graphite electrode, (b) Mn signal for blank sample, (c) Mn signal for graphite electrode taken from coated SC NMC532/graphite cell and (d) Mn signal for graphite electrode taken from uncoated SC NMC532/graphite cell. 204

Figure A10 Comparing the Ni (black) and Co (blue) μ-XRF signals to the Mn μ-XRF signal for the electrodes recovered from the cells described by Figure 7.7. The solid black and solid blue lines represent the expected ratios of all transition metals have equal probability for dissolution from NMC532. .... 205



## ABSTRACT

The energy density of lithium ion cells can increase when the charge cut-off potential increases or high Ni content positive electrode materials are used. However, this normally decreases the lifetime of cells because of the parasitic reactions that occur between the electrolyte and the charged electrodes. This thesis project focuses on developing high voltage lithium ion cells having high energy density and long lifetime.

Ethylene carbonate (EC) is normally used as an electrolyte solvent in all Li-ion cells due to its stability and most lithium ion battery scientists believe EC is essential for good Li-ion battery operation. Surprisingly, with an appropriate amount of electrolyte additive to passivate the graphite electrode, cells with only 1M LiPF<sub>6</sub> plus ethyl methyl carbonate (EMC) functioned well up to 4.4 V vs. graphite. In order to optimize the amount of electrolyte additive used in the cells, gas chromatography (GC) coupled with mass spectrometry (MS) was used to track the consumption of several additives and the trans-esterification of EMC during formation, cycling and storage. Some other advanced analysis methods were also used to obtain a better understanding of EC-free electrolytes.

The effect of lithium difluorophosphate (LiPO<sub>2</sub>F<sub>2</sub>) as an electrolyte additive on single crystal Li[Ni<sub>0.5</sub>Mn<sub>0.3</sub>Co<sub>0.2</sub>]O<sub>2</sub> (NMC532)/graphite pouch cells was examined. The combination of coated single crystal NMC532 and LiPO<sub>2</sub>F<sub>2</sub> is extremely useful for extending cell lifetime, especially when some other suitable electrolyte additives (e.g. fluoroethylene carbonate (FEC)) are used at the same time. The effect of a surface coating on single crystal NMC532 was also investigated systematically.

## LIST OF ABBREVIATIONS AND SYMBOLS USED

ARC	Accelerating rate calorimetry
CCCV	Constant current - constant voltage
CE	Coulombic efficiency
DEC	Diethyl carbonate
DiFEC	Difluoroethylene carbonate
DMC	Dimethyl carbonate
DTD	1,3,2-dioxathiolane-2,2-dioxide
EC	Ethylene carbonate
EELS	Electron energy-loss spectroscopy
EI	Electron impact ionization
EIS	Electrochemical impedance spectroscopy
EMC	Ethylmethyl carbonate
EV	Electric vehicle
$F_{\text{buoyant}}$	Buoyant force
$F_{\text{tension}}$	Force of tension
FEC	Fluoroethylene carbonate
FTIR	Fourier transform infrared spectroscopy
GC	Gas chromatography
HDI	Hexamethylene diisocyanate

LCO	$\text{LiCoO}_2$
LEDC	Lithium ethylene dicarbonate
LFP	$\text{LiFePO}_4$
LIB	Lithium ion batteries
LiBOB	Lithium bis(oxalato)borate
LiDFOB	Lithium difluoro (oxalate) borate
LiFSI	Lithium bis(fluorosulfonyl)imide
LiTFSI	Lithium bis (trifluoromethanesulfonyl)imide
LTO	Lithium titanium oxide ( $\text{Li}_{4/3}\text{Ti}_{5/4}\text{O}_4$ )
$m_p$	Mass of positive electrode
$m_n$	Mass of negative electrode
MA	Methyl acetate
MEC	Methylene ethylene carbonate
MMDS	Methylene methanedisulfonate
MS	Mass spectrometry
NCA	$\text{Li}(\text{Ni}_{0.8}\text{Co}_{0.15}\text{Al}_{0.05})\text{O}_2$
NMC	$\text{Li}(\text{Ni}_x\text{Mn}_y\text{Co}_z)\text{O}_2$ ( $x + y + z = 1$ )
NMC111	$\text{Li}(\text{Ni}_{1/3}\text{Mn}_{1/3}\text{Co}_{1/3})\text{O}_2$
NMC442	$\text{Li}(\text{Ni}_{0.42}\text{Mn}_{0.42}\text{Co}_{0.16})\text{O}_2$
NMC532	$\text{Li}(\text{Ni}_{0.5}\text{Mn}_{0.3}\text{Co}_{0.2})\text{O}_2$
NMC622	$\text{Li}(\text{Ni}_{0.6}\text{Mn}_{0.2}\text{Co}_{0.2})\text{O}_2$

NMC811	$\text{Li}(\text{Ni}_{0.8}\text{Mn}_{0.1}\text{Co}_{0.1})\text{O}_2$
NMP	N-methyl pyrrolidinone
NMR	Nuclear magnetic resonance
$\rho$	Density of the water
PBF	Pyridine trifluoroborate
PC	Propylene carbonate
PES	Prop-1-ene-1,3-sultone
PPF	Pyridine pentafluorophosphate
PTFE	Polytetrafluoroethylene
PVDF	Polyvinylidene difluoride
$Q_p$	Capacity of positive electrode
$Q_n$	Capacity of negative electrode
$q_p$	Specific capacity of positive electrode
$q_n$	Specific capacity of negative electrode
SC	Single crystal
SEI	Solid electrolyte interface
SEM	Scanning electron microscopy
TTSPi	Tris(trimethylsilyl) phosphite
UHPC	Ultra-high precision coulometry
VC	Vinylene carbonate
XPS	X-ray photoelectron spectroscopy

XRF	X-ray fluorescence
$Z_{+/+}$	Impedance of a positive symmetric cell
$Z_{-/-}$	Impedance of a negative symmetric cell
$Z_{+/-}$	Impedance of a full cell
$\delta_p$	Slippage of positive electrode
$\delta_n$	Slippage of negative electrode

## ACKNOWLEDGMENTS

First I would like to thank the *Natural Sciences and Engineering Research Council* (NSERC), the Killam Trust and the Donald R. Arnold scholarship for their financial support, along with Tesla for the partial funding of this work.

I would like to give special thanks to my supervisor Dr. Jeff Dahn for his extensive support and great guidance. I would also like to thank my committee members, Dr. Peng Zhang, Dr. Ian Hill and Dr. Harm Rotermund for their invaluable help and advice. I am also very grateful for the administrative help from Giselle Andrews and Lea Gawne.

I would like to thank all Dahn lab members for their support during the past years. Thanks to Robbie Sanderson, Simon Trussler and Michel Johnson for keeping the facilities operating well every day. Thanks to Rémi Petibon for developing the analysis method to measure electrolyte additive consumption. Thanks to S.L. Glazier for isothermal calorimetry experiment assistance. Thanks to L.D. Ellis and Rochelle Weber for X-ray photoelectron spectroscopy (XPS) experiment assistance.

Finally I would give thousands of thanks to my parents for endless spiritual encouragement and support.

## CHAPTER 1 INTRODUCTION

### 1.1 Motivation

Lithium-ion batteries (LIB) are now widely used in many applications from portable electronics (e.g. laptops, mobile phones, etc.) to transportation (e.g. electric vehicles (EVs)). Applications including EVs and grid energy storage systems have increased the requirements on cell lifetime, energy density, safety and rate capability. Meanwhile, battery manufacturers are also trying to decrease the cost of LIB.

For the past two decades, researchers devoted significant effort to increase the energy density of LIB using several methods. The first and most common way was to improve electrode materials. Take  $\text{Li}(\text{Ni}_x\text{Mn}_y\text{Co}_z)\text{O}_2$  (NMC,  $x + y + z = 1$ ) positive electrode materials as an example. In 2001, Lu et al. [1] showed that NMC materials, especially  $\text{Li}(\text{Ni}_{0.375}\text{Mn}_{0.375}\text{Co}_{0.25})\text{O}_2$ , demonstrated excellent electrochemical performance while Ohzuku et al. [2] showed that  $\text{Li}(\text{Ni}_{1/3}\text{Mn}_{1/3}\text{Co}_{1/3})\text{O}_2$  (NMC111) had similar performance. Since the  $\text{Ni}^{2+}/(\text{Ni}^{3+} \text{ or } \text{Ni}^{4+})$  redox couple is the main contributor to the capacity of NMC materials [3], researchers started to adjust the ratio between Ni, Mn and Co by increasing the Ni content in order to improve the specific capacity. Between 2001 and present, high Ni content containing positive electrode materials mainly including  $\text{Li}(\text{Ni}_{0.5}\text{Mn}_{0.3}\text{Co}_{0.2})\text{O}_2$  (NMC532) [4,5],  $\text{Li}(\text{Ni}_{0.6}\text{Mn}_{0.2}\text{Co}_{0.2})\text{O}_2$  (NMC622) [6,7] and  $\text{Li}(\text{Ni}_{0.8}\text{Mn}_{0.1}\text{Co}_{0.1})\text{O}_2$  (NMC811) [8] have been introduced into the LIB market gradually.

Additionally, increasing the upper cut-off voltage will increase the energy density of LIB. Petibon et al. [9] reported that a 36% energy density (of the positive electrode material) gain could be obtained if the upper cut-off voltage of  $\text{Li}(\text{Ni}_{0.42}\text{Mn}_{0.42}\text{Co}_{0.16})\text{O}_2$  (NMC442) vs.  $\text{Li}/\text{Li}^+$  increased from 4.28 V to 4.78 V. However, parasitic reactions between electrode materials and electrolytes occur, especially at high voltage, and compromise cell lifetime. In order to extend cell lifetime, electrolyte additives are used to modify the interphase between electrodes and electrolytes. Xu et al. [10] summarized much of the recent work on electrolyte additives in 2014. Knowing the fate of electrolyte additives during cell operation would allow novel electrolyte blends to be developed.

The first major part of this thesis concentrates on optimizing the amount of various electrolyte additives used in novel ethylene carbonate (EC)-free electrolytes for high voltage cells [9,11]. Gas chromatography (GC) coupled with mass spectrometry (MS) was used to track the fate of the electrolyte additives and some other electrolyte compositions during different operations (e.g. cycling, storage). Cells after long-term cycling were also subjected to degradation analysis including differential voltage analysis, electrochemical impedance spectroscopy (EIS) and gas evolution testing.

The application of single crystal (SC) positive electrode materials is thought to be a promising method to reduce parasitic reactions and extend lifetime of lithium-ion batteries [12,13]. However, there is a lack of systematic studies on the combined effect of



SC electrode materials and electrolyte additives. The second major part of this thesis will focus on a systematic study of the impact of lithium difluorophosphate ( $\text{LiPO}_2\text{F}_2$ ), which is one of the most useful electrolyte additives, on SC NMC532/graphite pouch cell performance.

Chapter 2 of this thesis gives an overview of the current understanding of the chemistry of the interphase between electrodes and electrolytes in a Li-ion cell. Chapter 3 describes the experimental techniques used in this thesis. Chapter 4 reports a study of EC-free electrolyte for high voltage lithium ion batteries. Chapter 5 then describes the effect of  $\text{LiPO}_2\text{F}_2$  as an electrolyte additive on SC NMC532/graphite pouch cells. Chapter 6 describes the combined effect of  $\text{LiPO}_2\text{F}_2$  and other electrolyte additives on SC NMC532/graphite pouch cell performance. Chapter 7 reports a comparative study on coated and uncoated SC NMC532 used in Li-ion pouch cells with electrolyte additives. Conclusions and suggestions for future work are described in Chapter 8.

## **1.2 Basic configuration of a Li-ion cell**

A lithium-ion cell has a positive electrode, a negative electrode, separators, some electrolyte and current collectors [14]. There are many choices of electrode materials that can act to host the lithium atoms. Since NMC and graphite are the main materials used in this thesis, Figure 1.1 shows a diagram of a lithium-ion cell with NMC111 as the positive electrode material and graphite as the negative electrode material. The electrode materials

are attached to their respective current collectors. The two electrodes are separated by an electronically insulating porous film called a separator.

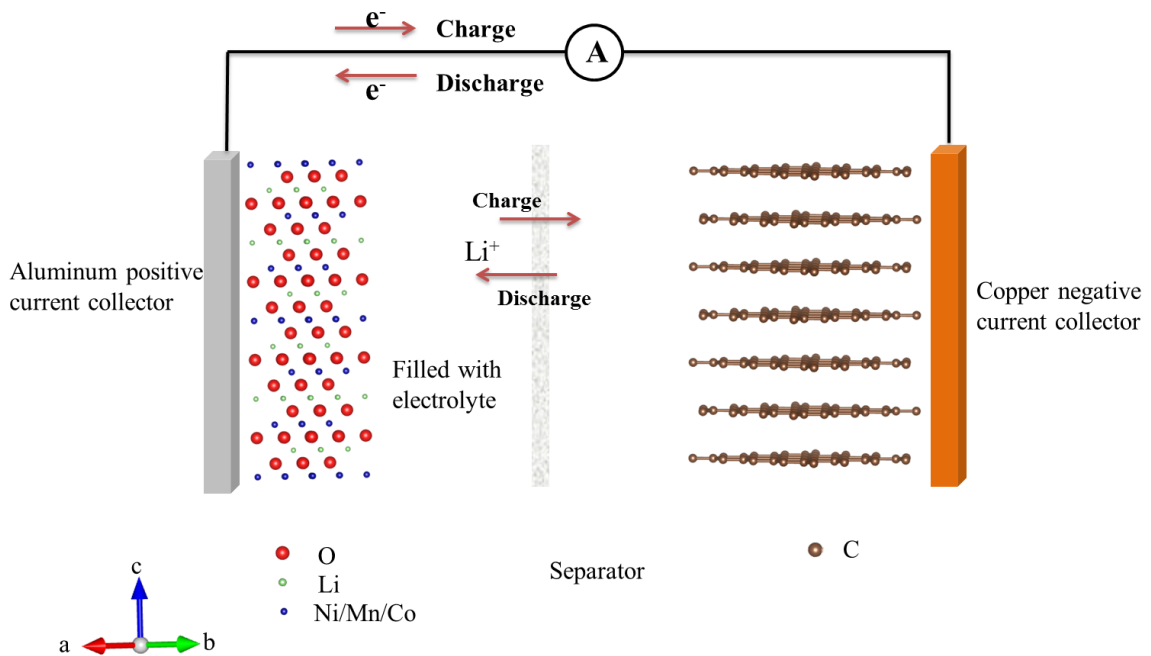
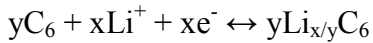


Figure 1.1 Schematic of a lithium-ion cell with a NMC111 positive electrode (left) and a graphite negative electrode (right). Taken with permission from Lin Ma, *Studies of the effects of electrolyte additives on the reactivity between charged electrodes and electrolytes in Li-ion batteries using accelerating rate calorimetry*, M.Sc. thesis, Dalhousie University, Halifax, NS (2014).

During the charge/discharge process, lithium ions are reversibly extracted from or inserted in the electrode materials. When a lithium-ion cell is charging, the electrons are forced to travel from the positive electrode towards the negative electrode through a circuit outside. Meanwhile, lithium ions delithiate from the positive electrode and travel

through the electrolyte to the negative electrode. When a lithium ion cell is discharging, the directions of both electrons and lithium ions are opposite to that of the charging process as shown in Figure 1.1. The two half reactions during charge or discharge are described by equations 1.1 and 1.2, respectively. In these reactions, M represents one type of transition metal or a combination of transition metals. The forward reactions occur when charging while the reverse reactions occur while discharging.



(1.2)

The voltage of a lithium ion cell is the difference between the potential of the positive electrode and the potential of the negative electrode.

### 1.3 Positive electrode materials

Many years of effort have been expended on the development of positive electrode materials for LIB.  $\text{LiCoO}_2$  (LCO),  $\text{Li}(\text{Ni}_{0.8}\text{Co}_{0.15}\text{Al}_{0.05})\text{O}_2$  (NCA), NMC and  $\text{LiFePO}_4$  (LFP) are relatively mature and dominate the commercial market now. Each material has its own advantages and disadvantages. For example, although LCO has high energy density, the use of Co increases cost and toxicity [15,16]. LFP has excellent safety performance [17] and is environmentally benign but has very low energy density [18].

The transition metal composition has a strong impact on the performance of NMC. Generally as the Ni content in NMC increases, the specific capacity to 4.2 V increases but the safety can be compromised [19].

Compared to conventional NMC (polycrystalline NMC), SC NMC [13,20] has larger primary particles (e.g.  $\sim 3\mu\text{m}$  for SC NMC532 [20]). Recently, Li et al. [12] reported that SC NMC532/graphite pouch cells with selected electrolyte additives showed excellent long lifetime at high voltage. This suggests that the application of SC positive electrode materials is a useful way of improving cell performance.

In order to increase energy density, lithium rich materials [21] and some new materials referred to as “5 V positive electrode materials” [22] (e.g.  $\text{LiNi}_{0.5}\text{Mn}_{1.5}\text{O}_4$  and  $\text{LiCoPO}_4$ ) are also being investigated. However, these materials suffer from different issues. Although the reversible specific capacity of Li-rich layered-oxide positive materials can reach around 250 mAh/g [21,23], a large irreversible capacity loss (IRC) [24] during the first cycle, poor rate capability [25], poor volumetric energy density and a significant voltage fade [26] limit their application. The development of suitable electrolyte systems is a bottleneck for high voltage positive electrode material [10].

#### **1.4 Negative electrode materials**

Instead of lithium metal, graphite, silicon-based materials and lithium titanium oxide ( $\text{Li}_{4/3}\text{Ti}_{5/4}\text{O}_4$ , LTO) are the dominant negative materials used in the LIB industry today.

Artificial graphite electrode materials have shown relatively high specific capacity and improved safety performance [27]. In order to decrease the cost of LIB, natural graphite has been regarded as a promising candidate [28,29]. LTO has relatively low cost, zero-strain during lithium lithiation/delithiation and excellent cycling performance. However, its voltage plateau is high (1.5 V vs. Li/Li<sup>+</sup>), which results in lower energy density, and its poor electronic conductivity is claimed to limit its rate capability [30,31].

Silicon-based materials have been used as negative electrodes in EVs because of their high volumetric capacity (~ 2200 Ah/L) [32]. However, they can suffer from capacity fade caused by the mechanical failure of active material or electrodes during the large volume expansion/contraction of Li<sub>x</sub>Si when LIB are charged or discharged [33,34]. Several solutions have been explored for the Si negative electrode. Nano-sized Si was developed because of the reduction of the mechanical stress [34–36]. Si/inactive (e.g. FeSi<sub>2</sub>) alloys were also designed to reduce the volume expansion and improve the cycling performance [34,37,38].

### **1.5 Electrolyte systems**

The typical components of an electrolyte system are solvents, lithium salts and electrolyte additives. Due to high dielectric constant, good compatibility with the electrode materials and film forming properties, EC is the most common electrolyte solvent component for LIB [39]. In order to expand the limited liquid range of EC-containing electrolytes and

lower the solvent viscosity, several linear carbonates are usually mixed with EC. Dimethyl carbonate (DMC), ethyl methyl carbonate (EMC) and diethyl carbonate (DEC) are the most common linear carbonates used with EC [10,39]. The chemical structures of the solvents mentioned above are shown in Figure 1.2. In addition to the carbonate solvents, some other non-carbonate solvents such as sulfones [40] and nitriles [41] have been investigated for special purpose applications such as high voltage cells.

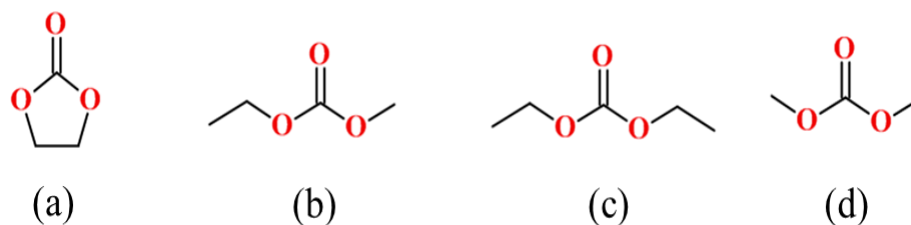


Figure 1.2 Chemical structures of some solvents used in lithium-ion batteries: (a) EC, (b) EMC, (c) DEC and (d) DMC.

The most common salt used in LIB is lithium hexafluorophosphate ( $\text{LiPF}_6$ ) [39]. It shows many superb characteristics such as high ionic conductivity when mixed with organic carbonates ( $> 10^{-3}$  S/cm), high lithium ion transference number ( $\sim 0.35$ ) and low corrosion of the Al positive electrode current collector at high potential [42].

Some other salts have also been studied for applications in LIB including lithium tetrafluoroborate ( $\text{LiBF}_4$ ) [43], lithium bis(oxalato)borate (LiBOB) [44], lithium bis(trifluoromethanesulfonyl)imide ( $(\text{LiN}(\text{SO}_2\text{CF}_3)_2$  called LiTFSI) [45], lithium

bis(fluorosulfonyl)imide ( $\text{LiNS}_2\text{O}_4\text{F}_2$  called LiFSI) [46] and so on. They have their own advantages and disadvantages. For example,  $\text{LiBF}_4$  has better thermal stability [43] but lower conductivity and poorer cation solvation [47] compared to  $\text{LiPF}_6$ . LiFSI-based carbonate electrolytes show higher ionic conductivities and higher lithium ion transference numbers compared to  $\text{LiPF}_6$ -based electrolyte but suffers from Al corrosion [48]. Figure 1.3 shows the chemical structures of the salts mentioned above.

Electrolyte additives, added at the 0.1 - 10% level [39] in electrolyte systems, contribute to improving cell performance (e.g. control impedance growth [49], suppress gas evolution and increase lifetime [50]). More details will be discussed in the next chapter.

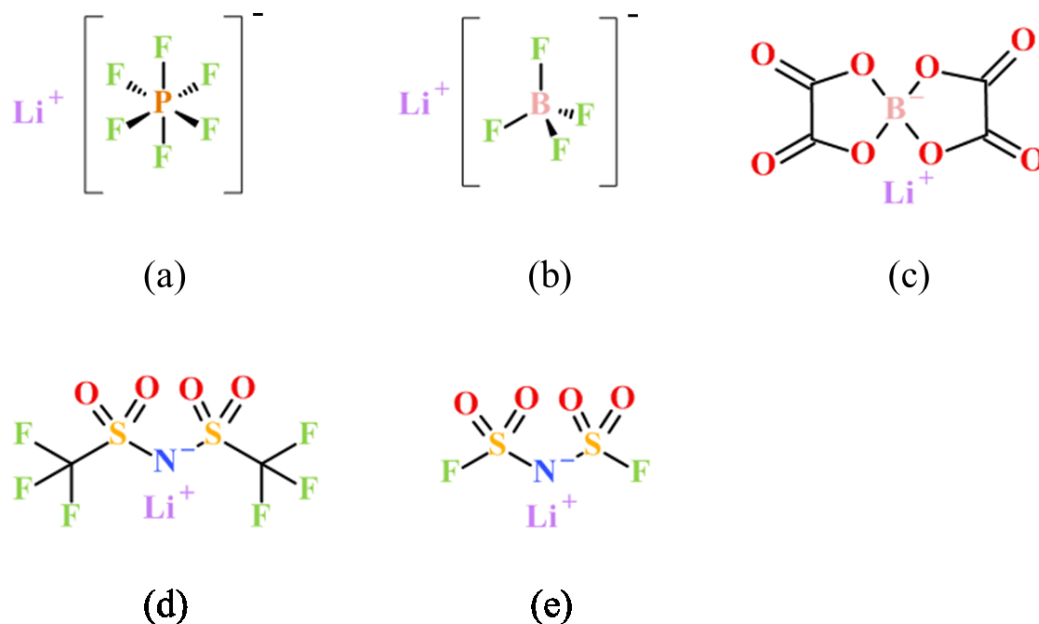


Figure 1.3 Chemical structures of some common salts used in lithium-ion batteries: (a)  $\text{LiPF}_6$  (b)  $\text{LiBF}_4$  (c) LiBOB (d) LiTFSI and (e) LiFSI. Taken with permission from Lin Ma, *Studies of the effects of electrolyte additives on the reactivity between charged electrodes and electrolytes in Li-ion batteries using accelerating rate calorimetry*, M.Sc. thesis, Dalhousie University, Halifax, NS (2014).

## CHAPTER 2 ELECTRODE/ELECTROLYTE INTERPHASE: WAYS TO CHANGE ITS CHEMISTRY

### 2.1 Solid electrolyte interphase

In lithium ion cells, both charged positive and negative electrodes can react with electrolyte to form layers composed of the products of the reactions. The layers, called solid electrolyte interphase (SEI) layers, are electronically insulating and ionically conducting. Peled [51] first suggested the formation of the SEI in 1979. The SEI allows reversible  $\text{Li}^+$  transport and dictates the kinetics of cell reactions. However, the SEI is very difficult to characterize clearly and is still being investigated by many researchers. Winter reported that it is “the most important but least understood component” in the LIB [52].

#### 2.1.1 Negative electrode/electrolyte interphase

This part will only focus on the interphase between the graphite negative electrode and carbonate-based electrolytes with or without electrolyte additives. The SEI contains both organic and inorganic compounds resulting from reacted electrolyte components. It has been reported that the SEI closer to the electrode is mainly composed of inorganic compounds while the SEI closer to the electrolyte is principally formed by organic compounds [53,54].

The mixture of EC and some other linear alkyl carbonates (e.g. DEC, EMC) with dissolved  $\text{LiPF}_6$  is a typical electrolyte (defined as the standard electrolyte in this thesis).



The SEI starts to form during the first charge process called the formation step. Substantial effort has been devoted to investigate the SEI formed in the standard electrolyte [54,55]. EC is well known to be the principle SEI film-forming agent on the graphite side. Figure 2.1 shows the reduction mechanism of EC [56]. Lithium ethylene dicarbonate (LEDC) and ethylene are the main products. Formed LEDC precipitates on the graphite surface to prevent further reduction of the electrolyte while gaseous ethylene needs to be removed during the pouch cell manufacturing process in order to decrease the mechanical stresses in devices containing lithium ion cells.

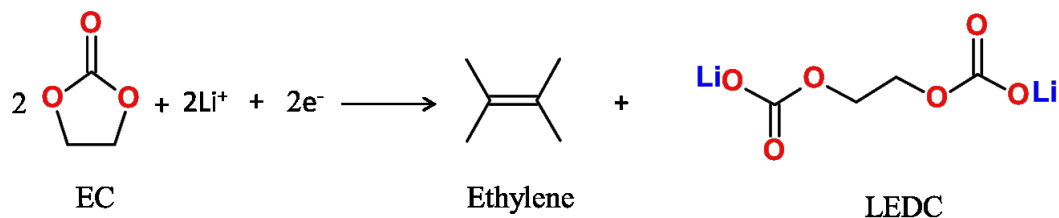


Figure 2.1 The reduction mechanism of EC on the graphite electrode.

The linear alkyl carbonates (e.g. DMC, EMC) can also be reduced on the graphite electrode and produce lithium alkyl carbonates [57–61], lithium alkoxides [57,59–62] and lithium carbonate [57,60,61,63] in the SEI.

The reaction (shown in Figure 2.2) activated by lithium alkoxides (ROLi) is called a trans-esterification reaction [64]. During EMC trans-esterification reactions, DMC and DEC are the main products. In this thesis, these reactions are a tell-tale indicator that EMC has been reduced at the graphite electrode.

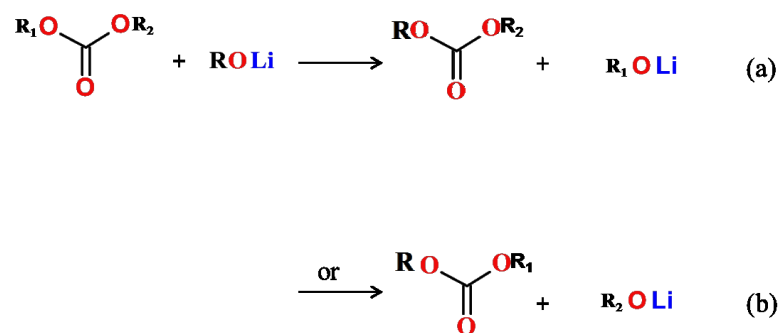


Figure 2.2 Possible mechanisms for the EMC trans-esterification reaction on the graphite electrode. ( $\text{R}_1$  represents methyl,  $\text{R}_2$  represents ethyl, R represents either methyl or ethyl).

LiF, resulting from the decomposition of  $\text{LiPF}_6$ , is another component that can be detected in the SEI on the graphite surface [56]. Equation 2.1 shows a possible mechanism of  $\text{LiPF}_6$  decomposition when trace amounts of water are in the cells [65–67].



The addition of film-forming electrolyte additives facilitates SEI formation by electrochemically forming film layers on the surface of graphite through a reduction process. The reduction potential of these electrolyte additives is normally higher than that of the main solvents (standard electrolyte), which means they will be reduced prior to the electrolyte solvents (e.g. EC). Vinylene carbonate (VC, shown in Figure 2.3(a)) is taken as an illustrative example. Ota et al. [68] showed that the reduction of VC occurs at a

potential more positive than 1.0 V vs. Li/Li<sup>+</sup>. VC can undergo polymerization on the surface of the graphite electrode during formation. Ouatani et al. [69] showed that the process of polymerization of VC can proceed either through the C=C double bond (polymer A) or the carbonate group (polymer B). The polymerization products are shown in Figures 2.3(b) and (c).

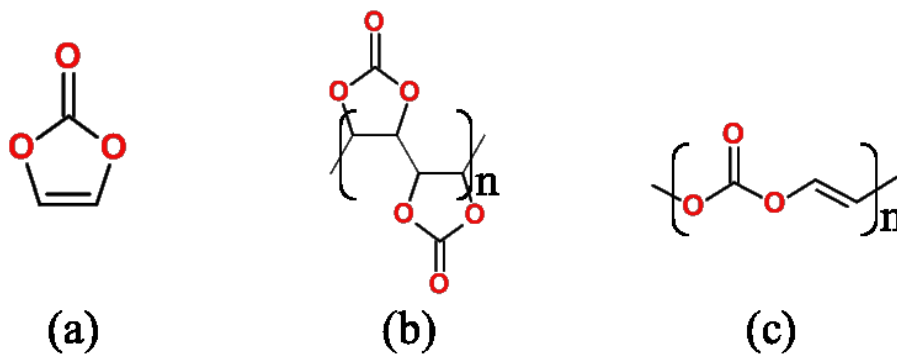


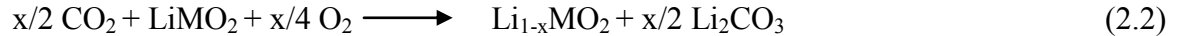
Figure 2.3 The chemical structure of VC (a) and its major reaction products on the graphite electrode during formation: polymer A (b) and polymer B (c).

### 2.1.2 Positive electrode/electrolyte interphase

Compared to the negative electrode/electrolyte interphase, limited work has been done on the positive electrode/electrolyte interphase because of the complicated species and their complex formation mechanisms. A review on the subject of electrode/electrolyte interphases was compiled by Xu in 2014, in which he summarized the previous limited work on the positive electrode/electrolyte interphase by categorizing their formation stages, including: (1) the formation of films during positive electrode manufacturing; (2)

spontaneous reactions when the positive electrode is soaked in the electrolyte; and (3) electrochemical rearrangement of the chemical species formed in stages (1) and (2) during charging [10].

A film consisting of  $\text{Li}_2\text{CO}_3$  usually forms on the surface of transition metal oxide-based positive electrode materials during their synthesis or processing in the atmosphere [70,71]. Equation 2.2 shows a possible chemical reaction [70].



(M represents a transition metal or a combination of transition metals)

Spontaneous chemical reactions can occur when positive electrode materials are exposed to electrolyte. Wang et al. [72,73] reported that direct contact of LCO with EC/DMC (1/1) containing 1M  $\text{LiPF}_6$  resulted in the decomposition of electrolyte and that precipitants formed (e.g.  $(\text{CH}_2\text{CO}_2\text{Li})_2$ ) on the surface of the electrode material. Accompanied by the dissolution of  $\text{Li}^+$  and the generation of  $\text{Co}_2\text{O}_3$ , the degradation of the LCO structure also occurred.

It is believed that the positive electrode/electrolyte interphase can be affected by the electrochemical processes during charging. Based on  $^7\text{Li}$  and  $^1\text{H}$  magic-angle spinning (MAS) nuclear magnetic resonance (NMR) studies, Ménétériér et al. [74] reported that a new organic film gradually formed on  $\text{Li}(\text{Ni}_{1-y-z}\text{Co}_y\text{Al}_z)\text{O}_2$  in 1M  $\text{LiPF}_6$  with propylene

carbonate (PC)/EC/DMC (1/1/3) during electrochemical charging. Duncan et al. [75,76] studied the interphase between  $\text{LiMn}_2\text{O}_4$  and the electrolyte (1M  $\text{LiPF}_6$  in EC/DEC (3/7)) using EIS, X-ray photoelectron spectroscopy (XPS) and Fourier transform infrared spectroscopy (FTIR). Some inorganic species such as  $\text{LiF}$ ,  $\text{Li}_x\text{PF}_y\text{O}_z$  as well as some organic species such as poly-ethers were detected after cycling. Electrolyte additives can also contribute to the formation of different species in the positive electrode/electrolyte interphase. Madec et al. [77] systematically compared the composition of the NMC111/electrolyte (1M  $\text{LiPF}_6$  in EC/EMC (3/7)) interphase with or without VC and prop-1-ene-1,3-sultone (PES) after cycling up to 4.2 V using XPS. Oligo-VC was detected in the interphase when VC was added meanwhile  $\text{RSO}_2\text{Li}$  was found when PES was added.

## **2.2 Electrolyte additives**

Electrolyte additives (up to 10 wt. %) are added to the electrolyte in order to improve the performance of LIB [10,39]. In the extensive reviews reported by Zhang et al. [53] and Xu et al. [10,39], the benefits brought by electrolyte additives can be generally divided into the following two categories: (1) modifying the properties of the SEI either on the positive side or the negative side and (2) overcharge protection. This thesis focuses on the study of electrolyte additives with the former function. They affect cell calendar or cycle life [78–80], safety [81,82], gas evolution [83–85] and impedance [86–88].

The three sections below present a brief overview of the present understanding of the effect of electrolyte additives on the graphite negative electrode, the Si-containing negative electrode and the positive electrode, respectively. The chemical structures of electrolyte additives described in this chapter are summarized in Figure 2.4.

### **2.2.1 Electrolyte additives for the graphite negative electrode**

Since graphite is now widely being used as the negative electrode material, researchers have put enormous effort into using all kinds of electrolyte additives to change the surface chemistries on the graphite side and improve cell performance. Many attempts [10] (e.g. XPS, FTIR, NMR) have also been executed to understand how additives work at a fundamental level while ultra-high precision coulometry (UHPC), long-term cycling and storage testing are some of the best ways to prove the actual usefulness of electrolyte additives.

VC, a representative of unsaturated additives, is the most popular electrolyte additive used in LIB because it helps extend the lifetime of LIB [68,89]. It can form polymers on the graphite side during cell formation and the relevant mechanism has been described by many researchers [53,68,78]. Some other organic electrolyte additives (e.g. sulfur-based, boron-based) have also been reported to have higher reduction potential than the solvents and change the composition of the interphase between the graphite and the electrolyte.

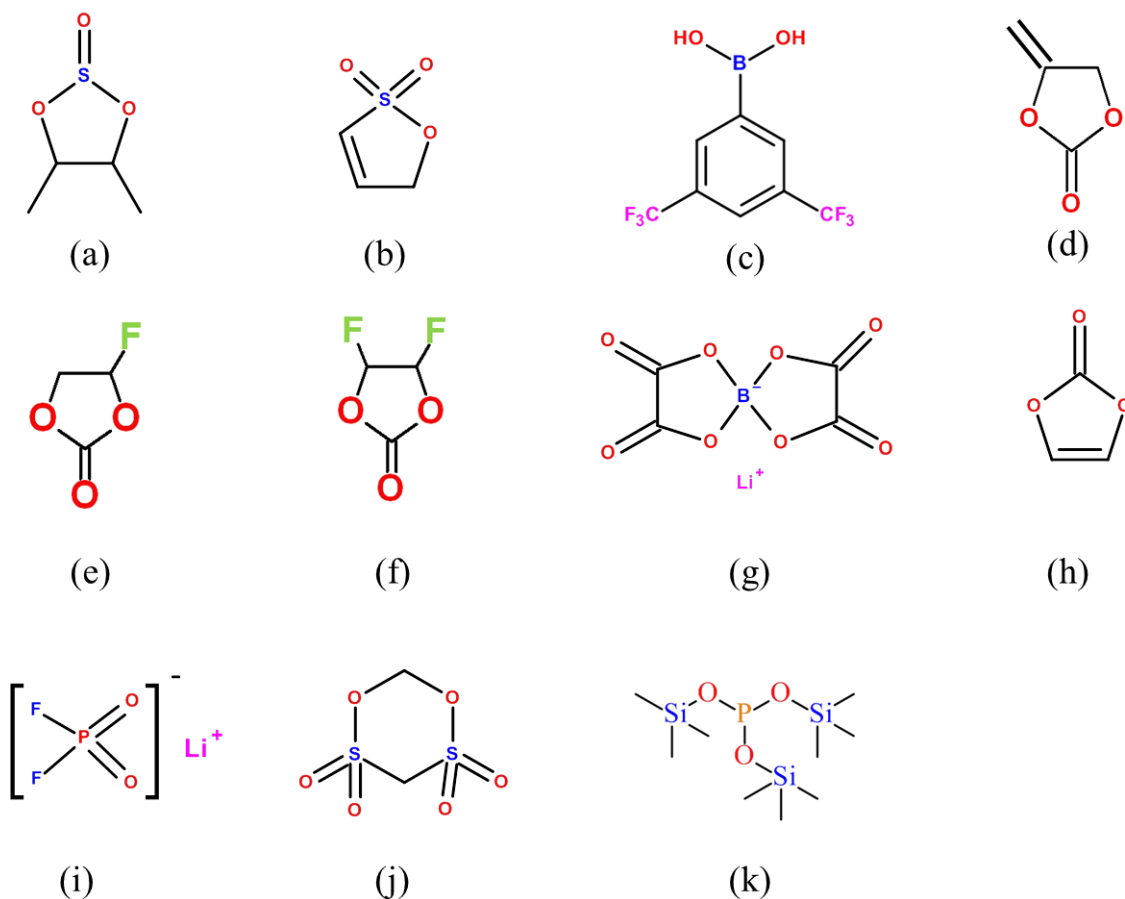


Figure 2.4 The chemical structures of BS (a), PES (b), BA (c), MEC (d), FEC (e), DiFEC (f), LiBOB (g), VC (h),  $\text{LiPO}_2\text{F}_2$  (i), MMDS (j) and TTSPi (k).

Chen et al. [90] synthesized butylene sulfite (BS) and demonstrated its film-forming capability on the graphite side in the PC-based electrolyte. The formation of a stable SEI (main products are  $\text{Li}_2\text{SO}_3$  and  $\text{ROSO}_2\text{Li}$ ) on the graphite surface is believed to improve the cell performance. Self et al. [84] proved that the reduction of PES on the graphite side during formation can suppress gas evolution in NMC442/graphite pouch cells. Based on SEM, FTIR, cycling and XPS measurements, Wang et al. [91] demonstrated that the addition of 3,5-bis(trifluoromethyl)benzeneboronic acid (BA) can improve the

electrochemical performance of the graphite electrode in PC-based electrolyte.

In addition to organic chemicals, researchers also investigated the effect of some inorganic chemicals when used as electrolyte additives. Because of the high reduction potential (1.7 V vs. Li/Li<sup>+</sup>) of BOB<sup>-</sup> anion, LiBOB can be a useful electrolyte additive. Xu et al. [92] reported that the addition of trace amounts (1 - 5 wt. %) of LiBOB could form a stable SEI on the graphite side even in PC-based electrolyte. Yang et al. [93,94] reported that the addition of LiPO<sub>2</sub>F<sub>2</sub> resulted in the formation of stable SEI on the graphite electrode and decreased its impedance during long term cycling.

### **2.2.2 Electrolyte additives for the silicon-containing negative electrode**

With the goal of increasing energy density, Si-containing negative electrode materials have been actively explored. Like graphite, Si is normally operated around 0.1 – 0.5 V vs. Li/Li<sup>+</sup> where most of the electrolyte components can be reduced and the products can change the surface chemistry of the interphase [34]. However, the interphase between Si and electrolyte is highly affected by the large volume changes during reversible lithiation/delithiation, which is totally different from graphite. During each cycling process, the formed SEI can be broken while new pristine Li<sub>x</sub>Si surface is created and another round of SEI formation starts [34].

Based on the success of some traditional electrolyte additives (e.g. VC, LiBOB) on the graphite electrode, researchers applied these electrolyte additives to the Si electrode. With



the addition of VC in carbonate-based electrolytes, Chen et al. [95] reported that the cell (Si/Li) capacity and the coulombic efficiency (CE) were improved. XPS results showed that the amount of LiF in the SEI was decreased compared to VC-free electrolyte, which indicated that the polymerized SEI formed by VC could prevent salt anion decomposition. LiBOB has also been shown to improve the cycle performance of Si/Li half cells in typical EC/DEC (3/7) electrolyte [96,97]. The reduction of BOB<sup>-</sup> resulted in the formation of a relatively stable SEI and decreased the consumption of active Si. FEC-containing electrolytes have been widely studied on the Si negative electrode because they contribute to improving electrochemical performance as judged by the capacity retention during long-term cycling [34,98,99]. According to surface analysis results [99], the interphase between Si and FEC-containing electrolytes is enriched with inorganic fluorides while the interphase resulting from FEC-free electrolytes mainly consists of the carbonate reduction products (as discussed in Section 2.1.1).

### **2.2.3 Electrolyte additives for the positive electrode**

Electrolyte additives can also affect the cell performance by changing the interphase between the positive electrode and the electrolyte. Smith and Burns et al. [100,101] developed UHPC which can accurately rank cell lifetime in a relatively short time period. Based on their report [102], with increasing amounts of VC content (up to 6 wt. %) in NMC/graphite cells, the charge end-point capacity slippage, which is caused by parasitic reactions at the positive side (e.g. electrolyte oxidation), decreased. This suggests that VC

is able to improve cell performance by affecting the SEI on the positive side, which subverts the viewpoint that VC only affects the SEI on the negative electrode.

In addition to the known ability to modify the SEI on the negative side, LiBOB also demonstrated its effect on the SEI at the positive electrode, which led to higher rate capability for NCA/Li cells [103]. In order to extend the cell lifetime at high voltage, LiBOB was also applied to  $\text{LiMn}_{1.5}\text{Ni}_{0.5}\text{O}_4/\text{Li}$  cells operated up to 4.9 V [104]. Compared with LiBOB-free cells, LiBOB-containing cells showed better capacity retention and smaller impedance. Surface analysis results suggested that the products of BOB oxidation on the positive electrode SEI prevent the oxidation of electrolyte and also suppress the dissolution of Mn (II) from the positive electrode [104].

$\text{LiPO}_2\text{F}_2$  is an extremely valuable electrolyte additive for controlling impedance growth on  $\text{LiNi}_{0.5}\text{Mn}_{0.25}\text{Co}_{0.25}\text{O}_2$  during long term cycling by modifying the interphase between positive electrode and electrolyte [105]. Zuo et al. [88] reported that the addition of methylene methanedisulfonate (MMDS) significantly increased the capacity retention of LCO/graphite cells cycled between 3.0 and 4.5 V by suppressing parasitic reactions on the positive side. MMDS has also been demonstrated to form stable SEI on the surface of  $\text{LiMn}_2\text{O}_4$ , thus leading to improved thermal stability [106] and suppression on the dissolution of Mn [107]. Xia et al. [108] reported that the addition of difluoroethylene carbonate (DiFEC) decreased charge-end-point capacity slippage, which indicated the

suppression of electrolyte oxidation on NMC442 electrode. Yang et al. [109] showed that the addition of DiFEC extended lifetime of LCO/graphite cell by forming stable SEI on LCO.

### **2.3 Introduction of coatings on the electrode materials**

Surface coating of electrode materials has been widely introduced to improve the performance of lithium ion cells (e.g. thermal stability [110], rate capability [111] and capacity retention [112,113]). The coating materials normally consist of metal oxides, carbon, metal carbonates, metal fluorides, metal aluminates and metal phosphates [114]. Various methods have been investigated to carry out surface coating including atomic layer deposition (ALD) [115], vapor decomposition processes [116], sol-gel methods [113] and so on. Since surface coating has been applied on both positive and negative electrode materials, the two sections below present a brief overview of the present understanding of the role of surface coating.

#### **2.3.1 Surface coatings on the positive electrode**

It is now accepted that the role of surface coating on the positive electrode material can be mainly classified into the following three categories [114,117]: (1) improved electron-conducting layer, (2) modification of surface chemistry and (3) physical protection layer.

Conductive carbon coatings have proven to be useful for improving the charge transfer process at the interphase of positive electrode materials. For example, with a surface coating of carbon, LFP showed better rate capability [116,118].

Surface chemistry of positive electrode materials has a strong impact on the electrochemical performance of cells [119,120]. Since the coating process often involves some physical treatment (e.g. heat treatment), this can change the surface chemistry of electrodes, which can contribute to changes in cell performance.

When  $\text{LiPF}_6$  reacts with trace amounts of moisture in the cells, HF will form (see equation 2.1) and corrode the electrode surface. Some researchers [114] reported that a surface coating (e.g.  $\text{Al}_2\text{O}_3$ ) could react with HF to eliminate its negative effect by an example reaction as shown in equation 2.3.



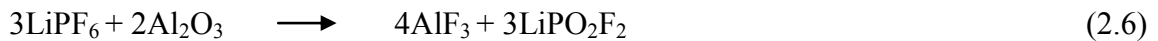
However,  $\text{H}_2\text{O}$ , the product of this reaction could produce more HF in cells. Therefore, some researchers do not believe that a surface coating can improve cell performance by eliminating acid species. A solid superacid model [117] was proposed to illustrate the role of coatings (e.g.  $\text{Al}_2\text{O}_3$ ) on modifying surface chemistry. In this model,  $\text{AlF}_3$  can be produced through equation 2.3 while LiF and  $\text{PF}_5$  can be produced from  $\text{LiPF}_6$ . In

equation 2.4,  $\text{Li}_3\text{AlF}_6$  can be produced and is regarded as a solid solution of  $\text{AlF}_3$  and  $\text{LiF}$  (see equation 2.5).



$\text{AlF}_3/\text{Al}_2\text{O}_3$  and  $\text{AlF}_3/\text{Li}_3\text{AlF}_6$  are solid superacids which form on the SEI around the positive electrode particles. Because of high acidic strength and catalytic effects, solid superacids are widely used as catalysts [121]. They improve electrochemical performance of LCO-containing cells by removing alkaline impurities [119] on the surface of LCO.

Chemically inactive material coatings can be a physical protection layer to suppress parasitic reactions (e.g. oxidation of electrolyte, oxygen release [122]) between electrodes and electrolytes. Some examples of these coating materials are  $\text{ZnO}$ ,  $\text{AlF}_3$ ,  $\text{Al}_2\text{O}_3$  and  $\text{ZrO}_2$  [113,114,123–125]. However, with the support of NMR technique, Hall et al. [126] recently found a possible reaction mechanism of  $\text{Al}_2\text{O}_3$  coating on positive electrode materials with  $\text{LiPF}_6$  as following equation.



### 2.3.2 Surface coatings on the negative electrode

Surface coating is also practiced on negative electrode materials in order to suppress side

reactions between electrolytes and electrodes and provide better electric contact networks. Carbon coating has been reported to protect natural graphite from attack by PC-based electrolyte [127,128]. Yoshio et al. [129] and He et al. [130] showed that carbon coating and  $\text{Al}_2\text{O}_3$  coating were both effective for improving Si-containing cell performance by stopping parasitic reactions on the surface, keeping integral electric contact around silicon particles and alleviating particle cracking.

Coating is an effective way of improving cell performance by affecting the interphase between electrodes and electrolytes. Meanwhile, electrolyte additives can also extend cell lifetime, control impedance growth and suppress gas production by modifying the SEI. Arumugam et al. [131] reported the special synergetic effect between  $\text{Al}_2\text{O}_3$  coated NMC622 and electrolyte additive combinations, called “PES211” (2% PES + 1% MMDS + 1% tris (trimethylsilyl) phosphite (TTSPi)), on cell performance. There is still wide space for fundamental investigation into the combined effect of electrolyte additives and coatings on cell performance. The relevant mechanisms could be of great help in fully understanding the interphases which affect the performance and lifetime of LIB.

## CHAPTER 3 EXPERIMENTAL TECHNIQUES

### 3.1 Cell chemistry and preparation

#### 3.1.1 Cell chemistry

Dry (no electrolyte) machine-made pouch cells were used through all the projects in this thesis. Four different cell chemistries were used including NMC111/graphite, NMC442/graphite, coated SC NMC532/graphite and uncoated SC NMC532/graphite. All the pouch cells were obtained from Li-Fun Technology (Xinma Industry Zone, Golden Dragon Road, Tianyuan District, Zhuzhou City, Hunan Province, PRC, 412000). The same artificial graphite negative electrode material (Kaijin AML-400 from Kaijin, China) was used in all the pouch cells. Table 3.1 summarizes the electrode formulations in the pouch cells used for this thesis.

The coating on the SC NMC532 was studied using electron microscopy since its detailed information was not disclosed by the supplier. Cross-sectional samples of the particles were first created using focused ion beam (FIB) milling in a scanning electron microscope (SEM). Once cross-sectioned, a line-scan was collected across the interface from the carbon substrate through the surface and into the bulk of the particle using electron energy-loss spectroscopy (EELS) and scanning transmission electron microscopy (STEM). At an accelerating voltage of 300 keV, EELS spectra were collected every 10 nm over a 500 nm span with an exposure time of 0.10 s at a dispersion of 0.5 eV/channel. Figure 3.1a shows the STEM image of a coated SC NMC532 particle. The red line indicates the direction of EELS line scan. Titanium was the only element

other than Li, Ni, Co and Mn observed in the sample.

Table 3.1 Electrode formulations used in the pouch cells of this thesis.

Cell Type	Ratio between the active electrode material, carbon black, polyvinylidene fluoride (PVDF) and graphite ( <u>only for SC NMC</u> ) of the NMC positive electrode (by weight)	Ratio between the active electrode material, carbon black and carboxymethyl cellulose-styrene-butadiene rubber (CMS-SBR) of the graphite positive electrode (by weight)	Cell balance (V)
NMC111/gr.	96:2:2	96:2:2	4.7
NMC442/gr.	96:2:2	96:2:2	4.7
coated SC NMC532/gr.	94:2:2:2	96:2:2	4.4
uncoated SC NMC532/gr.	94:2:2:2	96:2:2	4.4

To approximate the relative change in Ti concentration across the interface, each EELS spectrum in the line-scan was first background subtracted by least-squares fitting a generalized power law to the region between 370 and 445 eV as shown in Figure A1. Counts were integrated between the range of 445 eV and 460 eV to capture the characteristic Ti  $L_{2,3}$  edge. The counts were then normalized to 1.0. This is shown in Figure 3.1b. It can be observed that Ti is only present in the first 30-50 nm of the particle with few to no Ti counts found in the bulk of the particle. It should be noted that this analysis is entirely qualitative and the electron cross section, plural scattering and electron channeling effects were not taken into account for this analysis. Nevertheless,



the data show that the Ti is only present at the surface of the particles and therefore the coated samples have a Ti-based coating.

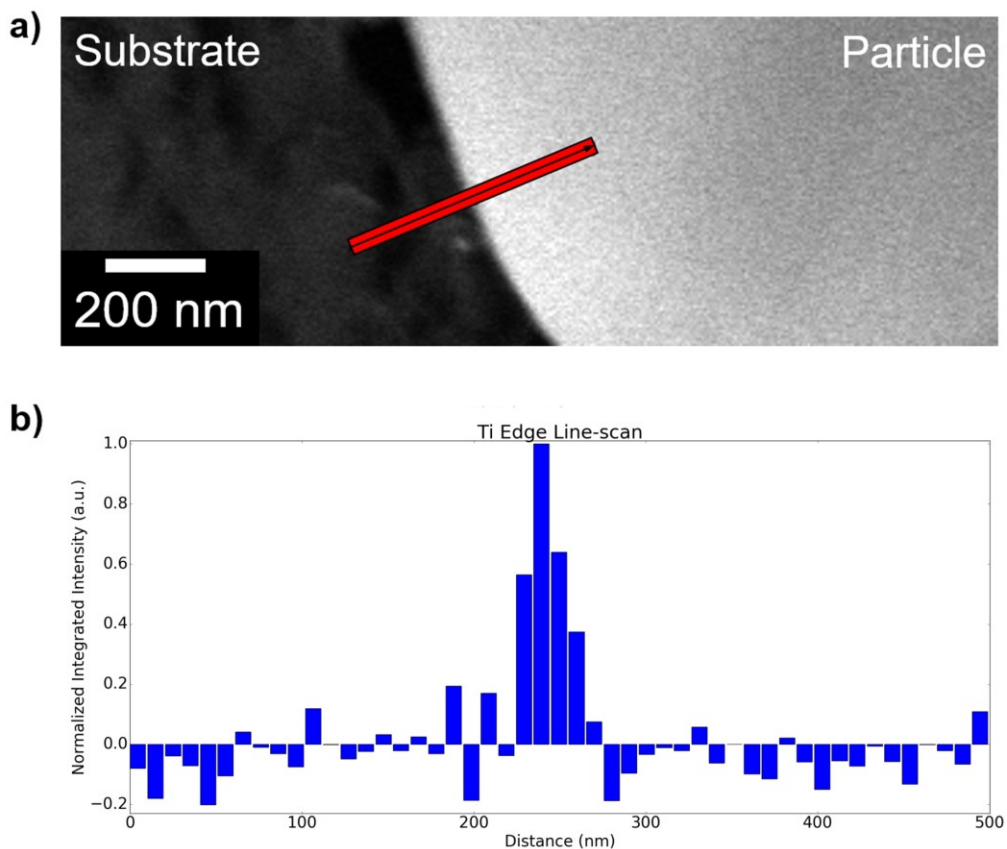


Figure 3.1 (a) STEM image of a fresh coated SC NMC532 particle. (b) EELS line scan profile of Ti.

XPS was also used for characterizing surface coating composition. Figure 3.2 shows the binding energy of Ti 2p peaks for both coated and uncoated NMC532. The binding energy of Ti 2p peaks for coated NMC532 is in excellent agreement with the reported literature

[132] values of  $\text{TiO}_2$ . We do not claim the coating is  $\text{TiO}_2$ , only that the data suggests the Ti is in the 4+ oxidation state and is in an octahedral oxygen environment.

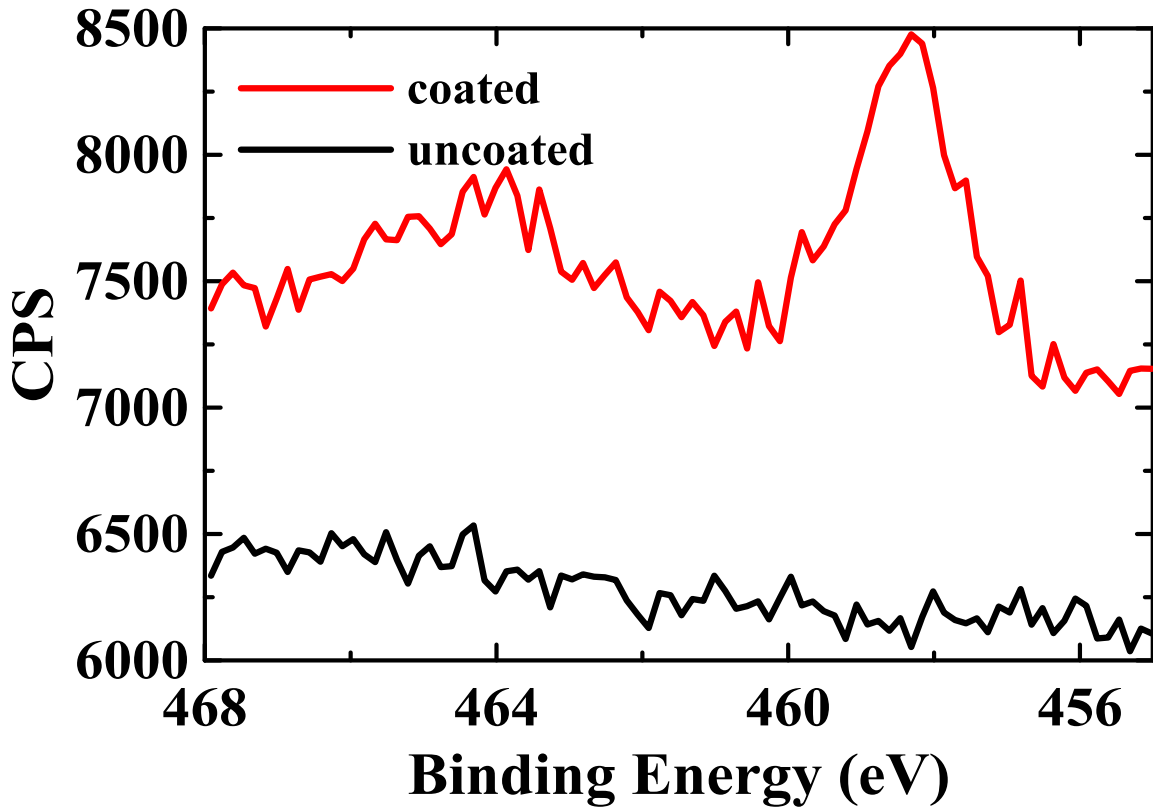
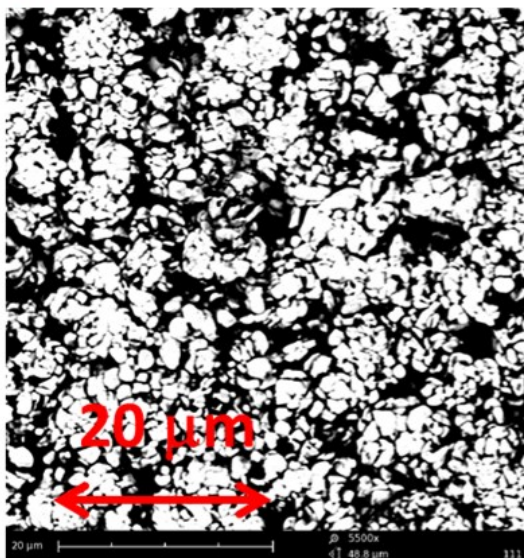


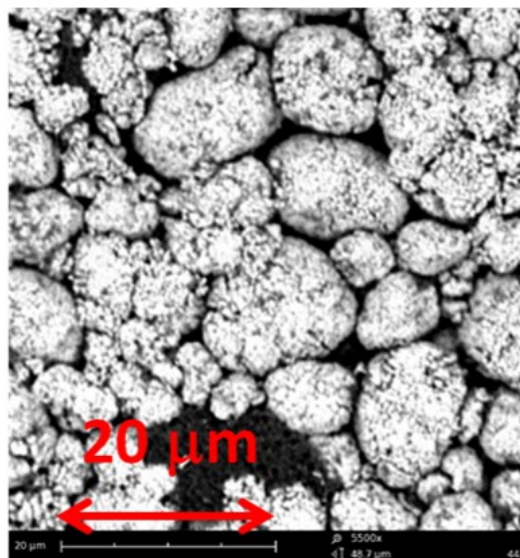
Figure 3.2 XPS spectra of Ti 2p peaks for coated and uncoated NMC532.

Figure 3.3 shows the SEM images for the fresh positive electrodes with different chemistries: (a) NMC111, (b) NMC442, (c) coated SC NMC532 and (d) uncoated SC NMC532.

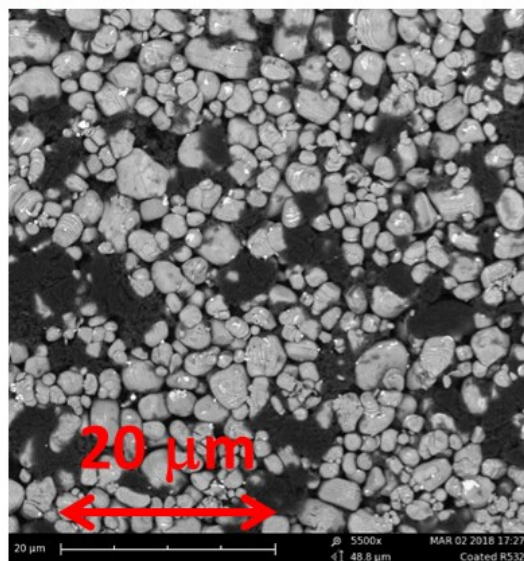
**(a) NMC111**



**(b) NMC442**



**(c) Coated SC NMC532**



**(d) Uncoated SC NMC532**

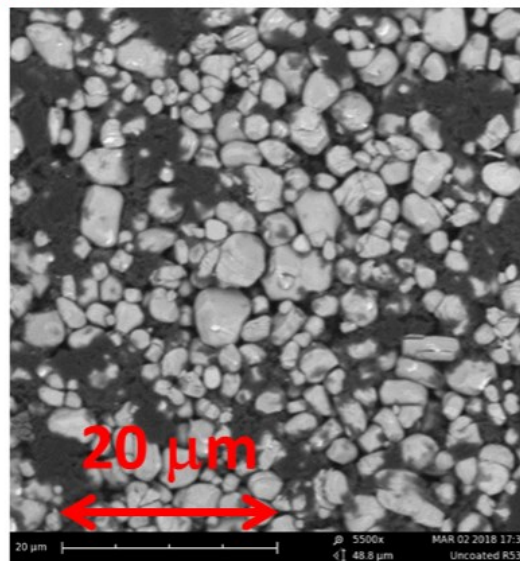


Figure 3.3 SEM images for fresh positive electrodes from the pouch cells used in this thesis: (a) NMC111, (b) NMC442, (c) coated SC NMC532 and (d) uncoated SC NMC532.

Figure 3.4 shows voltage vs. capacity for a coated SC NMC532/graphite pouch cell (black line), its corresponding coated SC NMC532 electrode (blue line) and graphite electrode (red line) during charging in order to illustrate the meaning of cell balance mentioned in Table 3.1.

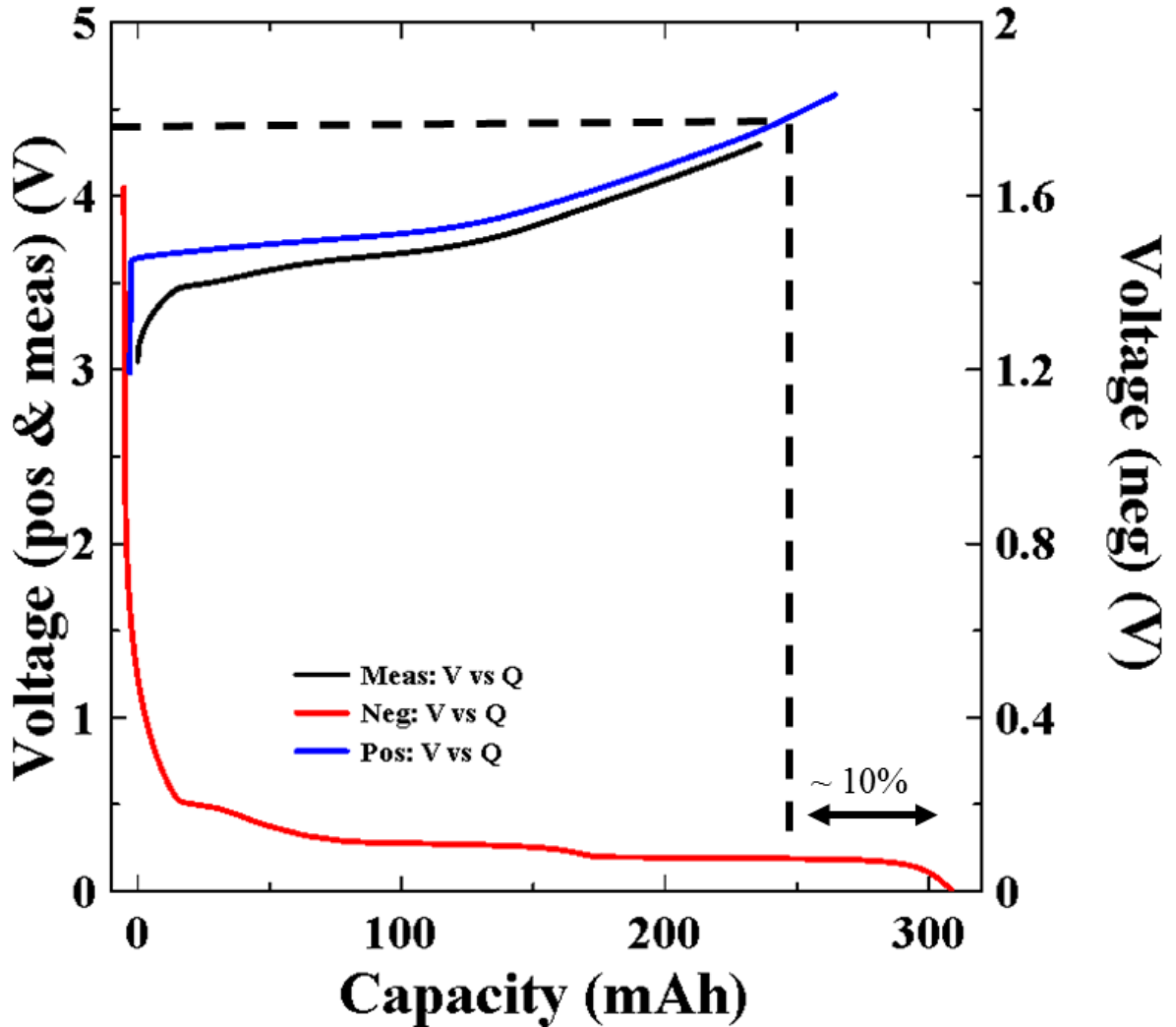


Figure 3.4 Voltage vs. capacity for a coated SC NMC532/graphite cell (black line), coated SC NMC532/lithium metal (blue line) and graphite/lithium metal (red line) with 1.2M LiPF<sub>6</sub> in EC/EMC 3/7 plus 2% FEC during charging process up to 4.3 V with current corresponding to C/20 at 40°C.

The data was measured using current corresponding to C/20 at 40°C. Theoretically, this coated SC NMC532/graphite pouch cell is balanced up to 4.4 V. As a result, when this pouch cell is charged to 4.4 V, there is still around 10% extra capacity in the graphite electrode as indicated in Figure 3.4.

### 3.1.2 Cell preparation

All pouch cells were vacuum sealed without electrolyte in a dry room in China and then shipped to our laboratory in Canada. Before electrolyte filling, the cells were cut just below the heat seal and dried at 100°C under vacuum for 14 hours to remove any residual water. Then the cells were transferred immediately to an argon-filled glove box for filling and vacuum sealing. All the pouch cells were filled with 0.9 g of electrolyte. After filling, cells were vacuum-sealed with a compact vacuum sealer (MSK-115A, MTI Corp.). Then cells were placed in a temperature box at 40. ± 0.1°C where they were hold at 1.5 V for 24 hours to allow for completion of wetting before formation. During formation all the cells were charged from 1.5 V to 3.5 V at a current corresponding to C/20 and then degassed and charged from 3.5 V to the high operation voltage.

Figure 3.5 shows a voltage (V) vs. capacity (Q) curve (a) and its relevant dQ/dV vs. voltage curve for a NMC442/graphite cell during formation up to 4.4 V with a current corresponding to C/20 at 40°C. Normally plateaus in the voltage vs. capacity appear as clearly identifiable peaks in the dQ/dV vs. V curve, which suggest the occurrence of redox reactions. In Figure 3.5(b), the peak at around 3.2 V suggests the reduction of EMC on the graphite electrode [9].

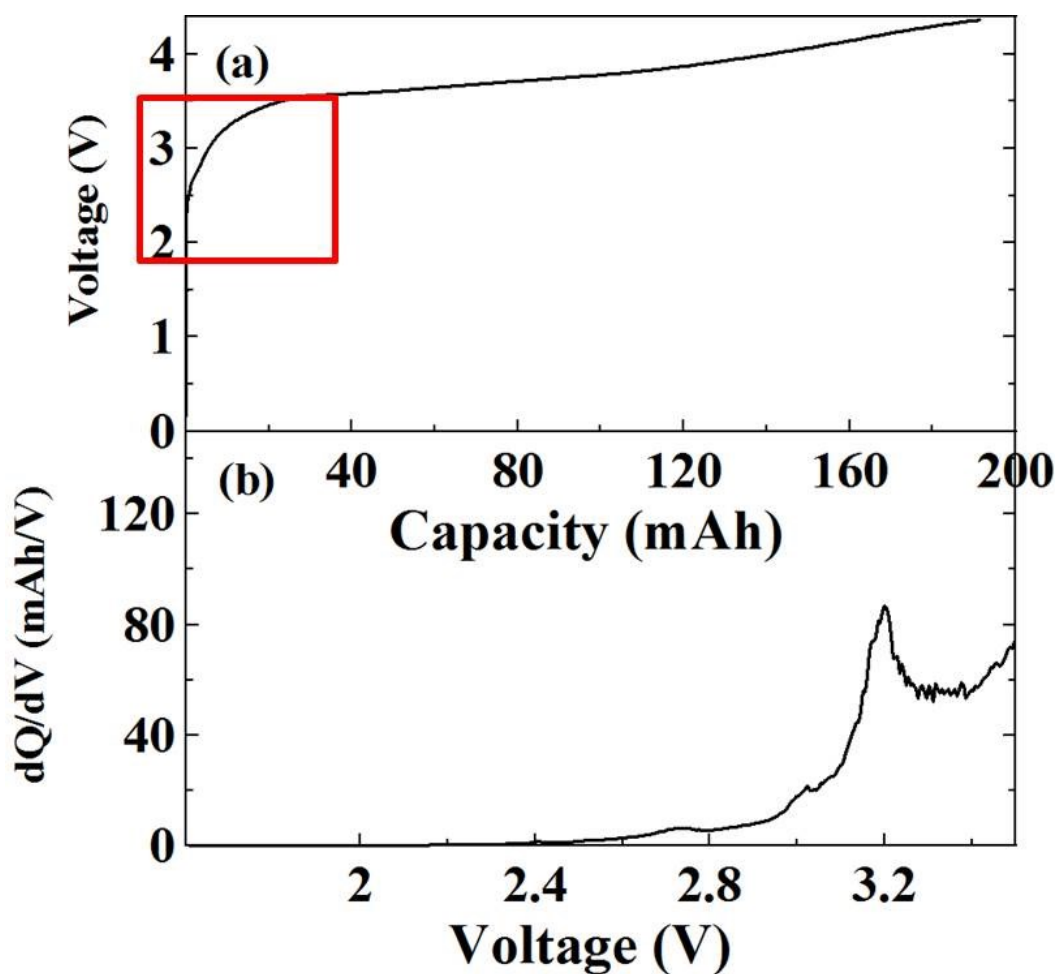


Figure 3.5 Voltage vs. capacity curve (a) and associated  $dQ/dV$  vs. voltage curve (b) for a NMC442/graphite cell with 1M  $\text{LiPF}_6$  in EMC during formation with a current corresponding to C/40 at 40°C. The  $dQ/dV$  vs. V curve only corresponds to the region of the V-Q curve in the highlighted box.

### 3.1.3 Electrolyte chemicals

Electrolyte chemicals used in this thesis were provided by different companies and used as received without any purification. Table 3.2 summarizes the supplier (if available), purity (if available) and water content (if available) of each electrolyte chemical.

Table 3.2 Detailed information of electrolyte chemicals used this thesis.

Chemical	Common name	Supplier	Purity (%)	Water content (ppm)
EC	ethylene carbonate	BASF	99.95	< 10
EMC	ethyl methyl carbonate	BASF	99.92	< 6
DMC	dimethyl carbonate	BASF	99.95	< 20
LiPF <sub>6</sub>	lithium hexafluorophosphate	BASF	99.94	< 20
VC	vinylene carbonate	BASF	99.8	< 100
FEC	fluoroethylene carbonate	BASF	99.94	< 20
DiFEC	difluoroethylene carbonate	HSC Corporation	99.5	NA
MEC	methylene ethylene carbonate	BASF	NA	NA
MMDS	methylene methanedisulfonate	Tinci Co. Ltd	98.7	NA
DTD	1,3,2-dioxathiolane-2,2-dioxide or ethylene sulfite	Tinci Co. Ltd	99.0	NA
TTSPi	tris(trimethylsilyl) phosphite	TCI America	> 95.0	NA
PES	prop-1-ene-1,3-sultone	Lianchuang Pharmaceutical	98.2	NA
PBF	pyridine trifluoroborate	3M Co. Ltd	99.0	NA
PPF	pyridine pentafluorophosphate	3M Co. Ltd	99.0	NA
MA	methyl acetate	BASF	99.95	< 20
CH <sub>2</sub> Cl <sub>2</sub>	dichloromethane	Fisher	99.9	NA
HDI	hexamethylene diisocyanate	Sigma-Aldrich	99.0	NA
LiPO <sub>2</sub> F <sub>2</sub>	lithium difluorophosphate	Tinci and Capchem Co. Ltd	99.73	180.04
LiBOB	lithium bis(oxalate)borate	Rockwood Lithium	99.9	NA
LiDFOB	lithium difluoro (oxalate) borate	Chemmetall	NA	NA

### 3.2 Storage testing

Storage experiments are simple and useful methods to compare the parasitic reaction rates of given electrode/electrolyte combinations at a selected cut-off voltage. These parasitic reactions mainly consist of electrolyte oxidation on the positive electrode, the dissolution of transition metals from the positive electrode and electrolyte reduction on the negative electrode [133]. This experiment can be applied to a single electrode (Li metal is the negative electrode) or a full cell configuration (usually graphite is the negative electrode). It is well known that the potential of an intercalation electrode depends on the amount of lithium residing in the electrode material. In a full cell configuration, if the negative electrode (graphite) is in a two-phase region and the positive electrode is not in a two-phase region, the voltage change of the cell during storage must be caused by a change of lithium content in the positive electrode because the electrode potential (vs.  $\text{Li}/\text{Li}^+$ ) in the two-phase region is constant.

Figure 3.6 shows the full cell voltage (or the half cell potential) vs. the state of charge curve for a LCO/graphite full cell and its corresponding half cell curves. It is clear that the change of the cell voltage results from a change of the lithium content in the positive electrode at high states of charge. The potential decrease of the positive electrode suggests the increase of lithium content inside. The lithium ions from the electrolyte combine with the electrons caused by the parasitic reactions on the surface of positive side to insert in the positive electrode. In the case of storage experiments on half cells, the



voltage change comes directly from the working electrode because the potential of the lithium metal electrode is constant.

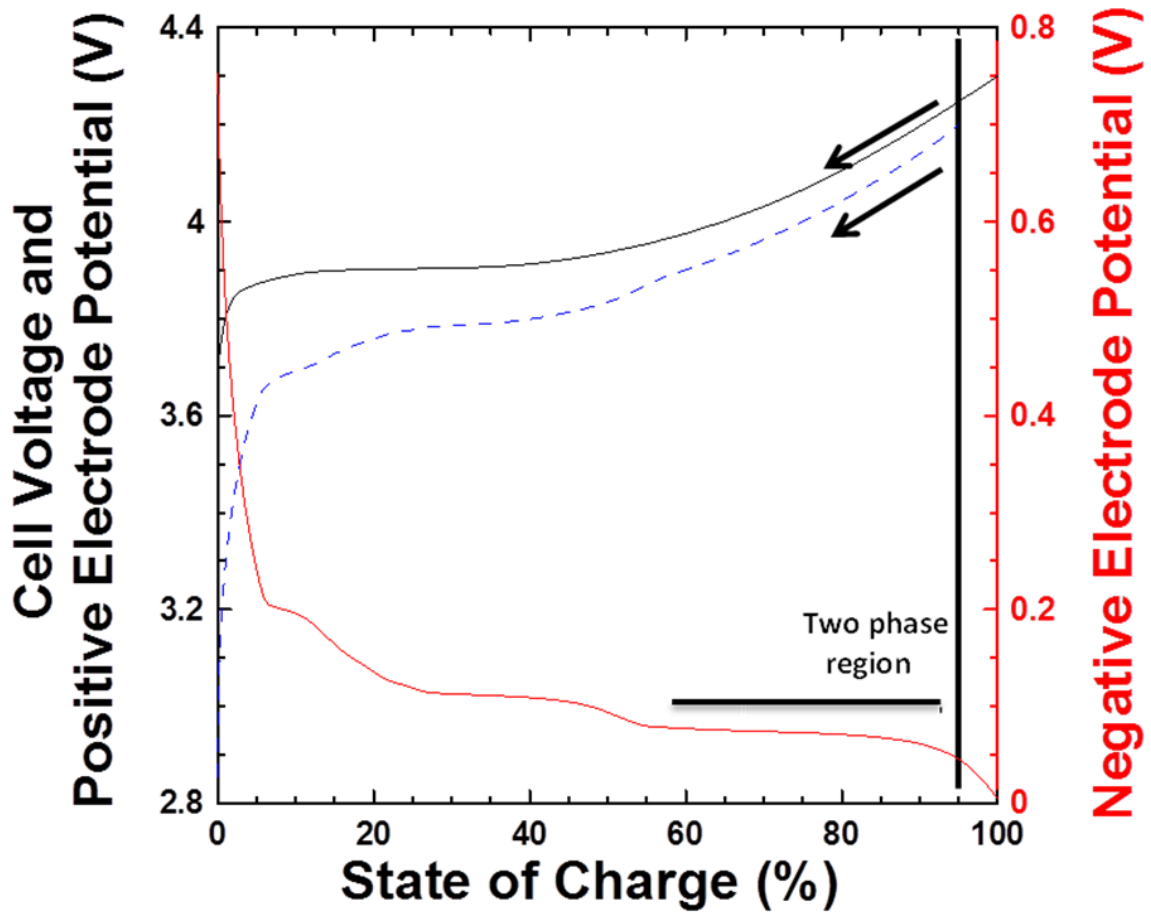


Figure 3.6 Voltage vs. state of charge curve for a LCO/graphite full cell (blue dashed curve). Potential (vs.  $\text{Li}/\text{Li}^+$ ) vs. state of charge curve for a graphite half cell (red solid curve) and a LCO half cell (black solid curve), respectively. Taken with permission from Deijun Xiong, *Surprising Chemistries in Li-ion Cells*, PhD thesis, Dalhousie University, Halifax, NS (2017).

The Dahn lab storage system, built in 2013, is used to test the open-circuit voltage of cells as a function of time at various temperatures. All the storage results presented in this

thesis are for the full cell configuration. Usually a Maccor series 4000 cycler was used to prepare cells for the storage tests. In this thesis, cells after formation were cycled between 2.8 V and the high cut-off voltage (4.3 or 4.4 V) twice with a current of 10 mA (C/20). Then the cells were held at the high cut-off voltage (4.3 or 4.4 V) for 24 hours and then were transferred to the storage system. The storage period lasts 500 hours at high temperature (40°C or 60°C) for each test.

### **3.3 Gas chromatography (GC)**

In order to obtain a deep understanding of the fate of electrolyte compositions, GC coupled with MS was used in this thesis to analyze the consumption of electrolyte additives and the change of solvent components semi-quantitatively in the cells during different operations (e.g. formation, long-term cycling and storage).

GC is a technique used to separate multiple species in a sample. A basic gas chromatograph, as shown in Figure 3.7, mainly consists of a heated injector, a carrier gas supply, a separation column located in a temperature programmable-oven and a detector. A mass spectrometer was the detector used in this thesis for detecting the volatile components of the electrolyte.

The carrier gas, namely the “mobile phase”, is helium in the column connected to the mass spectrometer here. The choice of carrier gas mainly depends on the quality of separation needed and the analyte mixture [134].

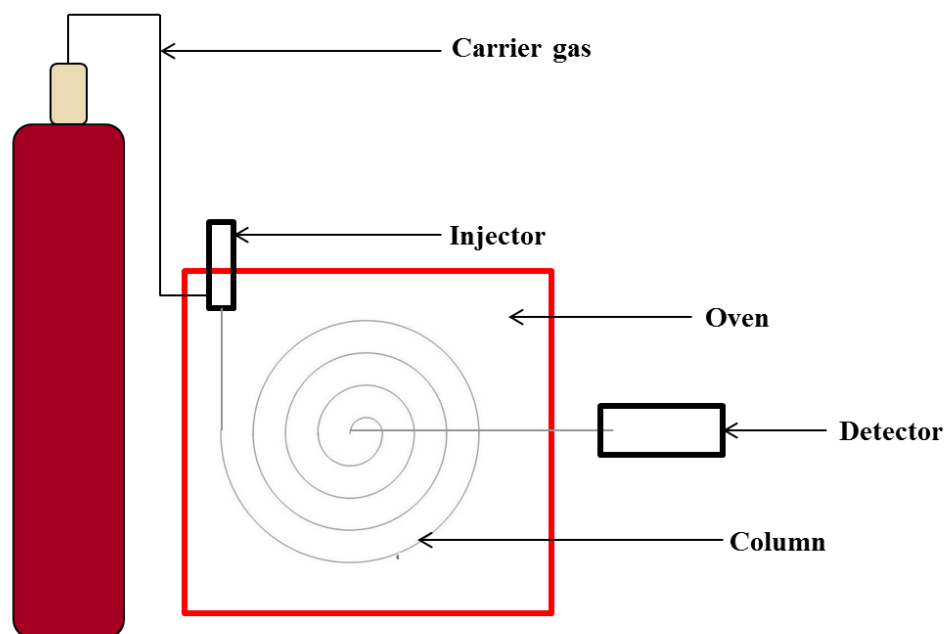


Figure 3.7 A schematic of a GC.

An analytical column, usually made of silica covered with a polymeric film outside, is a key part of the GC because the “stationary phase” is coated on the inner wall of the column. The stationary phase is usually a liquid phase or porous particulates. In addition to the stationary phase, the dimensions and coating thickness of the columns depend on the analytes, sample loading and so on. The column used for the experiment in this thesis is BR-5MS (Bruker, length: 30m, inner diameter: 0.25 mm, thickness of inside coating: 1.00  $\mu\text{m}$ ). The coating material inside the column is 5% phenyl plus 95% dimethyl arylene siloxane. Figure 3.8 shows the chemical structure of this coating material.

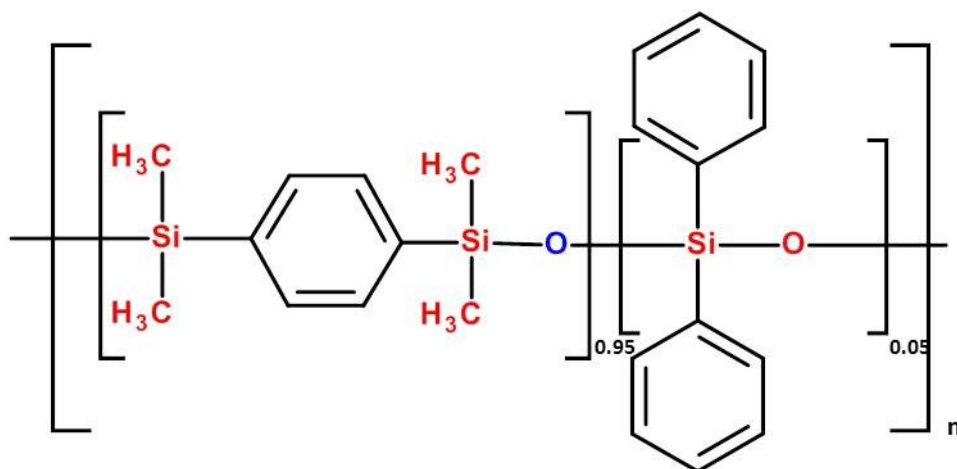


Figure 3.8 The chemical structure of 5% phenyl plus 95% dimethyl arylene siloxane.

After the sample is introduced in the injector, it will be volatilized and carried by the mobile phase through the column, during which the analytes in the sample will interact with the stationary phase inside. Since the partition coefficients of different analytes are different, different analytes will spend different times on the stationary phase, which results in the separation of the different analytes. In addition to the partition coefficient, the temperature of the oven also affects the retention time of the analytes. During the experiments in this thesis, a temperature ramp procedure was used to accelerate the separation process.

### 3.4 Mass spectrometry (MS)

MS, a powerful detection technique, was used in tandem with GC. Figure 3.9 shows a schematic of a typical mass spectrometer. A mass spectrometer mainly consists of a

sample inlet, an ionization chamber, a mass analyzer and an ion detector. The sample is initially introduced into the sample inlet then transferred to the ionization chamber where the sample is ionized. The charged atoms or molecules are separated based on the mass to charge ratio ( $m/z$ ) by the mass analyser. Then the ions exit the mass analyser and hit the detector to create a signal. Generally more ions mean a stronger signal, which lays the foundation for quantitative analysis.

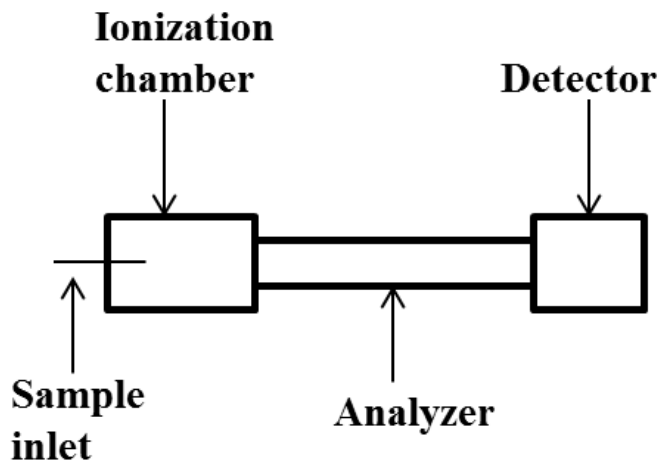


Figure 3.9 A schematic of a mass spectrometer.

Electron impact ionization (EI) was the ionization method used to produce results for this thesis. The essential idea of an EI source is to accelerate electrons to a set energy (usually 70 eV), and allow these electrons to hit the neutral gas phase molecules, causing ionization. The electrons are generated using a heated tungsten filament and a strong electric field. The whole process is illustrated in Figure 3.10.

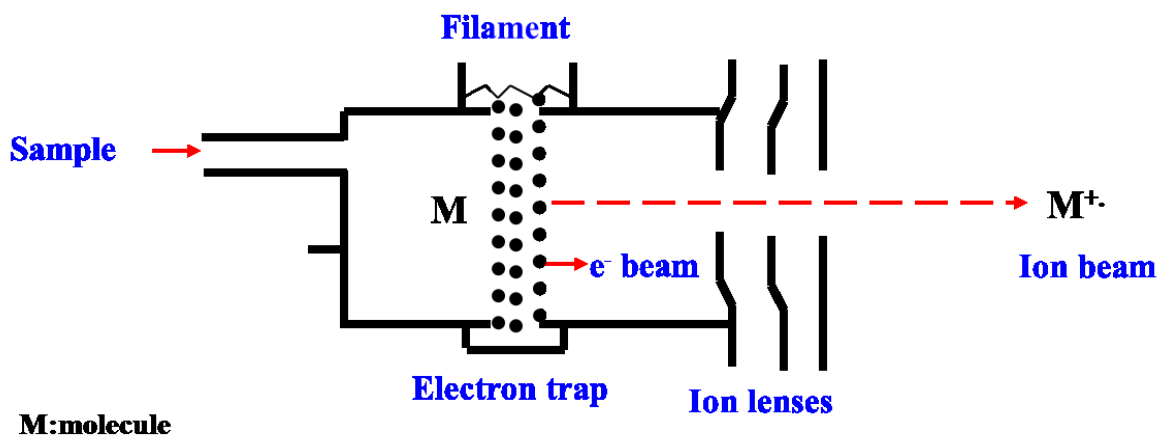


Figure 3.10 A schematic of an EI source.

There are several common types of mass analyzer such as ion trap, time of flight, quadrupole and magnetic sector. A quadrupole mass analyzer was used to produce the results for this thesis. The basic principle of a quadrupole analyzer is to allow the ions to travel through a set of four rods which create an oscillating electric field. Only those ions at a specific  $m/z$  ratio will make it through this field while the rest of the ions will hit the sides of the rods, and never reach the detector. The detailed theory can be found in reference [134]. Figure 3.11 shows a simple schematic of a quadrupole analyzer.

### 3.5 Ultra-high precision coulometry (UHPC)

UHPC developed by Smith et al. [135,136] was extensively used in the work presented in this thesis in order to gain an understanding about the effect of different electrolyte systems and cell chemistry on the anticipated cell lifetime.

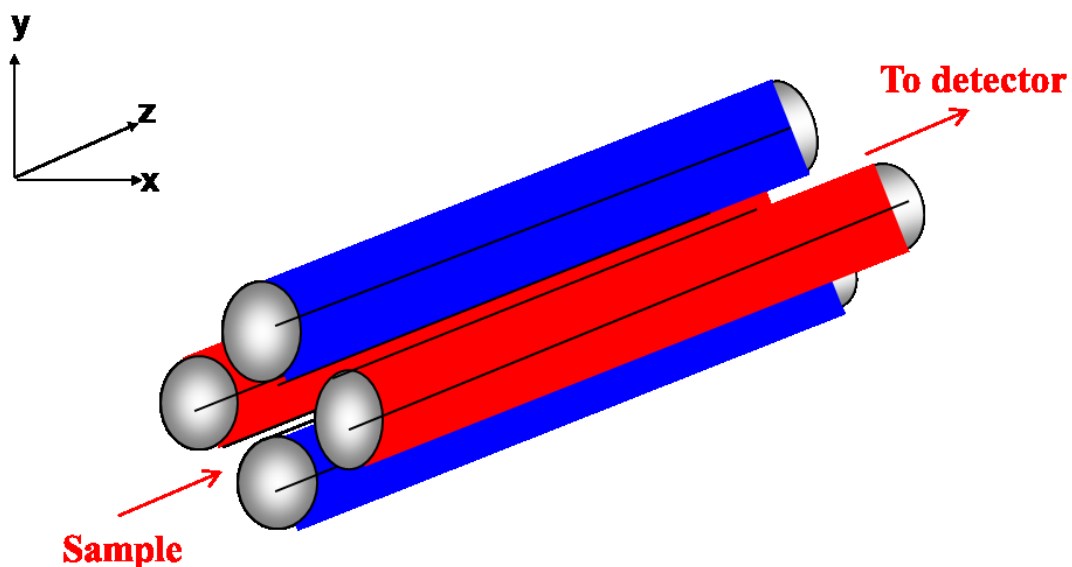


Figure 3.11 A schematic of a quadrupole mass analyzer.

Figure 3.12 shows the 100-channel UHPC system at Dalhousie University. Several significant parameters such as CE, the charge and discharge endpoint capacity slippages per cycle ( $\Delta_c$  and  $\Delta_d$ , respectively) and the fractional fade per cycle can be measured accurately by UHPC to compare the rate of parasitic reactions between different cells.

According to the lithium inventory model proposed by Smith et al. [100], the fractional fade per cycle,  $\text{fade}/Q$ , represents lithium loss due to SEI growth at the negative electrode and the fractional charge endpoint capacity slippage per cycle,  $\text{slippage}/Q$ , indicates the electrolyte oxidation at the positive electrode.



Figure 3.12 The UHPC test channels at Dalhousie University.

The relationship between fade/Q, slippage/Q and CE can be summarized by the following equation:

$$1 - CE = \text{coulombic inefficiency (CIE)} = \text{Fade}/Q + \text{Slippage}/Q \quad (3.1)$$

Generally lower slippage/Q, lower fade/Q and higher CE result in longer lived cells [101].



### 3.6 Gas evolution

In a lithium ion cell, electrode materials can react with electrolyte to produce gaseous products during formation, cycling or storage. The production of gas can result in the deformation of a pouch cell, loss of electrical contact between a cell and its device and even safety issues. Electrolyte compositions affect the production of gas [84]. Therefore, it is important to measure the gas produced in a cell accurately to determine the effect of electrolyte composition on gas evolution. *In-situ* and *ex-situ* gas measurement systems [83] were built in the Dahn lab in 2013. In these systems Archimedes' Principle is used to measure the buoyant force on the cell. Figure 3.13 shows a photograph of the set-up used for the *ex-situ* gas measurement. A pouch cell is hooked under a balance. The details of the test procedure are discussed by Self et al [84].

When a pouch cell is immersed in water, the following forces act on it: buoyant force ( $F_{\text{buoyant}}$ ), force of the tension due to the hook ( $F_{\text{tension}}$ ) and gravity ( $G$ ). This can be described in equation 3.2.

$$\Sigma F = F_{\text{tension}} + F_{\text{buoyant}} - G = 0 \quad (3.2)$$

When the volume of a pouch cell changes due to gas evolution,  $F_{\text{buoyant}}$  will change but  $G$  will stay constant. As a result, the change of  $F_{\text{tension}}$  is opposite to the change of  $F_{\text{buoyant}}$  on the cell.

$$\Delta F_{\text{tension}} = -\Delta F_{\text{buoyant}} \quad (3.3)$$

The change of  $F_{\text{buoyant}}$  is described by equation 3.4.

$$\Delta F_{\text{buoyant}} = \Delta v g \rho \quad (3.4)$$

where  $\Delta v$  is the volume change of a pouch cell,  $\rho$  is the density of the liquid (water)

where the pouch cell is immersed and  $g$  is the magnitude of gravitational acceleration.

The change of  $F_{\text{tension}}$  can be determined by the balance, which is described by equation 3.5.

$$\Delta F_{\text{tension}} = \Delta m_{\text{balance}} g \quad (3.5)$$

where  $\Delta m_{\text{balance}}$  is the mass change measured by the balance and  $g$  is the magnitude of gravitational acceleration.

As a summary of equations 3.3 – 3.5, the volume change of a pouch cell, which is equal to the amount of produced gas, is directly proportional to the mass change measured by the balance. This is described by equation 3.6.

$$\Delta v = -\Delta m / \rho \quad (3.6)$$

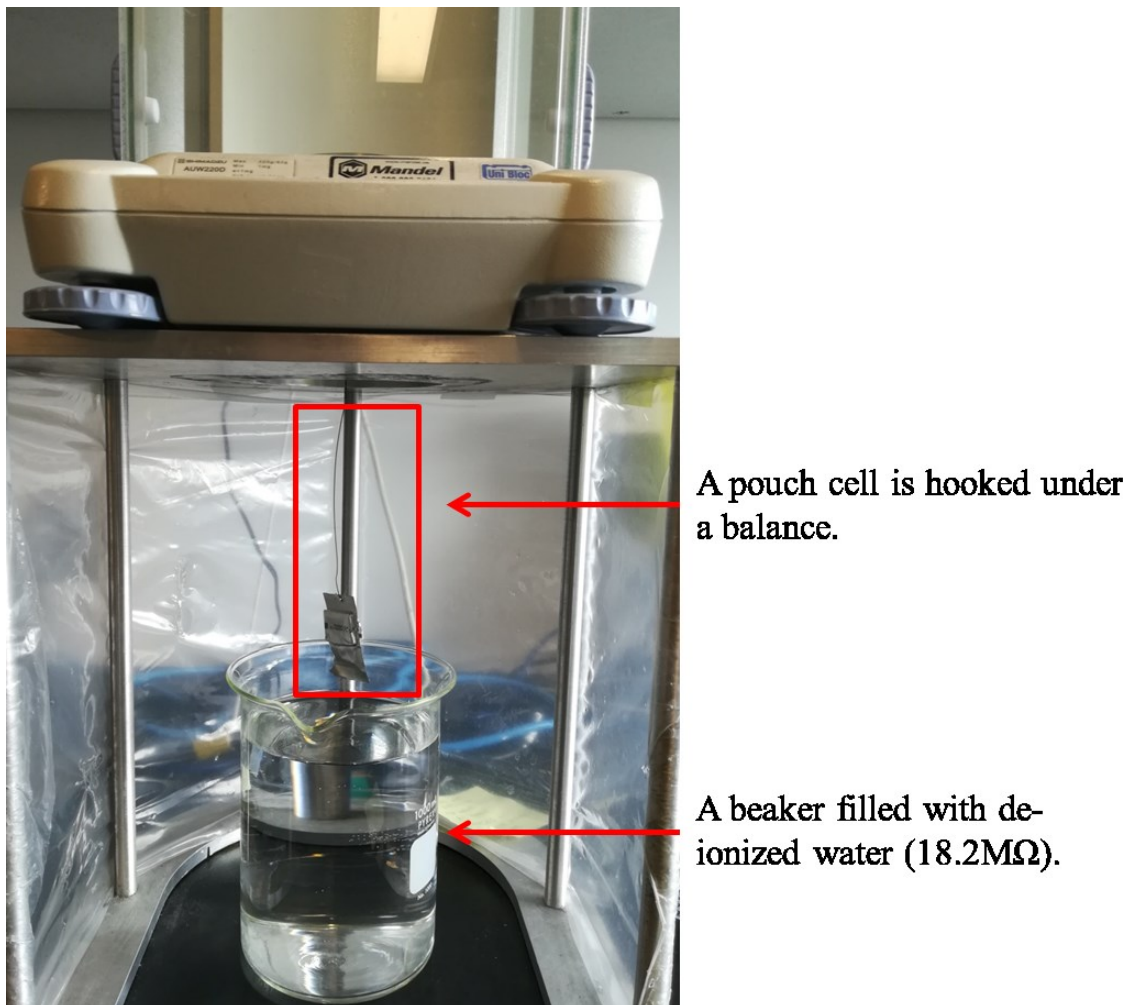


Figure 3.13 The *ex-situ* gas measurement set-up.




In this thesis, the volume of a dry pouch cell is around 2.5 mL.

### 3.7 Electrochemical impedance spectroscopy (EIS)

EIS is a quick and non-destructive technique to measure the current resulting from an alternating voltage applied to an electrochemical cell over a range of frequencies. This was used in this thesis to obtain an understanding of the impedance changes when

different electrode/electrolyte systems were used. Electrolyte compositions affect the composition and thickness of the SEI, which impacts the resistance of the SEI layer. Therefore EIS measurements are important to characterize the effectiveness of the SEI. In order to illustrate the impedance of a Li-ion cell, some simple electronic components are used to model the different contributions to the impedance. Table 3.3 summarizes the electronic components used and their impedance.

Table 3.3 Basic electronic components and their calculated impedance.

Component	Circuit Symbol	Impedance
Resistor		R
Capacitor		$1/(i\omega C)$
Inductor		$i\omega L$

The simple equivalent circuit model reported by Petibon [137] is used in this thesis to interpret the impedance of a Li-ion cell. Figure 3.14 shows a simple model for a hypothetical single active particle (a) and its equivalent circuit model (b). In Figure 3.14(b), the resistor models the charge transfer resistance for the incorporation of lithium in the active particle including lithium ions passing through SEI. The Warburg resistor (W) models the solid state lithium diffusion from the edge of the particle to the center of the particle while the capacitor in parallel models the double layer capacitance. Figure

3.14 also shows a simplified equivalent circuit for a full Li-ion cell. This model consists of the charge transfer resistance and double layer capacitance from both the positive electrode and the negative electrode. A resistor ( $R_e$ ) in series with the two parallel circuits models the impedance for lithium passing through the electrolyte.

A small amplitude alternating voltage signal, usually in the  $\pm 5 - 10$  mV range, is used so that the current response is linear with the applied voltage. The EIS spectra were collected using a BioLogic VMP3 equipped with two EIS boards. EIS measurements in this thesis were taken in temperature-controlled boxes at  $10.0 \pm 0.1^\circ\text{C}$  when the cells were at 3.8 V. A frequency range from 10 mHz to 100 kHz was applied during each measurement.

### **3.7.1 EIS of Symmetric Cells**

The application of symmetric cells [138] in this thesis was used to measure the impedance of both positive and negative electrodes independently. As a result, the impedance contributions of positive electrode and negative electrode to the full cell impedance can be distinguished. A symmetric cell is a coin Li-ion cell composed of two positive electrodes or two negative electrodes.

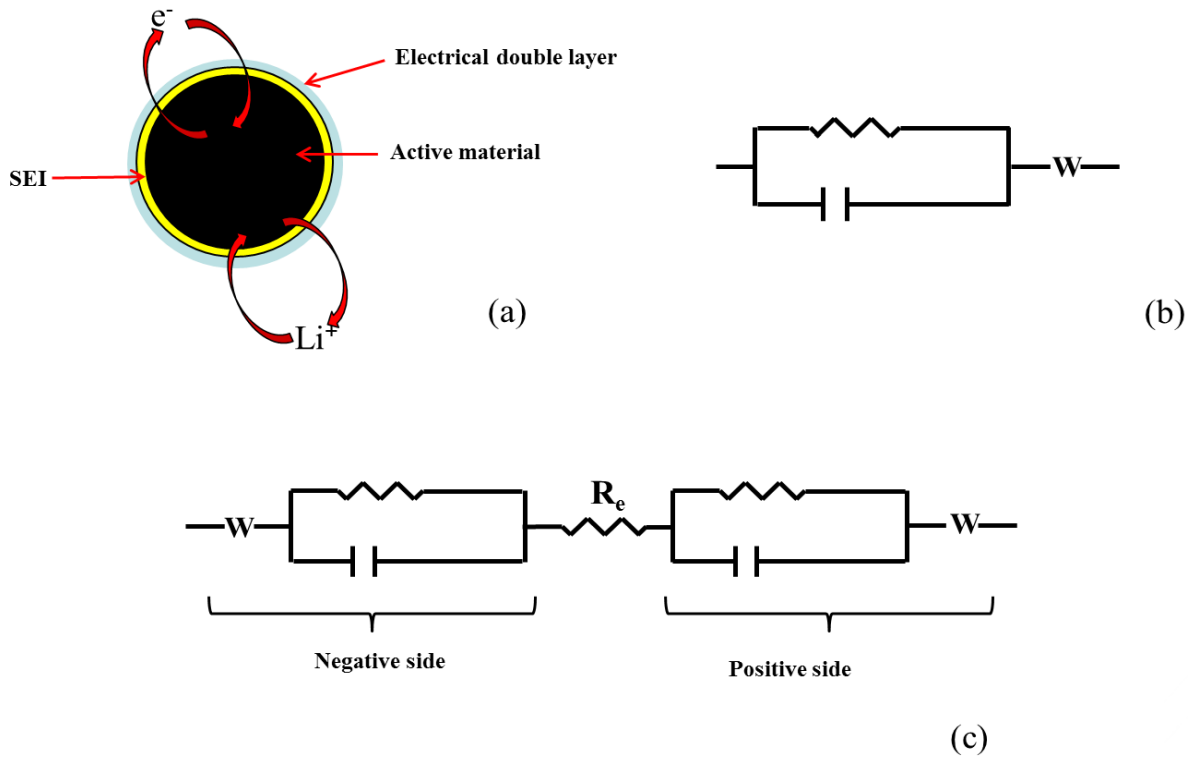


Figure 3.14 Schematic of a single active particle immersed in the electrolyte (a) and its corresponding simple equivalent circuit (b) and a simple equivalent circuit of a lithium-ion full cell.

The relationship between the impedance of a positive symmetric cell,  $Z_{+/+}$ , negative symmetric cell,  $Z_{-/-}$ , and a full cell,  $Z_{+/-}$ , is described in the following equations [137].

$$Z_{+/+} = Z_+ + Z_e + Z_+ = 2Z_+ + Z_e \quad (3.7)$$

$$Z_{-/-} = Z_- + Z_e + Z_- = 2Z_- + Z_e \quad (3.8)$$

$$Z_{+/-} = Z_+ + Z_e + Z_- \quad (3.9)$$

$$Z_{+/+} + Z_{-/-} = 2Z_+ + 2Z_- + 2Z_e = 2Z_{+/-} \quad (3.10)$$

$Z_+$  represents the impedance of a positive electrode,  $Z_-$  represents the impedance of a negative electrode and  $Z_e$  represents the resistance of the electrolyte.

### 3.8 Differential voltage analysis

Generally, cell capacity loss can result from unequal slippage of both electrodes [100], mechanical damage to the electrodes [139] or impedance growth [140] during long term cycling. Differential voltage analysis is a useful way of distinguishing the capacity loss in a cell between electrode slippage and loss of active material, respectively. This method, first proposed by Bloom et al. [141,142], showed that  $dV/dQ$  vs.  $Q$  curve of a full cell,  $Q(f)$ , can be calculated from  $dV/dQ$  vs.  $Q$  data of positive and negative half cells.

$$dV/dQ \text{ vs. } Q(f) = dV/dQ \text{ vs. } Q(p) - dV/dQ \text{ vs. } Q(n) \quad (3.11)$$

The capacity,  $Q$ , of positive electrode ( $Q_p$ ) and negative electrode ( $Q_n$ ) can be calculated using following equations.

$$Q_p = q_p m_p + \delta_p \quad (3.12)$$

$$Q_n = q_n m_n + \delta_n \quad (3.13)$$

where  $q_p$  and  $q_n$  are specific capacities of positive electrode and negative electrode,  $m_p$  and  $m_n$  are masses of positive electrode and negative electrode,  $\delta_p$  and  $\delta_n$  are slippages of positive electrode and negative electrode. The slippage is relative to zero represented by a

full Li-ion cell in the discharged state.

In order to make the best agreement between calculated  $dV/dQ$  vs.  $Q$  data and measured data for a full cell, there are four parameters can be adjusted during differential voltage analysis: positive electrode mass, negative electrode mass, positive electrode slippage and negative electrode slippage. As a result, the active electrode masses and relative slippages can be compared between an early cycle and later in cell life (e.g. long term cycling, high temperature storage) to investigate the extent of relative slippages and electrode material mass losses.

As an example, Figure 3.15 shows voltage vs. capacity for a fresh coated SC NMC532/graphite pouch cell (black line) and its corresponding  $dV/dQ$  vs.  $Q$  curve (grey line) during charging process. In order to fit the grey line,  $dV/dQ$  vs.  $Q$  for a fresh coated SC NMC532/lithium half cell (blue line) and a fresh graphite/lithium half cell (red line) were also collected. The fitting curve (green) and relevant parameters (slippage and electrode mass) are also shown in this Figure. All the data was collected using the UHPC with current corresponding to  $C/20$  at  $40^{\circ}\text{C}$ . All the fitting was performed using home-made software [143].



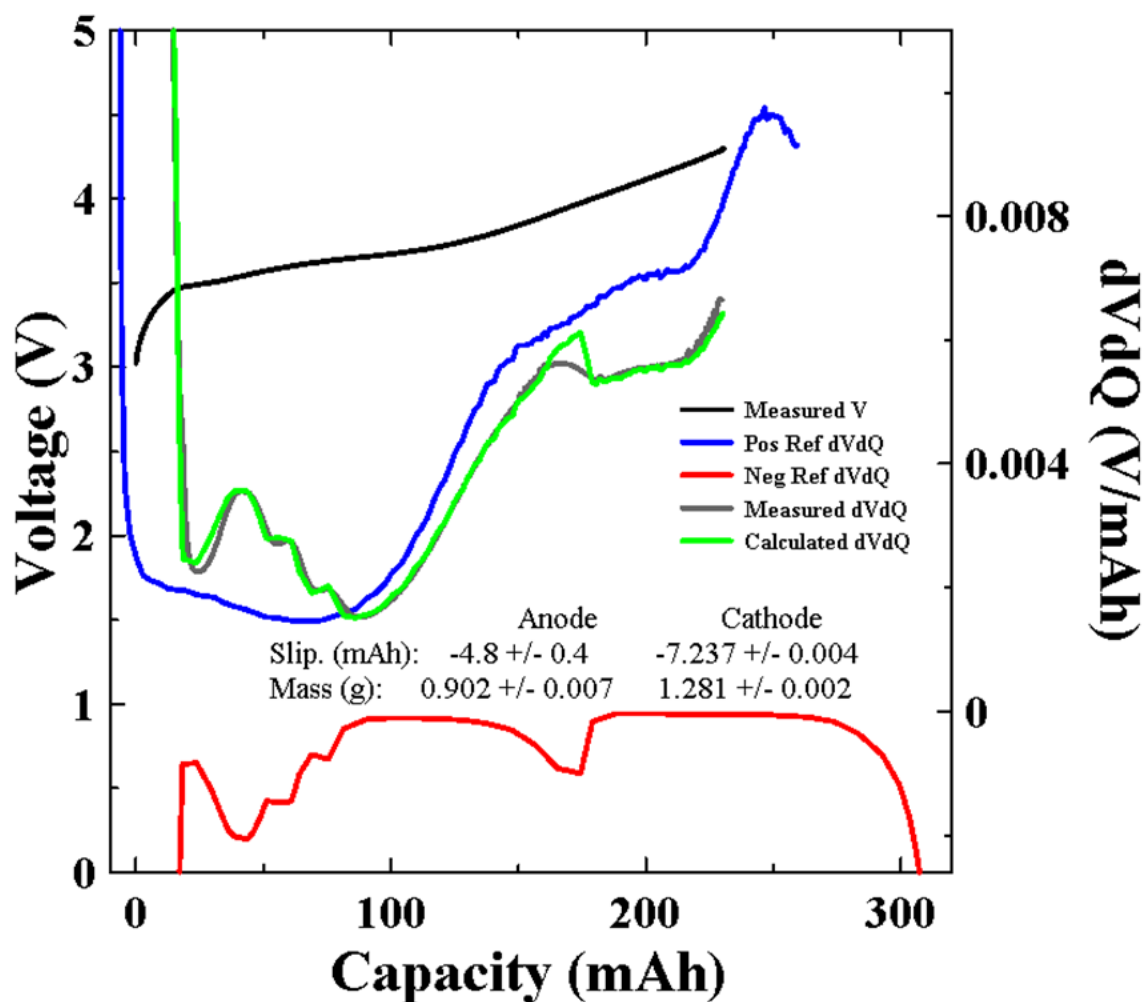


Figure 3.15 Voltage vs. capacity for a fresh coated SC NMC532/graphite cell (black line) with 2% FEC in 1.2M LiPF<sub>6</sub> in EC/EMC 3/7 and its corresponding dV/dQ vs. Q curve (grey line). dV/dQ vs. Q for a fresh coated SC NMC532/lithium half cell (blue line), a fresh graphite/lithium half cell (red line) and calculated coated SC NMC532/graphite (green line). All the data was collected using the UHPC with current corresponding to C/20 at 40°C. All the fitting results (i.e. slippage and electrode mass) are shown in the legend.

## CHAPTER 4 A GUIDE TO ETHYLENE CARBONATE-FREE ELECTROLYTE MAKING FOR LI-ION CELLS

The majority of this work was adapted from the following peer-reviewed article:

- L. Ma, S.L. Glazier, R. Petibon, J. Xia, J.M. Peters, Q. Liu, J. Allen, R.N.C. Doig, J.R. Dahn, A Guide to Ethylene Carbonate-Free Electrolyte Making for Li-ion Cells, *J. Electrochem. Soc.* 164 (2017) A5008-A5018.

Lin Ma performed pouch cell preparation, gas evolution measurements, impedance measurements and storage testing. S.L. Glazier performed UHPC cycling testing. Lin Ma performed GC-MS analysis with R. Petibon. Lin Ma performed dV/dQ cell failure analysis with J. M. Peters. Dr. J. R. Dahn provided guidance, participated in the interpretation of all the data and edited all manuscripts. Lin Ma prepared the first draft of the manuscript.

In this chapter, NMC442/graphite pouch cells demonstrate superb performance at high voltage when EC-free electrolytes, using a solvent mixture that is > 95% EMC and between 2 and 5% of an “enabler”, are used. The “enablers”, required to passivate graphite during formation, can be VC, methylene-ethylene carbonate (MEC), FEC or DiFEC among others. In order to optimize the amount of “enabler” added to EMC, GC-MS was used to track the consumption of “enabler” during the formation step. Storage testing, EIS, UHPC, long-term cycling, differential voltage analysis and isothermal microcalorimetry were used to determine the optimum amount of enabler to

add to the cells. It was found that the graphite negative electrode cannot be fully passivated when the amount of “enabler” is too low resulting in gas production and capacity fade. Using excess “enabler” can cause large impedance and gas production in most cases. The choice of “enabler” also impacts cell performance. A solvent blend of 5% FEC with 95% EMC (by weight) provides the best combination of properties in NMC442/graphite cells operated to 4.4 V. The experiments and their interpretation presented here represent a primer for the design of EC-free electrolytes. Meanwhile, the disadvantages of EC-free electrolytes are also illustrated in this chapter.

## **4.1 Experimental**

### **4.1.1 The preparation of pouch cells**

NMC111/graphite and NMC442/graphite pouch cells were prepared according to the procedure described in Section 3.1.2. 1.0 M LiPF<sub>6</sub> in EMC was used as the control electrolyte. Electrolytes with additives were formulated by adding 1, 2, 3, 4 or 5 wt% VC, MEC, FEC or DiFEC.

### **4.1.2 EIS testing**

EIS measurements were conducted on NMC111/graphite and NMC442/graphite pouch cells before and after UHPC testing, storage testing and long-term charge-discharge cycle testing. Cells were charged or discharged to 3.8 V before they were moved to a 10. ± 0.1°C temperature box. Alternating current (AC) impedance spectra were collected with ten points per decade from 100 kHz to 10 mHz with a signal amplitude of 10 mV. A Biologic VMP-3 was used to collect this data.

### **4.1.3 Charge-discharge cycling testing**

All the cells were prepared for long-term cycling at  $40. \pm 0.1^\circ\text{C}$ . The cells were charged and discharged at 80 mA (C/2.5) between 2.8 and 4.4 V with constant current - constant voltage (CCCV) mode using a Neware (Shenzhen, China) charger system. The cut-off current for CCCV mode was 10 mA (C/20). All pouch cells were cycled with external clamps to ensure a firm stack pressure of about 25 kPa (gauge pressure) even if gas was produced during cycling. The gas, if produced, was forced to the edges of the pouch due to the action of the clamps.

### **4.1.4 Storage testing**

A Maccor series 4000 cycler was used to prepare the cells for the storage tests. Cells after formation were cycled between 2.8 V and 4.4 V twice with a current of 10 mA (C/20). Then the cells were held at 4.4 V for 24 hours and then were transferred to the storage system. The open circuit voltage of the cells was monitored automatically for 1 second every 6 hours for a total storage time of 500 h at  $40.^\circ\text{C}$ .

### **4.1.5 GC-MS testing**

The extraction of the electrolyte components from the cell jelly roll followed the procedure described by Petibon et al. [144]. In this method, dichloromethane was used as the solvent to extract the electrolyte from the jelly rolls of pouch cells. Then the extracted sample was filtered and put in a mixture of dichloromethane:water (100:1 wt/wt) to remove damaging chemicals such as  $\text{PF}_5$  and HF which reside in the aqueous phase. A sample from the organic phase was then injected into the GC-MS.

#### **4.1.6 UHPC testing**

Both formed NMC111/graphite and NMC442/graphite pouch cells underwent UHPC cycling between 2.8 V and 4.2 V at C/20, 40°C for 16 cycles. Since a power failure interrupted the test, extended cycling was done to ensure the CE was stable. The UHPC allows the CE and charge-end-point capacity slippage to be measured with great accuracy and relevant interpretation can be found in reference [100].

### **4.2 Results and discussion**

#### **4.2.1 The effect of electrolyte additives in EC-free electrolytes on Li-ion cell performance**

Figure 4.1 shows the differential capacity vs. cell voltage of NMC442/graphite pouch cells filled with 1M LiPF<sub>6</sub> in EMC and with 1M LiPF<sub>6</sub> in EMC with different concentrations (from 1% to 5% by weight) of enablers: (a) VC, (b) MEC, (c) FEC and (d) DiFEC during the formation charge to 3.5 V at 40°C with a current corresponding to C/20. Data for two cells of each type, to demonstrate reproducibility, are shown.

Cells with 1M LiPF<sub>6</sub> in EMC and no enabler showed a large peak in the differential capacity plot at around 3.1 V. This results from the reduction of EMC on the surface of graphite. Adding enablers to the electrolyte suppressed this peak, indicating that the reduction of these enablers produced a good passivation layer which prevented EMC reduction. The passivation of graphite is evidenced by the presence of small differential capacity peaks at around 2.8 V, 2.3 V, 2.5 V and 2.3 V for VC, MEC, FEC and DiFEC,

respectively. In panel (d), a cell with 1% DiFEC still shows a substantial peak corresponding to EMC reduction. This shows that when the amount of enabler is too small, it may not be enough to fully passivate the graphite surface.

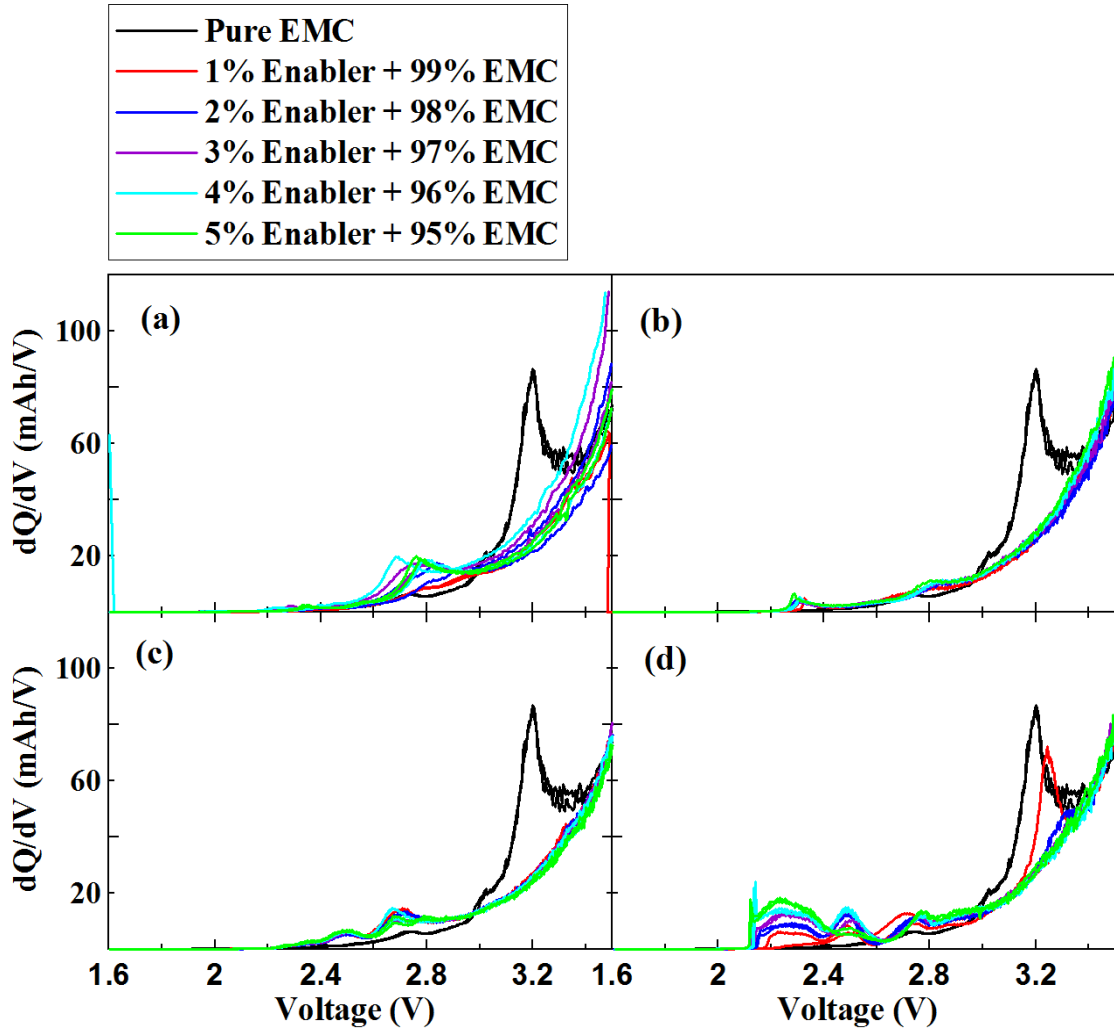


Figure 4.1  $dQ/dV$  vs. voltage for NMC442/graphite pouch cells with 1M  $\text{LiPF}_6$  EMC electrolyte or 1M  $\text{LiPF}_6$  EMC containing different amounts of “enablers”, as indicated, during formation at 40°C with a current corresponding to C/20. The enabler is (a) VC, (b) MEC, (c) FEC and (d) DiFEC. Data for two cells of each type is shown in each panel to demonstrate reproducibility.

Figures 4.2a and 4.2b show the amount of enabler left and the percent of EMC trans-esterification (see Section 2.1.1) after the first cycle (formation) as a function of the initial enabler content of cells that underwent formation at 40°C with a current of C/20 up to 4.4 V. The dashed blue line in Figure 4.2a is a line of slope 1. Comparing the data for cells with FEC in Figure 4.2a to the dashed blue line shows that only about 2% FEC was consumed during formation even if the initial FEC content was 3, 4 or 5%. By contrast, when MEC was used, the amount of MEC consumed increases with the initial MEC content, since only about 0.5% MEC was left when the initial MEC content was 5% VC and DiFEC show intermediate behavior between FEC and MEC where some additional VC and DiFEC beyond 2% are consumed as the initial loading increases. This will have an impact on the cell as will be shown later. Figure 4.2b shows the percentage of EMC that underwent trans-esterification producing DMC and DEC [57]. The presence of lithium alkoxides caused by the reduction of linear alkyl carbonates causes these trans-esterification reactions. Therefore, when trans-esterification of EMC occurs it is a signal that EMC was reduced at the graphite negative electrode during formation. The presence or absence of DMC and DEC allows one to determine how well the graphite has been passivated by the products of the reduction of the enabler. Figure 4.2b shows that EMC trans-esterification is eliminated when the initial enabler content is more than a certain amount, generally about 3%. Figure 4.2b shows that the minimum amount of enabler required to passivate the graphite surface and prevent substantial EMC reduction

should be about 3% (by weight) for the type of cell used in this study.

In order to explore the consumption of the enablers during the formation process itself, Figures 4.2c and 4.2d show the amount of enabler remaining and the percentage of EMC trans-esterification as a function of time during formation, respectively. The experiments described in Figures 4.2c and 4.2d were made with an initial enabler content of 2% (by weight).

Figures 4.2c and 4.2d suggest that FEC is the most effective enabler since the least FEC is consumed and the amount of EMC undergoing trans-esterification is the smallest when FEC is used. By contrast, at a 2% loading it appears that DiFEC is the least effective enabler (on a percent weight basis) as it is totally consumed and 20% of EMC still undergoes transesterification. Figures 4.2c and 4.2d show that most of the enabler was consumed before 3.5 V and the amount of EMC undergoing trans-esterification roughly stabilizes after 3.5 V suggesting that the enablers were reduced on the graphite surface early in the formation cycle.

Based on Figure 4.2, three enabler contents were chosen for study using EIS, storage and long-term cycling to compare the impact of different enabler content. The loadings chosen were as follows: 1% (insufficient amount), 3% (in the optimal range based on Figure 4.2) and 5% (possibly too much in the cases of VC, MEC and DiFEC based on Figure 4.2a).



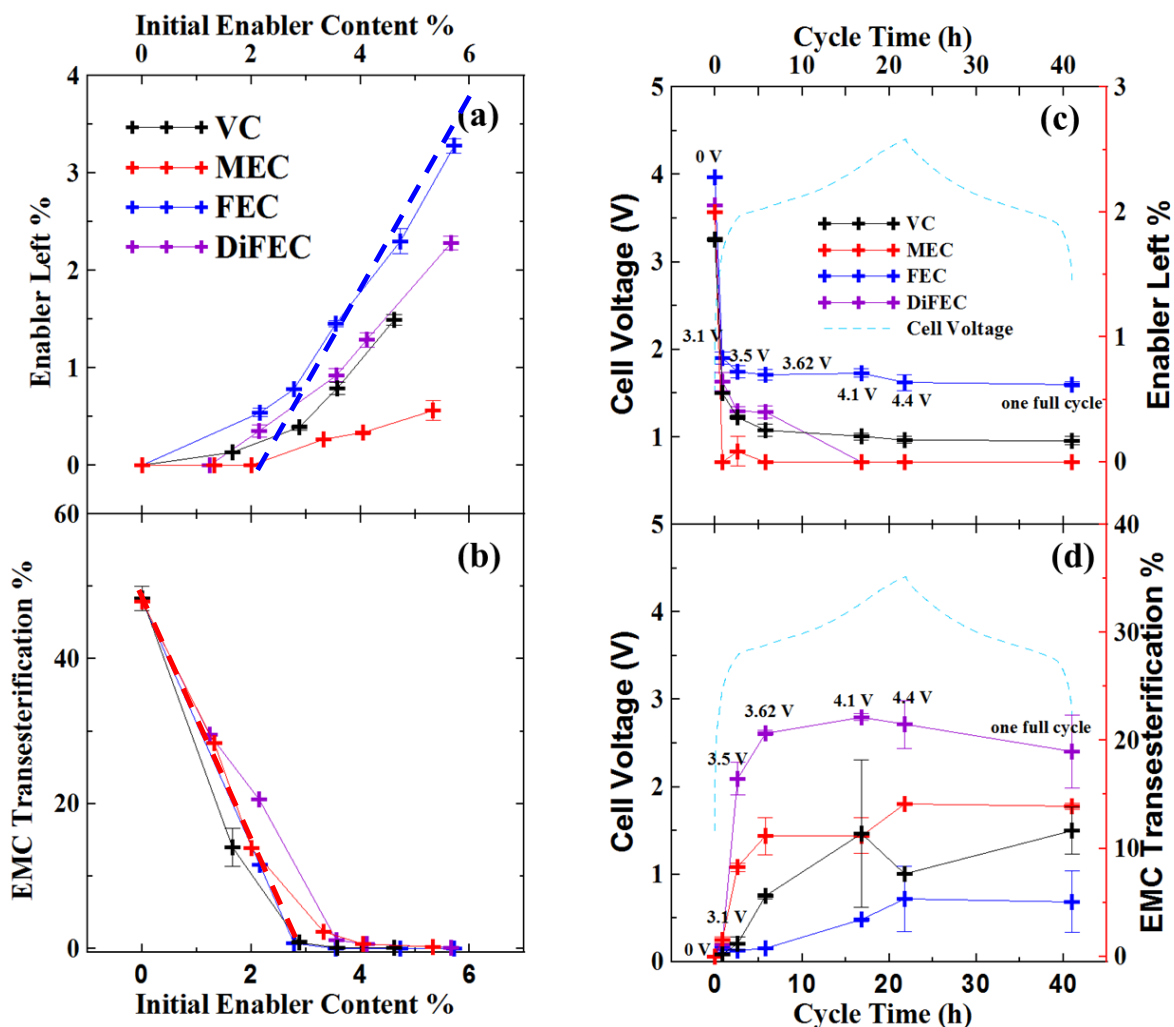


Figure 4.2 Amount of enabler left (a) and % EMC trans-esterification (b) vs. initial enabler content in NMC442/graphite pouch cells that underwent their first full (formation) cycle between 2.8 – 4.4 V at 40°C, C/20. The blue dashed line in Figure 4.2a is a line of slope = 1 and the same line is shown in Figures 4.11a and 4.11c. The red dashed line in Figure 4.2b is a guide to the eye and the same line is shown in Figures 4.11b and 4.11d. (c) shows the amount of enabler left and % EMC trans-esterification (d) vs. time during the first cycle at 40°C in NMC442/graphite pouch cells initially filled with 1M LiPF<sub>6</sub> EMC electrolyte containing ~ 2% enabler.

Figure 4.3 shows Nyquist plots measured after formation for NMC442/graphite pouch cells containing 1M LiPF<sub>6</sub> in EMC and 1M LiPF<sub>6</sub> in EMC with different enabler contents:

(a) VC, (b) MEC, (c) FEC and (d) DiFEC. The impedance spectra were measured at 3.8 V and at 10.0°C. The diameter of the semi-circle arises from the sum of the charge-transfer resistances and the transport of lithium ions through the SEI layers at both the positive and negative electrodes. In this thesis, the diameter of the semicircle is called  $R_{ct}$ . [Note: The interpretation of the impedance spectra in this work follows that of Atebamba et al. [145] and  $R_{ct}$  is regarded as the main contribution to the diameter of the semi-circle]. In the case of VC, MEC and DiFEC, the diameter of the semicircle increases dramatically when 5% enabler is used, while with FEC it does not. According to Figure 4.2a, the amount of enabler consumed increases for VC, MEC and DiFEC when the initial enabler content increased beyond 3% which would thicken the negative electrode SEI layer causing impedance increase as observed in Figure 4.3. In the case of FEC, Figure 4.2a shows that only 2% FEC was consumed even if 3, 4 or 5% FEC was initially loaded in the cell. This is consistent with the results in Figure 4.3 which show the impedance of cells with FEC does not increase with FEC loading for the cells with 3% and 5% FEC.

#### **4.2.2 Storage and cycling tests**

Figure 4.4 shows a summary of the voltage drop of NMC442/graphite pouch cells containing 1M LiPF<sub>6</sub> in EMC and 1M LiPF<sub>6</sub> in EMC with different enabler contents: VC, MEC, FEC and DiFEC during the storage test at 40°C. Two cells were measured for each data point and the error bars in Figure 4.4 are the difference between the two results.

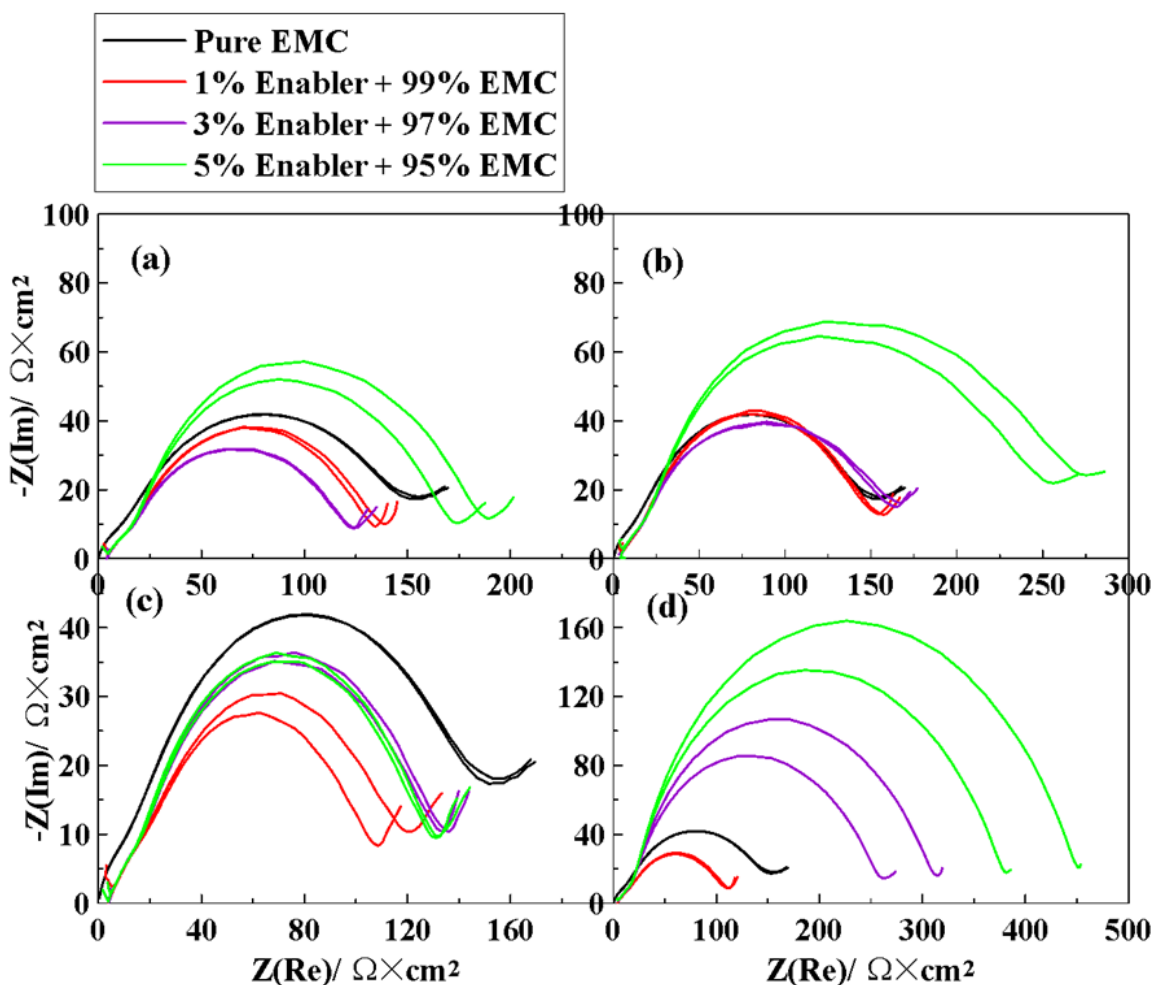


Figure 4.3 Nyquist plots for NMC442/graphite pouch cells with 1M LiPF<sub>6</sub> EMC electrolyte or 1M LiPF<sub>6</sub> EMC with different enabler contents after formation. (a) VC, (b) MEC, (c) FEC and (d) DiFEC. All the data was measured at 3.8 V and 10°C. Data for two cells of each type are presented in each panel to demonstrate reproducibility.

The voltage drop during the storage test indicates the occurrence of parasitic reactions at the surface of the positive electrode. The lithium alkoxides created by EMC reduction are probably responsible for the rapid self-discharge as they can be involved in shuttle type reactions [100]. Compared to the cells with 1M LiPF<sub>6</sub> in EMC and the cells with 1%

enabler, the cells with 3% or 5% enabler show a significantly smaller voltage drop. Based on Figure 4.2b, there were little to no Li alkoxides present in the electrolyte when the enabler content was 3% or greater so the self-discharge during storage should be less severe, as observed. For each enabler, there is little or no difference between cells with 3% or 5% enabler based on the storage data. In addition, the choice of enabler does not affect the voltage drop during storage when the enabler content is 3% or 5%.

Figures 4.5a-d show the capacity versus cycle number for NMC442/graphite pouch cells containing 1M LiPF<sub>6</sub> in EMC and 1M LiPF<sub>6</sub> in EMC with different enabler contents: (a) VC, (b) MEC, (c) FEC and (d) DiFEC during CCCV cycling up to 4.4 V at 40°C with a current that corresponded to C/2.5. The constant voltage cut-off current corresponded to C/20. Figures 4.5e-h show the difference between the average charge and the average discharge potential ( $\Delta V$ ) vs. cycle number corresponding to the cells shown in Figures 4.5a-d, respectively. The value of  $\Delta V$  is a measure of the polarization in the cells [146]. Compared to cells with 1M LiPF<sub>6</sub> in EMC and cells with 1% enabler, cells with 3% or 5% enabler show better capacity retention and smaller polarization growth during long-term cycling. Figures 4.5g and 4.5h show that FEC and DiFEC control polarization growth during cycling better than VC and MEC. Even with a 1% loading of FEC or DiFEC, the polarization of the cells after 200 cycles is comparable to that of cells with a 5% loading of VC or MEC.

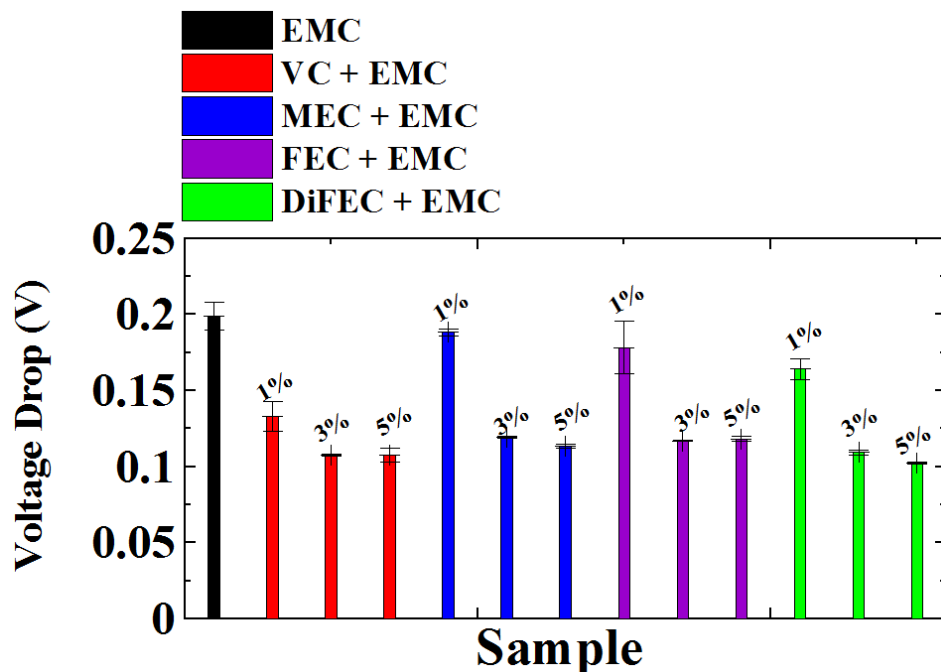


Figure 4.4 Summary of voltage drop during 500 hour storage at 4.4 V and 40°C for NMC442/graphite pouch cells with 1M LiPF<sub>6</sub> EMC electrolyte or 1M LiPF<sub>6</sub> EMC with different enabler content as indicated.

#### 4.2.3 Cell failure mechanism analysis

Differential voltage analysis was performed on NMC442/graphite pouch cells after long term cycling to determine the reason for the capacity loss and to compare differences between various enablers with different concentrations. Loss of Li inventory due to SEI growth and repair as well as loss of active material are the possible causes of low rate capacity loss. Impedance growth can reduce cell capacity at high rate. Dahn et al. [143], among others [141,147] showed that differential voltage analysis allows the active masses of both electrodes and the relative capacity slippages of each electrode to be determined. In this work, these parameters were obtained using reference differential voltage curves measured in NMC442/Li and graphite/Li half cells to fit  $dV/dQ$  vs.  $Q$  of

the full cells.

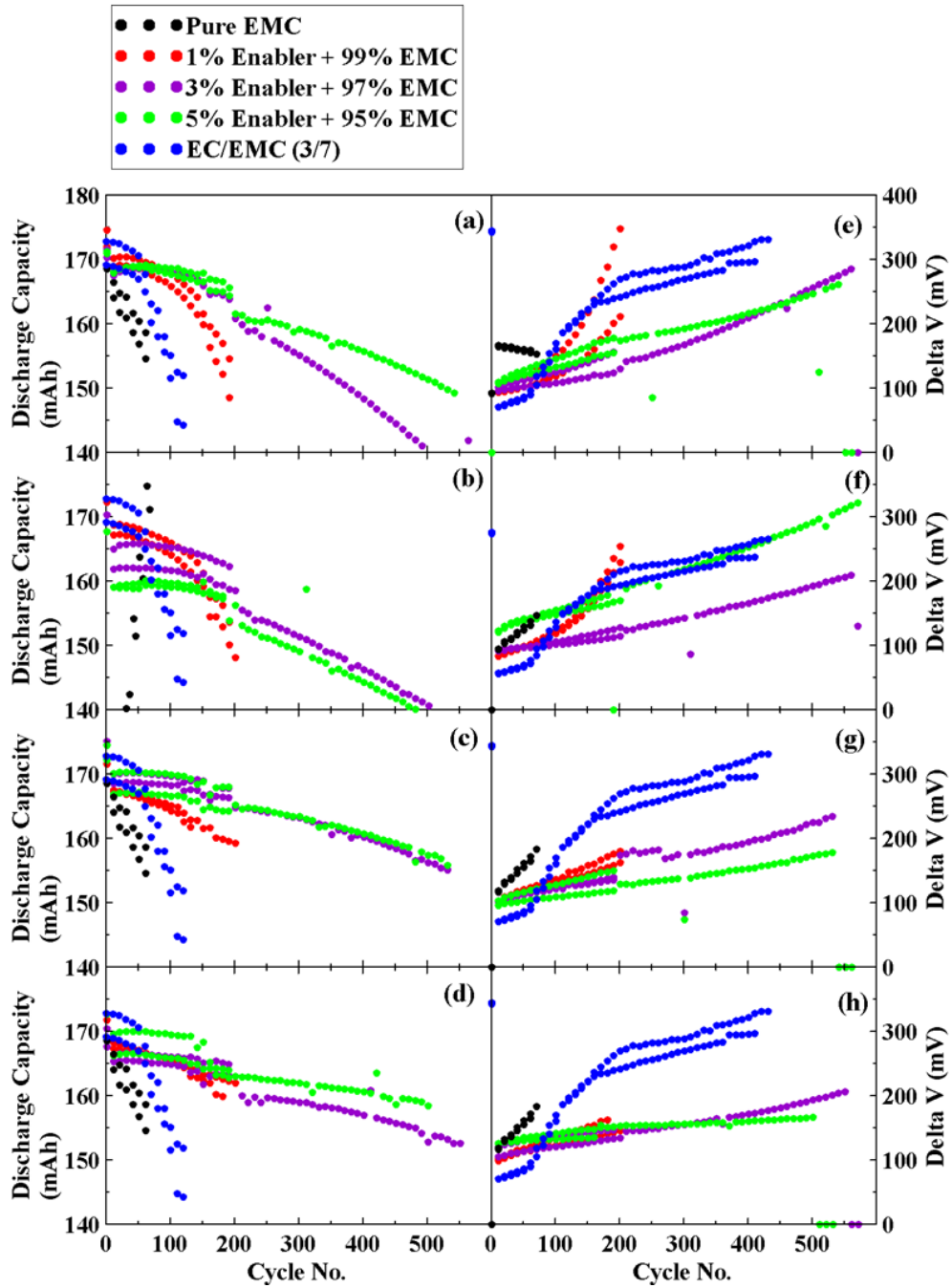


Figure 4.5 Discharge capacity (a) to (d) and cell polarization (e) to (h) vs. cycle number for NMC442/graphite pouch cells with 1M LiPF<sub>6</sub> EMC electrolyte or 1M LiPF<sub>6</sub> EMC with different enabler content during long term CCCV cycling at 40°C between 2.8 V and 4.4 V using currents corresponding to C/2.5. A constant voltage step at the top of charge was applied until the current dropped below C/20. (a), (e) VC; (b), (f) MEC; (c), (g) FEC and (d), (h) DiFEC. Data for two cells of each type are included in each panel to demonstrate reproducibility.

Figure 4.6(a) shows the measured Li-ion cell (after 200 cycles of CCCV cycling shown in Figure 4.5) voltage vs. capacity curve at C/20, 40°C. Figures 4.6(c) and 4.6(e) show the potential vs. capacity curves for the fitted positive and negative electrodes, respectively. Figures 4.6(b), 4.6(d) and 4.6(f) are enlargements of Figures 4.6(a), 4.6(c) and 4.6(e), respectively, near the zero of the capacity axis. Cells with 1M LiPF<sub>6</sub> in EMC containing 3% FEC or 3% DiFEC are selected as examples to discuss here. The electrode masses and slippages used in Figure 4.6 and Figures 4.7c and 4.7d are those that gave the best fits between the measured and calculated dV/dQ vs Q curves. The point Q = 0 indicated by the dashed line in Figure 4.6 is taken as the point where the full Li-ion cell reaches the fully discharged state. The positive or negative electrode slippage can be negative or positive compared to Q = 0 as shown in Figures 4.6(d) and 4.6(f). The relative slippage is very small indicating that very little capacity loss had occurred by loss of Li inventory at the negative electrode.

This is consistent with the data in Figures 4.5a and 4.5b where the low rate C/20 cycle at the beginning of the testing (cycles 1 and 2) has virtually the same capacity as the C/20 cycles after 200 cycles (plotted as the star-shaped data points at cycle 240, for clarity).

Therefore, Figures 4.6 and 4.7 show that the reason for capacity loss in these cells with 3% FEC or 3% DiFEC is impedance growth. Although not shown, the same conclusions can be made about all cells with 3% and 5% enabler. The low rate C/20 capacity after 200

cycles is virtually the same as the low rate C/20 capacity during cycles 1 and 2. Thus, the capacity fade of 3% or 5% enabler-containing cells shown in Figures 4.5a-d is predominantly due to impedance growth.

The situation is more complex for the capacity fade of cells with 1M LiPF<sub>6</sub> in EMC and cells with 1% enabler in 1M LiPF<sub>6</sub> in EMC shown in Figures 4.5a-d. In those cases the low rate (C/20) cycles collected after 200 cycles did not match the capacity of cycles 1 and 2 at C/20 (see Figure 4.8).

Even when the same cells were tested at C/40 and C/80 after 200 cycles, their capacities were still about 5 to 10% less than their initial low rate capacity (see Figure 4.8). This suggests loss of Li inventory as well as impedance growth for the cells with no enabler or 1% enabler. This is consistent with a poorly passivated negative electrode as shown in Figures 4.2a and 4.2b for cells with no enabler or 1% enabler.

Figure 4.9 shows a summary of the impedance ( $R_{ct}$ , diameter of the EIS semicircle) of NMC442/graphite pouch cells containing 1M LiPF<sub>6</sub> in EMC or 1M LiPF<sub>6</sub> in EMC with different enabler (VC, MEC, FEC or DiFEC) contents. Data are shown for  $R_{ct}$  collected after formation (Figure 4.3), after storage (Figure 4.4) and after long-term CCCV cycling (Figure 4.5). Cells using FEC as the enabler showed the lowest  $R_{ct}$  compared to all other cells, and  $R_{ct}$  remained small even when the FEC content in the electrolyte was initially 5%. By contrast, when VC, MEC or DiFEC were used,  $R_{ct}$  increased with enabler content.



Cells with 3% FEC or 5% FEC showed similar values of  $R_{ct}$  after formation, after storage and after CCCV cycling. Again, FEC appears to be the best choice among these four enablers.

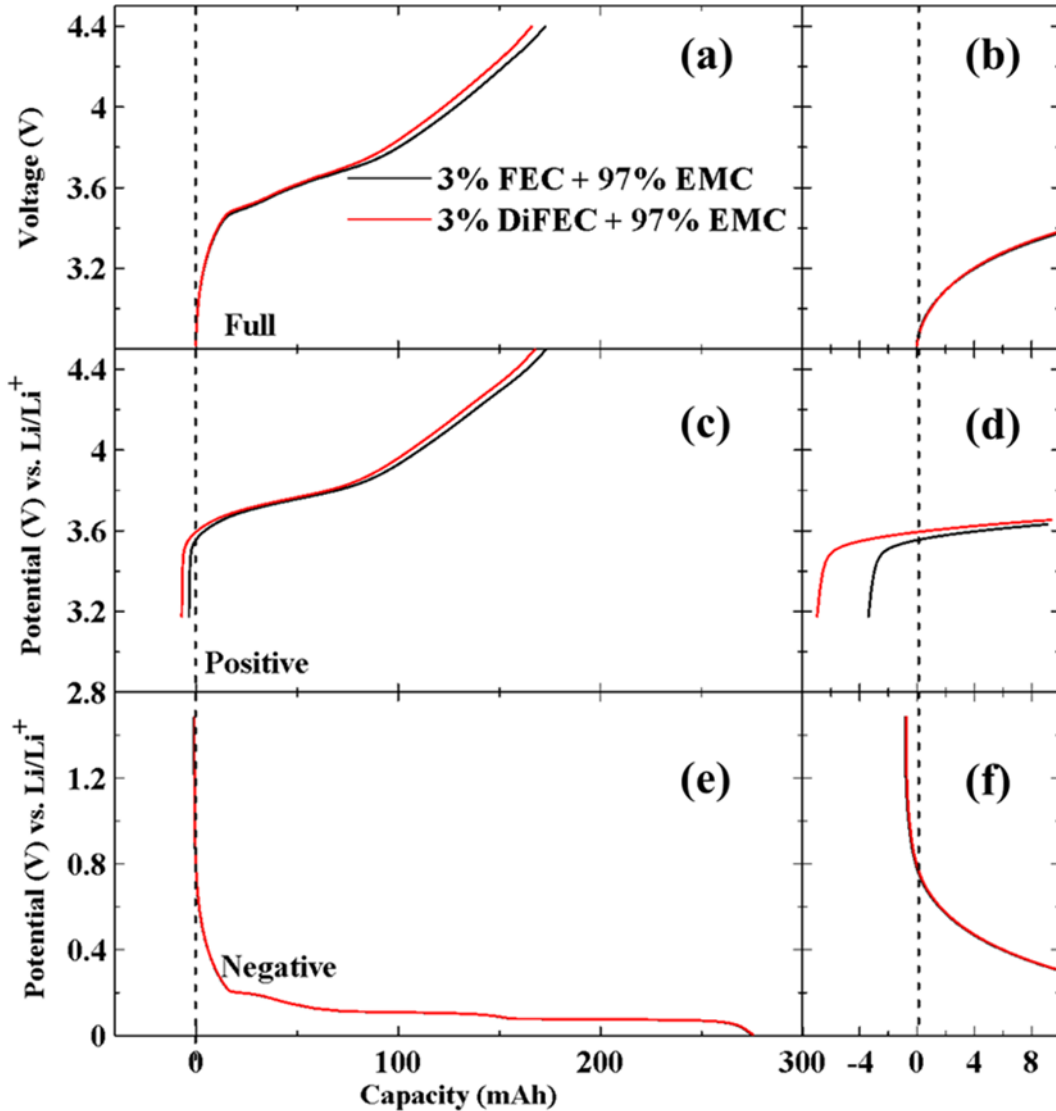


Figure 4.6 (a) Measured NMC442/graphite cell (after long term cycling shown in Figure 4.7)  $V(Q)$  curves cycled at  $C/20$  at  $40^{\circ}\text{C}$ . Extracted  $V_p(Q)$  (b) and  $V_n(Q)$  (c) curves, respectively, from the  $dV/dQ$  analysis software. These  $V_p(Q)$  and  $V_n(Q)$  curves are the potentials of the positive electrode (NMC442) and negative electrode (graphite) vs.  $\text{Li}/\text{Li}^+$  and these curves are aligned along the capacity axis just as they are in the full cell. The right inset panels (b), (d) and (f) show an expanded view of the region near  $Q = 0$  for panels (a), (c) and (e), respectively.

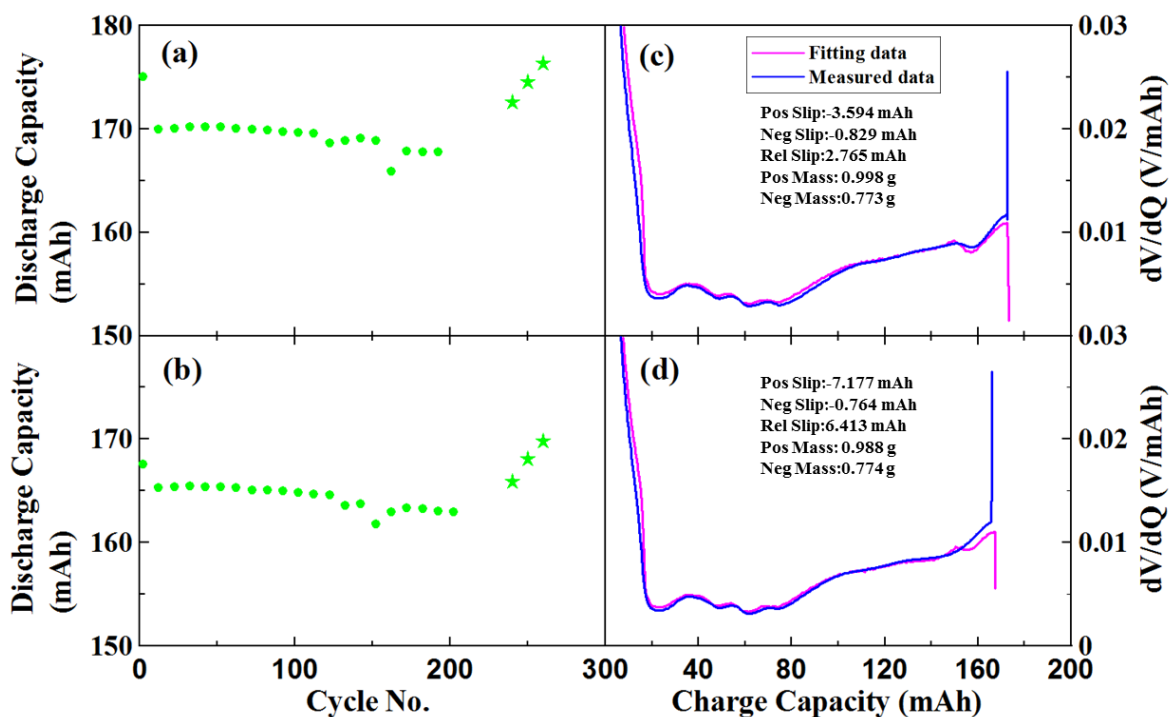


Figure 4.7 Discharge capacity vs. cycle number (a and b, for NMC442/graphite pouch cells with 1M LiPF<sub>6</sub> EMC containing 3% FEC or 3% DiFEC, respectively, during CCCV long term cycling at 40°C between 2.8 V and 4.4 V with currents corresponding to C/2.5. A constant voltage step at the top of charge was applied until the current dropped below C/20. The star-shaped points in each panel are the low rate cycling data collected after the long term cycling. The first one was measured at C/20, the second one was measured at C/40 and the third one was measured at C/80. Panels (c) and (d) show the differential voltage vs. capacity curve and the fitted curve for the cells in panels (a) and (b) after 200 cycles. A C/20 charge curve collected after 200 cycles was used for the fitting.

Figure 4.10 shows a summary of the gas production in NMC442/graphite pouch cells containing 1M LiPF<sub>6</sub> in EMC and 1M LiPF<sub>6</sub> in EMC with different enabler contents (VC, MEC, FEC or DiFEC) after long-term CCCV cycling to 4.4 V at 40°C (a), after storage (4.4 V, 500 h, 40°C) (b) and after formation (c).

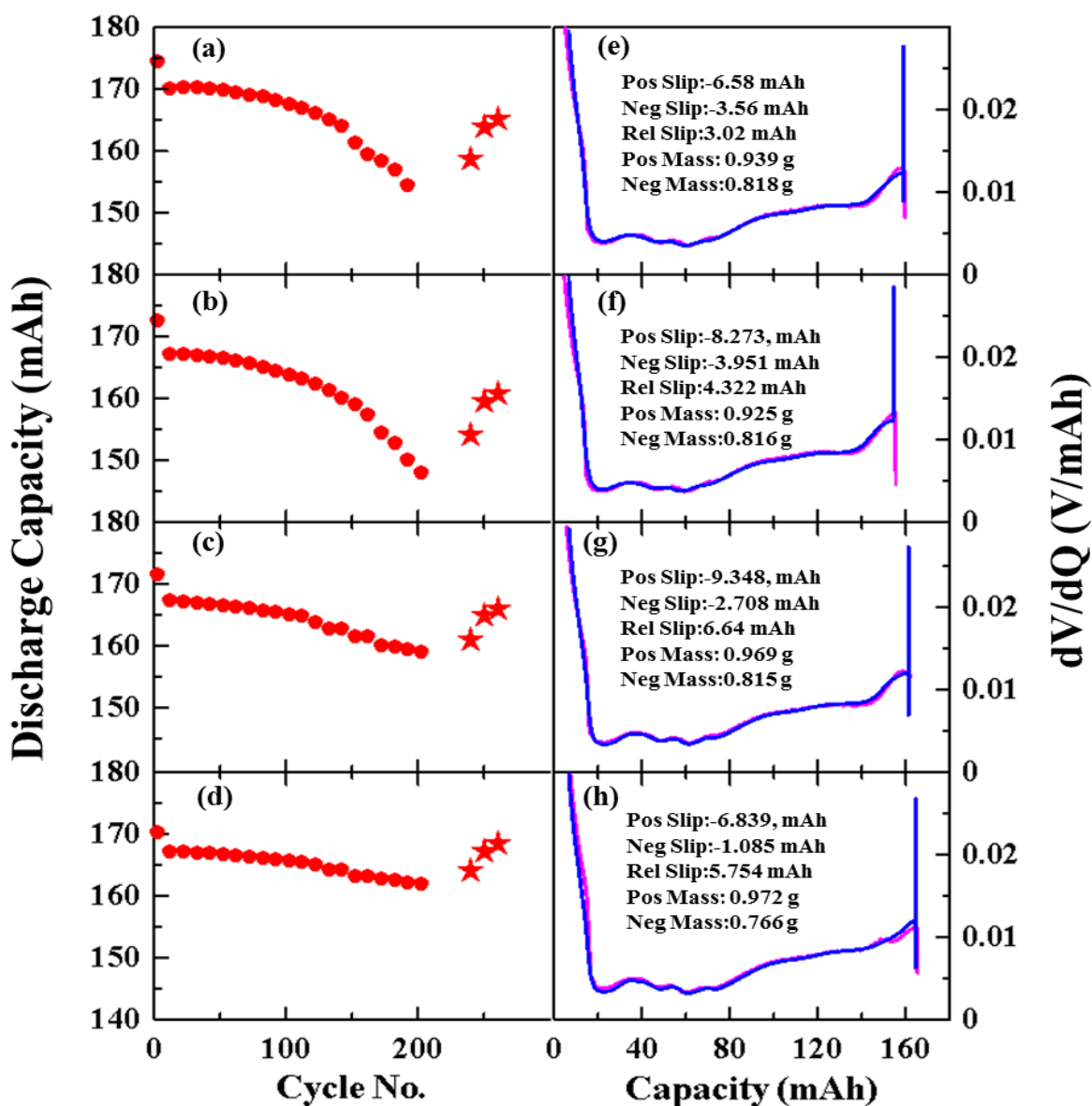


Figure 4.8 Discharge capacity vs. cycle number (a, b, c and d for NMC442/graphite pouch cells with 1M LiPF<sub>6</sub> EMC containing 1% VC, 1% MEC, 1% FEC and 1% DiFEC, respectively), during CCCV long term cycling at 40°C between 2.8 V and 4.4 V with currents corresponding to C/2.5. A constant voltage step at the top of charge was applied until the current dropped below C/20. The star-shaped points in each panel are the low rate cycling data collected after the long term cycling. The first one was measured at C/20, the second one was measured at C/40 and the third one was measured at C/80. Panels e-h show the differential voltage vs. capacity curve and the fitted curve for the cells in panels a-d after 200 cycles. A C/20 charge curve collected after 200 cycles was used for the fitting.

Figure 4.10 is very interesting. During formation, cells with only 1% enabler produced more gas than those with 3% or 5% enabler, most likely due to poorly passivated graphite. During storage and CCCV cycling, cells with 5% VC, 5% MEC or 5% DiFEC produced more gas than those with 3% of the same enablers, presumably due to oxidation of excess enabler. During storage and CCCV cycling, cells with 1% MEC, 1% FEC and 1% DiFEC produced more gas than those with 3% of the same enablers presumably due to poor passivation of the graphite and resulting EMC reduction. Cells that had 3% MEC, 3% FEC, 5% FEC and 3% DiFEC showed very little gas generation in these tests presumably because the graphite was well passivated and, in the cases of MEC and DiFEC, little excess enabler remained to be oxidized at the positive electrode. In the case of FEC, excess FEC above 3% did not lead to gassing at 40°C presumably due to the oxidative stability of FEC.

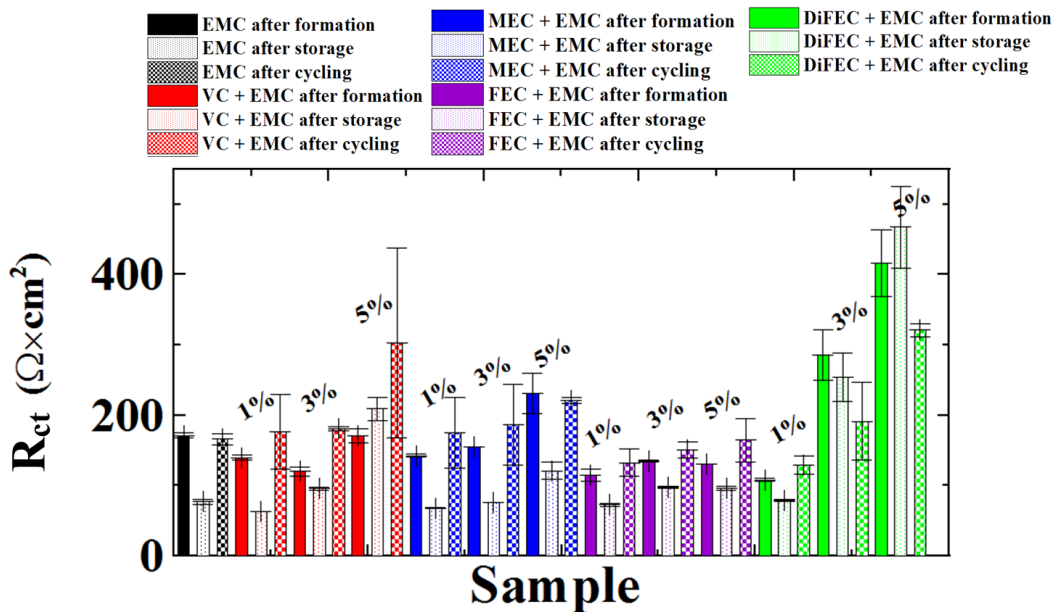


Figure 4.9 A summary of the impedance results for NMC442/graphite pouch cells with 1M LiPF<sub>6</sub> in EMC electrolyte or 1M LiPF<sub>6</sub> EMC with different enabler content as indicated after formation (40°C, C/20), after 500 h storage (4.4 V, 40°C) and after ~ 200 CCCV cycles (2.8 – 4.4 V, 40°C, C/2.5). All the EIS data was measured at 3.8 V and 10°C. The data shown is the average of two cells and the error bars represent the range of the measurements.

Figures 4.11a and 4.11c show the amount of enabler left in the electrolyte after storage (4.11a) and long term CCCV cycling (4.11c) as a function of the initial enabler content.

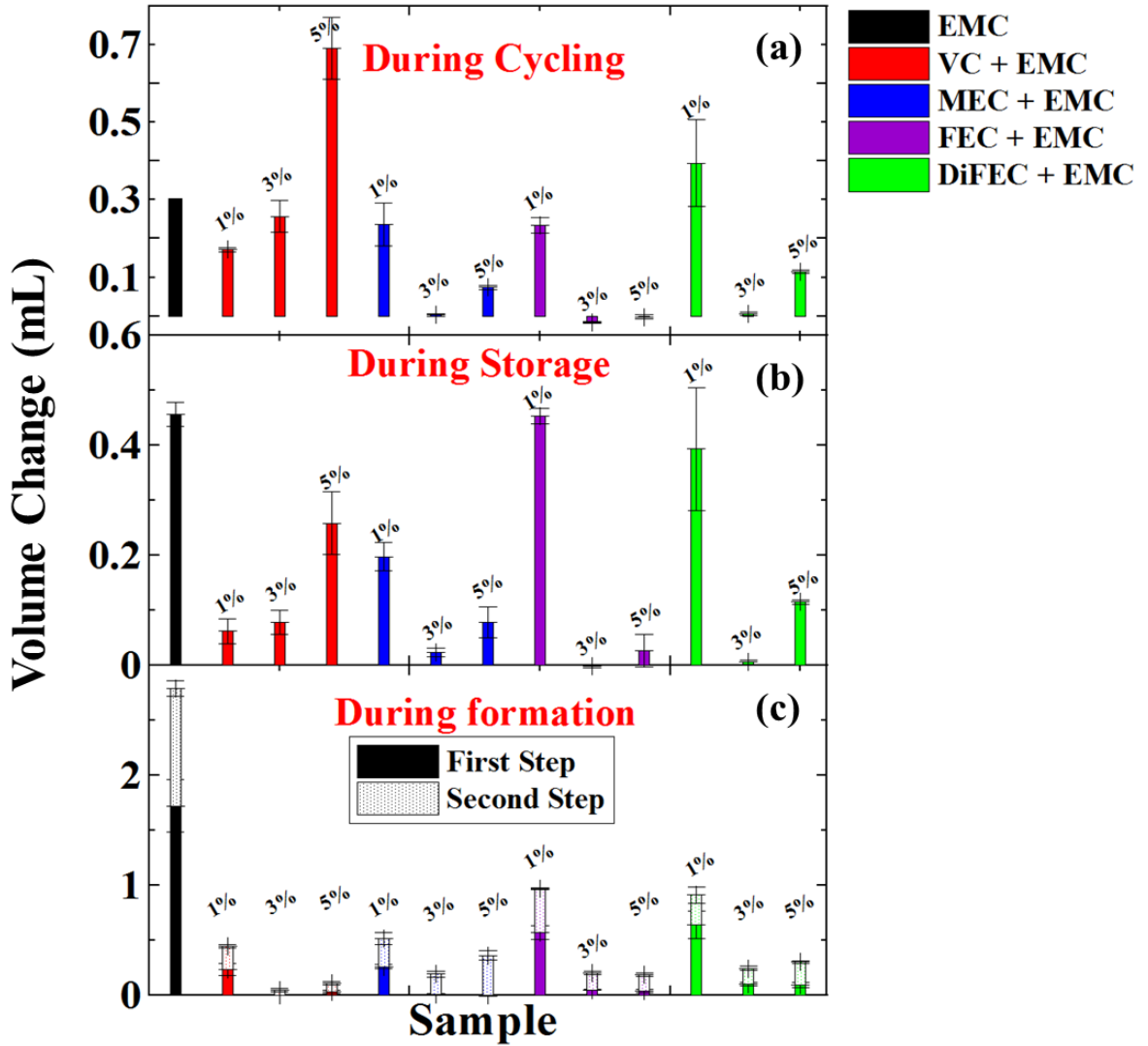


Figure 4.10 A summary of the gas volumes in NMC442/graphite pouch cells with 1M LiPF<sub>6</sub> EMC electrolyte or 1M LiPF<sub>6</sub> EMC with different enabler content as indicated: (a) after ~ 200 CCCV cycles (2.8 – 4.4 V, 40°C, C/2.5), (b) after 500 h storage (4.4 V, 40°C) and (c) after formation (40°C, C/20). All the data was measured at 1 atm. and 20°C. The data shown is the average of two cells and the error bars represent the range of the measurements.

These data should be compared to the data in Figure 4.2a which showed the amount of enabler left after formation. The blue dashed lines in Figures 4.2a, 4.11a and 4.11c are the same and can be used to see that the concentration of FEC in the electrolytes containing 3% or 5% FEC was virtually unchanged after storage or cycling compared to the concentration after formation. By contrast, the concentration of all the other enablers decreased during storage and during long term cycling. Figures 4.11b and 4.11d show the amount of EMC trans-esterification that occurred after storage (4.11b) and after long term cycling (4.11d) as a function of the initial enabler content. The red dashed lines in Figures 4.2b, 4.11b and 4.11d are the same and can be used to see that the amount of transesterification increased dramatically during storage and cycling for all cells that initially had 1% of enabler added. This, again, shows that 1% enabler is insufficient to passivate the graphite electrode. However, with an initial loading of 3% or 5% enabler, the percentage of EMC trans-esterification did not increase during storage (500 hours) or long-term cycling (~ 200 cycles). This suggests the formation of a robust SEI on the negative electrode when the enough enabler was added initially.

#### **4.2.4 Prediction of cell lifetime at a lower upper cut-off voltage**

In a further attempt to determine the optimum amount of VC or FEC to use in EC-free electrolytes based on 1M LiPF<sub>6</sub> in EMC, some NMC111/graphite and NMC442/graphite pouch cells were subjected to UHPC cycling (16 cycles) between 2.8 and 4.2 V with a current corresponding to C/20 at 40°C.

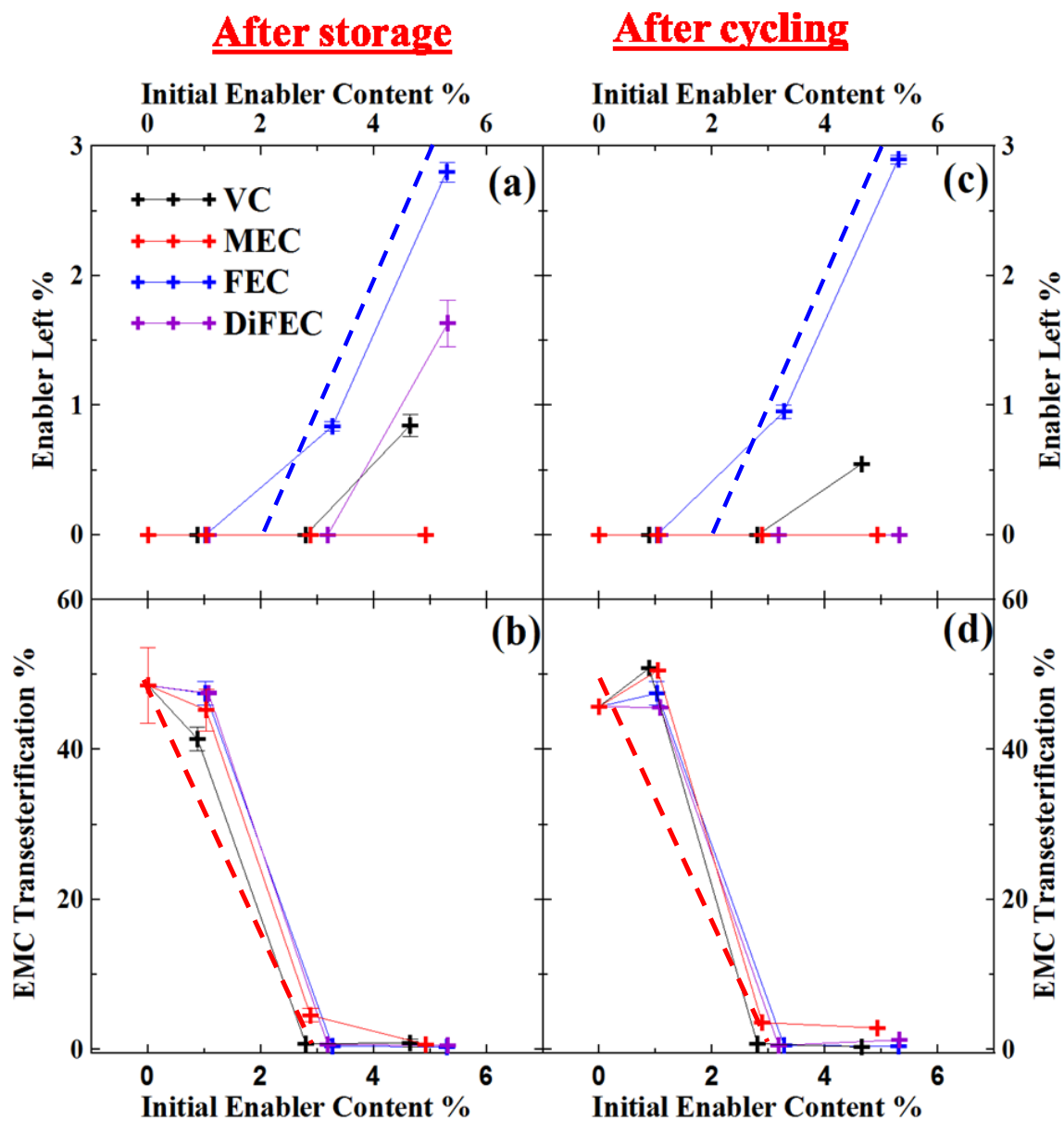


Figure 4.11 Amount of enabler left (a) and % EMC trans-esterification (b) vs. initial enabler content in NMC442/graphite pouch cells that underwent 500 h storage at 40°C, 4.4 V; amount of enabler left (c) and % EMC trans-esterification (d) vs. initial enabler content in NMC442/graphite pouch cells that underwent ~ 200 CCCV cycles (2.8 – 4.4 V, 40°C, C/2.5). A constant voltage step at the top of charge was applied until the current dropped below C/20. The data shown is the average of two cells and the error bars represent the range of the measurements. The blue dashed and red dashed lines are the same lines shown in Figure 4.2 and are reproduced here so data from Figure 4.2 and 4.11 can be compared.

Figure 4.12 shows the significant parameters from the UHPC test: (a) CE, (b) charge end-point capacity slippage, (c) discharge capacity and (d)  $\Delta V$  (the difference between the average charge voltage and the average discharge voltage) vs. cycle number. Test results for one cell are used as an example in each panel to show the method of determining the UHPC results in this thesis. In panel (a), the CE values from the last five cycles (12-16 cycles) were fitted with a line to predict the CE value at cycle 16. The CIE was calculated by taking  $CIE = 1 - CE$ , where CE is the value of the CE from the fitted line at cycle 16. The CIE is then divided by the time of one cycle to get CIE/hour as shown in Figure 4.13a.

In Figures 4.12b, 4.12c and 4.12d, the values from the last five cycles (12-16 cycles) were fitted with a line. The slopes of the charge end-point capacity versus cycle number and the discharge capacity versus cycle number curves were then divided by the time of one cycle and the discharge capacity of the first cycle. These give the fractional charge endpoint capacity slippage per hour and the fractional capacity fade per hour, respectively. The relevant results are summarized in Figures 4.13b and 4.13c, respectively. The slope of the  $\Delta V$  versus cycle number graph was divided by the time of one cycle to get the polarization growth rate as shown in Figure 4.13d.

In Figure 4.13, each data point is the average for two nominally identical cells. The error bar plotted at each value consists of two parts: (1) the variation from cell to cell and (2)



the error associated with the measured value based on quality of the fitted line to the last five points. These two contributions to the error have been combined according to standard practices in error propagation [148].

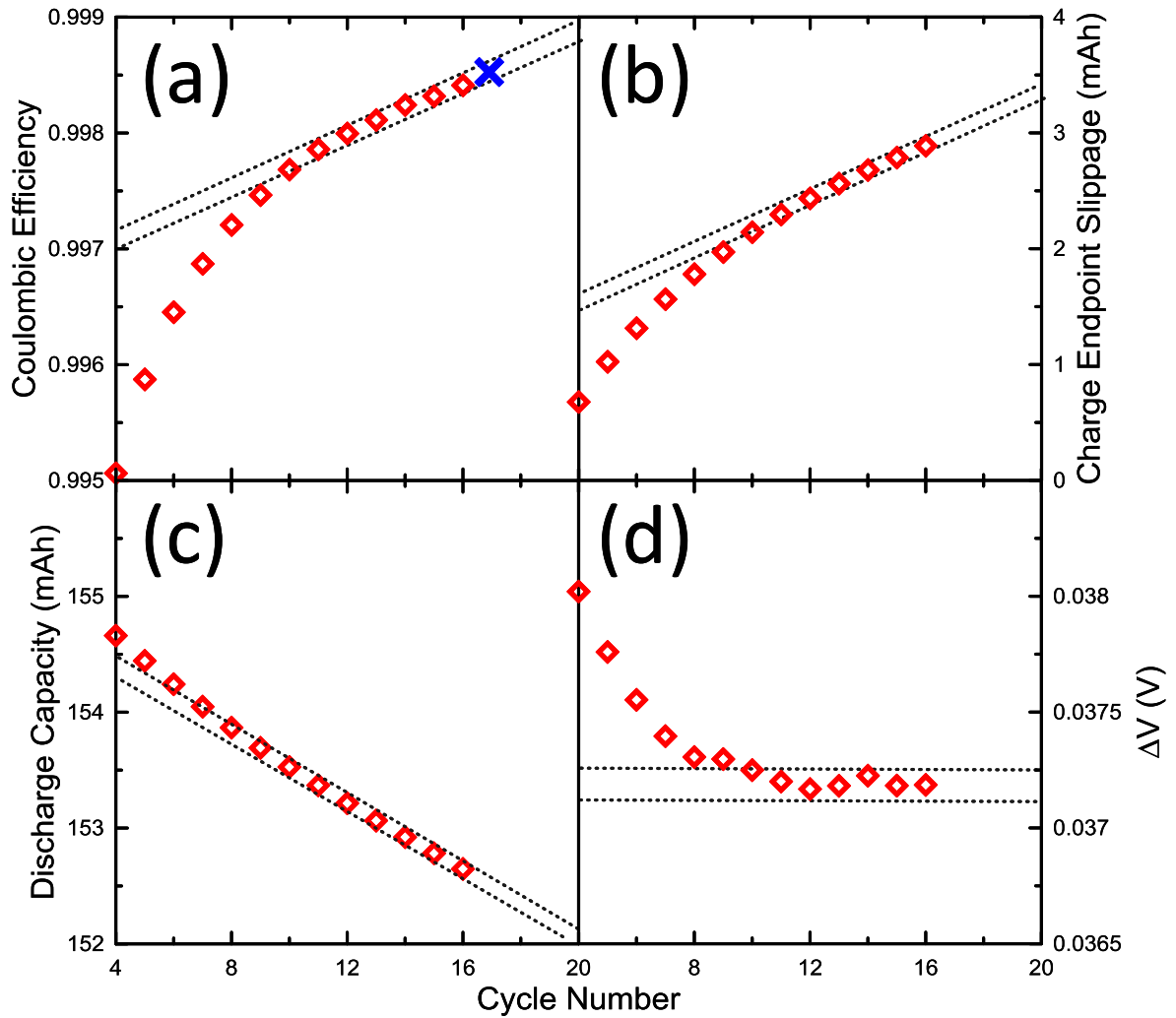


Figure 4.12 The typical measurables of a UHPC test including (a) CE, (b) charge end-point capacity, (c) discharge capacity and (d)  $\Delta V$  vs. cycle number. Dashed lines in each panel indicate the linear fit for the last five data points in each panel. The blue cross in panel (a) represents the predicted CE value at cycle 17 based on the linear fit.

The fractional fade per hour (Figure 4.13c) represents lithium loss due to SEI growth at the negative electrode while the fractional charge end-point capacity slippage per hour (Figure 4.13b) measures the rate of the electrolyte oxidation at the positive electrode[100]. Generally, lower fractional charge end-point capacity slippage, lower fractional fade and lower CIE lead to the cells with longer lifetime [101].

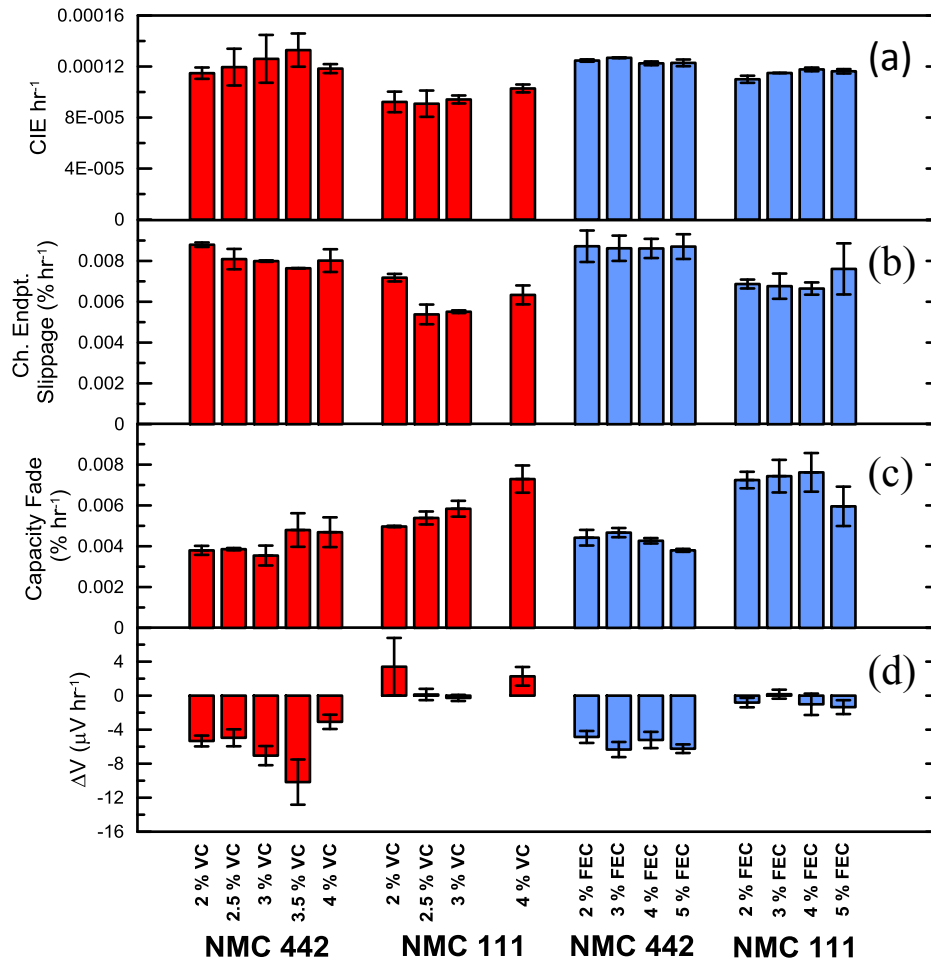


Figure 4.13 A summary of UHPC test results for NMC111/graphite and NMC442/graphite pouch cells filled with 1M LiPF<sub>6</sub> in EMC plus different concentrations of VC (2%, 2.5%, 3%, 3.5%, 4%) or FEC (2%, 3%, 4%, 5%) during 16 cycles between 2.8 and 4.2 V with currents corresponding to C/20 at 40°C including (a) CIE/h, (b) fractional charge end-point capacity slippage per hour, (c) fractional discharge capacity fade per hour and (d) increase in ΔV per hour. Each data point shown in Figure 4.15 is based on a linear fit to the last five cycles. The data shown is the average of two cells and the error bars were calculated as described in the text.

When cells were operated to 4.2 V, the concentration of FEC (from 2% to 5%) barely affected cell performance while 4% VC led to higher capacity fade compared to other cells with smaller amounts of VC. The impedance test results and gas evolution during UHPC cycling can be found in Figure 4.14. Figure 4.14 clearly shows that there are penalties with respect to impedance if increased amounts of VC are used. Finally, the UHPC results (Figures 4.12 and 4.13) suggest that there is little to distinguish between cells with between 2 and 4% VC from a lifetime standpoint and between cells with 3 and 5% FEC from a lifetime standpoint. The volume of a dry pouch cell is around 2.5 mL as mentioned in Section 3.6.

#### **4.2.5 The disadvantages of EC-free electrolyte systems**

Rate capability is an important factor for lithium ion cells because of increasing demands on fast-charging lithium ion cells for current and forthcoming applications [149]. Various strategies have been devoted to the development of high-rate lithium ion cells. Klopsch et al. [150] synthesized new  $\text{Li}[\text{Li}_{0.2}\text{Mn}_{0.56}\text{Ni}_{0.16}\text{Co}_{0.08}]\text{O}_2$  positive electrode material with small and homogenous particles to improve cell rate capability. Yue et al. [151] synthesized  $\text{LiMn}_2\text{O}_4/\text{C}$  composite using a hydrothermal method to improve the contact between  $\text{LiMn}_2\text{O}_4$  and C and enhance the cell rate capability.

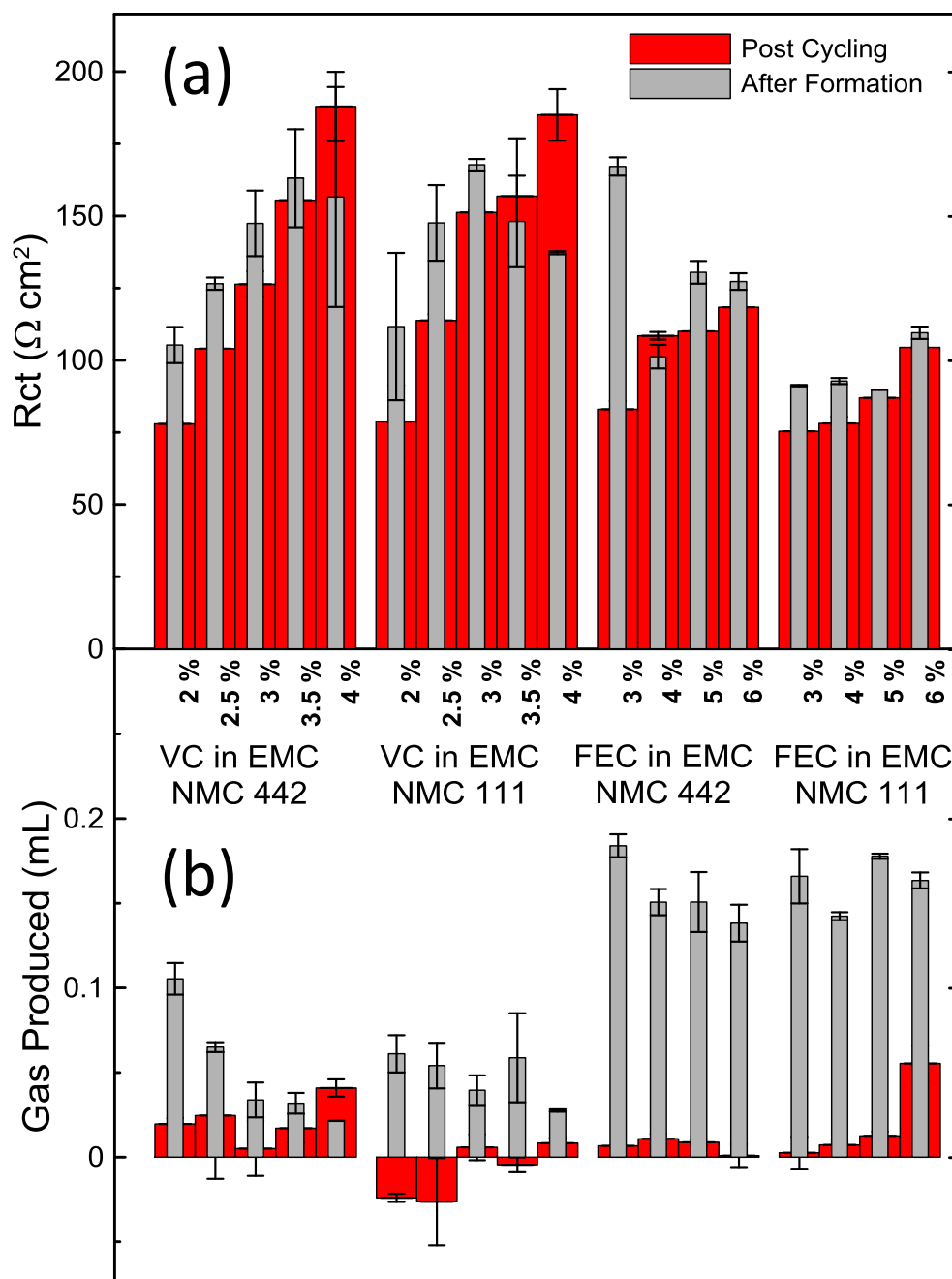


Figure 4.14 A summary of impedance results (a) and gas volumes (b) for NMC111/graphite or NMC442/graphite pouch cells with 1M LiPF<sub>6</sub> EMC electrolyte or 1M LiPF<sub>6</sub> EMC with different enabler content, as indicated, before and after UHPC cycling. All the impedance data was measured at 3.8 V and 10°C. All the cell volume change data was measured at 20°C and 1 atm. The data shown is the average of two cells and the error bars represent the range of the measurements.

EC-free electrolyte systems were also used in NMC111/graphite pouch cells for fast charging rate testing by Liu et al. [152]. Figure 4.15 shows discharge capacity versus cycle number for NMC111/graphite pouch cells with 1M LiPF<sub>6</sub> in the electrolytes indicated in the legend using different charge rates at 22°C. The capacity loss during 2C cycling results from lithium plating which has been verified in reference [152].

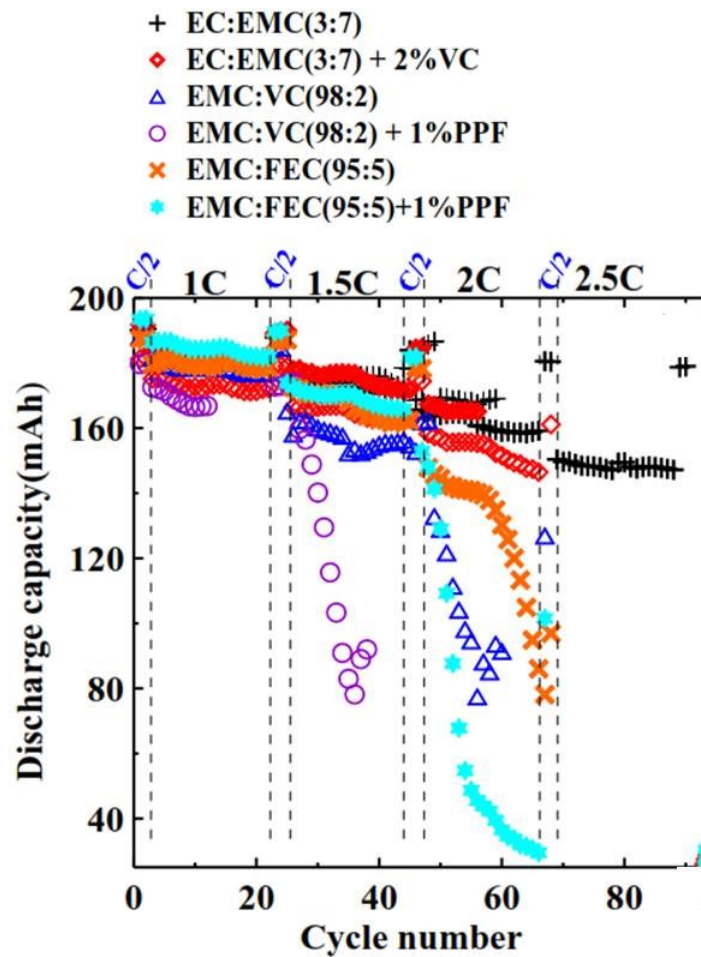


Figure 4.15 Discharge capacity versus cycle number for NMC111/graphite pouch cells with 1M LiPF<sub>6</sub> in the electrolytes indicated in the legend using different charge rates at 22°C. The discharge rate was always C/2. This Figure is taken with permission from Q.Q. Liu, D.J. Xiong, R.Petibon, C.Y. Du, J.R. Dahn, Gas Evolution during Unwanted Lithium Plating in Li-ion Cells with EC-based or EC-free Electrolytes, *J.Electrochem. Soc.* 164 (2016) A3010-A3015.

The volume change of these cells during cycling was monitored using the in-situ gas measurement setup. Figures 4.16 and 4.17 show the volume change of these cells versus time during cycling. When lithium plating occurred at 2C, cells with EC-free electrolytes produced lots of gas while cells with EC-based electrolytes do not. This suggests that EC can preferentially react with freshly deposited Li and form a stable SEI to prevent gas evolution in EC-containing electrolytes.

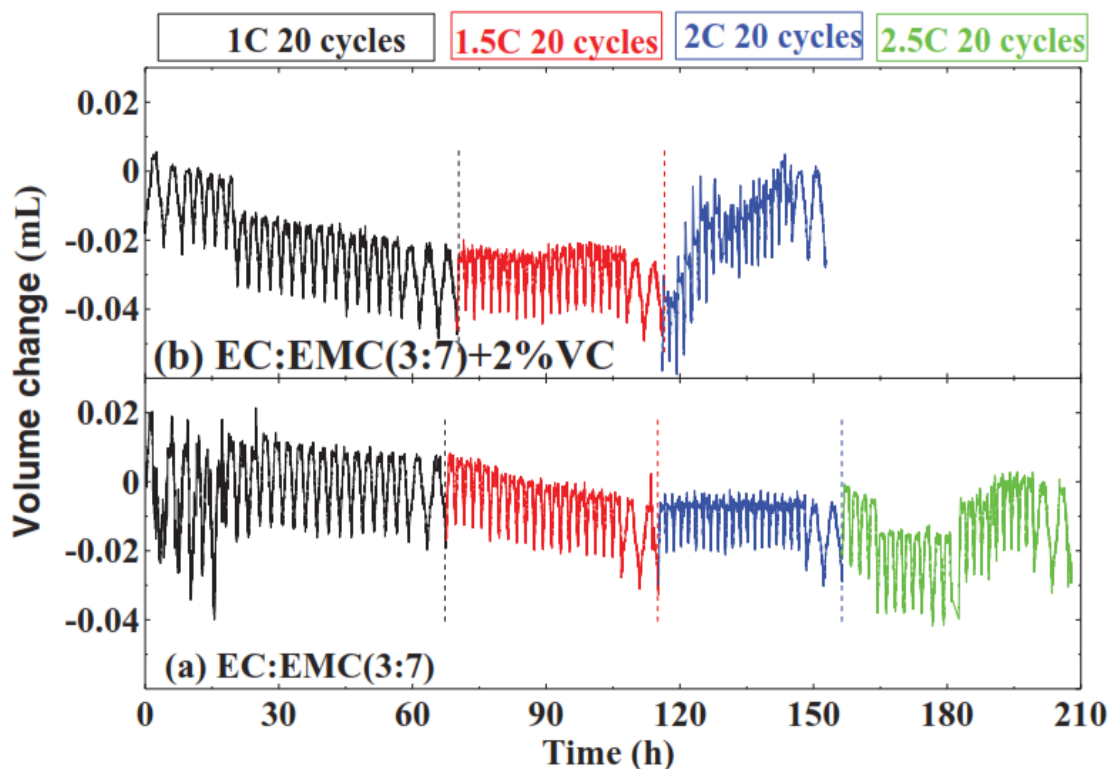


Figure 4.16 In-situ gas measurement of NMC111/graphite pouch cells with 1M LiPF<sub>6</sub> in (a) EC/EMC 3/7 and (b) EC/EMC 3/7+2%VC during cycling at different charge rates at 22°C. This Figure is taken with the permission from Q.Q. Liu, D.J. Xiong, R.Petibon, C.Y. Du, J.R. Dahn, Gas Evolution during Unwanted Lithium Plating in Li-ion Cells with EC-based or EC-free Electrolytes, *J.Electrochem. Soc.* 164 (2016) A3010-A3015.

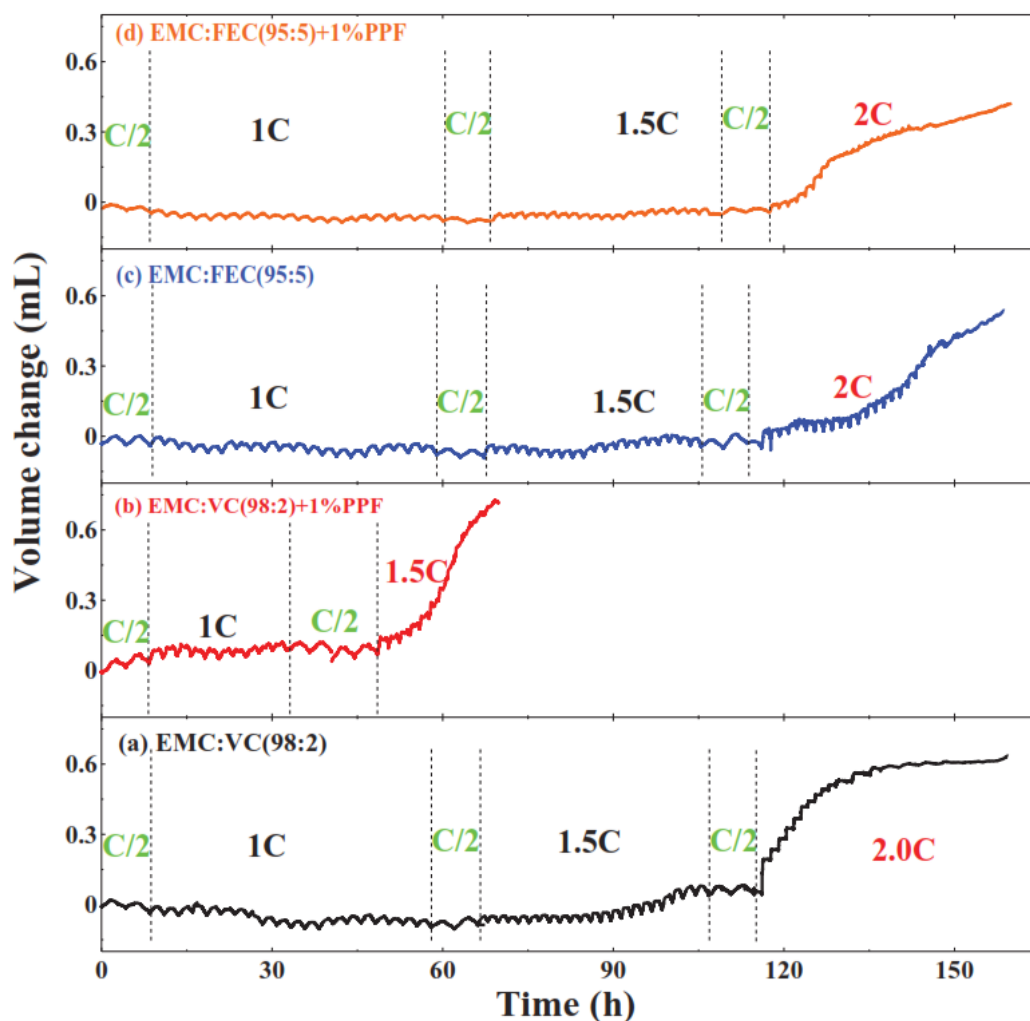


Figure 4.17 In-situ gas measurement of NMC111/graphite pouch cells with 1M LiPF<sub>6</sub> in (a) EC/VC 98/2, (b) EC/VC 98/2+1%PPF, (c) EMC/FEC 95/5 and (d) EMC/FEC 95/5+1%PPF during cycling at different charge rates at 22°C. This Figure is taken with permission from Q.Q. Liu, D.J. Xiong, R.Petibon, C.Y. Du, J.R. Dahn, Gas Evolution during Unwanted Lithium Plating in Li-ion Cells with EC-based or EC-free Electrolytes, *J.Electrochem. Soc.* 164 (2016) A3010-A3015.

The concentration of LiPF<sub>6</sub> has an impact on cell performance. Wang et al. [153] showed that the concentration of LiPF<sub>6</sub> affected the impedance and lifetime of LCO/graphite pouch cells with EC-based electrolytes. Therefore it is necessary to investigate the effect

of  $\text{LiPF}_6$  concentration on EC-free electrolyte systems. Figure 4.18 shows the conductivity of  $\text{LiPF}_6/\text{EMC}$  solutions with different concentrations of  $\text{LiPF}_6$  at different temperatures. When the concentration of  $\text{LiPF}_6$  is lower than 0.4 M, the conductivity of the solution drops dramatically because  $\text{LiPF}_6$  (low concentration) cannot be dissociated well by EMC (low dielectric constant solvent).

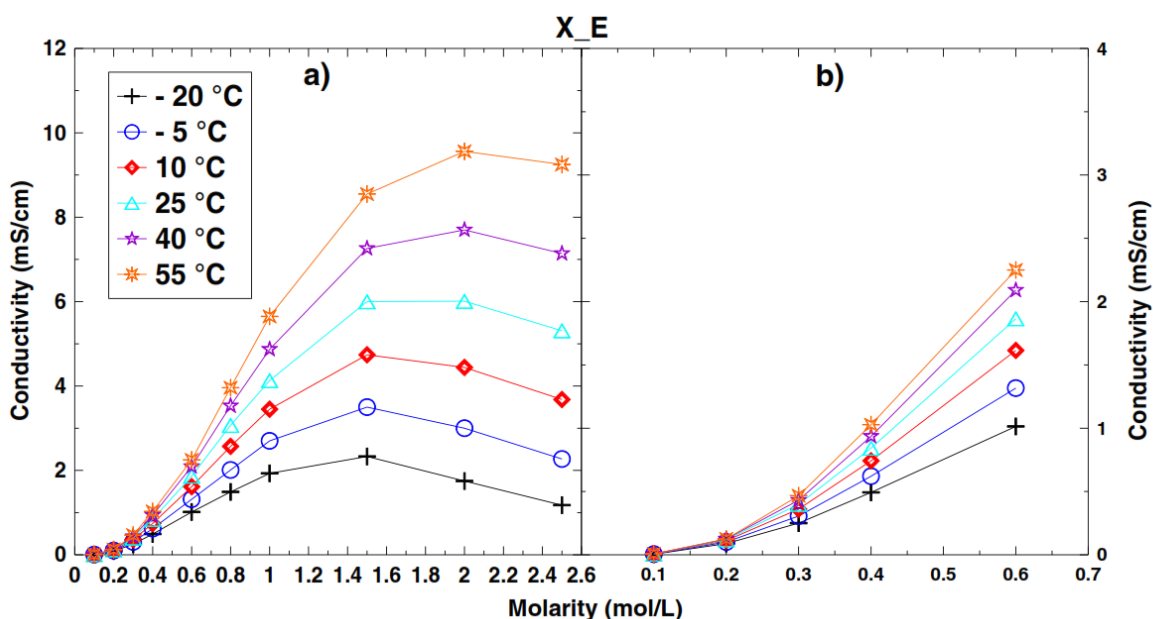


Figure 4.18 Ionic conductivity of X\_E (EMC with different concentrations of  $\text{LiPF}_6$ ) electrolytes ( $X = 0.1, 0.2, 0.3, 0.4, 0.6, 1, 1.5, 2$  and  $2.5\text{M LiPF}_6$ ) measured at different temperatures ( $-20^\circ\text{C}, -5^\circ\text{C}, 10^\circ\text{C}, 25^\circ\text{C}, 40^\circ\text{C}$  and  $55^\circ\text{C}$ ). This Figure is taken with permission from D.J. Xiong, T. Hynes, J.R. Dahn, Dramatic Effects of Low Salt Concentrations on Li-ion Cells Containing EC-free Electrolytes, *J.Electrochem. Soc.* 164 (2017) A2089-A2100.

### 4.3 Conclusions for Chapter 4

Electrolytes consisting of  $1\text{M LiPF}_6$  in EMC plus a small amount of “enabler” have been demonstrated to be useful for NMC442/graphite pouch cells operated at high potential.



The work in this chapter focused on strategies for finding the best EC-free electrolyte for high voltage LIB. In addition to the selected “enablers” studied in this work, there are many more “enablers” that need to be identified and carefully tested. Studies of EC-free electrolytes have remarkable clarity because there is no EC present in the electrolyte to contribute to a complex negative electrode SEI that contains decomposition products from EC as well as from the electrolyte additives. The clear reduction peak of EMC observed during formation (Figure 4.1) as well as the trans-esterification of EMC which occurs when Li alkoxides are created by EMC reduction (Figure 4.2) allows one to easily determine when enough enabler has been added to the EC-free electrolyte to passivate the graphite negative electrode effectively. Such clear and remarkable data, of an almost tutorial nature, cannot be collected for electrolytes that contain EC.

In order to optimize the amount of “enabler” added to 1M LiPF<sub>6</sub> in EMC, GC-MS was used to track the consumption of “enabler” and the trans-esterification of EMC during formation. Cells containing different initial amounts of “enabler” were systematically investigated using storage testing, EIS, long-term CCCV cycling and UHPC tests. The tools used here are very appropriate to use to understand the impact of electrolyte additives in Li-ion cells.

If the amount of “enabler” added to 1M LiPF<sub>6</sub> in EMC was not enough (e.g. 1%), the graphite negative electrode could not be passivated well, which resulted in gas production

during formation, storage and cycling, rapid capacity fade and polarization increase during cycling. If the amount of “enabler” was in excess (e.g. 5%), it resulted in large impedance and gas production during storage and cycling, except in the case of FEC. FEC was the only enabler that was only consumed to a level of about 2% during formation, even if excess FEC was added, which explains why the impedance did not increase when excess FEC was added. In addition, the amount of FEC in the electrolyte did not diminish during the storage and cycling tests performed here. Cells with 3% FEC or 5% FEC in 1M LiPF<sub>6</sub> with EMC appear to be the best in the testing performed here.

Although EMC-based electrolytes without EC demonstrate outstanding performance at high voltage and high temperature, serious gas evolution occurs when unwanted lithium plating exists in NMC/graphite pouch cells at high charge rate. Since the concentration of LiPF<sub>6</sub> can affect cell performance with EC-based electrolytes, the effect of LiPF<sub>6</sub> concentration on EC-free electrolyte systems was investigated. Unfortunately, the conductivity of EC-free electrolyte systems is extremely low when low concentrations of LiPF<sub>6</sub> are used.

## CHAPTER 5 LITHIUM DIFLUOROPHOSPHATE AS AN ELECTROLYTE ADDITIVE IN $\text{Li}[\text{Ni}_{0.5}\text{Mn}_{0.3}\text{Co}_{0.2}]\text{O}_2/\text{GRAPHITE POUCH CELLS}$

The majority of this work was adapted from the following peer-reviewed article:

- L.Ma, Leah Ellis, S. L. Glazier, Xiaowei Ma, Qianqian Liu, Jing Li and J.R. Dahn, Lithium Difluorophosphate as An Electrolyte Additive in  $\text{Li}(\text{Ni}_{0.5}\text{Mn}_{0.3}\text{Co}_{0.2})\text{O}_2/\text{graphite Pouch Cells}$ , *J. Electrochem. Soc.* 165 (2018) A891-A899.

Lin Ma performed pouch cell preparation, gas evolution measurements, impedance measurements, storage testing, UHPC cycling testing and NMR testing. S.L. Glazier performed isothermal microcalorimetry testing. Leah Ellis performed XPS testing and XPS data analysis. Dr. J.R. Dahn provided guidance, participated in the interpretation of all the data and edited the manuscript. Lin Ma prepared the first draft of the manuscript mentioned above.

In this chapter, the effect of  $\text{LiPO}_2\text{F}_2$  as an electrolyte additive in NMC532/graphite pouch cells was examined using UHPC, EIS, storage testing, gas evolution measurements, isothermal microcalorimetry and long term charge-discharge cycling. Comparisons to the well-known additive, VC were made.  $\text{LiPO}_2\text{F}_2$  is an effective additive for NMC532/graphite pouch cells since it was found to improve CE, decrease parasitic heat flow, improve charge-discharge cycle lifetime and decrease impedance growth. The composition of the SEI on both electrodes was examined by XPS in cases where  $\text{LiPO}_2\text{F}_2$

was used or not used. The effect of combining methyl acetate, as a co-solvent to improve rate capability, and  $\text{LiPO}_2\text{F}_2$  was also investigated using long term cycling testing at  $20^\circ\text{C}$ . Overall,  $\text{LiPO}_2\text{F}_2$  is shown to be an extremely valuable electrolyte additive, more effective than VC in these cells.

## **5.1 Experimental**

### **5.1.1 The preparation of pouch cells**

Coated SC NMC532/graphite and NMC442/graphite pouch cells were prepared according to the procedure described in Section 3.1.2. 1.2 M  $\text{LiPF}_6$  in EC/EMC 3/7 (by weight) was used as the control electrolyte. Electrolytes with additives were formulated by dissolving 2 wt.% VC, 0.5 or 1.0 wt%  $\text{LiPO}_2\text{F}_2$  in control electrolyte. 20 wt.% methyl acetate (MA) was mixed with control electrolyte when needed.

### **5.1.2 EIS testing**

EIS measurements were conducted on NMC532/graphite pouch cells before and after both storage testing and long-term charge-discharge cycle testing. Cells were charged or discharged to 3.8 V before they were moved to a  $10. \pm 0.1^\circ\text{C}$  temperature box. AC impedance spectra were collected with ten points per decade from 100 kHz to 10 mHz with a signal amplitude of 10 mV. A Biologic VMP-3 was used to collect this data.

### **5.1.3 Charge-discharge cycling tests**

Some cells were prepared for long-term cycling at  $40. \pm 0.1^\circ\text{C}$  or  $20. \pm 0.1^\circ\text{C}$  (room temperature). The cells were charged and discharged at 77 mA (C/3) between 3 and 4.3 V

using CCCV mode with a Neware (Shenzhen, China) charger system. The cut-off current for CCCV mode was 11.5 mA (C/20).

Some cells were prepared for high-rate long-term cycling at  $20. \pm 0.1^\circ\text{C}$  (room temperature). The cells were discharged at a current corresponding to C/2 and charged with currents corresponding to 1C, 1.5C, 2C, 2.5C and 3C between 3 and 4.1 or 4.3 V using a Neware (Shenzhen, China) charger system. The charging rate was changed every 30 cycles. The purpose of this test was to determine at what current unwanted Li plating would occur.

All pouch cells were cycled with external clamps to ensure a firm stack pressure of about 25 KPa even if gas was produced during cycling. The gas, if produced, was forced to the edges of the pouch due to the action of the clamps.

#### **5.1.4 Storage testing**

A Maccor series 4000 cycler was used to prepare cells for storage tests. Cells after formation were cycled between 2.8 V and 4.4 V twice with a current corresponding to C/10. Then the cells were held at 4.4 V or 2.5 V for 24 hours and then were transferred to the storage system. The open circuit voltage of the cells was monitored automatically for 1 second every 6 hours for a total storage time of 500 h at  $60.^\circ\text{C}$  [154].

#### **5.1.5 Solution nuclear magnetic resonance (SNMR) tests**

SNMR was used to identify  $\text{LiPO}_2\text{F}_2$  [155] before and after cell formation.  $^{19}\text{F}$ -NMR spectra were collected at room temperature using a Bruker AC-250 (5.9 T) NMR

spectrometer. Chemical shifts are reported in ppm relative to external reference standards ( $^{19}\text{F}$ -NMR, 0.5%  $\text{CF}_3\text{C}_6\text{H}_5$ ). Since HF, generated from the hydrolysis of  $\text{LiPF}_6$ , can react with typical NMR tubes, a thin walled fluoro-ethylene propylene (FEP) liner with a polytetrafluoroethylene (PTFE) plug (Sigma-aldrich) inserted into a glass NMR tube was used for testing. All the SNMR samples were made by mixing 100 mg electrolyte with 1g dimethyl sulfoxide- $d_6$  (Sigma-Aldrich, 99.9 atom% D). The electrolyte after formation was removed from the formed pouch cells by a centrifuge (IEC Centra GP8R, 2500 revolutions/min, 30 min,  $20^\circ\text{C}$ ). A small slit was cut in the base of the pouch cell and the pouch cell was placed in a sealed tube before the centrifuge operation started. About 0.4 mL of electrolyte was extracted through the slit by the action of the centrifuge.

#### **5.1.6 XPS for surface analysis**

XPS was used for analysis of the surfaces of graphite and NMC532 electrodes from selected pouch cells after formation. The sample preparation procedure and instrument details can be found in Madec et al. [156]. After formation, certain cells were transferred to an Ar-filled glove box. The electrodes were removed, and rinsed several times with EMC, to remove  $\text{LiPF}_6$  and EC. Removal of these species is essential for the underlying SEI components to be observed by XPS. Removal of EC and  $\text{LiPF}_6$  is also important for maintaining low pressures in the XPS system. Rinsing with EMC is not expected to dissolve any SEI components, as EMC is the major component of the electrolyte in which the SEI was formed. Once the rinsed samples were dried, they were mounted onto a molybdenum sample holder, using double-sided, ultra-high vacuum-compatible copper tape. The sample holder was transferred into the XPS system, without exposure to air, using a specially designed air-tight apparatus that could be evacuated to low pressures.

Electrodes were left under ultra-high vacuum overnight to allow for off-gassing of any remaining volatile components. The samples were then transferred to the analysis chamber of the XPS, which has a base pressure of  $1 \times 10^{-10}$  mbar and was maintained below  $2 \times 10^{-9}$  mbar during the experiments. Analysis was performed with a SPECS spectrometer equipped with a Phoibos 150 hemispherical analyser, using unmonochromatized Mg K $\alpha$  radiation and a pass energy of 20 eV. Preliminary and final survey scans were compared to ensure that no photochemical degradation was induced during analysis. Data analysis was done using CasaXPS software (v. 2.3.18). Charge correction was done by fitting the adventitious carbon peak and shifting the x-axis down such that this peak fell at 285.0 eV. XPS spectra were fit with a non-linear Shirley-type background. This background was subtracted from the signal to allow for visual comparison of atomic concentrations between samples using relative peak heights. Elemental analysis was done using relative sensitivity factors for the SPECS instrument. Peaks were fit with a mixed Gaussian (70%) /Lorentzian (30%) line shape. All XPS measurements and XPS data analysis and interpretation were done by Leah Ellis.

#### **5.1.7 Isothermal microcalorimetry tests**

In order to form stable SEI layers before calorimetry measurements, the formed cells were cycled four times between 3.0 V and 4.2 V at 10 mA ( $\sim C/20$ ). Then cells were transferred into a TAM III Microcalorimeter (TA Instruments) at 40.00°C where the temperature was kept stable to  $\pm 0.0001^\circ\text{C}$ . Cells were connected to a Maccor series 4000 charger (Maccor Inc.) for cycling the cells while in the microcalorimeter. All the experimental details can be found in reference [157]. Heat flow measurements were

recorded to an accuracy of  $\pm 1.0 \mu\text{W}$  and the baseline drift over the course of the experiments did not exceed  $\pm 0.5 \mu\text{W}$ . After 24 hours of temperature stabilization in the calorimeter, cells were charged and discharged at 1.5 mA ( $\approx C/150$ ) between 4.0 V and a sequence of upper cutoff voltages: 4.2 V, 4.3 V (twice), 4.4 V (twice) and then 4.2 V once again. All microcalorimetry measurements and data analysis were made by Stephen Glazier.

#### **5.1.8 UHPC tests**

Formed NMC532/graphite pouch cells underwent UHPC cycling between 2.8 V and various upper cut-off voltages (4.1, 4.2, 4.3 and 4.4 V) at C/20 and 40°C for 16 cycles. The UHPC allows the CE and charge-end-point capacity slippage to be measured with great accuracy and the interpretation of high precision coulometry data can be found in reference [100].

#### **5.1.9 Frequency response analyzer (FRA) tests**

The testing system [158], built in-house at Dalhousie University, consists of Neware (Shenzhen, China) cyclers connected to computers with Gamry frequency response analyzer (FRA) cards via appropriate computer controlled relays. Formed NMC532/graphite pouch cells underwent cycling between 3 and 4.4 V at 40°C using protocol #1 described by Nelson et al. [158]. The cells were cycled between 3 and 4.4 V at C/3. Every 10 cycles, the cells underwent an “FRA cycle” consisting of a charge and discharge cycle at C/20 between 3 and 4.4 V while the FRA measured the cell impedance



every 0.1 V between 3.5 and 4.4 V. After the FRA cycle, the cells were cycled again between 3 and 4.4 V at C/3 for 10 cycles. This protocol was repeated many times.

## **5.2 Results and Discussion**

### **5.2.1 The effect of LiPO<sub>2</sub>F<sub>2</sub> in EC-free electrolyte on cell formation**

Figure 5.1 shows the differential capacity vs. cell voltage of NMC442/graphite pouch cells during the formation charge to 3.5 V at 40°C with a current corresponding to C/20. The electrolytes used in the cells were 1.0 M LiPF<sub>6</sub> in EMC plus different concentrations (0.5% and 1%) of LiPO<sub>2</sub>F<sub>2</sub> or 5% FEC. With the addition of 5% FEC, the reduction peak of EMC (~ 3.2 V) was suppressed as reported in Section 4.2.1. However, with the addition of LiPO<sub>2</sub>F<sub>2</sub>, the reduction peak of EMC was not affected. This suggests that LiPO<sub>2</sub>F<sub>2</sub> alone cannot produce a good passivation layer on the graphite electrode.

Figure 5.2 shows the percentage of EMC that underwent trans-esterification producing DMC and DEC [57] vs. the initial content of LiPO<sub>2</sub>F<sub>2</sub> during the first full cycle for NMC442/graphite pouch cells (up to 4.4 V) at 40°C with a current corresponding to C/20.

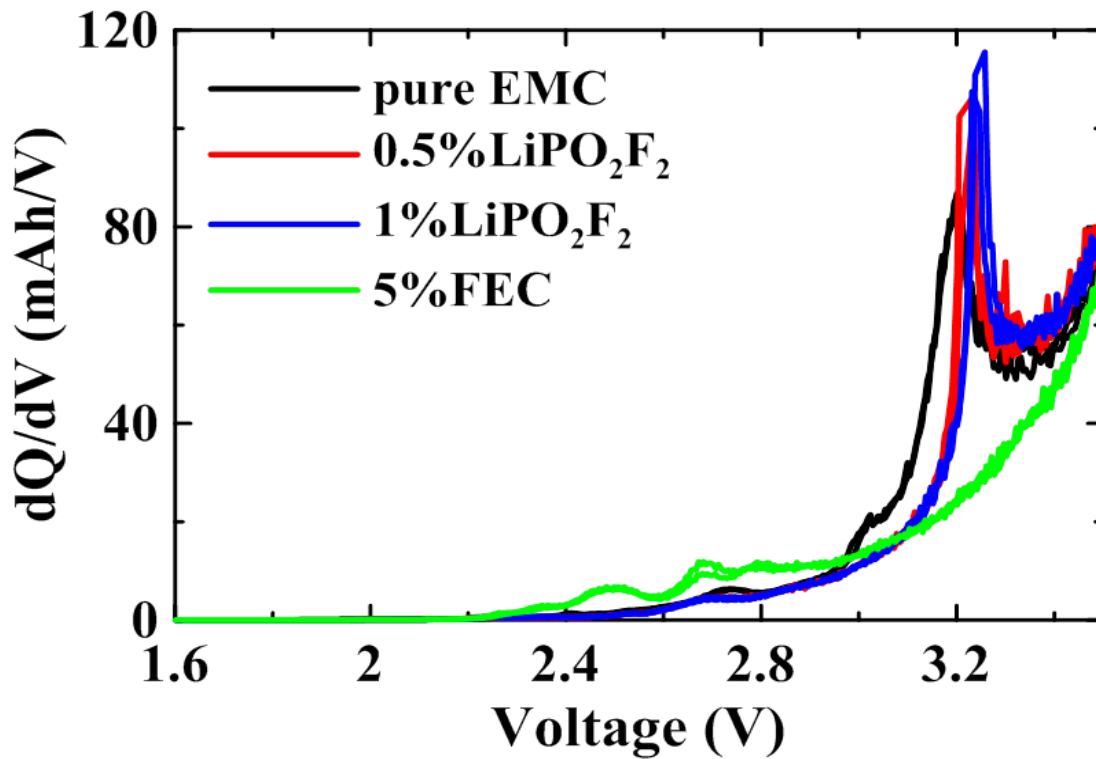


Figure 5.1 dQ/dV vs. voltage for NMC442/graphite pouch cells with different electrolytes as shown in the legend during formation at 40°C. The charging current corresponded to C/20.

As reported in Section 4.2.1, these trans-esterification reactions were caused by the presence of lithium alkoxides due to the reduction of linear alkyl carbonates. It is a signal that EMC was reduced at the graphite negative electrode during formation, which helps determine how well the graphite electrode was passivated by the electrolyte additives. Figure 5.2 shows that EMC trans-esterification was barely affected when only  $\text{LiPO}_2\text{F}_2$  was added into the electrolyte. This suggests that  $\text{LiPO}_2\text{F}_2$  alone cannot passivate the graphite electrode well, which is consistent with the result shown in Figure 5.1.

### 5.2.2 The effect of $\text{LiPO}_2\text{F}_2$ in EC-based electrolyte on cell formation

Figure 5.3 shows the differential capacity vs. cell voltage of NMC532/graphite pouch cells during the formation charge to 3.5 V at 40°C with a current corresponding to C/20. The electrolytes used in the cells were control electrolyte, control electrolyte with different concentrations (0.5% and 1%) of  $\text{LiPO}_2\text{F}_2$ , control electrolyte with 20% MA and control electrolyte with 20% MA plus different concentrations (0.5% and 1%) of  $\text{LiPO}_2\text{F}_2$ .

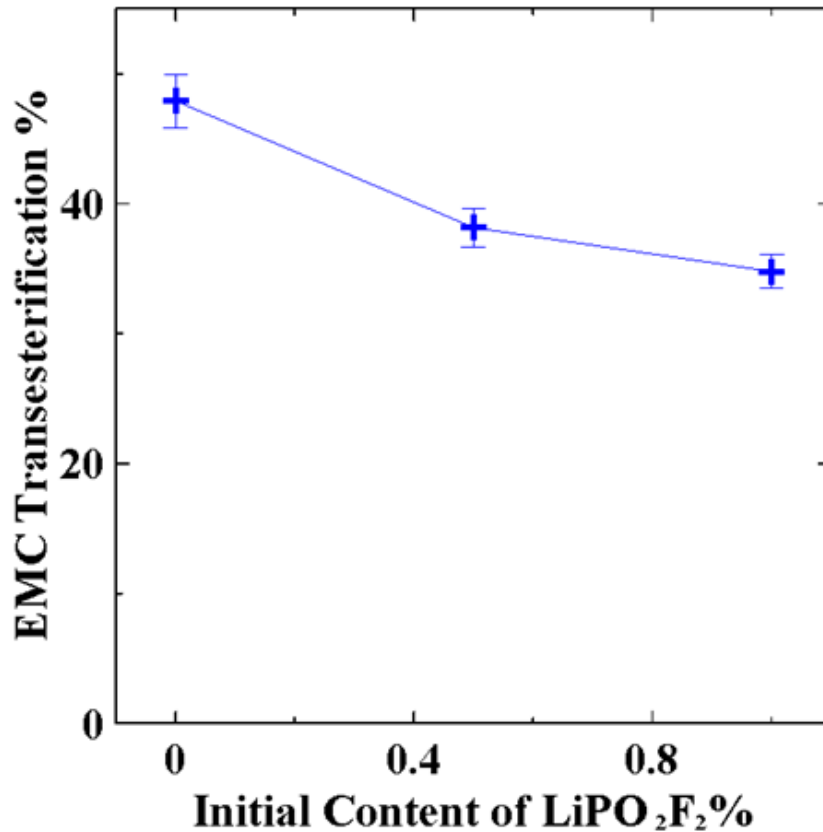


Figure 5.2 % EMC trans-esterification vs. initial content of  $\text{LiPO}_2\text{F}_2$  in NMC442/graphite pouch cells that underwent their first full (formation) cycle between 2.8 – 4.4 V at 40°C, C/20.

All the cells show a reduction peak in the differential capacity plot at a full cell potential around 2.9 V. This results from the reduction of EC on the surface of graphite [11]. Adding  $\text{LiPO}_2\text{F}_2$  to the electrolyte does not affect this peak, suggesting that  $\text{LiPO}_2\text{F}_2$  is electrochemically stable in the electrolyte during the formation step. This is consistent with a previous report [105] and the results shown in Figure 5.1.

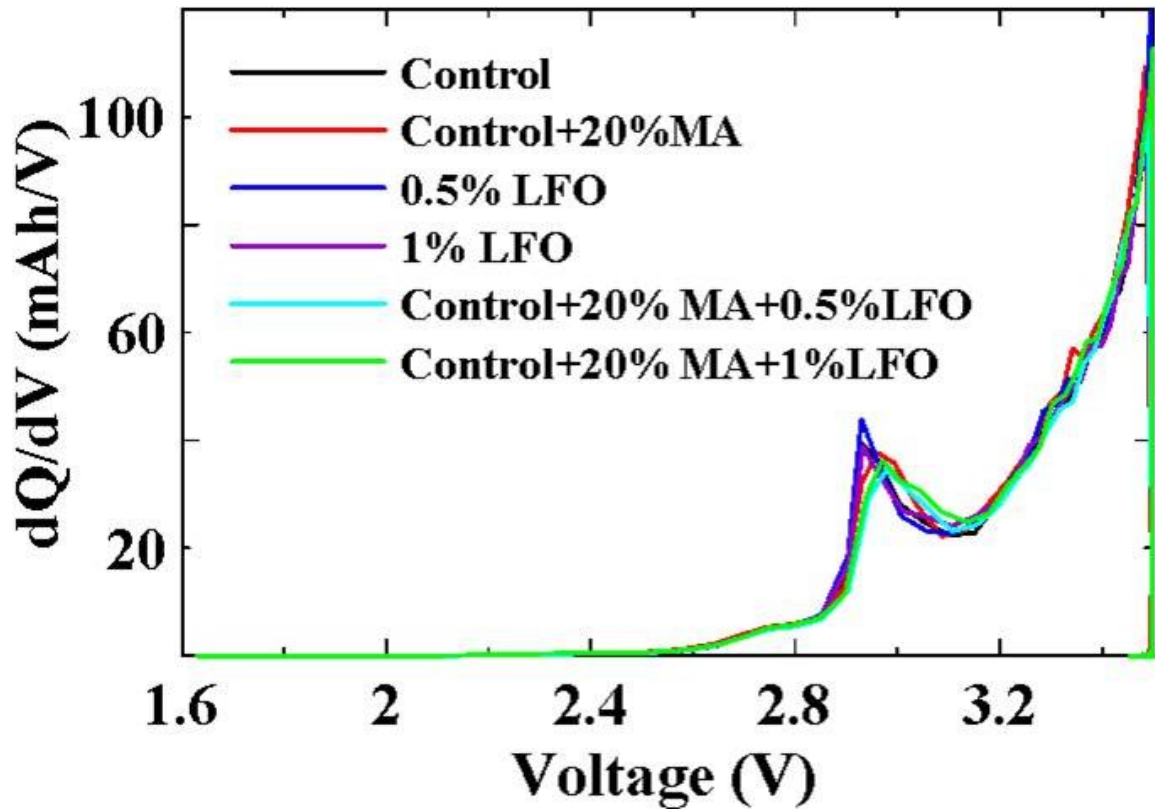


Figure 5.3  $dQ/dV$  vs. voltage for NMC532/graphite pouch cells with different electrolytes as shown in the legend during formation at  $40^\circ\text{C}$ . The charging current corresponded to C/20.  $\text{LiPO}_2\text{F}_2$  is called LFO in the Figure legend.

Figure 5.4 shows the  $^{19}\text{F}$  NMR spectra for a) fresh control electrolyte; b) fresh control electrolyte + 0.5%  $\text{LiPO}_2\text{F}_2$ ; c) fresh control electrolyte + 1%  $\text{LiPO}_2\text{F}_2$ ; d) control electrolyte + 0.5%  $\text{LiPO}_2\text{F}_2$  centrifuged out of cells after formation; and e) control electrolyte + 1%  $\text{LiPO}_2\text{F}_2$  centrifuged out of cells after formation. Figure 5.4a shows the doublet from the  $\text{PF}_6^-$  anions in the control electrolyte. Figures 5.4b – 5.4e, show, in addition to the doublet from  $\text{PF}_6^-$ , a second doublet from  $\text{PO}_2\text{F}_2^-$  anions which is indicated by a red circle in the  $^{19}\text{F}$  NMR spectra [155]. Moreover, Figures 5.4b – 5.4e show that the intensity ratio between  $\text{PO}_2\text{F}_2^-$  and  $\text{PF}_6^-$  of the fresh electrolyte (Figures 5.4b and 5.4c) is higher than that in the electrolyte centrifuged out of the cells after formation (Figures 5.4d and 5.4e). This suggests that some of the  $\text{LiPO}_2\text{F}_2$  has been consumed during formation.

To understand and compare the impact of the  $\text{LiPO}_2\text{F}_2$  additive and MA on the electrode/electrolyte interphase and study how these interphases are related to the corresponding electrochemical performance, the nature of SEI, when different electrolyte blends were used, was characterized using XPS after cell formation at 3.8 V. The top row of Figure 5.5 shows XPS spectra of the graphite negative electrode, formed in control electrolyte, 1%  $\text{LiPO}_2\text{F}_2$ , and 1%  $\text{LiPO}_2\text{F}_2$  with 20% MA.

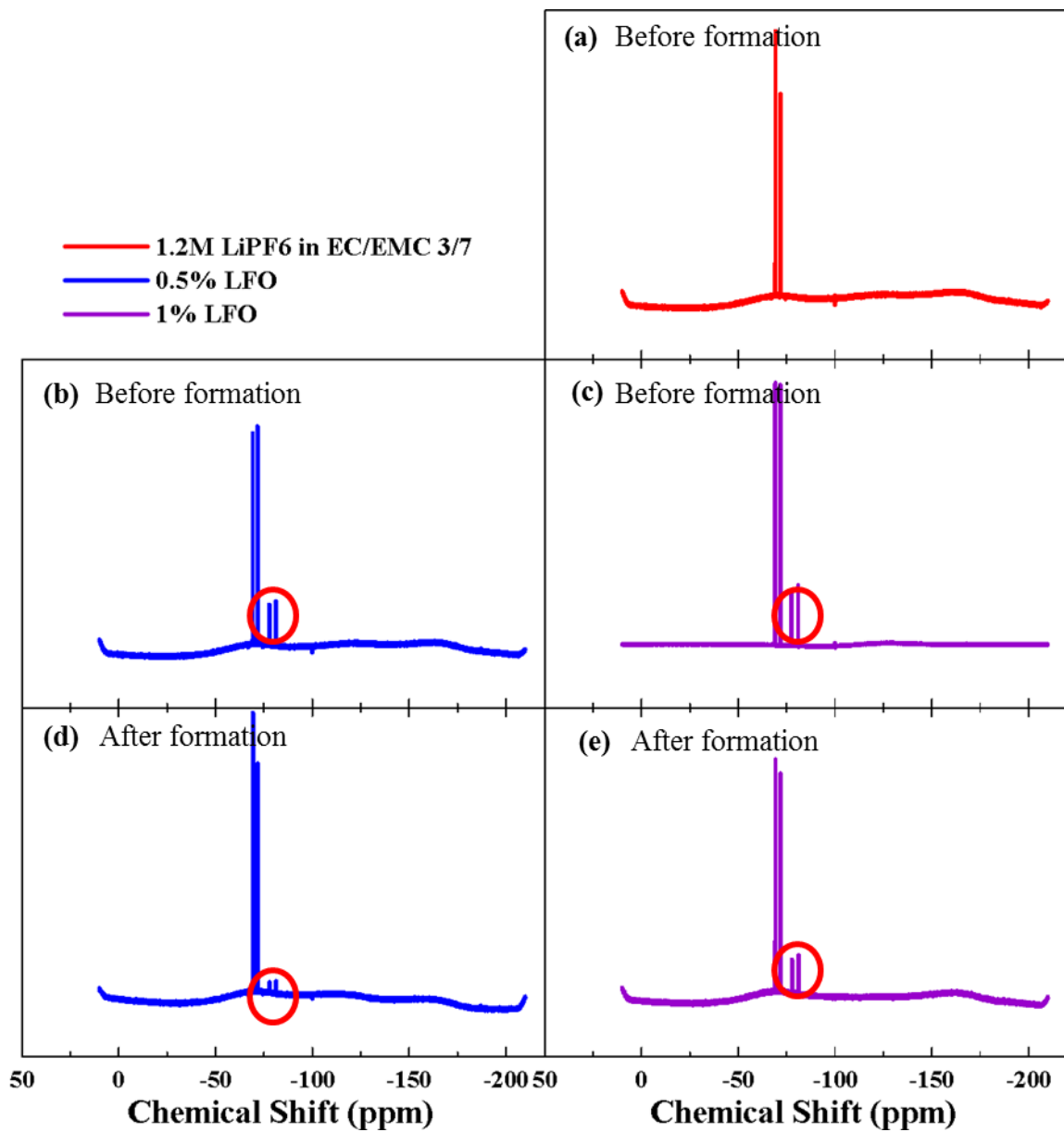
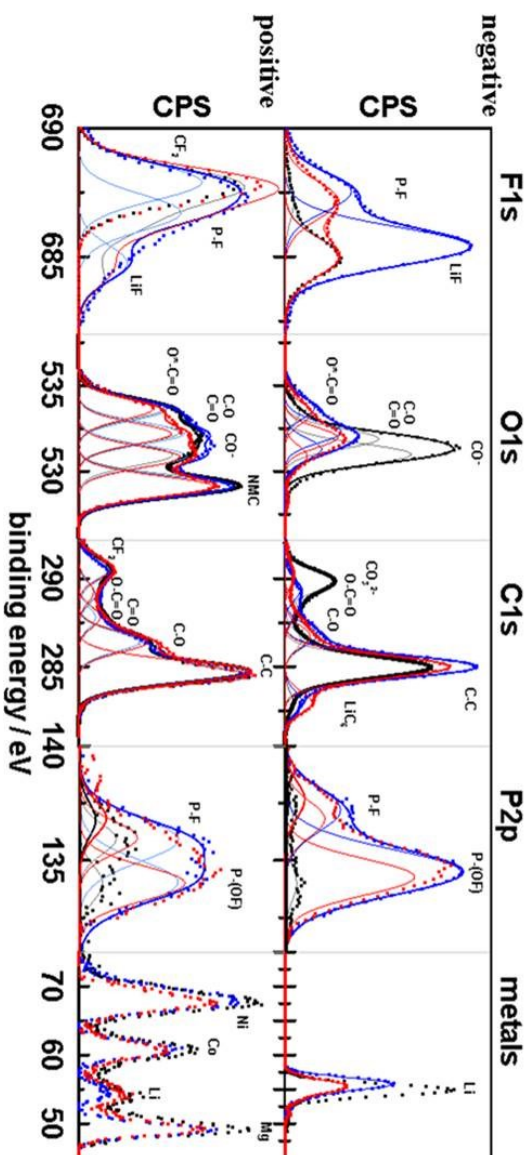


Figure 5.4  $^{19}\text{F}$  NMR spectra for fresh control electrolyte (a), fresh control electrolyte + 0.5%  $\text{LiPO}_2\text{F}_2$  (b), fresh control electrolyte + 1%  $\text{LiPO}_2\text{F}_2$  (c), control electrolyte + 0.5%  $\text{LiPO}_2\text{F}_2$  centrifuged out of cells after formation (d) and control electrolyte + 1%  $\text{LiPO}_2\text{F}_2$  centrifuged out of cells after formation (e).  $\text{LiPO}_2\text{F}_2$  is called LFO in the Figure legend.

The peak from lithiated graphite ( $\text{LiC}_6$ ), at 284.3 eV, is larger in cells containing 1%  $\text{LiPO}_2\text{F}_2$ . This suggests that the SEI layer, covering the lithiated graphite, is thinner in

cells containing  $\text{LiPO}_2\text{F}_2$ . The SEI formed with  $\text{LiPO}_2\text{F}_2$  contains fewer carbonate species (evidenced by smaller peaks at 291 eV in the  $\text{C}^{1s}$  spectra, and 531 eV in the  $\text{O}^{1s}$  spectra), and more fluorophosphate species (evidenced by larger peaks in the  $\text{P}^{2p}$  spectra, and at 687 eV in the  $\text{F}^{1s}$  spectra). The presence of more fluorophosphate species suggests that  $\text{LiPO}_2\text{F}_2$  participates in the formation of the negative electrode SEI. The reduction in the amount of carbonate species suggests that the SEI formed by  $\text{LiPO}_2\text{F}_2$  hinders the carbonate solvents from breaking down and forming the SEI. Fluorophosphate species appear to passivate the electrode and may be a cause of improved cell performance (as will be shown later). The bottom row of Figure 5.5 shows XPS spectra of the corresponding NMC532 positive electrode. Again, greater amounts of fluorophosphates occur in cells with  $\text{LiPO}_2\text{F}_2$ . This suggests that  $\text{LiPO}_2\text{F}_2$  reacts at the positive electrode, as well as the negative electrode, to form a beneficial SEI. The addition of  $\text{LiPO}_2\text{F}_2$  does not obviously change the thickness of the positive electrode SEI, judging from the relative heights of the underlying positive electrode peaks (Ni, Co, Mn, and the  $\text{O}^{1s}$  peak at 528 eV). The addition of MA to cells with  $\text{LiPO}_2\text{F}_2$  does not have an impact on the surface chemistry of the positive electrode, but it appears to somewhat increase the amount of LiF in the negative electrode SEI. The reason why there is more LiF in the presence of MA is unknown.



**Negative electrode**

Atom %	control	1% LFP02F2	1% LFP02F2+ 20% MA
F 1s	4.1	9.6	16.0
O 1s	29.3	17.8	16.3
C 1s	30.4	45.6	37.6
P 2p	0.4	3.9	3.1
Li 1s	35.9	23.1	27.1

**Positive Electrode**

Atom %	control	1% LFP02F2	1% LFP02F2+ 20% MA
F 1s	15.5	18.4	17.5
O 1s	20.2	18.2	21.1
C 1s	56.5	55.2	53.2
P 2p	0.8	1.6	1.6
Li 1s	4.5	4.8	4.3
Ni+Co+Mn	2.5	1.8	0.0

Figure 5.5 Typical F 1s (a, f), O 1s (b, g), C 1s (c, h), P 2p (d, i) and metal XPS core spectra for graphite electrodes and NMC532 electrodes, respectively, at 3.8 V after formation with different electrolytes as indicated.



### 5.2.3 The effect of $\text{LiPO}_2\text{F}_2$ on storage testing

Figure 5.6 shows a summary of (5.6a and 5.6b) voltage drop, (5.6c and 5.6d) gas evolution and (5.6e and 5.6f) impedance change of NMC532/graphite pouch cells containing control electrolyte, control electrolyte with different concentrations (0.5% and 1%) of  $\text{LiPO}_2\text{F}_2$ , control electrolyte with 2% VC, control electrolyte with 20% MA and control electrolyte with 20% MA plus different concentrations (0.5% and 1%) of  $\text{LiPO}_2\text{F}_2$  during the storage testing at  $60^\circ\text{C}$ . Two cells were measured for each experiment and the error bars on the data points in Figure 5.6 are the difference between the two results. The data point is located at the average value of the results from the two experiments. The starting voltage before storage for Figures 5.6a, 5.6c and 5.6e was 4.4 V while the starting voltage for Figures 5.6b, 5.6d and 5.6f was 2.5 V. The voltage drop during the storage testing indicates the occurrence of parasitic reactions at the surface of the positive electrode (4.4 V) and the negative electrode (2.5 V), respectively [154]. The cells with 0.5%  $\text{LiPO}_2\text{F}_2$ , 1%  $\text{LiPO}_2\text{F}_2$  and 2% VC show smaller voltage drops compared to other cells. Figures 5.6c and d show that with the addition of  $\text{LiPO}_2\text{F}_2$  or VC, the amount of gas produced during storage was reduced.

Figures 5.6e and f show a summary of the impedance before and after storage. All the impedance spectra were measured at 3.8 V and at  $10.0^\circ\text{C}$ . The impedance in this Figure is the diameter of the semi-circle in the Nyquist plot that arises from the sum of the charge-transfer resistances and the transport of lithium ions through the SEI layers at both

the positive and negative electrodes [79]. The addition of different electrolyte additives results in the formation of different SEI layers. This has an impact on cell impedance. Cells using  $\text{LiPO}_2\text{F}_2$  as an electrolyte additive showed smaller impedance compared to all other cells. Figure 5.6c shows that with the addition of  $\text{LiPO}_2\text{F}_2$  or VC, the amount of gas produced during storage was reduced compared to control electrolyte. This shows that the addition of electrolyte additives can suppress the production of gaseous by-products resulting from parasitic reactions as is well known.

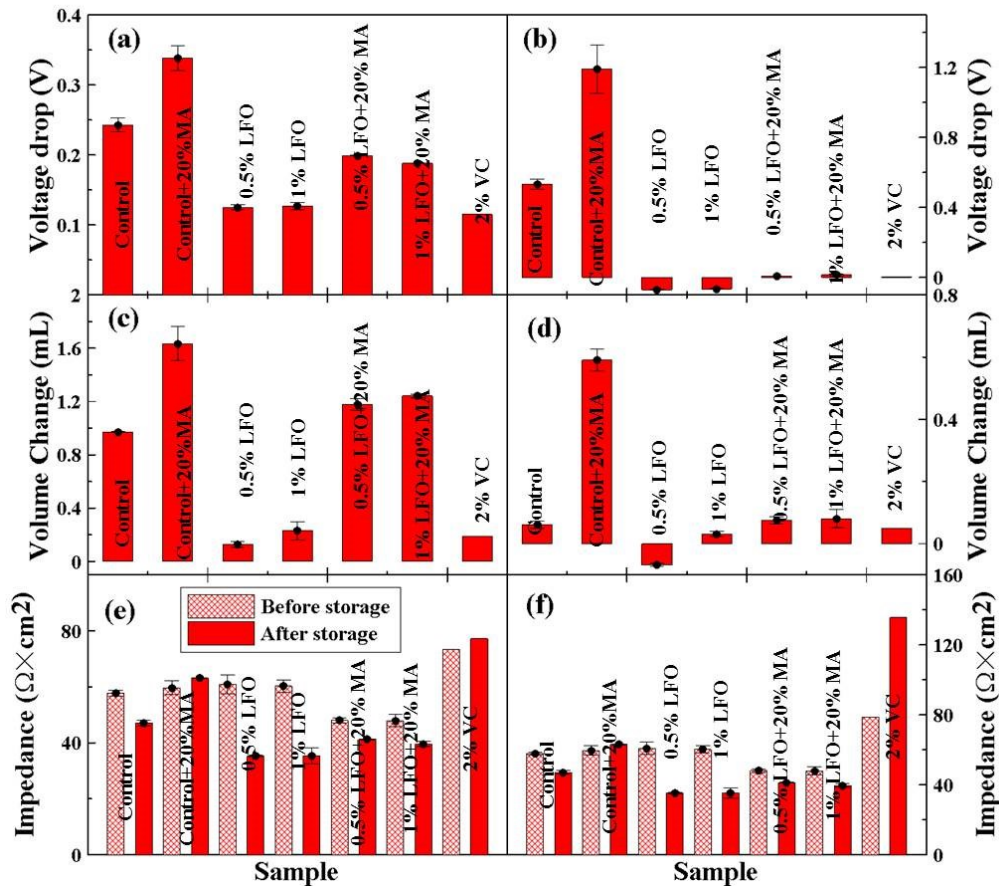


Figure 5.6 Summary of voltage drop at 4.4 V (a) and 2.5 V (b), cell volume change at 4.4 V (c) and 2.5 V (d), charge transfer impedance (diameter of “semicircle” in the Nyquist plot) before and after storage at 4.4 V (e) and 2.5 V (f) during 500 hour storage at 60°C for NMC532/graphite pouch cells with different electrolytes as indicated.  $\text{LiPO}_2\text{F}_2$  is called LFO in the Figure legend.

#### 5.2.4 The effect of $\text{LiPO}_2\text{F}_2$ on cell lifetime

In Figures 5.7a – 5.7c, the data points for cells with control electrolyte cannot be seen because they are off scale (Their CIE is too large to be seen on this graph). Figure 5.7 summarizes the CIE (a), fractional fade (b) and fractional charge endpoint capacity slippage (c) versus upper cut-off voltage of NMC532/graphite pouch cells during UHPC testing at 40°C with currents corresponding to C/20. Based on previous work [100], the fractional fade represents lithium loss due to SEI growth at the negative electrode and the fractional charge endpoint capacity slippage indicates electrolyte oxidation at the positive electrode. The relationship between fractional fade, fractional slippage and CE can be found in Section 3.5.

Figures 5.7a – 5.7c show that as the upper cut-off voltage increased the CIE and fractional charge end point capacity slippage increased while the fractional fade decreased. Cells with 2% VC, 0.5%  $\text{LiPO}_2\text{F}_2$  or 1%  $\text{LiPO}_2\text{F}_2$  show similar CIE, fractional fade and fractional charge end point capacity slippage at different upper cut-off voltages. With the addition of MA, the CIE, fractional fade and fractional charge end point capacity slippage increased dramatically. This suggests that there will be a penalty in cell lifetime when MA is used as a co-solvent in these cells with these additives.

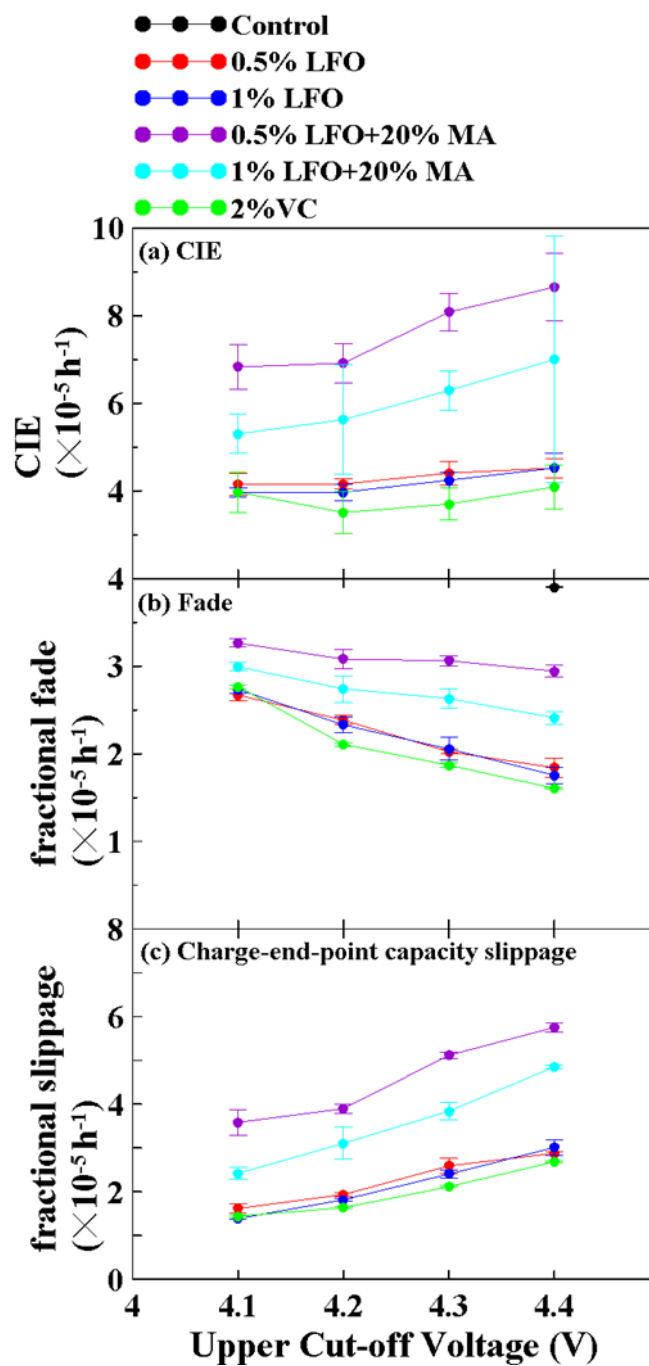


Figure 5.7 A summary of UHPC test results for NMC532/graphite pouch cells filled with different electrolytes as indicated after 16 cycles between 3 and upper cut-off voltages (4.1, 4.2, 4.3, 4.4 V) with currents corresponding to C/20 at 40°C including (a) coulombic inefficiency per hour, (b) fractional charge end-point capacity slippage per hour and (c) fractional discharge capacity fade per hour. The data shown is the average of two cells and the error bars were calculated as described in the text.  $\text{LiPO}_2\text{F}_2$  is called LFO in the Figure legend.

Figures 5.8a and 5.8c show the normalized discharge capacity versus cycle number for NMC532/graphite pouch cells containing control electrolyte, control electrolyte with 2% VC, 0.5% LiPO<sub>2</sub>F<sub>2</sub>, 1% LiPO<sub>2</sub>F<sub>2</sub> and control electrolyte with 20% MA plus different concentrations (0.5% and 1%) of LiPO<sub>2</sub>F<sub>2</sub> during CCCV cycling up to 4.3 V using currents that correspond to C/3 at 20°C and 40°C, respectively. The constant voltage cut-off current at the top of charge corresponded to C/20. Figures 5.8b and 5.8d show the difference between the average charge and the average discharge potential ( $\Delta V$ ) vs. cycle number corresponding to the cells shown in Figures 5.8a and 5.8c, respectively. The value of  $\Delta V$  is a measure of the polarization in the cells [146]. Compared to the other cells, cells with 1% LiPO<sub>2</sub>F<sub>2</sub> show the best capacity retention and the smallest rate of polarization increase during long-term cycling. The addition of MA decreased cell lifetime, which agrees with the results shown in Figure 5.7.

### **5.2.5 The effect of LiPO<sub>2</sub>F<sub>2</sub> on gas evolution at high voltage**

To further investigate the stability of LiPO<sub>2</sub>F<sub>2</sub>-containing electrolyte at the NMC532 positive electrode surface, cells with different electrolytes were charged and held at 4.1, 4.2, 4.3, 4.4 and 4.5 V for 20 h while the volumes of gas produced in the cells at high voltages were measured using an in-situ gas measurement setup [83]. The temperature of the cells during the experiment was 40.0°C.

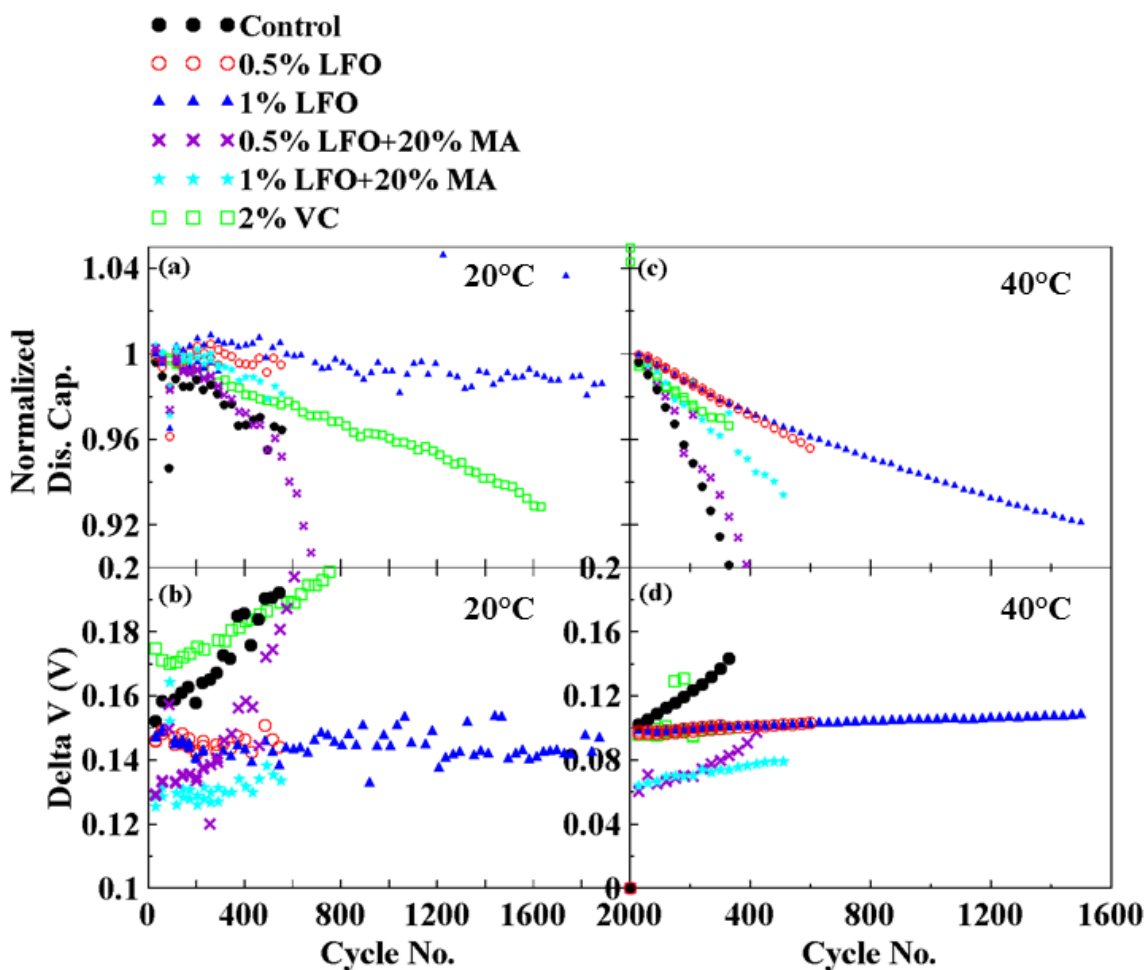


Figure 5.8 Normalized discharge capacity (panel a for 20°C, panel c for 40°C) and cell polarization (panel b for 20°C, panel d for 40°C) vs. cycle number for NMC532/graphite pouch cells with different electrolytes as indicated during long term CCCV cycling between 3 and 4.3 V using currents corresponding to C/3. A constant voltage step at the top of charge was applied until the current dropped below C/20. LiPO<sub>2</sub>F<sub>2</sub> is called LFO in the Figure legend.

Figure 5.9a shows the cell voltage versus time while Figure 5.9b shows the volume change of the NMC532/graphite cells versus time. Figure 5.9b shows that incorporating MA as a co-solvent resulted in larger amounts of gas production at high voltage.

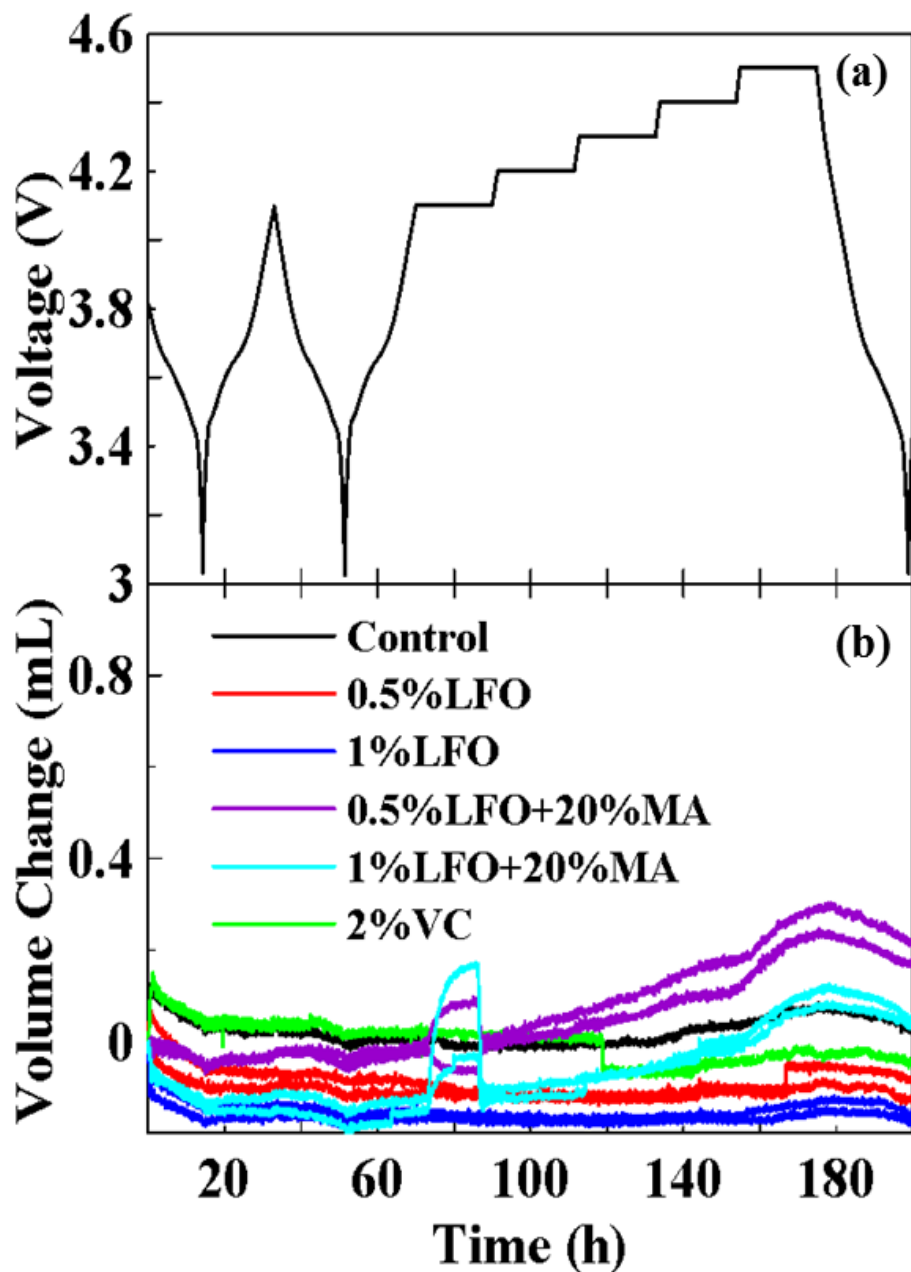


Figure 5.9 The in-situ gas evolution cell voltage as a function of time (a), and the gas volume of NMC532/graphite pouch cells with different electrolytes as a function of time (b).  $\text{LiPO}_2\text{F}_2$  is called LFO in the Figure legend.

### 5.2.6 The effect of $\text{LiPO}_2\text{F}_2$ at fast charge rate

In order to investigate the charging rate capability of NMC532/graphite pouch cells with

selected electrolytes, cells were cycled between 3 V and 4.1 V (Figures 5.10a and 5.10b) or 4.3 V (Figures 5.10c and 5.10d) using different charging rates at 20°C. The charging rates were 1C, 1.5C, 2C, 2.5C and 3C (30 cycles at each C-rate) while the discharging rate was always C/2. Figures 5.10a and 5.10c show the discharge capacity versus cycle number for NMC532/graphite pouch cells with different electrolytes during cycling. The discharge capacity fade behavior at high C-rate charge depended strongly on the electrolyte used. Based on previous work [159], MA helps improve high charging rate capability because of its low viscosity while LiPO<sub>2</sub>F<sub>2</sub> functioned well here by decreasing impedance from both positive and negative electrodes as shown in Figures 5.6e and 5.6f [160]. However, unwanted lithium plating eventually causes capacity fade at sufficiently high C-rates of charge even though cell impedance was decreased using LiPO<sub>2</sub>F<sub>2</sub>. This is consistent with the results reported by Liu et al. [160].

### **5.2.7 The effect of LiPO<sub>2</sub>F<sub>2</sub> on impedance growth during cycling**

Figures 5.11a and 5.11b show the normalized discharge capacity (a) and  $\Delta V$  (b) versus cycle number for the NMC532/graphite pouch cells undergoing the FRA cycling method. The cells containing control electrolyte and MA exhibited rapid discharge capacity fade compared to 1% LiPO<sub>2</sub>F<sub>2</sub> and 2% VC-containing cells. Cells with 1% LiPO<sub>2</sub>F<sub>2</sub> + 20% MA show less change in  $\Delta V$  compared to cells with 0.5% LiPO<sub>2</sub>F<sub>2</sub> + 20 % MA during cycling, which demonstrates that adding LiPO<sub>2</sub>F<sub>2</sub> decreases impedance growth.



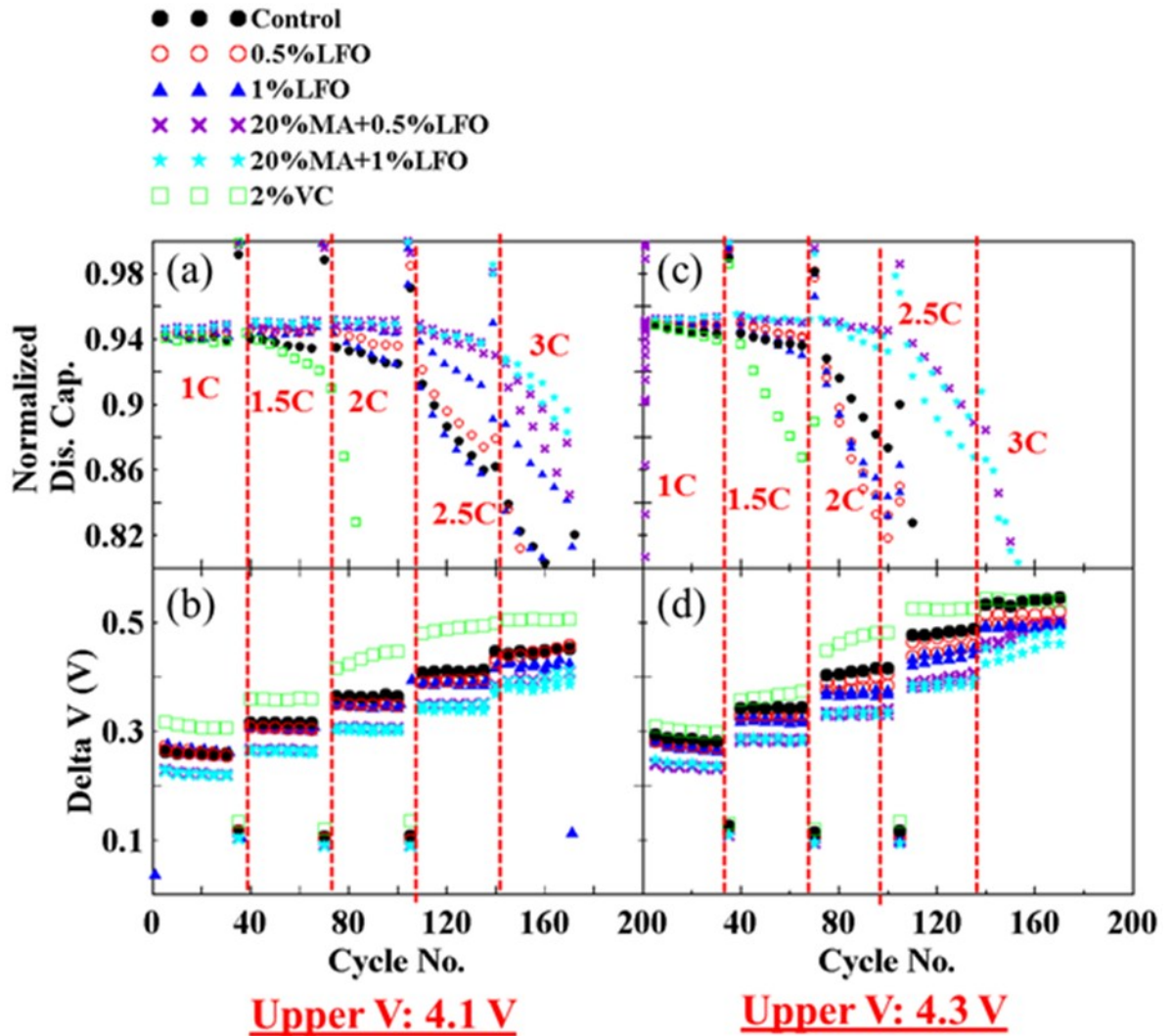


Figure 5.10 Normalized discharge capacity (panel a for 4.1 V, panel c for 4.3 V) and cell polarization (panel b for 4.1 V, panel d for 4.3 V) vs. cycle number for NMC532/graphite pouch cells with different electrolytes at 20°C during rate capability testing between 3 V and different upper cut-off voltages (4.1 or 4.3 V). The charging rate was changed every 30 cycles as indicated while discharging rate was always kept at C/2. LiPO<sub>2</sub>F<sub>2</sub> is called LFO in the Figure legend.

Figures 5.11c and 5.11d show the resistance,  $R_{ct}$ , at cycle 2 (a), cycle 68 (b), cycle 211 (c) and cycle 350 (d) as a function of voltage for the cells depicted in Figure 5.11a. Each

panel shows the resistance measured during the charge and discharge of the indicated FRA cycles for the cells containing the different electrolyte blends. All cells exhibited an increase in resistance as the voltage increased from 3.8 V to 4.4 V as reported by Nelson et al. [158]. Control electrolyte and 0.5%  $\text{LiPO}_2\text{F}_2$  + 20% MA-containing cells show a larger resistance at all voltages and as the cycle number increased. Cells with 1%  $\text{LiPO}_2\text{F}_2$  showed the lowest impedance at all states of charge with increasing cycle number. Cells with 2% VC showed relatively higher impedance at all states of charge and cycle numbers compared to the other cells.

### **5.2.8 The effect of $\text{LiPO}_2\text{F}_2$ on heat flow**

Isothermal microcalorimetry is a useful method to study parasitic reactions in lithium ion cells. The parasitic heat flow can be calculated as the average of the heat flows during charge and discharge, minus the heat flow due to cell overpotential at each voltage point when currents are sufficiently low [161,162].

In this study, the parasitic heat flow was calculated as the average heat flow minus the heat flow due to overpotential at each voltage point during charge-discharge cycles at 1.5 mA (about  $C/150$ ) between 4.0 V and upper cutoff voltages between 4.2 V and 4.4 V at 40°C. The isothermal calorimetry studies were used to try to optimize the concentration of  $\text{LiPO}_2\text{F}_2$  in the electrolyte.

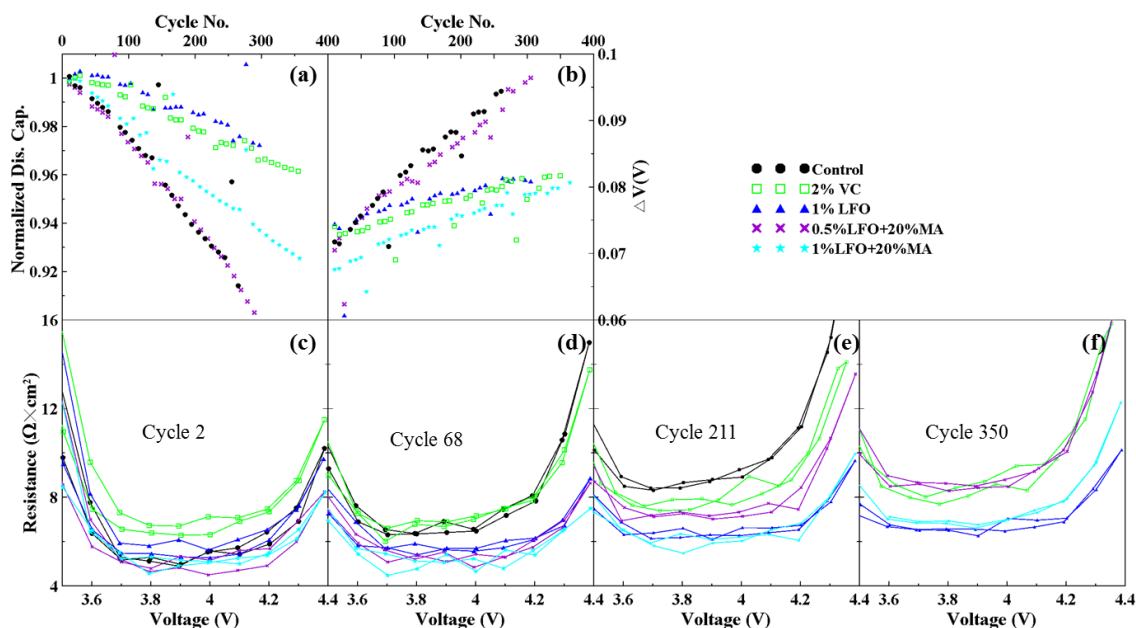


Figure 5.11 The normalized discharge capacity (a) and cell polarization (b) as a function of cycle number for NMC532/graphite pouch cells with different electrolytes undergoing cycling tests and FRA measurements according to the method reported by Nelson et al. [158] at 40°C. The combination of charge transfer resistance (both positive and negative electrodes) and resistance due to motion of ions through the SEI layers (both positive and negative electrodes),  $R_{ct}$ , as a function of voltage measured at different cycles (c – 2 cycles, d – 68 cycles, e – 211 cycles, f – 350 cycles) corresponding to the cells shown in (a, b) measured at 40°C.  $\text{LiPO}_2\text{F}_2$  is called LFO in the Figure legend.

Figures 5.12a to 5.12e show the calculated parasitic heat flow versus potential for cells containing different amounts of  $\text{LiPO}_2\text{F}_2$  (0.5%, 1% and 1.5%) or 2% VC in control electrolyte. Figures 5.12a to 5.12e follow in chronological order, i.e. the experiments reported in Figure 5.12a were performed first. Results for cycles to 4.3 V, 4.3 V a second time, 4.4 V and 4.4 V a second time shown in Figures 5.12b, 5.12c, 5.12d and 5.12e, respectively, were performed in sequence. Interphase layers on both the negative and positive electrode thicken to some degree during cycling so it is normal for the parasitic

heat flow to decrease in subsequent cycles. Therefore, the heat flow of the second cycle at the same voltage is lower than that of the first cycle. For example, the heat flow of the same electrolyte at 4.3 V in Figure 5.12c is lower than that of Figure 5.12b. Figures 5.12a to 5.12e show that 1%  $\text{LiPO}_2\text{F}_2$  is the “winner” (i.e. the lowest parasitic heat flow) in these sensitive tests.

Figure 5.12f shows the average parasitic heat flow of the cells with the indicated electrolytes during each cycle. Cells with 1%  $\text{LiPO}_2\text{F}_2$  had lower parasitic heat flow at all voltages compared to cells with 0.5%  $\text{LiPO}_2\text{F}_2$  or 1.5%  $\text{LiPO}_2\text{F}_2$ . Even though Figures 5.10 and 5.11c, 5.11d, 5.11e and 5.11f show clear advantages of cells with 1%  $\text{LiPO}_2\text{F}_2$  over cells with 2% VC, Figure 5.12f suggests that the parasitic heat flow of cells with 2% VC and cells with 1%  $\text{LiPO}_2\text{F}_2$  is similar.

### **5.3 Conclusions for Chapter 5**

$\text{LiPO}_2\text{F}_2$  alone cannot passivate the graphite electrode well, which resulted in EMC reduction on the graphite electrode. Although  $\text{LiPO}_2\text{F}_2$ , itself, was not reduced during formation in EC-based electrolyte, it was involved in the formation of SEI layer on both positive and negative electrode based on the results shown in Figure 5.5.

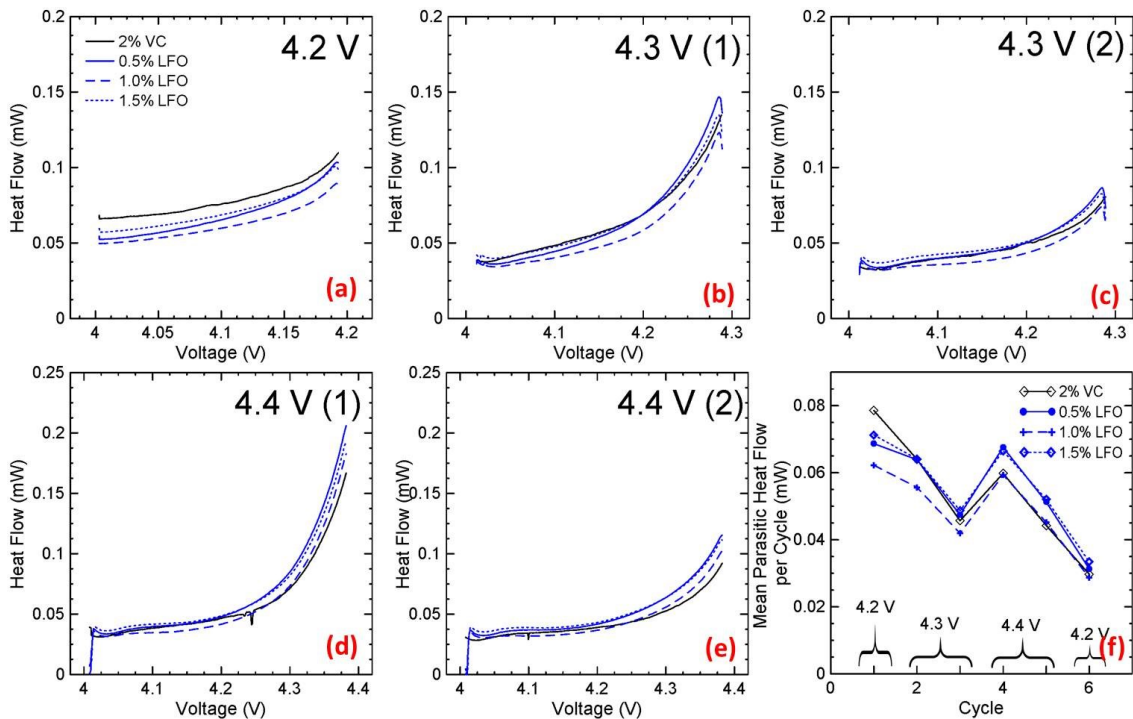


Figure 5.12 The parasitic heat flow of NMC532/graphite cells with different electrolytes as indicated. The data from panel a to panel e in Figure 5.12 follows a chronological order, i.e. Figure 5.12a was performed first. Cycles to 4.3 V, 4.3 V, 4.4 V and 4.4 V are shown in panels b, c, d and e, respectively. The average parasitic heat flow during each cycle is shown in Figure 5.12f for the cells described in Figures 12a-e.  $\text{LiPO}_2\text{F}_2$  is called LFO in the Figure legend.

In EC-based electrolyte, electrolytes containing  $\text{LiPO}_2\text{F}_2$  as an electrolyte additive have been demonstrated to be very useful in NMC532/graphite pouch cells. The use of  $\text{LiPO}_2\text{F}_2$  suppressed parasitic reaction rates between the charged electrodes and the electrolyte, improved cell cycle lifetime, decreased cell impedance at different states of charge and during long term cycling. Isothermal microcalorimetry showed that the optimum amount of  $\text{LiPO}_2\text{F}_2$  is around 1% in these cells. Overall, 1%  $\text{LiPO}_2\text{F}_2$  looks to be as effective or more effective than 2% VC as a general-purpose additive.

Methyl acetate (MA) is a useful co-solvent in NMC532/graphite pouch cells containing  $\text{LiPO}_2\text{F}_2$  in order to improve fast charging rate capability. However, the addition of MA causes a penalty in cell lifetime as suggested by UHPC results and demonstrated by long-term cycling results.

In the next chapter, a systematic study of the combination of  $\text{LiPO}_2\text{F}_2$  and other promising electrolyte additives will be presented.

**CHAPTER 6 COMBINATIONS OF LITHIUM DIFLUOROPHOSPHATE  
AND OTHER ELECTROLYTE ADDITIVES IN  
Li[Ni<sub>0.5</sub>Mn<sub>0.3</sub>Co<sub>0.2</sub>]O<sub>2</sub>/GRAPHITE POUCH CELLS**

The majority of this work was adapted from the following peer-reviewed article:

- L. Ma, Leah Ellis, S.L. Glazier, Xiaowei Ma and J.R. Dahn, Combination of LiPO<sub>2</sub>F<sub>2</sub> and Other Electrolyte Additives in Li(Ni<sub>0.5</sub>Mn<sub>0.3</sub>Co<sub>0.2</sub>)O<sub>2</sub>/graphite Pouch Cells, *J. Electrochem. Soc.* 165 (2018) A1718-A1724.

Lin Ma performed pouch cell preparation, gas evolution measurements, impedance measurements, storage testing and UHPC cycling testing. Xiaowei Ma filled the pouch cells. S.L. Glazier performed isothermal microcalorimetry testing. Leah Ellis performed XPS testing and XPS data analysis. Dr. J.R. Dahn provided guidance, participated in the interpretation of all the data and edited the paper. Lin Ma prepared the first draft of the manuscript mentioned above.

LiPO<sub>2</sub>F<sub>2</sub> is a useful electrolyte additive for Li-ion cells as shown in the last chapter. In this chapter, combinations of several selected additives and LiPO<sub>2</sub>F<sub>2</sub> were explored in NMC532/graphite pouch cells using high temperature storage testing (60°C), UHPC, EIS, isothermal microcalorimetry and long term charge-discharge cycling. Several useful additives to use in combination with LiPO<sub>2</sub>F<sub>2</sub>, were found, especially VC, DiFEC and FEC. These electrolyte additive combinations (e.g. LiPO<sub>2</sub>F<sub>2</sub> + FEC, LiPO<sub>2</sub>F<sub>2</sub> + VC, LiPO<sub>2</sub>F<sub>2</sub> + DiFEC) are effective in NMC532/graphite pouch cells since they were found

to improve CE, extend charge-discharge cycle lifetime, decrease parasitic heat flow and control impedance growth. The composition of the SEI on both positive and negative electrodes was examined by XPS when  $\text{LiPO}_2\text{F}_2$  was used with or without other selected electrolyte additives. The combination of  $\text{LiPO}_2\text{F}_2$  with other additives can improve the lifetime and performance of Li-ion cells.

## **6.1 Experimental**

### **6.1.1 The preparation of pouch cells**

Coated SC NMC532/graphite pouch cells were prepared according to the procedure described in Section 3.1.2. Two types of control electrolytes were used in this study. Control electrolyte A was 1.2 M  $\text{LiPF}_6$  in EC/EMC 3/7 (by weight). Control electrolyte B was 1.2 M  $\text{LiPF}_6$  in EC/DMC 3/7 (by weight). Control electrolyte A was used in storage testing, long-term cycling testing, XPS analysis and automated EIS measurements during charge-discharge cycling. Control electrolyte B was used for UHPC cycling and isothermal microcalorimetry testing. Electrolytes with additives or additive combinations were formulated by dissolving different amounts of VC,  $\text{LiPO}_2\text{F}_2$ , FEC, DiFEC, MEC, PBF, PPF, DTD, MMDS, LiBOB, LiDFOB and HDI in control electrolyte. Figure 6.1 shows chemical structures of all the electrolyte additives mentioned above.



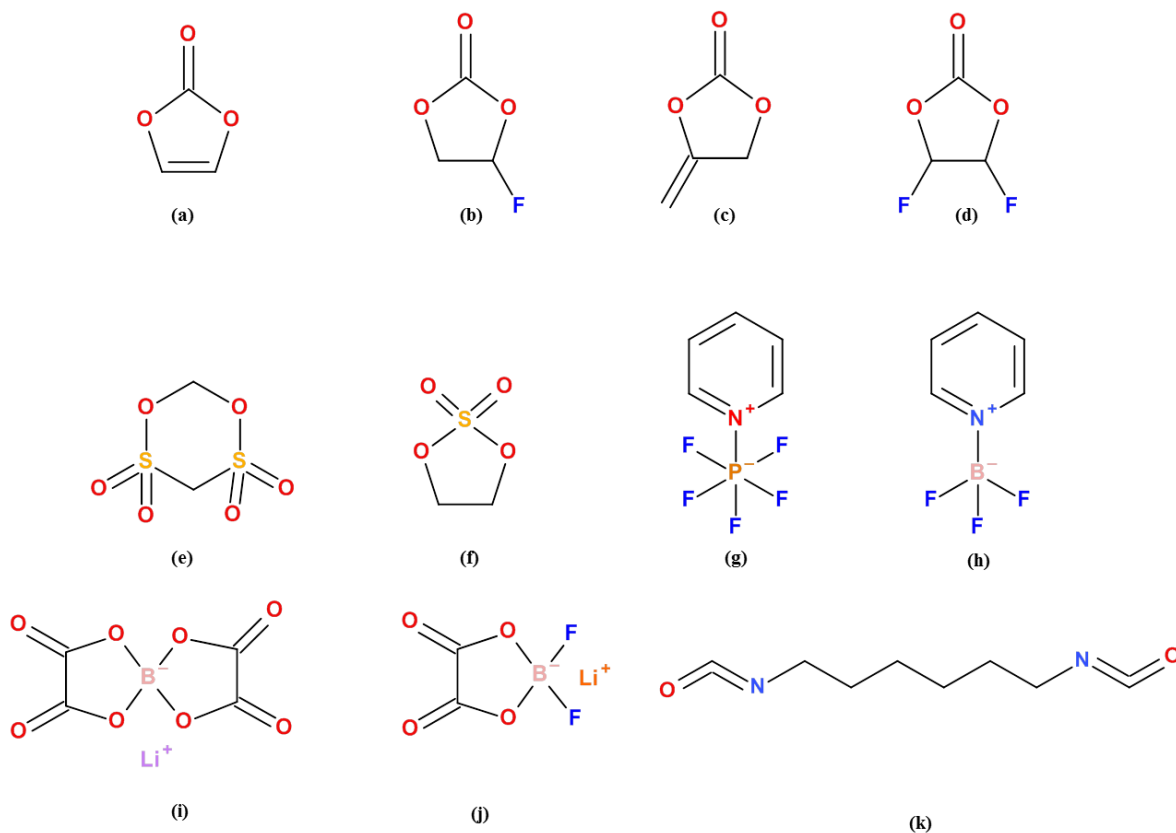


Figure 6.1 Chemical structures of the electrolyte additives used in this work: (a) VC, (b) FEC, (c) MEC, (d) DiFEC, (e) MMDS, (f) DTD, (g) PPF, (h) PBF, (i) LiBOB, (j) LiDFOB and (k) HDI.

### 6.1.2 EIS testing

See Section 5.1.2.

### 6.1.3 Charge-discharge cycling tests

The cells were charged and discharged at 77 mA ( $C/3$ ) between 3 and 4.3 V using CCCV mode with a Neware (Shenzhen, China) charger system at  $40. \pm 0.1^\circ\text{C}$ . The cut-off

current in CV mode was 11.5 mA (C/20).

External clamps were applied to all the pouch cells to ensure a firm stack pressure of about 25 KPa even if gas was produced during cycling. The gas, if produced, was forced to the edges of the pouch due to the action of the clamps.

#### **6.1.4 Storage testing**

See Section 5.1.4.

#### **6.1.5 XPS for surface analysis**

See Section 5.1.6.

#### **6.1.6 Isothermal microcalorimetry tests**

See Section 5.1.7.

#### **6.1.7 UHPC tests**

See Section 5.1.8.

#### **6.1.8 Automated EIS measurements during charge-discharge cycling**

See Section 5.1.9.

## 6.2 Results and discussion

### 6.2.1 The effect of $\text{LiPO}_2\text{F}_2$ -containing electrolyte additive combinations on storage testing

Figure 6.2 shows a summary of (6.2a-6.2b) voltage drop and (6.2c-6.2d) impedance change of NMC532/graphite pouch cells containing control electrolyte, control electrolyte with different concentrations of electrolyte additives or additive combinations during storage testing at  $60^\circ\text{C}$ . Measurements for two cells were averaged to obtain each data point in Figure 6.2 and the error bars are the difference between the two results. The starting voltage for Figures 6.2a and 6.2c was 4.4V while the starting voltage for Figures 6.2b and 6.2d was 2.5V. The voltage drop during the storage testing suggests the occurrence of parasitic reactions at the surface of the positive electrode (4.4 V) and the negative electrode (2.5 V), respectively [154]. The addition of VC, FEC, DiFEC and PPF into the  $\text{LiPO}_2\text{F}_2$ -containing cells leads to smaller voltage drops during storage compared to the other cells when the starting voltage was 4.4 V. This suggests that the combinations of  $\text{LiPO}_2\text{F}_2$  with VC, FEC, DiFEC and PPF are promising for suppressing parasitic reactions on the positive electrode at high voltage.

Figures 6.2c and 6.2d show a summary of the impedance before and after storage testing. All the impedance spectra were measured at 3.8 V and at  $10.0^\circ\text{C}$ . The impedance reported here is the diameter of the semi-circle (in the Nyquist plot) that arises from the sum of the charge-transfer resistances and the transport of lithium ions through the SEI

layers at both the positive and negative electrodes [79]. All the additive combinations showed decreased impedance after high temperature storage testing when the starting voltage was 4.4 V. The addition of MEC, MMDS and HDI resulted in higher impedance compared to other additive combinations during storage testing when the starting voltage was 2.5 V.

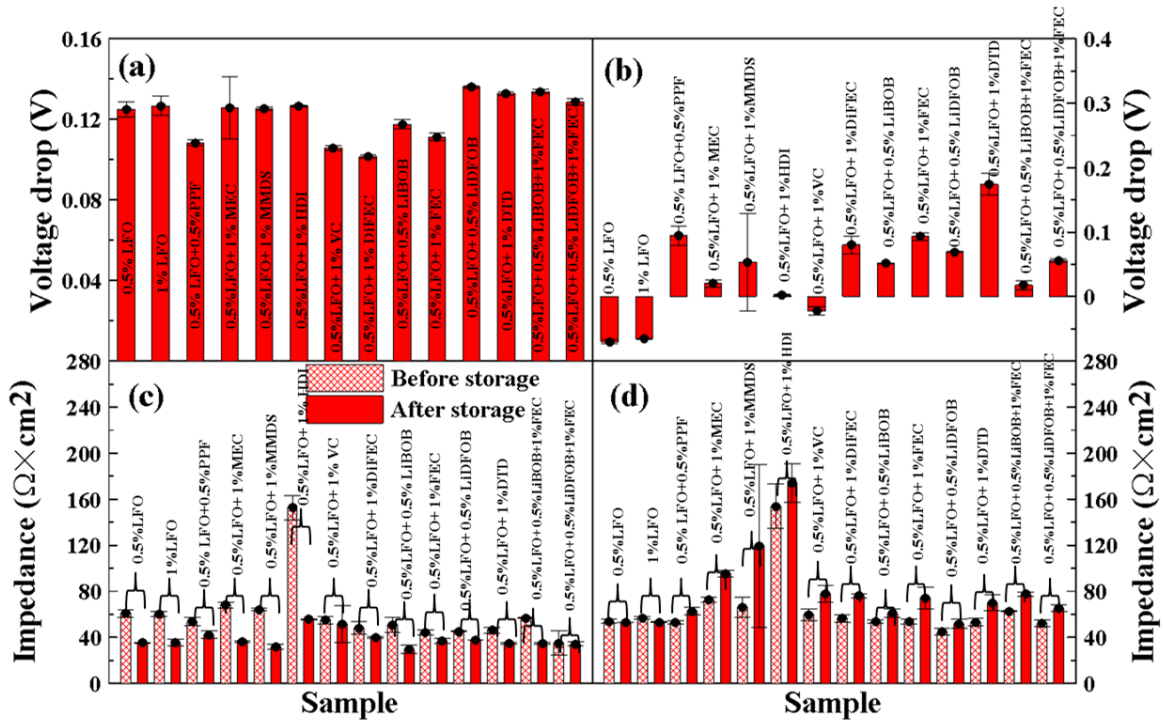


Figure 6.2 Summary of voltage drop at 4.4 V (a) and 2.5V (b) impedance change at 4.4 V (c) and 2.5 V (d) during 500 hour storage at 60°C for NMC532/graphite pouch cells with different electrolytes as indicated.  $\text{LiPO}_2\text{F}_2$  is called LFO in the Figure legend.

## 6.2.2 The effect of $\text{LiPO}_2\text{F}_2$ -containing electrolyte additive combinations on electrode surface chemistry, cell heat flow and cell lifetime

Figure 6.3 summarizes CIE (a), fractional fade (b) and fractional charge-end-point

capacity slippage (c) versus upper cut-off voltage of NMC532/graphite pouch cells during UHPC testing at 40°C with a current corresponding to C/20. The explanation of CIE, fractional fade and fractional charge-end-point capacity slippage can be found in Section 3.5. Generally, lower CIE, lower fractional fade and lower fractional charge-end-point capacity slippage result in lithium ion cells with longer lifetime [101].

In Figures 6.3a-6.3c, generally CIE and fractional charge-end-point capacity slippage increased while fractional fade decreased with increasing of upper cut-off voltage. These phenomena are widely observed in NMC/graphite cells as a function of upper cut-off voltage [163]. Except for 1% LiPO<sub>2</sub>F<sub>2</sub> + 0.5% PBF, cells with all the other additive combinations yielded smaller CIE, fractional fade and fractional charge-end-point capacity slippage than 1% LiPO<sub>2</sub>F<sub>2</sub> alone at the different upper cut-off voltages. This suggests a synergetic effect of these additive combinations on cell lifetime.

Figure 6.4 summarizes the impedance changes for NMC532/graphite pouch cells with different electrolytes during UHPC cycling. LiPO<sub>2</sub>F<sub>2</sub> controls impedance growth on both positive side and negative electrodes during cell cycling [160]. However, the combination of VC with LiPO<sub>2</sub>F<sub>2</sub> results in an increase of impedance before and after UHPC cycling. The other selected additive combinations show similar impedance performance compared to 1% LiPO<sub>2</sub>F<sub>2</sub> alone.

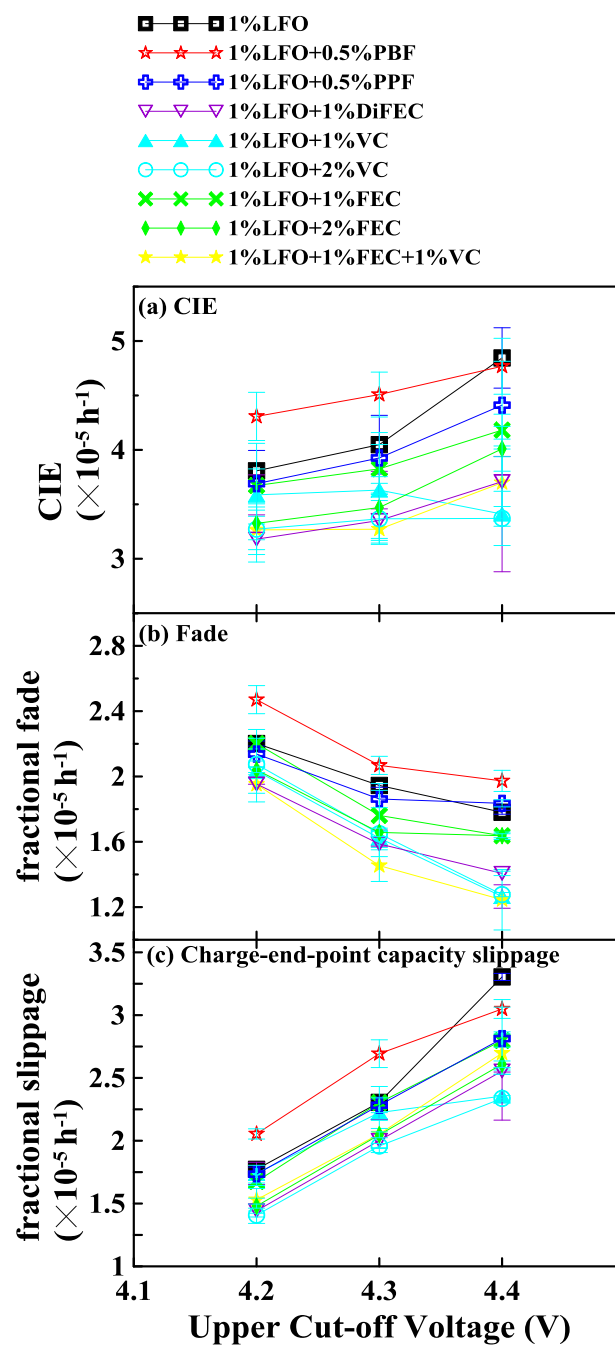


Figure 6.3 A summary of UHPC testing results for NMC532/graphite pouch cells filled with different electrolytes as indicated during 16 cycles between 3.0 V and different upper cut-off voltages (4.2, 4.3, 4.4 V). Cells were tested with currents corresponding to C/20 at 40°C including (a) coulombic inefficiency per hour (b) fractional discharge capacity fade per hour and (c) fractional charge end-point capacity slippage per hour. The data shown is the average of two cells and the error bars are the difference between the individual measurements.  $\text{LiPO}_2\text{F}_2$  is called LFO in the Figure legend.

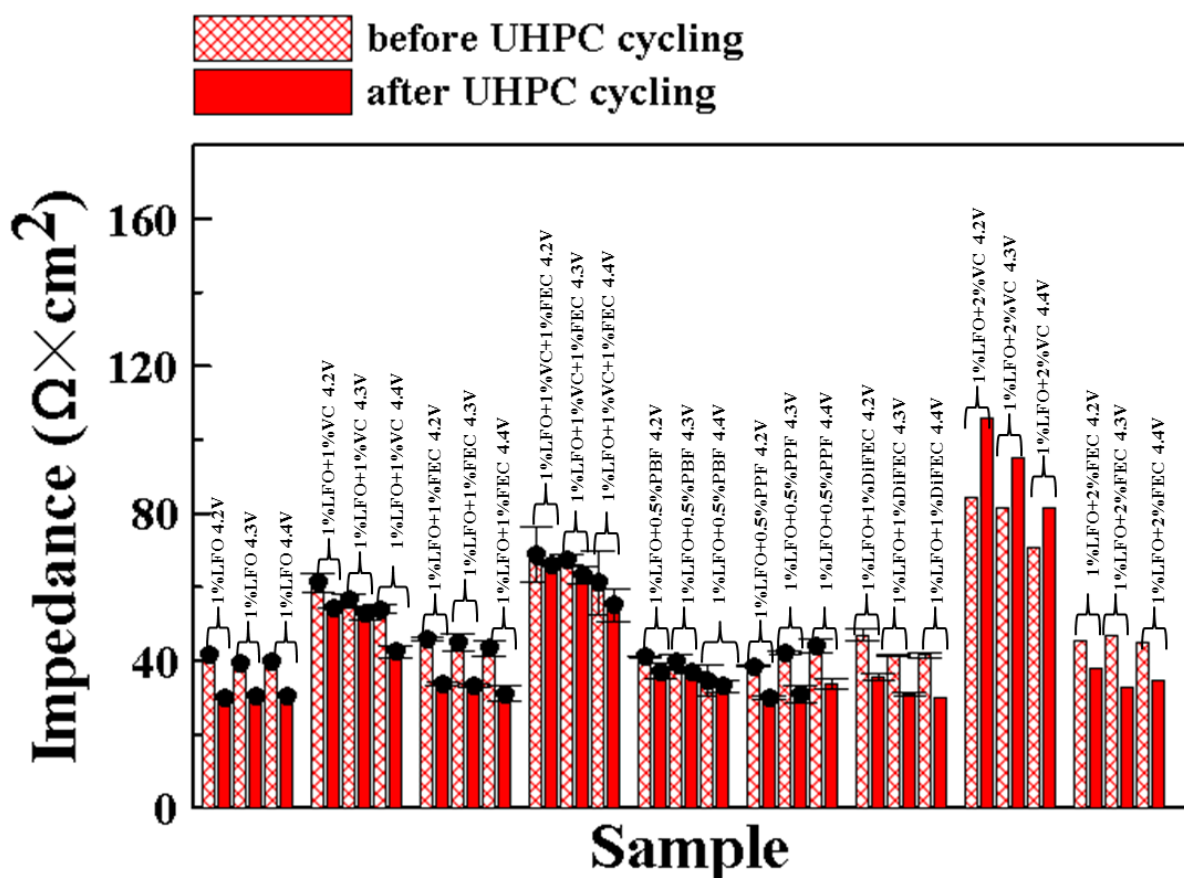


Figure 6.4 Summary of impedance before and after 16 UHPC cycles between 3.0 and various upper cut-off voltages (4.2, 4.3, 4.4 V). Cells were tested with currents corresponding to C/20 at 40°C for NMC532/graphite pouch cells with different electrolytes as indicated. LiPO<sub>2</sub>F<sub>2</sub> is called LFO in the Figure legend.

Figure 6.5 shows XPS spectra of A) negative and B) positive electrodes from cells that were formed without electrolyte additives, with 1% LiPO<sub>2</sub>F<sub>2</sub>, 1% LiPO<sub>2</sub>F<sub>2</sub> + 2% FEC and 1% LiPO<sub>2</sub>F<sub>2</sub> + 2% VC.

In Section 5.2.2, it was shown that the addition of 1% LiPO<sub>2</sub>F<sub>2</sub> to the electrolyte significantly increases the amount of inorganic SEI species—LiF (685 eV), phosphates

(~134 eV) and fluorophosphates (~136 eV and 687 eV)—on both the negative and positive electrodes [164]. The addition of 2% FEC or VC to electrolyte containing 1%  $\text{LiPO}_2\text{F}_2$  further increases the amount of these inorganic species (LiF, phosphate and fluorophosphates) on both electrodes. This is evidenced by the increased peak area in the phosphate regions, and by the relative atomic ratios shown in Table 6.1. The additional inorganic species brought about by  $\text{LiPO}_2\text{F}_2$  and VC appear to thicken the positive electrode SEI, evidenced by a smaller NMC lattice oxygen peak at ~529 eV. With the addition of  $\text{LiPO}_2\text{F}_2$  to control electrolyte, the negative electrode SEI was thinner, as it appeared to prevent the formation of  $\text{Li}_2\text{CO}_3$  (~290 eV). With the addition of FEC and VC, the SEI of the negative electrode thickens, evidenced by the smaller lithiated graphite peak at 284 eV. It is possible that  $\text{LiPO}_2\text{F}_2$ , VC and FEC benefit cell performance by increasing the amount of inorganic species, such as LiF, in the SEIs of both electrodes. DFT studies [165] suggest that a 2 nm layer of LiF is sufficient to block electron tunneling from a lithium electrode, while 3 nm of  $\text{Li}_2\text{CO}_3$  is required to block electron tunnelling. This suggests that LiF is more passivating, and perhaps a more desirable SEI component. It is also possible that FEC and VC benefit cell performance by increasing the thickness of the negative electrode SEI, since the thickness of the SEI is sometimes correlated to the degree of passivation [166] The relationship between an SEI's physical properties (chemical composition, thickness and morphology) to its performance (passivation and impedance) is complicated, and not well-understood [167].



Empirical observation of SEI chemistry in cells with varying degrees of performance may contribute to the understanding of the SEI and its effect on cell performance.

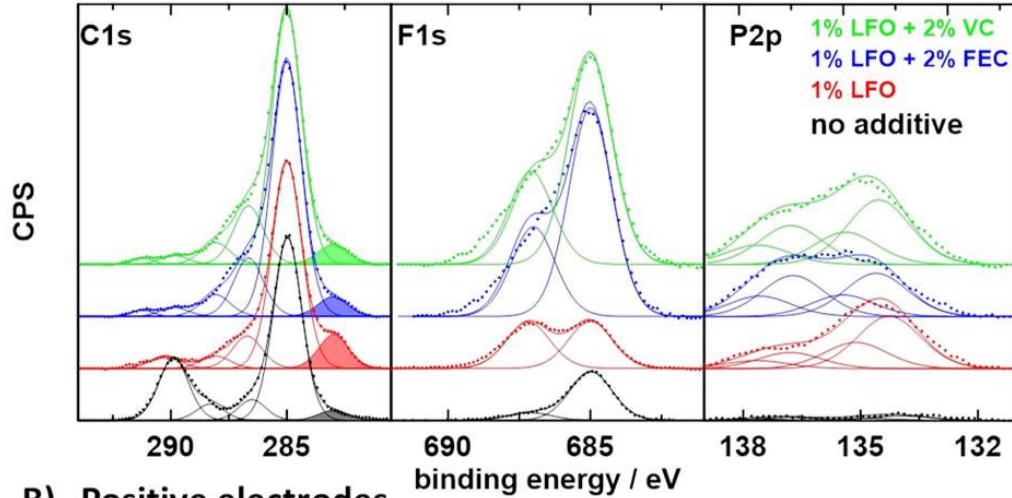
Table 6.1 Atomic ratios of the elements on the surfaces of negative and positive electrodes cycled without additives, 1% LiPO<sub>2</sub>F<sub>2</sub>, 1% LiPO<sub>2</sub>F<sub>2</sub> + 2%FEC and 1% LiPO<sub>2</sub>F<sub>2</sub> + 2%VC.

		<b>F</b>	<b>O</b>	<b>C</b>	<b>P</b>	<b>Li</b>
<i>Negative</i>	<b>No additive</b>	4.3 ± 0.2	31.8 ± 0.4	33.4 ± 0.4	0.26 ± 0.07	30.3 ± 0.6
	<b>1% LiPO<sub>2</sub>F<sub>2</sub></b>	9.4 ± 0.2	19.6 ± 0.4	47.5 ± 0.6	3.22 ± 0.09	20.2 ± 0.8
	<b>1%LiPO<sub>2</sub>F<sub>2</sub>+2% FEC</b>	21.6 ± 0.4	13.3 ± 0.2	41.2 ± 0.6	2.8 ± 0.1	21 ± 1
	<b>1%LiPO<sub>2</sub>F<sub>2</sub>+2% VC</b>	19.5 ± 0.4	16.3 ± 0.3	37.4 ± 0.5	3.1 ± 0.1	23.8 ± 0.9
<i>Positive</i>	<b>No additive</b>	16.1 ± 0.4	22.1 ± 0.4	57.1 ± 0.7	0.4 ± 0.2	4.2 ± 0.8
	<b>1% LiPO<sub>2</sub>F<sub>2</sub></b>	18.6 ± 0.5	20.2 ± 0.4	56.6 ± 0.8	1.3 ± 0.1	3.5 ± 0.8
	<b>1%LiPO<sub>2</sub>F<sub>2</sub>+2% FEC</b>	28.2 ± 0.6	17.4 ± 0.4	43 ± 1	1.4 ± 0.2	10 ± 1
	<b>1%LiPO<sub>2</sub>F<sub>2</sub>+2% VC</b>	24.2 ± 0.5	16.8 ± 0.3	48 ± 0.7	1.2 ± 0.2	9.7 ± 0.9

In this work, isothermal microcalorimetry was used to investigate the heat flow of parasitic reactions in lithium ion cells. The parasitic heat flow was calculated using the methods outlined in Section 5.2.8 during charge-discharge cycles at 1.5 mA between 4.0 V and upper cutoff voltages between 4.2 V and 4.4 V at 40°C. The isothermal microcalorimetry studies were used to investigate the effect of the combinations of

additives with  $\text{LiPO}_2\text{F}_2$ .

### A) Negative electrodes



### B) Positive electrodes

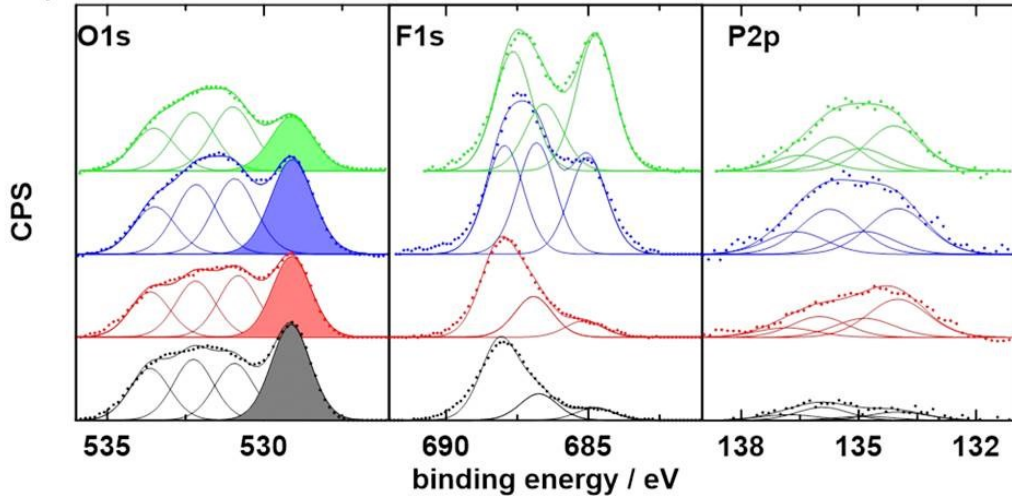


Figure 6.5 Regions of the XPS spectra of A) negative electrodes and B) positive electrodes that underwent formation in cells with no additive (black), 1%  $\text{LiPO}_2\text{F}_2$  (red), 1%  $\text{LiPO}_2\text{F}_2$  + 2% FEC (blue), and 1%  $\text{LiPO}_2\text{F}_2$  + 2% VC (green).  $\text{LiPO}_2\text{F}_2$  is called LFO in the Figure legend.

Figures 6.6a-6.6f show the measured parasitic heat flow versus potential of cells containing different electrolytes as labeled in the legend. Figures 6.6a-6.6f follow a chronological order, i.e. Figure 6.6a was performed first. Cycles to 4.3 V, 4.3 V, 4.4 V, 4.4

V and 4.2 V shown in Figures 6.6b, 6.6c, 6.6d, 6.6e and 6.6f, respectively, were performed in sequence in order to determine to which extent the exposure to high voltage had damaged the electrolyte. Figures 6.6a-6.6f show that the addition of VC or FEC into LiPO<sub>2</sub>F<sub>2</sub>-containing electrolyte decreases the parasitic heat flow and hence should improve cell lifetime.

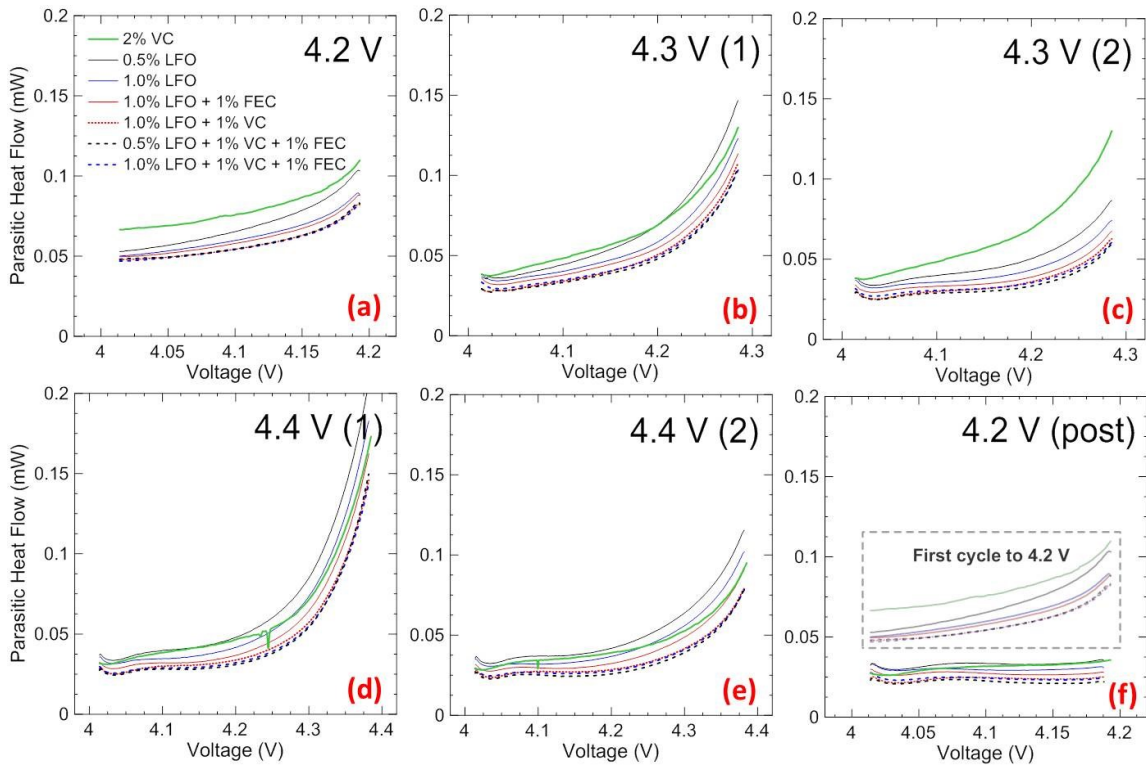


Figure 6.6 The calculated parasitic heat flow of NMC532/graphite cells with different electrolytes as indicated. The data from a to f in Figure 6.6 follows a chronological order, ie. Figure 6.6a was performed first. Cycles from 3.9 V to 4.3 V, 4.3 V, 4.4 V, 4.4 V and 4.2 V are shown in Figures 6.6b, 6.6c, 6.6d, 6.6e and 6.6f, respectively. LiPO<sub>2</sub>F<sub>2</sub> is called LFO in the Figure legend.

Figure 6.7 shows the average parasitic heat flow of cells with various electrolytes during

each cycle.  $\text{LiPO}_2\text{F}_2$  has been shown to be very useful for depressing the parasitic heat flow in Li-ion cells as shown in Section 5.2.8. When VC or FEC are combined with  $\text{LiPO}_2\text{F}_2$ , cells with such electrolytes show smaller parasitic heat flow at all voltages compared to cells with  $\text{LiPO}_2\text{F}_2$  alone.

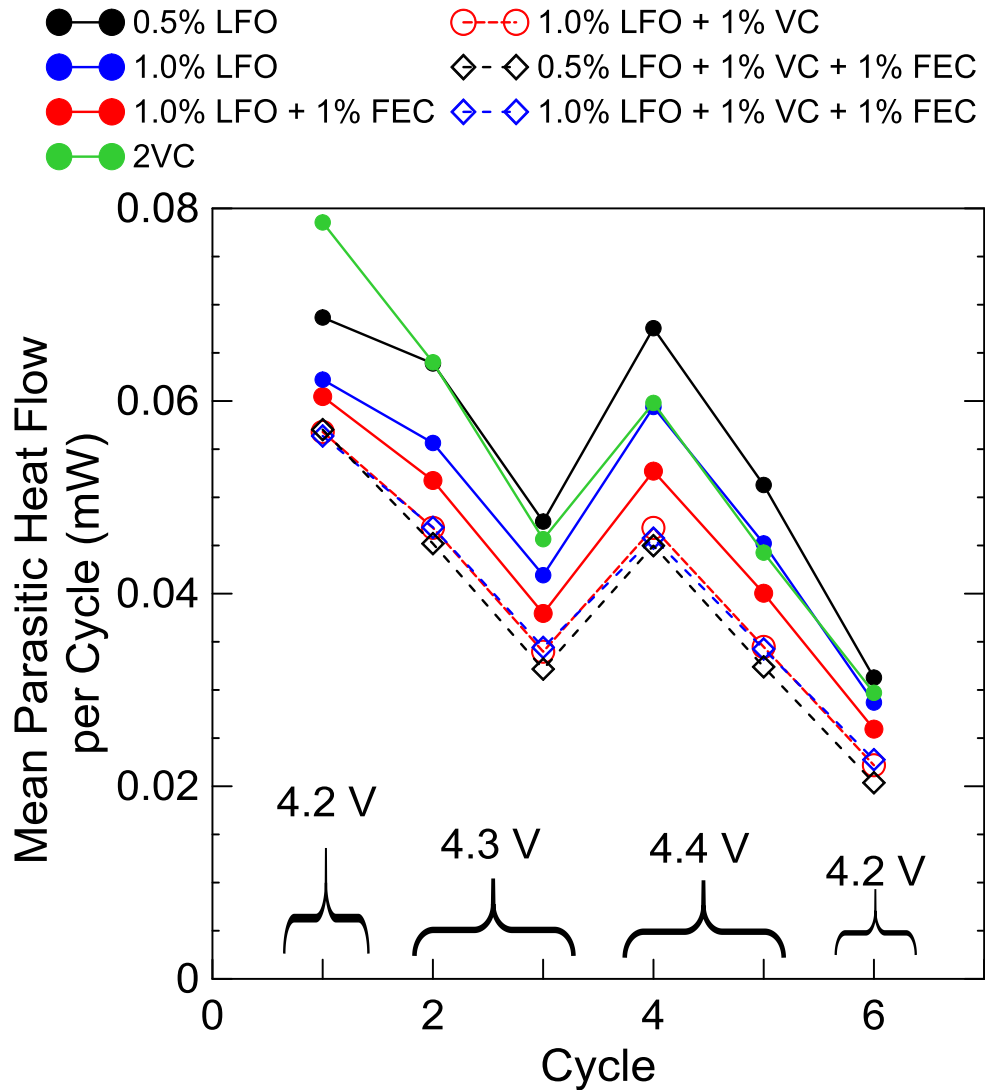


Figure 6.7 The average parasitic heat flow during each cycle for cells shown in Figures 6.6a-f is plotted in Figure 6.7.  $\text{LiPO}_2\text{F}_2$  is called LFO in the Figure legend.

Figure 6.8a shows the normalized discharge capacity versus cycle number for NMC532/graphite pouch cells at 40°C containing different electrolytes during CCCV cycling up to 4.3 V with currents that corresponding to C/3. The constant voltage cut-off current corresponded to C/20. Figure 6.8b shows the normalized difference between the average charge and the average discharge potential ( $\Delta V\%$ ) vs. cycle number corresponding to the cells shown in Figure 6.8a. The value of  $\Delta V\%$ , starting at 100% for the C/3 cycles of each cell, is a measure of the polarization in the cells [146]. Compared to cells with only  $\text{LiPO}_2\text{F}_2$ , cells with additive combinations show better capacity retention during long-term cycling.

### **6.2.3 The effect of $\text{LiPO}_2\text{F}_2$ -containing electrolyte additive combinations on impedance growth during cycling**

Figures 6.9a-6.9b show the normalized discharge capacity (a) and  $\Delta V$  (b) versus cycle number for NMC532/graphite pouch cells with different electrolytes during the FRA cycling method, respectively. All cells showed similar small rates of capacity loss per cycle (slope of the data in Figure 6.9a) while cells with 1%  $\text{LiPO}_2\text{F}_2$  + 2% DiFEC and 1%  $\text{LiPO}_2\text{F}_2$  + 2% FEC showed the smallest rates of polarization ( $\Delta V$ ) increase in Figure 6.9b. Cells with 1%  $\text{LiPO}_2\text{F}_2$  + 2% VC and 1%  $\text{LiPO}_2\text{F}_2$  + 1% FEC + 1% VC showed larger increases in polarization than cells with  $\text{LiPO}_2\text{F}_2$  alone. This indicates that the combination of VC and  $\text{LiPO}_2\text{F}_2$  will result in more impedance growth than  $\text{LiPO}_2\text{F}_2$  alone.

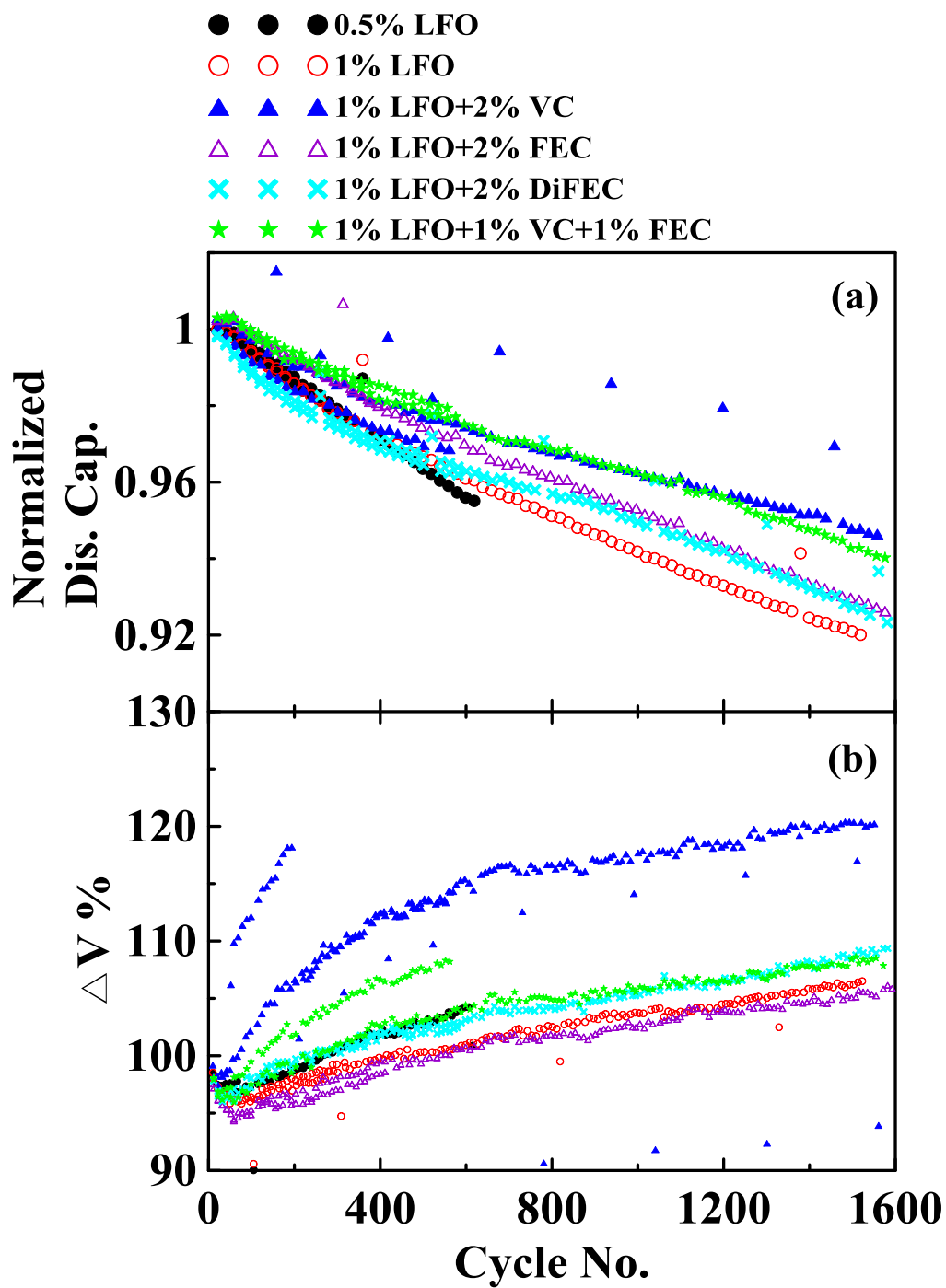


Figure 6.8 Normalized discharge capacity (a) and normalized cell polarization (difference between average charge and average discharge voltage ( $\Delta V$  %)) (b) vs. cycle number for NMC532/graphite pouch cells with different electrolytes as indicated during long term CCCV cycling between 3 and 4.3 V using currents corresponding to C/3 at 40°C. A constant voltage hold at the top of charge was applied until the current dropped below C/20.  $\text{LiPO}_2\text{F}_2$  is called LFO in the Figure legend.

Figures 6.9c-6.9e show the resistance (diameter of the semi-circle in the Nyquist plot of the impedance spectrum),  $R_{ct}$ , at cycle 2 (6.9c), cycle 100 (6.9d) and cycle 200 (6.9e) as a function of voltage for the corresponding cells in Figures 6.9a and 6.9b. The impedance spectra were measured at 40°C during the C/20 cycle that occurred sequentially after every 10 C/3 cycles. Each panel shows  $R_{ct}$  measured during each charge and discharge of the FRA cycle for the cells containing different electrolyte additive combinations. In all cases,  $R_{ct}$  increases at high and low voltages as has been observed before [158]. As the cycle number increases the value of  $R_{ct}$  at a particular voltage increases slowly. Careful examination of Figures 6.9c-6.9e shows that  $R_{ct}$  increases most slowly with cycle number for the cells with 1% LiPO<sub>2</sub>F<sub>2</sub> + 2% FEC and 1% LiPO<sub>2</sub>F<sub>2</sub> + 2% DiFEC, in agreement with Figure 6.9b. Similarly Figures 6.9c-6.9e show that  $R_{ct}$  increases most rapidly with cycle number for the cells with 1% LiPO<sub>2</sub>F<sub>2</sub> + 2%VC and 1% LiPO<sub>2</sub>F<sub>2</sub> + 1% VC + 1% FEC, in agreement with Figure 6.9b.

### **Summary of results:**

To give readers a better appreciation of the method used to down-select the initial set of additives to the final “preferred” set, the following summary is provided. Based on the results in Figures 6.2-6.4 and 6.6-6.9 the following summary can be made

1. Based on Figures 6.2a, 6.2c and 6.2d the co-additives PPF, FEC, DiFEC and VC were selected for further evaluation. Cells containing co-additives HDI, MEC, DTD,

LiBOB, LiDFOB and MMDS had larger voltage drops during 4.4 V storage tests and/or had large impedance after the storage period. These were not evaluated further.

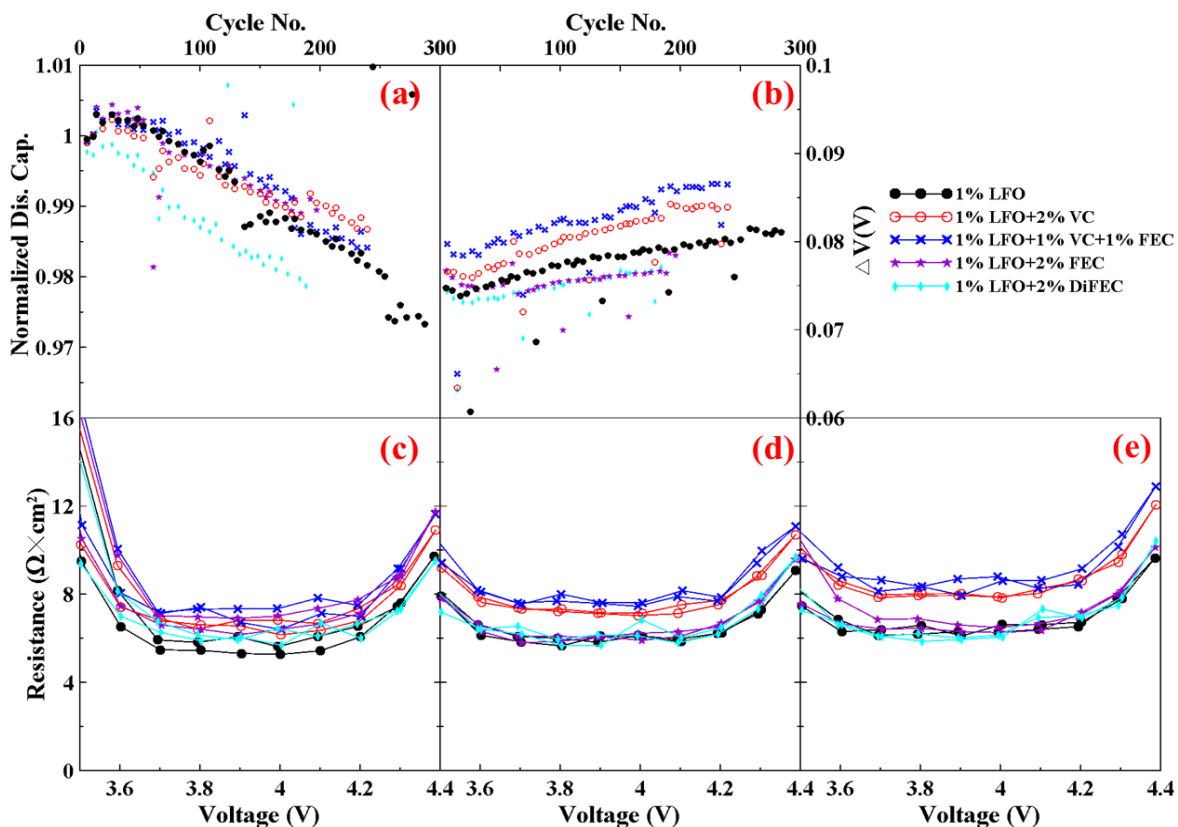


Figure 6.9 The normalized discharge capacity (a) and cell polarization (difference between average charge and average discharge voltage ( $\Delta V$ )) (b) as a function of cycle number for NMC532/graphite pouch cells with different electrolytes undergoing cycling tests and simultaneous EIS measurements according to the FRA method reported by Nelson et al. [158] at 40°C. The combination of charge transfer resistance (both positive and negative electrodes) and resistance due to motion of ions through the SEI layers (both positive and negative electrodes),  $R_{ct}$ , as a function of voltage at different cycles: 2 cycles c); 100 cycles d); 200 cycles e) for the the cells shown in panels a) and b) measured at 40°C.  $\text{LiPO}_2\text{F}_2$  is called LFO in the Figure legend.

2. Based on Figure 6.3, the co-additives PPF and PBF, along with  $\text{LiPO}_2\text{F}_2$  yielded cells with similar CE, charge endpoint capacity slippage and capacity fade to cells with only  $\text{LiPO}_2\text{F}_2$ . Therefore PPF and PBF were eliminated from further evaluation.



3. Based on Figures 6.3, 6.4, 6.6 and 6.7, the co-additives, 2% VC, 2% FEC, 1% DiFEC as well as 1% VC + 1% FEC were identified as combinations that when combined with 1% LiPO<sub>2</sub>F<sub>2</sub> should yield long lived cells. Figure 6.4, however identified that VC, in combination with LiPO<sub>2</sub>F<sub>2</sub> led to impedance increases compared with LiPO<sub>2</sub>F<sub>2</sub> alone, while the co-additives FEC and DiFEC did not.

4. Figure 6.8 showed that the additive combinations identified in #3 above did, in fact, yield cells with better capacity retention than cells with only 1% LiPO<sub>2</sub>F<sub>2</sub>.

5. Figure 6.8b and Figure 6.9 showed that impedance and impedance growth during long term cycling at 40°C were worse for cells with 1% LiPO<sub>2</sub>F<sub>2</sub> + 2% VC and 1% LiPO<sub>2</sub>F<sub>2</sub> + 1% VC + 1% FEC than for cells with 1% LiPO<sub>2</sub>F<sub>2</sub> + 2% FEC and 1% LiPO<sub>2</sub>F<sub>2</sub> + 2% DiFEC. These observations mirror the conclusions based on Figure 6.4.

6. The microcalorimeter experiments in Figures 6.6 and 6.7 point to the benefits of VC as the co-additive to use with LiPO<sub>2</sub>F<sub>2</sub> because the parasitic heats are smaller in cells that have VC and LiPO<sub>2</sub>F<sub>2</sub>.

Based on the summary above, the systems 1% LiPO<sub>2</sub>F<sub>2</sub> + 2% FEC, 1% LiPO<sub>2</sub>F<sub>2</sub> + 2% DiFEC and 1% LiPO<sub>2</sub>F<sub>2</sub> + 1% VC + 1% FEC look to be excellent choices for additives in these NMC532/graphite cells designed for 4.3 V operation. The latter ternary combination may give longer lifetime than the two binaries based on the

microcalorimetry results. However, the two binaries show lower impedance, less impedance growth and will be more suitable for high rate cells.

### **6.3 Conclusions for Chapter 6**

Electrolytes containing  $\text{LiPO}_2\text{F}_2$  as an electrolyte additive are especially useful in NMC532/graphite pouch cells [164]. The work in this thesis focused on studying NMC532/graphite cells having electrolytes containing combinations of  $\text{LiPO}_2\text{F}_2$  and other electrolyte additives. Combinations of  $\text{LiPO}_2\text{F}_2$  and preferred electrolyte additives (e.g. VC, FEC, DiFEC) dramatically suppressed parasitic reaction rate between electrodes and electrolytes, decreased parasitic reaction heat flow, extended cell cycle lifetime and controlled cell impedance growth during cycling. Electrolytes with 1%  $\text{LiPO}_2\text{F}_2$  + 2% FEC, 1%  $\text{LiPO}_2\text{F}_2$  + 2% DiFEC or 1%  $\text{LiPO}_2\text{F}_2$  + 1% VC + 1% FEC look to be excellent choices for these NMC532/graphite cells designed for 4.3 V operation.

It is beyond the scope of this work to report the mechanisms of the synergistic action of  $\text{LiPO}_2\text{F}_2$  and other electrolyte additives in NMC532/graphite pouch cells. It is hoped that this work can motivate other researchers to help understand the relevant mechanisms.

## CHAPTER 7 IMPACT OF A SURFACE COATING ON $\text{Li}[\text{Ni}_{0.5}\text{Mn}_{0.3}\text{Co}_{0.2}]\text{O}_2$ ON LI-ION CELL PERFORMANCE

The majority of this work was adapted from the following peer-reviewed article:

- Lin Ma, Scott Young, L.D. Ellis, Que Huang, Xiaowei Ma, M. Chatzidakis, Hongyang Li, Lauren Thompson, Ahmed Eldesoky, C.R.M. McFarlane, G.A. Botton, Ian G. Hill and J. R. Dahn, Impact of a surface coating on  $\text{Li}[\text{Ni}_{0.5}\text{Mn}_{0.3}\text{Co}_{0.2}]\text{O}_2$  on Li-ion cell performance, submitted to Tesla for approval (2018).

Lin Ma performed pouch cell preparation, gas evolution measurements, impedance measurements, storage testing, SEM image collection, long term cycling testing and UHPC cycling testing. Scott Young prepared all the symmetric cells. Xiaowei Ma performed storage testing and cycling testing relevant to 2% VC and 2% FEC. Que Huang performed accelerating rate calorimetry (ARC) testing. Leah Ellis performed XPS testing and XPS data analysis. Hongyang Li performed ion milling experiment. Lauren Thompson and Ahmed Eldesoky performed XRF experiment. Dr. J.R. Dahn provided guidance, participated in the interpretation of all the data and edited the paper. Lin Ma prepared the first draft of the manuscript mentioned above.

The effect of a Ti-based surface coating on NMC532 positive electrode material in NMC532/graphite Li-ion pouch cells has been investigated using high temperature storage testing (60°C), UHPC, EIS, ARC and long term cycling. Several superior

electrolyte additive combinations were selected for this study. Comparing data from cells containing coated and uncoated NMC532 showed that the surface coating generally contributed to improved cell performance from many perspectives, however for one electrolyte additive combination, cells containing coated and uncoated NMC532 had virtually identical excellent performance. In an effort to understand why the coating was effective, XPS was used to study the SEI on both coated and uncoated NMC532. X-ray fluorescence (XRF) studies of negative electrodes harvested from aged cells showed that the coating helped to prevent transition metal dissolution, although the amounts of metal dissolved were very small from both coated and uncoated NMC532. The “pouch bag” method was also used to study the effect of interactions between delithiated NMC532 (coated or uncoated) and lithiated graphite on gas evolution and impedance growth.

## **7.1 Experimental**

### **7.1.1 The preparation of pouch cells and pouch bags**

Coated SC NMC532/graphite and uncoated SC NMC532/graphite pouch cells were prepared according to the procedure described in Section 3.1.2.

The pouch bag method developed by Xiong et al. [168] was used to demonstrate the effect of interactions between different positive electrodes and negative electrodes on cell impedance growth and gas evolution when different electrolyte additives were used. Cells after formation were cycled at 40°C between 2.8 V and 4.4 V twice with a current

corresponding to  $C/10$ . Then the cells were held at 4.4 V for 24 hours before opening to recover the individual charged electrodes for the fabrication of pouch bags. The positive electrode (with its electrolyte) was sealed inside a pouch bag and the negative electrode (with its electrolyte) was sealed inside another pouch bag. Since some EMC evaporated during the pouch bag construction process, a suitable amount (0.15 g) of EMC was added to each pouch bag prior to sealing in order to create a similar electrolyte environment to that in the original pouch cells.

### **7.1.2 EIS testing**

See Section 5.1.2.

### **7.1.3 Charge-discharge cycling tests**

The cells were cycled using currents corresponding to  $C/3$  between 3 and 4.3 V using CCCV mode with a Neware (Shenzhen, China) charger system. All the cells were cycled twice using a slow rate (the first charge process was at  $C/3$  while the subsequent discharge, charge and discharge processes were at  $C/20$ ) every 50 cycles. The CCCV cut-off current was  $C/20$ .

External clamps were applied to all the pouch cells to ensure a firm stack pressure of about 25 KPa even if gas was produced during cycling. The gas, if produced, was forced to the edges of the pouch due to the action of the clamps.

#### **7.1.4 Storage testing**

See Section 5.1.4.

#### **7.1.5 XPS for surface analysis**

See Section 5.1.6.

#### **7.1.6 UHPC tests**

See Section 5.1.8.

#### **7.1.7 Accelerating rate calorimetry (ARC) experiments**

Cells after formation were discharged to 3.0 V and charged to 4.4 V at C/20. After holding at 4.4 V for 3 h, cells were transferred to an Ar-filled glovebox for ARC sample preparation. The details of sample preparation can be found in reference [169]. The capacity of delithiated positive electrode material added to each ARC tube was kept consistent (around 15 mAh) so that all the ARC data can be comparable. As a result, the masses of positive electrode material and electrolyte were adjusted for each ARC sample. In each ARC sample, 70 mg of charged electrode materials plus 23 mg of electrolyte were added.

### 7.1.8 Micro X-ray fluorescence (XRF) spectroscopy

All XRF imaging and analysis were carried out using a Bruker M4 Tornado Micro-XRF instrument with a rhodium X-ray source housed at the University of New Brunswick. The negative electrode was removed from the pouch cell by cutting it open in air after discharging it to a safe handling voltage of 2.8 V. A 3 x 2 cm piece of the negative electrode was then taped directly to a motion stage to ensure a flat surface; and mapping of the negative electrodes was carried out under vacuum between 0 and 50 keV with a tube current of 200  $\mu\text{A}$ , and over 2 scanning cycles at a rate of 4.00 mm/second with a 40  $\mu\text{m}$  spot size. Complete elemental analysis was performed at each position along the sample.

#### *Mn Calibration for XRF analysis*

A Mn calibration curve was prepared using a Corona Vacuum Coaters (Vancouver, BC, Canada) model V-3T sputtering system. This method, developed by Dahn et al. [170], uses a mask opening over the target and a rotating substrate table to create gradients in the amount of deposited material on a substrate. The linear mask used in this work generates a linear mass per unit area increase versus position on the substrate. Pre-weighed aluminum foil discs were used to measure the mass per unit area deposited versus position. Deposition increased from 0.0  $\mu\text{g cm}^2$  to about 30  $\mu\text{g cm}^2$  across the 76 mm long sputtering track.

During the same sputtering run, fresh graphite negative electrodes were mounted on the substrate table next to the aluminum foil weigh discs. The same “wedge” of Mn was deposited onto the graphite negative electrodes. Several of these Mn-coated electrodes were then used to record the Mn XRF signal versus position on the electrode to be compared with the mass per unit area versus position of the weigh discs, thus allowing a calibration curve to be constructed.

### **7.1.9 Scanning electron microscopy (SEM) imaging**

A Hitachi S-4700 SEM coupled with an 80 mm<sup>2</sup> silicon drifted detector (Oxford Instrument) was used to characterize the morphology of uncoated and coated SC NMC532 electrodes. The images of samples were obtained using an accelerating voltage of 5 kV and current of 10 μA. Uncoated and coated SC NMC532 electrodes were obtained from pouch cells after formation or after long term cycling. Samples were prepared by an ion beam cross-section polisher (IB-19530CP). Electrodes were milled by the cross section polisher with an Ar ion beam during a coarse step (voltage 6 kV, current 40 μA) and a fine step (voltage 6 kV, current 5 μA).

## **7.2 Results and discussion**

### **7.2.1 The effect of surface coating on storage testing**

Figure 7.1 shows a summary of the voltage drop during 500 h of 60°C storage (starting voltage was 4.4 V) of NMC532/graphite pouch cells (with either coated or uncoated SC



NMC532) containing different electrolytes. Two cells were measured for each data point and the error bars are the difference between the two results. During storage, a larger voltage drop indicates the occurrence of more parasitic reactions at the surface of the positive electrode [154]. Figure 7.1 shows that the application of the Ti-based surface coating on the positive electrode decreased the voltage drops compared to cells without surface coating on the positive electrode when electrolyte additives were used. The data for uncoated cells with 2% FEC was not included because the voltage-time curves for those cells were not normal and hence judged to be unreliable (see Figure A7).

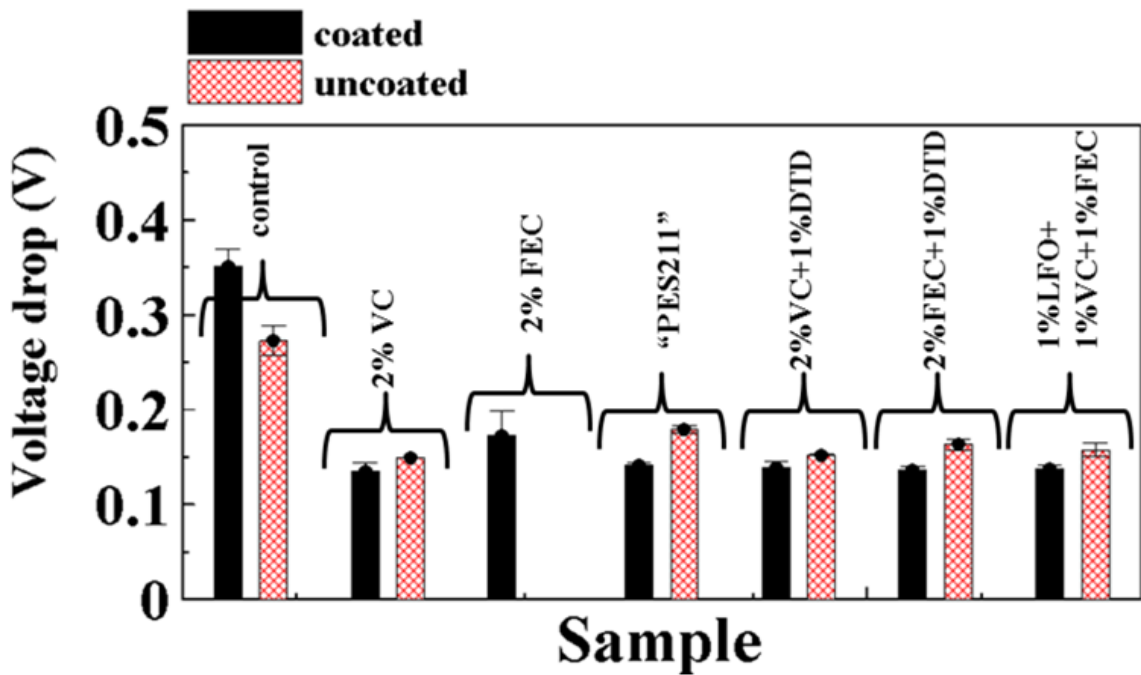


Figure 7.1 Summary of voltage drop at 4.4 V during 500h storage at 60°C for coated and uncoated SC NMC532/graphite pouch cells with different electrolytes as indicated.  $\text{LiPO}_2\text{F}_2$  is called LFO in the Figure legend.

### **7.2.2 The effect of surface coating on impedance growth and gas evolution**

Figure 7.2 summarizes the positive electrode charge transfer impedance measurements for charged (a) coated SC NMC532 and (b) uncoated SC NMC532 electrodes before and after storage testing (in pouch cells or pouch bags) with different electrolytes as indicated. All of these measurements were made in positive/positive electrode symmetric cells. The values reported in Figure 7.2 are the “diameters” of the “semicircles” in the impedance spectra for the positive/positive symmetric cells shown in Figures A1b and A1c to Figures A5b and A5c. Xiong et al. [171] showed that the interaction between the positive electrode and the negative electrode in a pouch cell during storage helps control impedance growth on the positive electrode and that the impedance of charged positive electrodes obtained from pouch bags is larger than those obtained from pouch cells. Figure 7.2 shows that the Ti-based surface coating on the SC NMC532 electrode material helps to control impedance growth when electrolyte additives were used. When electrolyte additives were used, the impedance of coated positive electrodes harvested from pouch bags shown in Figure 7.2(a) is smaller than that of uncoated electrodes shown in Figure 7.2(b). This strongly suggests that the coating helps limit parasitic reactions at the positive electrode that lead to impedance growth.

Figure 7.3 summarizes the negative electrode charge transfer impedance measurements for charged (a) coated SC NMC532 and (b) uncoated SC NMC532 electrodes before and after storage testing (in pouch cells or pouch bags) with different electrolytes as

indicated.

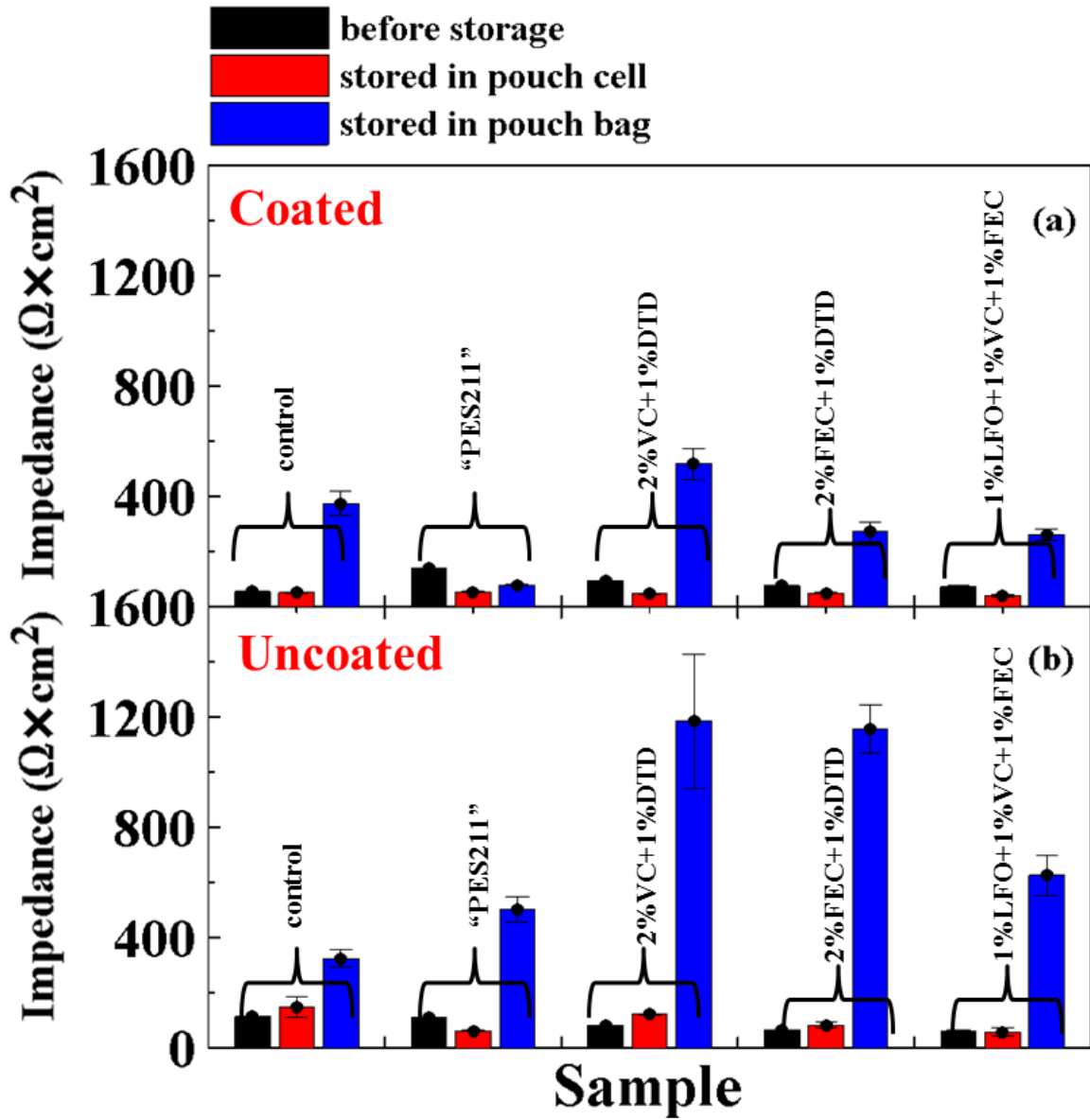


Figure 7.2 Summary of impedance change for (a) coated delithiated SC NMC532 and (b) uncoated delithiated SC NMC532 electrodes before or during 500h storage testing (stored in either pouch cells or pouch bags) at 60°C with different electrolytes as indicated.  $\text{LiPO}_2\text{F}_2$  is called LFO in the Figure legend.

All of these measurements were made in negative/negative electrode symmetric cells.

The values reported in Figure 7.3 are the “diameters” of the “semicircles” in the impedance spectra for the negative/negative symmetric cells shown in Figures A1d and A1e to Figures A5d and A5e.

The impedance of the negative electrode was much smaller than that of the positive electrode (compare the axis scales of Figures 7.2 and 7.3). Comparing Figures 7.3a and 7.3b for the same electrolyte additives, one learns that the presence or absence of the coating on the positive electrode has virtually no impact on the impedance of the negative electrode. The choice of electrolyte additives used does have an obvious impact on the impedance of the lithiated graphite electrode before and after storage testing. Compared to other electrolyte additives, “PES211” shows the largest impedance on the lithiated graphite electrode.

Figure 7.4 shows a summary of the gas volumes generated in the pouch bags containing delithiated coated SC NMC532 (a), lithiated graphite taken from coated SC NMC532/graphite cells (a), coated SC NMC532/graphite pouch cells (a), pouch bags containing delithiated uncoated SC NMC532 (b), lithiated graphite taken from uncoated SC NMC532/graphite cells (b) and uncoated SC NMC532/graphite pouch cells (b) after 500 h storage testing at 60°C with the different electrolytes, as indicated.

Almost no volume changes were detected for pouch bags containing lithiated graphite, which is consistent with a previous report [171]. In most cases, pouch bags with

delithiated positive electrodes produced more gas than the corresponding pouch cells.

The volume of gas evolved in the pouch bags containing charged coated SC NMC532

was generally larger than in the corresponding pouch bags with uncoated SC NMC532.

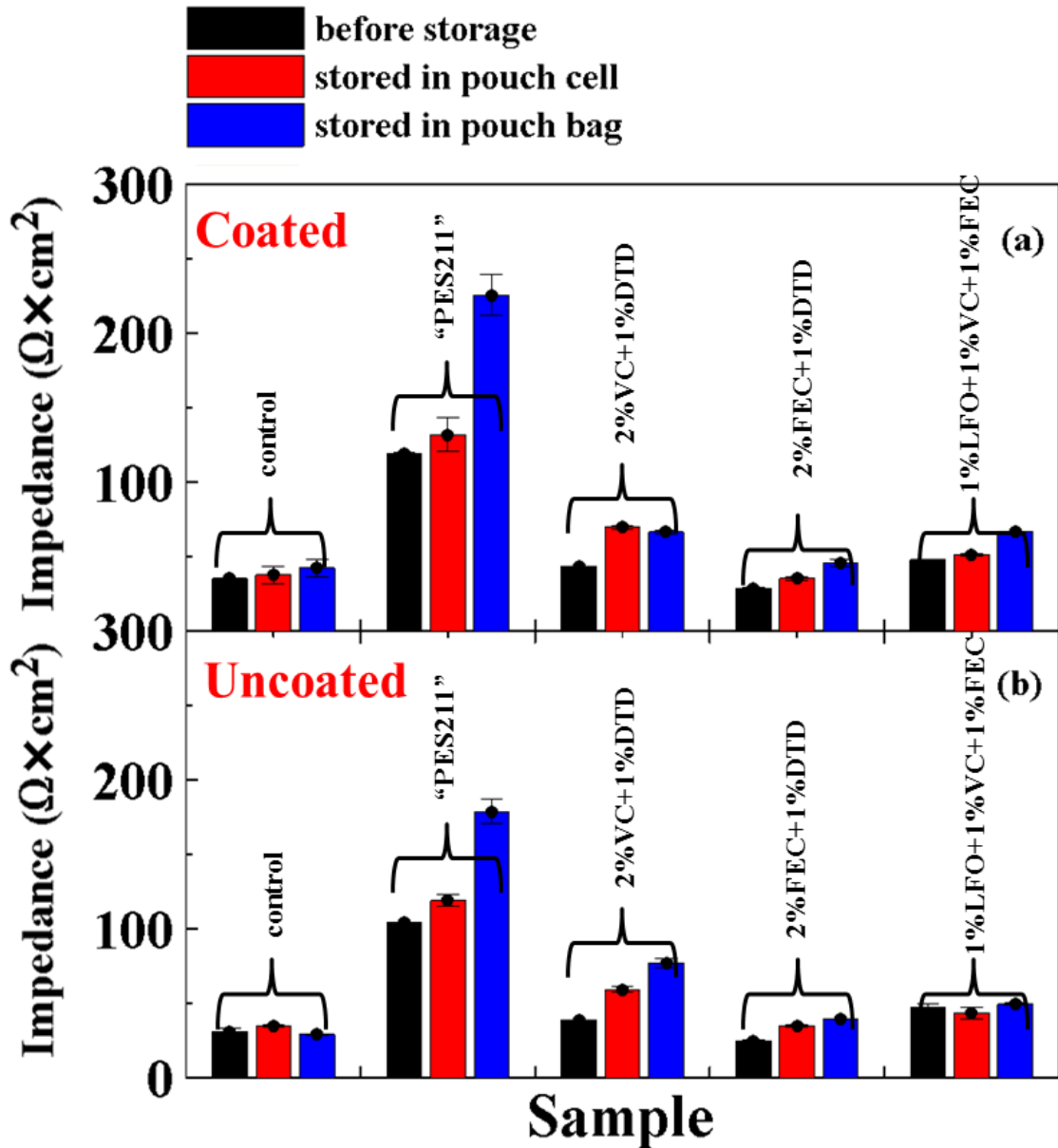


Figure 7.3 Summary of impedance change for lithiated graphite taken from (a) coated SC NMC532/graphite pouch cells and (b) uncoated SC NMC532/graphite pouch cells before or during 500h storage testing (stored in either pouch cells or pouch bags) at 60°C with different electrolytes as indicated. LiPO<sub>2</sub>F<sub>2</sub> is called LFO in the Figure legend.

This appears to correlate well with the results in Figure 7.2, because gaseous reaction products are not expected to increase the charge transfer resistance [172]. The volume of gas evolved in pouch cells containing coated SC NMC532 was generally smaller than in the corresponding pouch cells containing charged uncoated SC NMC532. Ellis et al. [172], recently showed that gases such as CO<sub>2</sub> created at the positive electrode can be removed by the negative electrode. It is possible that the gas product distributions created by the coated and uncoated NMC532 electrodes in contact with electrolyte are different, which could help explain the results in Figure 7.4.

### **7.2.3 The effect of surface coating on cell lifetime**

Figure 7.5 summarizes the CIE per hour (CIE/h) (a), fractional fade per hour (b) and fractional charge endpoint capacity slippage per hour (c) of coated and uncoated SC NMC532/graphite pouch cells with different electrolytes as indicated during UHPC testing at 40°C between 3.0 and 4.3 V with currents corresponding to C/20.

Based on explanations from previous work [101], lower fractional fade, fractional slippage and CIE (higher CE) generally result in cells with longer lifetimes. Figures 7.5a – 7.5c show that generally CIE, fractional charge end point capacity slippage and fractional fade are less (better) for cells with coated SC NMC532 compared to cells with uncoated SC NMC532 when the same electrolytes are used.

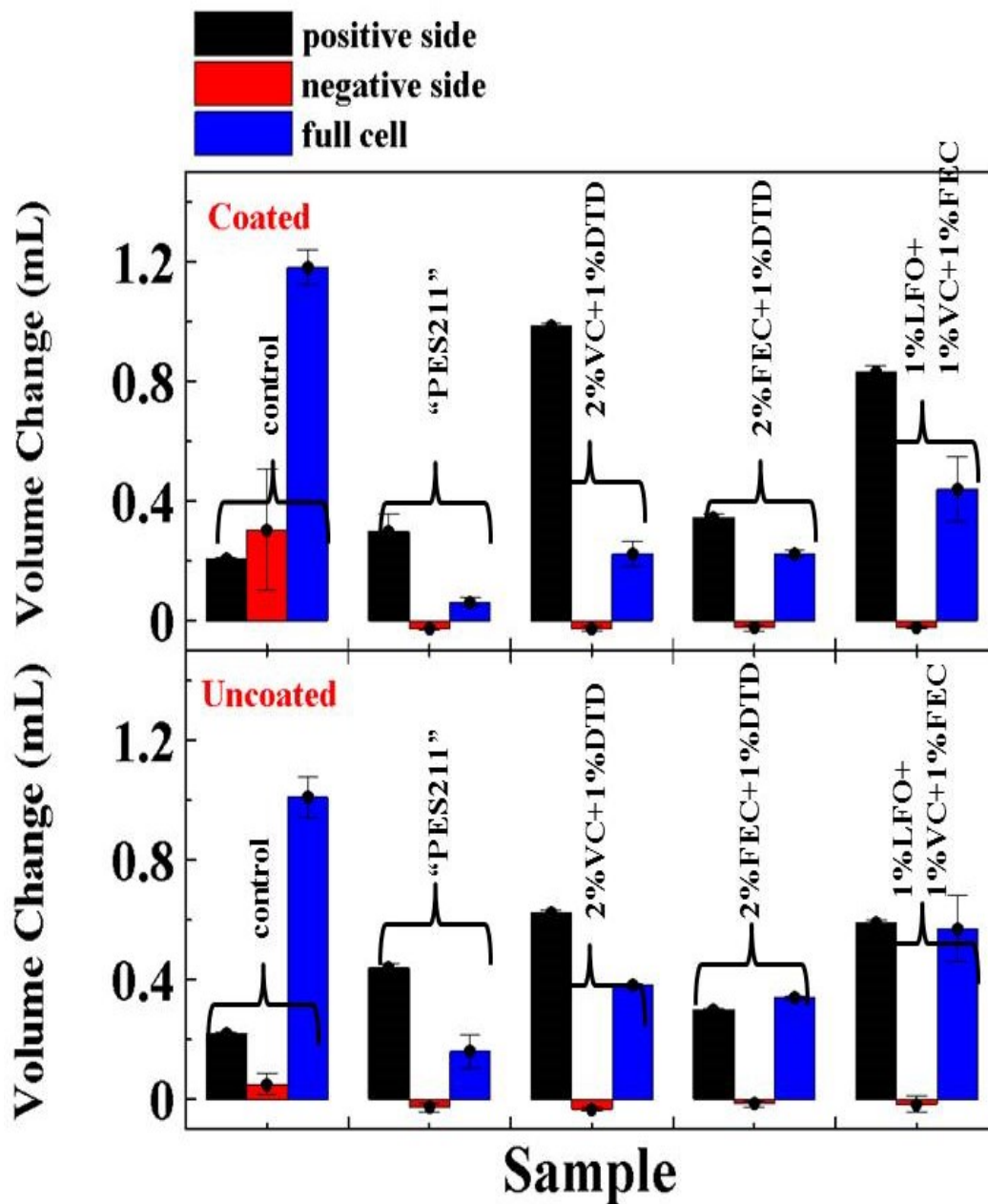


Figure 7.4 Gas evolution of pouch bags containing delithiated coated SC NMC532 (a) or lithiated graphite taken from coated NMC532/graphite cells (a), coated SC NMC532/graphite pouch cells (a), pouch bags containing delithiated uncoated SC NMC532 (b) or lithiated graphite taken from uncoated SC NMC532/graphite cells (b) and uncoated SC NMC532/graphite pouch cells during 500h storage testing at 60°C with different electrolytes as indicated. LiPO<sub>2</sub>F<sub>2</sub> is called LFO in the Figure legend.

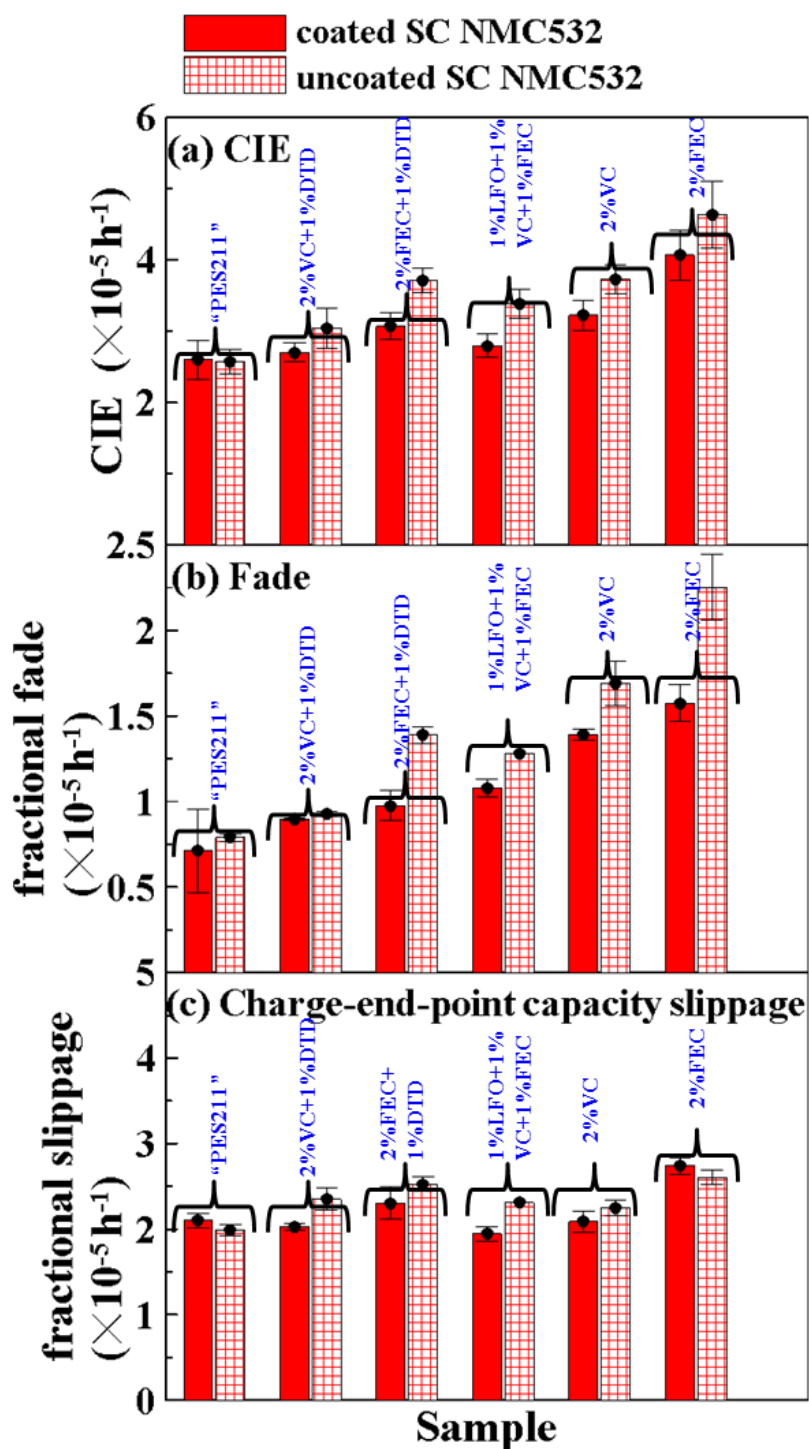


Figure 7.5 A summary of UHPC testing results for coated and uncoated SC NMC532/graphite pouch cells filled with different electrolytes as indicated during 16 cycle between 3 and 4.3 V with currents corresponding to C/20 at 40°C including (a) CIE per hour (b) fractional discharge capacity fade per hour and (c) fractional charge end-point capacity slippage per hour. The data shown is the average of two cells and the error bars were calculated as described in the text.  $\text{LiPO}_2\text{F}_2$  is called LFO in the Figure legend.



One exception is for the electrolyte “PES211” where the CIE, fade and slippage are almost the same for the coated and uncoated cells. Therefore, it is expected that cells with coated SC NMC532 will have longer lifetimes than cells with uncoated SC NMC532, except in the case of “PES211”, where the lifetimes should be similar.

Figure 7.6 summarizes the full cell charge transfer impedance (diameter of the “semicircle” in the Nyquist plot) changes for coated (a) and uncoated (b) SC NMC532/graphite pouch cells with different electrolytes during UHPC cycling. For simple electrolyte additives like VC and FEC, the presence of the coating caused an impedance decrease while the impedance of cells with uncoated SC NMC532 with these additives increased during cycling. It is our opinion that many coatings were initially developed to improve the performance of cells with simple additive systems. When more sophisticated electrolyte additive systems were used such as “PES211”, 2% VC + 1% DTD, 2% FEC + 1% DTD and 1% LiPO<sub>2</sub>F<sub>2</sub> + 1% VC + 1% FEC, the impedance decreased after testing for cells using both coated and uncoated SC NMC532.

Figures 7.7a and 7.7c show the normalized discharge capacity versus cycle number during long-term testing for cells with uncoated SC NMC532 (7.7a) and cells with coated SC NMC532 (7.7c) containing different electrolytes as labeled during CCCV cycling up to 4.3 V with currents that correspond to C/3 at 40°C. The upper cut-off current was C/20.

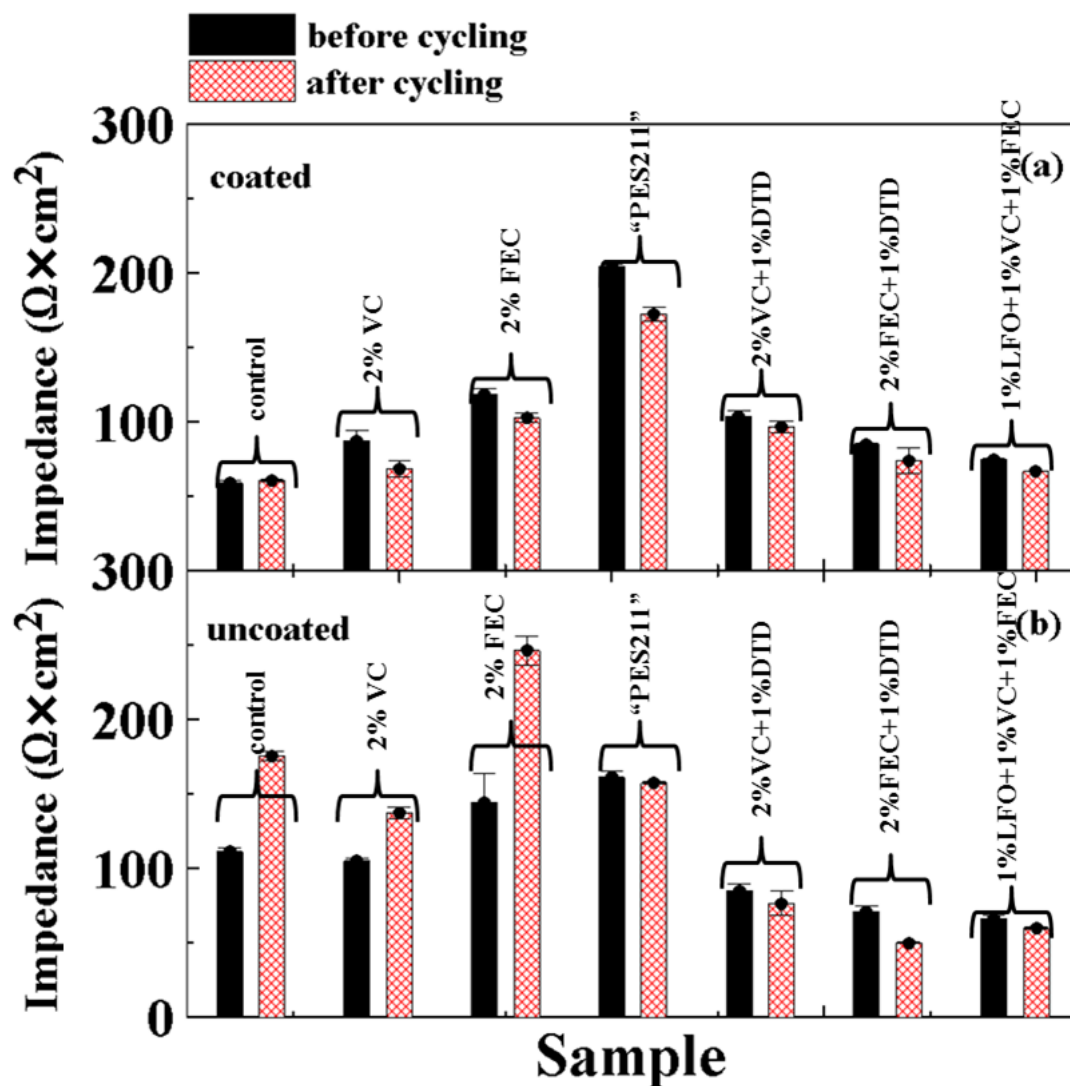


Figure 7.6 Summary of impedance change during 16 UHPC cycles between 3 and 4.3 V with currents corresponding to C/20 at 40°C for (a) coated SC NMC532/graphite and (b) uncoated SC NMC532/graphite pouch cells with different electrolytes as indicated.  $\text{LiPO}_2\text{F}_2$  is called LFO in the Figure legend.

Figures 7.7b and 7.7d show the difference between the average charge and the average discharge potential ( $\Delta V$ ) vs. cycle number corresponding to the cells shown in Figures 7.7a and 7.7c, respectively. This indicates the polarization in the cells [146] during

cycling.

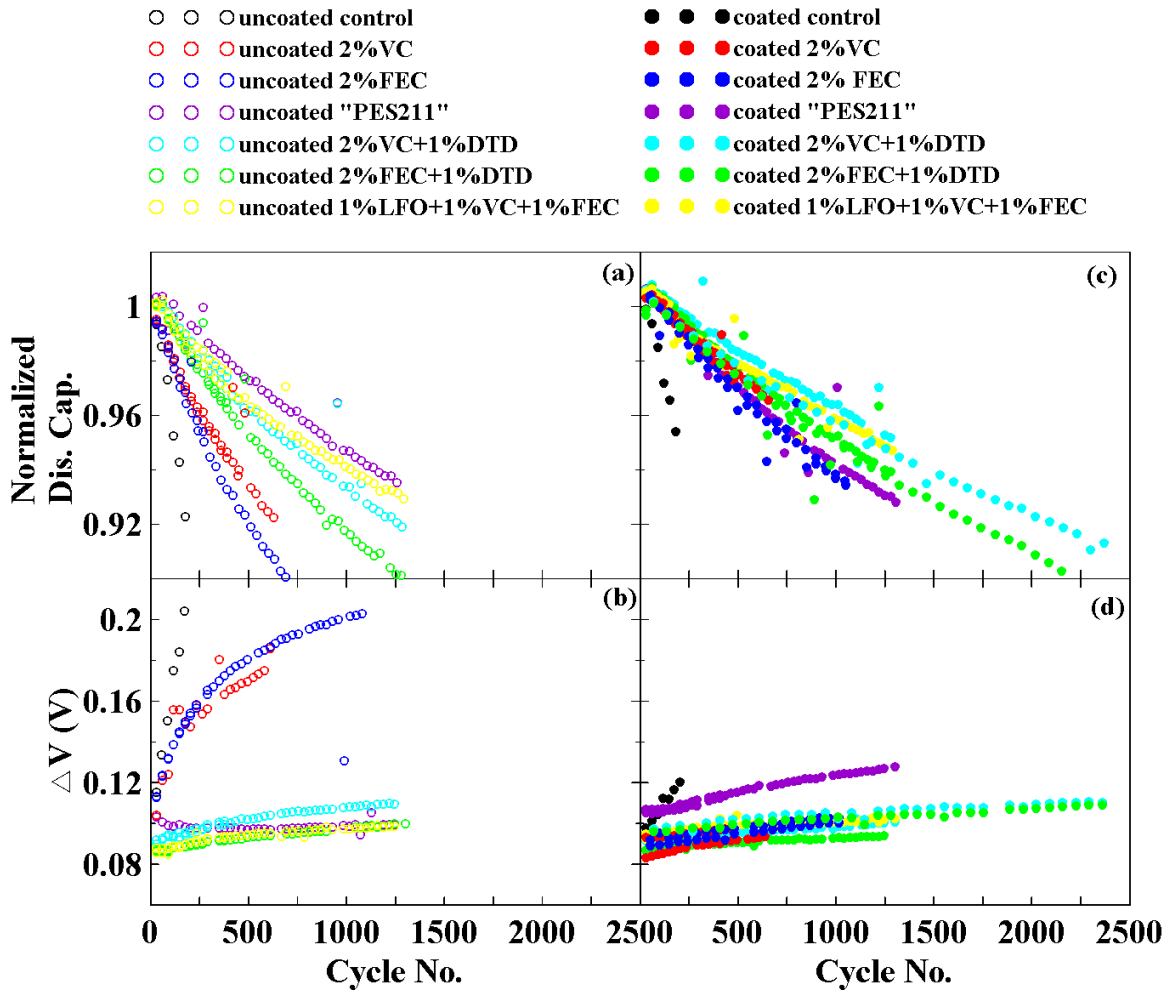


Figure 7.7 Normalized discharge capacity (a, c) and cell polarization (b, d) vs. cycle number for uncoated (a, b) and coated (c, d) SC NMC532/graphite pouch cells with different electrolytes as indicated during long term CCCV cycling between 3 and 4.3 V using currents corresponding to C/3 at 40°C. A constant voltage step at the top of charge was applied until the current dropped below C/20. LiPO<sub>2</sub>F<sub>2</sub> is called LFO in the Figure legend.

Except for "PES211"-containing cells, cells with coated SC NMC532 with or without electrolyte additives demonstrated better capacity retention and smaller polarization

during long-term cycling testing compared to cells with uncoated SC NMC532. This suggests that this type of surface coating improves the lifetime of SC NMC532/graphite cells consistent with the UHPC results shown in Figure 7.5.

#### **7.2.4 Cell failure mechanism analysis**

Differential voltage analysis was performed on cells with coated SC NMC532 and on cells with uncoated SC NMC532 having 2% VC after long term cycling to determine the reason for the capacity loss. Cell capacity loss can result from lithium inventory loss during SEI growth and repair as well as loss of active material. Furthermore, cell capacity loss during high rate cycling can occur when impedance increases. Dahn et al. [143] and Bloom et al. [173,142] showed that differential voltage analysis is a useful way to determine the active masses of both electrodes and the capacity loss due to Li inventory loss, which is called “shift loss” here. In this study, electrode mass and relative electrode capacity shifts were obtained using reference differential voltage curves to fit  $dV/dQ$  vs.  $Q$  of the full pouch cells. The reference curves were measured with C/40 rates in NMC532/Li and graphite/Li half coin cells.

Figures 7.8a and 7.8b show the discharge capacity versus cycle number for cells with coated SC NMC532 and cells with uncoated SC NMC532 containing 2% VC during CCCV cycling up to 4.3 V with C/3 rate at 40°C. After every 50 cycles, all the cells were cycled using slow rate (the first charge process was at C/3 while the subsequent

discharge, charge and discharge process were at C/20). The low rate C/20 discharge capacity after ~650 cycles is higher than the capacity measured during the last C/3 cycle for both cell types. This is partly caused by the impedance growth in these cells with 2% VC as shown in Figures 7.7b and 7.7d. Notice that the difference between the last C/20 and C/3 capacity at the end of test is larger for the cell with uncoated SC NMC532 (Figure 7.8b) than for the cell with coated SC NMC532 (Figure 7.8a) consistent with the results in Figures 7.7b and 7.7d. Figures 7.8c and 7.8d show dV/dQ vs. Q for the cells with coated SC NMC532 and uncoated SC NMC532 before long term cycling, respectively. Figures 7.8e and 7.8f show dV/dQ vs. Q for the cells with coated SC NMC532 and uncoated SC NMC532 after long term cycling, respectively. The fitting parameters are listed in these Figures. The initial shift between the positive and negative electrode capacity curves was about -2 mAh and -4 mAh for cells with coated SC NMC532 and uncoated SC NMC532, respectively. After cycling, the shift was about +12 mAh for the cell with coated SC NMC532 and about +18 mAh for the cell with uncoated SC NMC532. The shift loss for the cell with coated SC NMC532 was therefore about 14 mAh and about 22 mAh for the cell with uncoated SC NMC532. The black double headed arrow in Figure 7.8a has a length of 13.7 mAh and represents the difference in capacity between the first C/20 cycle and the last C/20 cycle for the cell with coated SC NMC532. The red double headed arrow in Figure 7.8b has a length of 21.6 mAh represents the difference in capacity between the first C/20 cycle and the last C/20 cycle

for the cell with uncoated SC NMC532. These results are consistent with the shift loss (i.e. the difference of relative slippage between the results shown before cycling and after cycling) obtained from fitting.

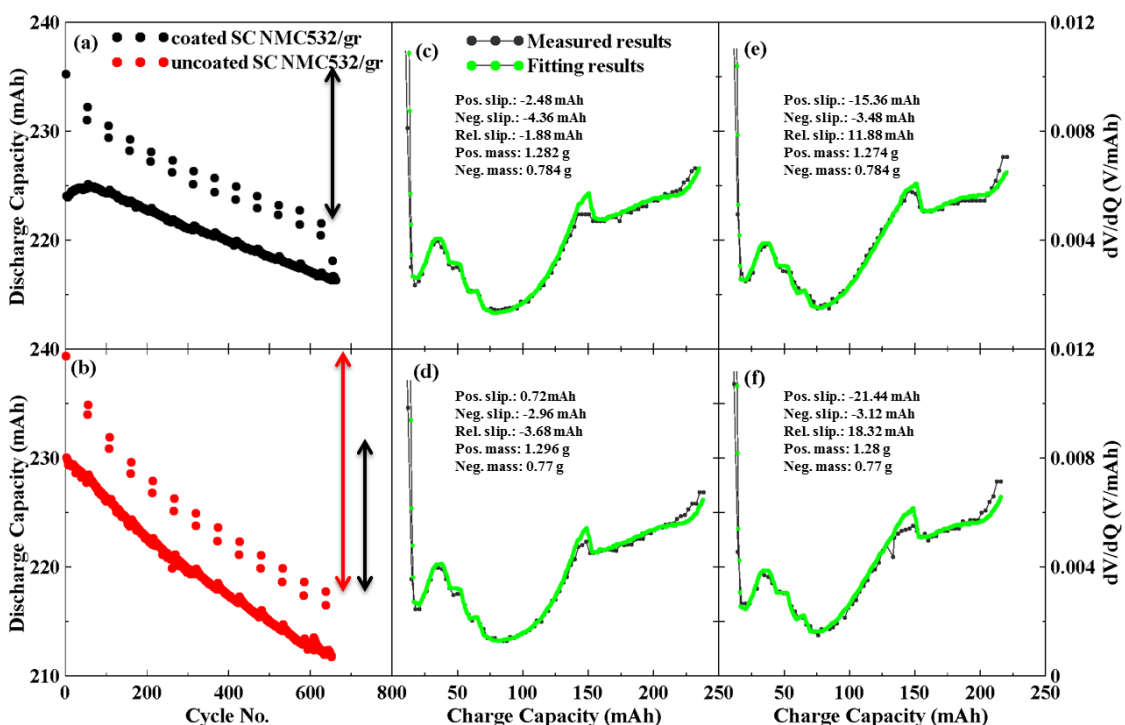


Figure 7.8 Discharge capacity vs. cycle number (a and b) for coated and uncoated SC NMC532/graphite pouch cells with 1.2M LiPF<sub>6</sub> EC/EMC 3/7 containing 2% VC, respectively, during CCCV long term cycling at 40°C between 3 V and 4.3 V with currents corresponding to C/3. A constant voltage step at the top of charge was applied until the current dropped below C/20. Panels c and d show the differential voltage vs. capacity curve and the fitted curve for the cells in panels a) and b) before ~650 cycles. A C/20 charge curve collected before ~650 cycles was used for the fitting. Panels e and f show the differential voltage vs. capacity curve and the fitted curve for the cells in panels a) and b) after ~650 cycles. A C/20 charge curve collected after ~650 cycles was used for the fitting.

Transition metal dissolution from the positive electrode and its subsequent deposition on the negative electrode is known to be one of the reasons for cell capacity fade [174,175]. At the end of the 650 cycles shown in Figures 7.8a and 7.8b, the amount of loading of Mn

found of the negative electrode of the cell with coated SC NMC532 was  $1.1 \pm 0.1 \mu\text{g}/\text{cm}^2$  and was  $3.6 \pm 0.3 \mu\text{g}/\text{cm}^2$  for the cell with uncoated SC NMC532. The corresponding XRF images are shown in Figure A9. This suggests surface coating on positive electrode suppresses the dissolution of Mn. The Mn loading on the negative electrode taken from a cell with coated SC NMC532 directly after formation was found to be  $0.53 \pm 0.1 \mu\text{g}/\text{cm}^2$  of Mn. The Mn loading on the negative in the cells with coated SC NMC532 only doubled compared to that found after formation during the 650 cycles to 4.3 V at  $40^\circ\text{C}$ . Unfortunately, results for cells with uncoated SC NMC532 after formation are not available. A  $3.6 \mu\text{g}/\text{cm}^2$  loading corresponds to 0.1% of the Mn that was initially in the positive electrode. Previous reports [174–177] mentioned that the deposition of Mn on negative electrode caused capacity loss of Li-ion cells. However, in this work, the amount of Mn deposition on negative electrode is much smaller for both coated and uncoated SC NMC532 containing cells compared to the results shown by Gilbert et al. [174]. Thompson et al. [178] made a careful comparison between Gilbert’s work and Mn dissolution found on the negative electrodes in cells like those of the present work. Even though the cells tested by Thompson et al. were cycled 5 times longer than Gilbert’s and at a temperature of  $55^\circ\text{C}$  compared to  $20^\circ\text{C}$  for Gilbert the negative electrodes in Thompson’s cells had about an order of magnitude less Mn on the negative electrode. In addition, Thompson’s cells lost a maximum of 12% capacity after 750 cycles to 4.4 V at  $55^\circ\text{C}$  while Gilbert’s lost about 37% capacity after 200 cycles to 4.4 V at  $20^\circ\text{C}$ . Thompson et al. attributed this to the

effectiveness of the electrolyte additives used in her cells and to the SC morphology of the positive electrode. It is possible that the increased Mn dissolution from the uncoated material in the experiment described here is responsible for the increased capacity loss. However, many more studies are required, involving cells with other electrolytes like “PES211”, where the capacity retention of coated and uncoated cells is similar in order to be sure that differences in Mn deposition are responsible for the increased rate of capacity loss due to an increase in shift loss. Since the instrument was not calibrated for any other elements besides Mn, the dissolution of Co and Ni was not quantified. However, the raw signal counts of Ni and Co per  $\text{cm}^2$  of negative electrode are approximately proportional to the number of atoms deposited. Figure A10 shows the Co and Ni signals compared to the Mn signals. Lines to guide the eye are drawn based the 5:3:2 ratio of Ni:Mn:Co in the positive electrode material. Most interesting in Figure A10 is that the Ni and Co signals are approximately the same for the electrodes taken from coated and uncoated cells, suggesting that transition metal dissolution is not the cause for the increased shift loss in the uncoated cells. However, many more studies are required, involving cells with other electrolytes like “PES211”, where the capacity retention of coated and uncoated cells is virtually identical, in order to be sure that differences in transition metal deposition are linked to increased rates of capacity loss due to an increase in shift loss.

S. Watanabe et al. [179,180] reported that the capacity loss and impedance growth of NCA/graphite cells were partially due to micro-crack generation on NCA particle



surfaces during cycling. However, SC material has been reported to deliver superior performance by maintaining particle integrity [181,182]. In this work, uncoated and coated SC NMC532 electrode materials, taken from pouch cells with 2% VC after formation or after long term cycling (electrodes taken from the same cells as described by Figure 7.9 and the same cells used for XRF analysis discussed above), were polished by Ar ion milling and then used for SEM image collection. Figure 7.9 shows cross sectional SEM images of uncoated SC NMC532 (after formation (a) and after cycling (b)) and coated SC NMC532 (after formation (c) and after cycling (d)). There are very few or no micro-cracks observed in this Figure. This suggests that the impedance growth of uncoated SC NMC532/graphite pouch cells during long term cycling resulted from the interphase between the electrode and electrolyte.

Figure 7.10A shows XPS spectra of coated and uncoated positive electrodes taken from cells (which had 2% VC in the electrolyte) after formation and after long term cycling (shown in Figure 7.8). Titanium peaks from the coating were not observable by XPS. The XPS spectra in Figure 7.10 are not normalized, and are plotted as raw counts per second (CPS) with a Shirley background subtracted from the peaks. This way the relative amounts of the SEI species can be assessed qualitatively by eye. After formation the SEIs on the uncoated and coated positive electrodes are similarly thin ( $< \sim 10$  nm, since the NMC lattice oxygen and PVDF peaks are visible). After formation, the SEIs are composed of organics, fluorophosphates and LiF. After cycling the SEIs on the uncoated

and coated positive electrodes are thicker (the NMC lattice oxygen and PVDF peaks are no longer visible). The aged SEI is composed of phosphates, in addition to the species that were present on the SEI after formation. The SEI on the coated electrode appears to be thinner than that on the uncoated electrode after formation (the NMC lattice peak is taller). After cycling, there appears to be more LiF on the surface of the coated electrode.

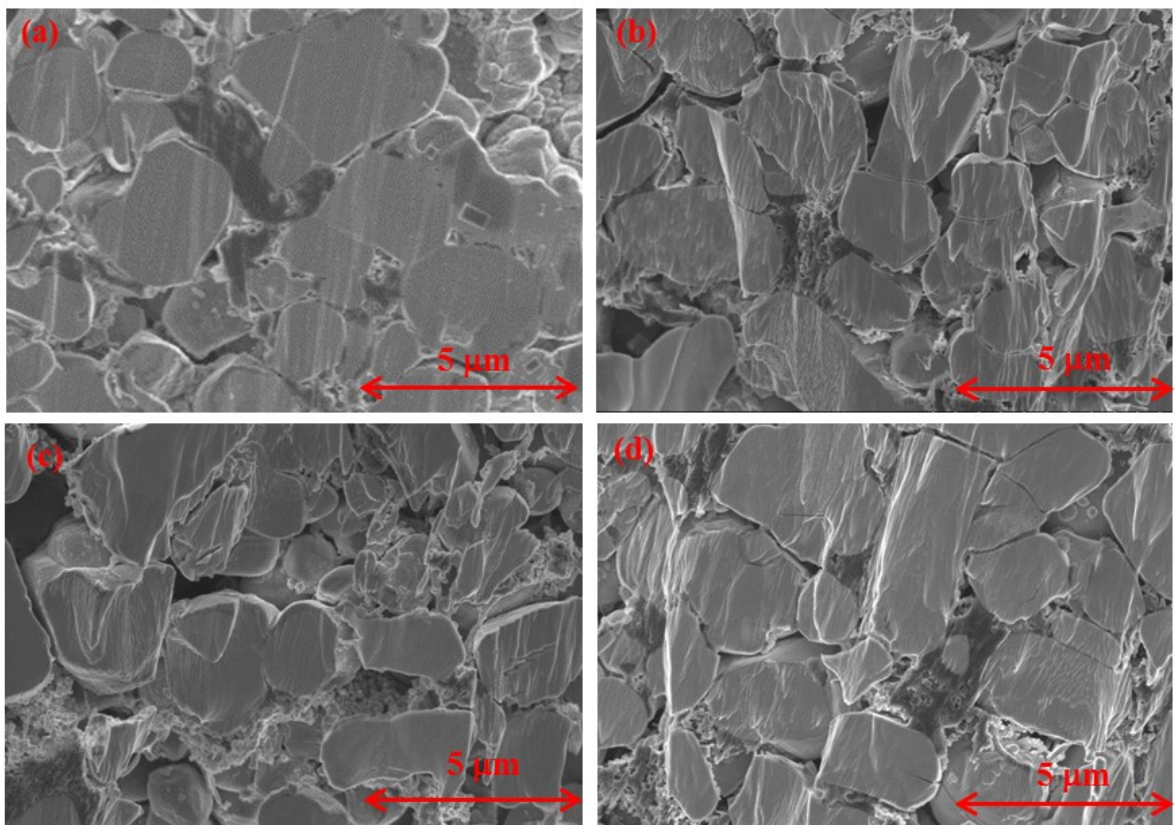
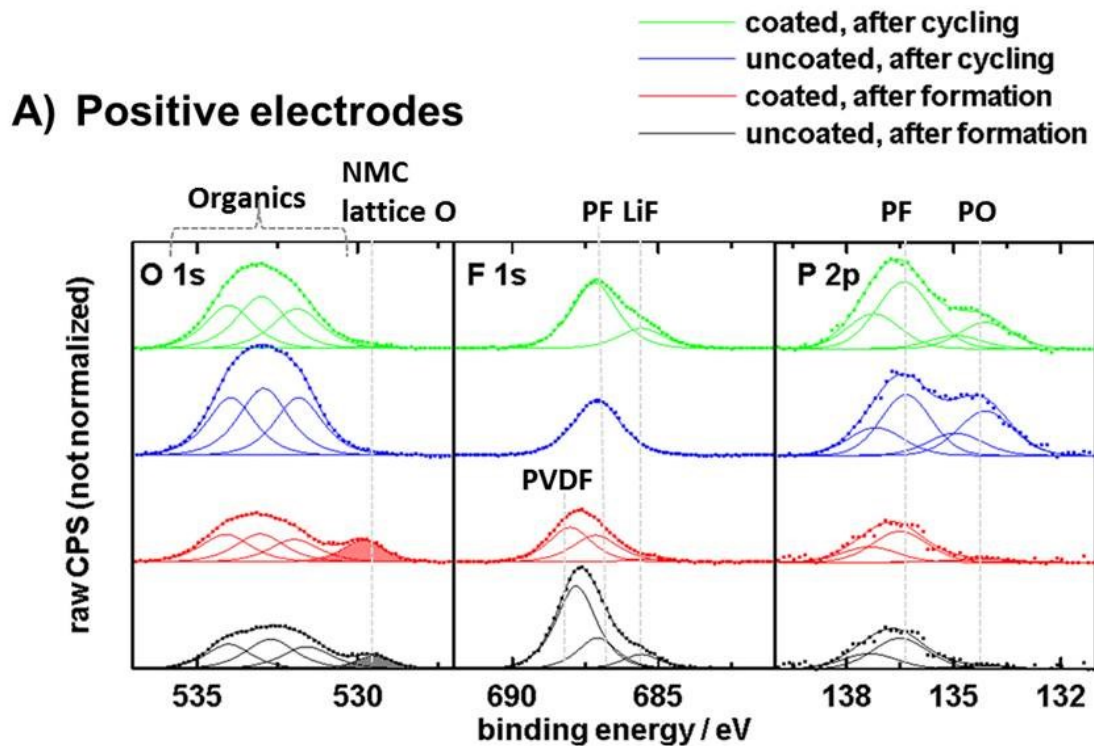


Figure 7.9 SEM images of cross sections of positive electrodes taken from uncoated SC NMC532/graphite pouch cells (after formation (a), after cycling (b)) and from coated SC NMC532/graphite pouch cells (after formation (c), after cycling (d)). All the cells were filled with 2% VC containing electrolyte. The corresponding long term cycling process was shown in Figure 7.8.

Figure 7.10B shows XPS spectra of negative electrodes taken from coated or uncoated SC NMC532/graphite cells (which had 2% VC in the electrolyte) after formation and after long term cycling (shown in Figure 7.8). After formation the SEIs on both negative electrodes are virtually identical. They are composed of organics, fluorophosphates, phosphates and LiF. The initial SEIs are relatively thin, since the  $\text{LiC}_6$  peak from the underlying electrode is still somewhat visible. After cycling the SEIs on both negative electrodes become thicker. The composition of the aged SEI is similar to that of the SEI after formation, but the aged negative electrodes contain more ether-type compounds (287 eV) and phosphates (as was the case for the aged positive electrodes).

There is not a big difference between the negative electrode SEIs from cells with coated and uncoated SC positive electrodes. After cycling, there appears to be more LiF on the surface of the negative electrode from the cell with the coated positive electrode. The increased amounts of LiF in the SEIs of both electrodes from the cell with the coated positive electrode, may be related to the superior performance of this cell in cycling tests. LiF is known to be a passivating SEI component [183]. Recent work from Ellis et al. [184] shows that the amount of LiF in the negative electrode SEI increases as the SEI matures and becomes more passivating.



**B) Negative electrodes**

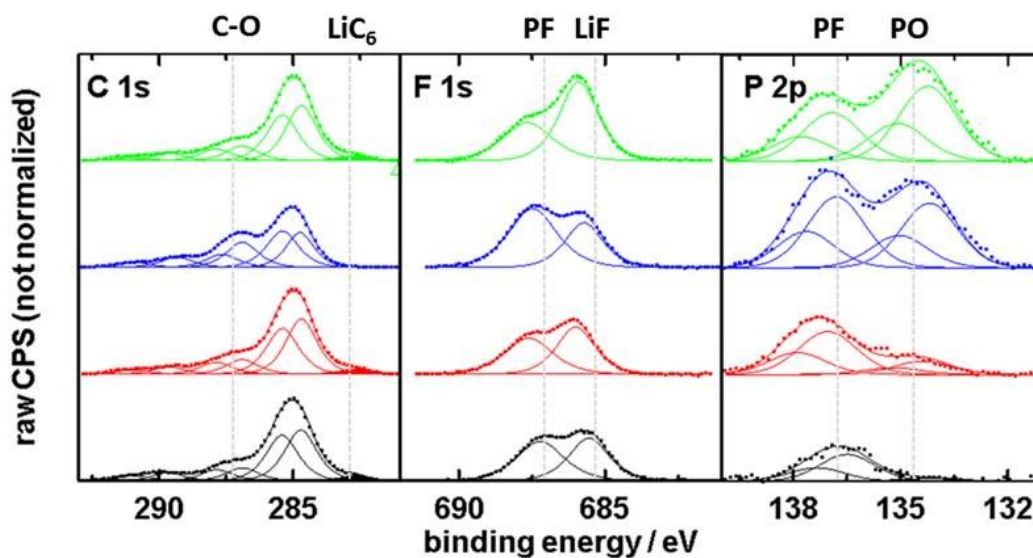


Figure 7.10 Regions of the XPS spectra of A) positive electrodes and B) negative electrodes that underwent formation or long term cycling (shown in Figure 8) in coated or uncoated SC NMC532/graphite pouch cells with 2% VC.

### **7.2.5 The effect of surface coating on safety performance**

Figure 7.11 shows the self-heating rate (SHR) versus temperature results for delithiated coated and uncoated SC NMC532 harvested after formation at 4.4 V (vs. graphite) reacting with different electrolytes: (a) 1% LiPO<sub>2</sub>F<sub>2</sub> + 1% VC + 1% FEC, (b) 2% FEC + 1% DTD, (c) 2% VC + 1% DTD and (d) 2% PES + 1% DTD + 1% TTSPi (“PES211”). Dashed lines in each panel are the results for duplicate samples.

Figures 7.11a-c show that the SHR of coated SC NMC532 is higher than that of uncoated SC NMC532 between ~ 150°C and ~ 200°C. Figures 7.11a-d show that the SHR of coated SC NMC532 and uncoated SC NMC532 is similar before 150°C. This suggests that surface coating on the positive electrode did not bring an obvious benefit to the cell safety performance. As a note, it was not possible to measure the results for “PES211” blends reacting with delithiated coated SC NMC532 due to corrosion of the stainless steel ARC tube (reasons for this are unknown) at elevated temperatures.

### **7.2.6 The effect of surface coating on gas evolution at high voltage**

To further compare the stability of different electrolyte additives containing electrolytes at the coated or uncoated SC NMC532 positive electrode surface, coated or uncoated SC NMC532/graphite pouch cells with different electrolytes as labeled were charged and held at 4.1, 4.2, 4.3, 4.4 and 4.5 V for 20 h while the amount of gas evolved in the cells

during the whole process was monitored using an in-situ gas measurement setup [83].

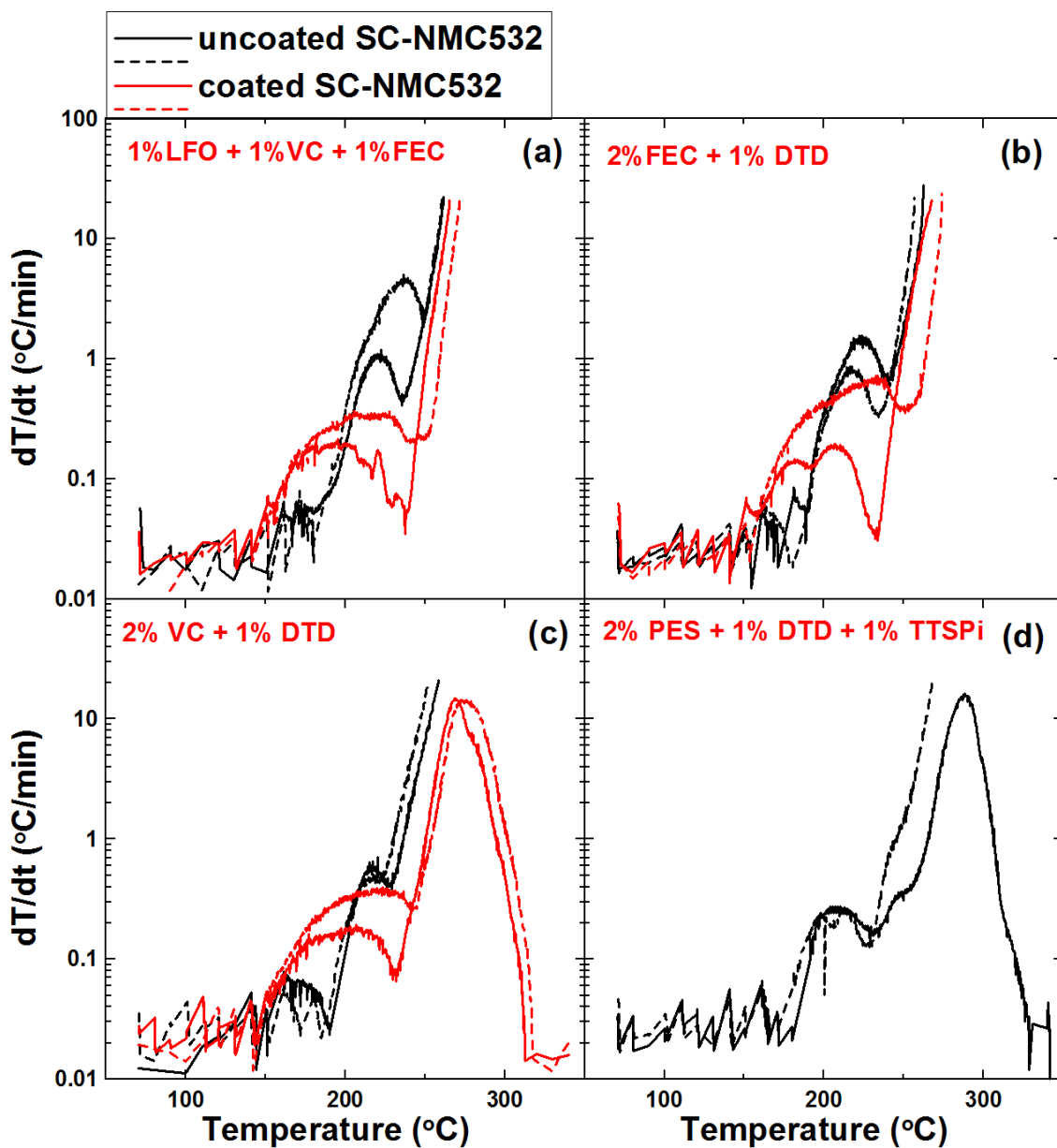


Figure 7.11 SHR vs. temperature for delithiated coated and uncoated SC NMC532 electrodes reacting with different electrolytes: (a) 1% LFO + 1% VC + 1% FEC, (b) 2% FEC + 1% DTD, (c) 2% VC + 1% DTD and (d) 2% PES + 1% DTD + 1%TTSPi (“PES211”) at 4.4V (vs. graphite). The results for duplicate samples are given as a dashed line in each panel.  $\text{LiPO}_2\text{F}_2$  is called LFO in the Figure legend.

The temperature of the in-situ gas testing experiment was 40.0°C. Figures 7.12a-f show the cell voltage versus time while Figures 7.12g-l show the volume change of the coated or uncoated SC NMC532/graphite pouch cells versus time.

Figures 7.12g-l show that uncoated SC NMC532/graphite cells produced more gas than coated SC NMC532/graphite cells at high voltages (4.4 and 4.5V) when the same electrolytes were used. This suggests that the surface coating on the SC positive electrode material helps suppress gas production in full Li-ion pouch cells with electrolyte additives at high voltage, consistent with the 60°C storage experiments on full pouch cells reported in Figure 7.4.

However, the reader is reminded that pouch bags with charged coated SC NMC532 produced more gas than pouch bags with charged uncoated SC NMC532 having the same electrolyte (including additives) during 60°C storage. This strongly suggests that the gas product distribution, and hence the electrolyte oxidation reactions, are different on the surfaces of the coated and uncoated SC NMC532 particles. If the electrolyte oxidation reactions are different, then different species can transport to the surface of the negative electrode causing different rates of capacity loss.

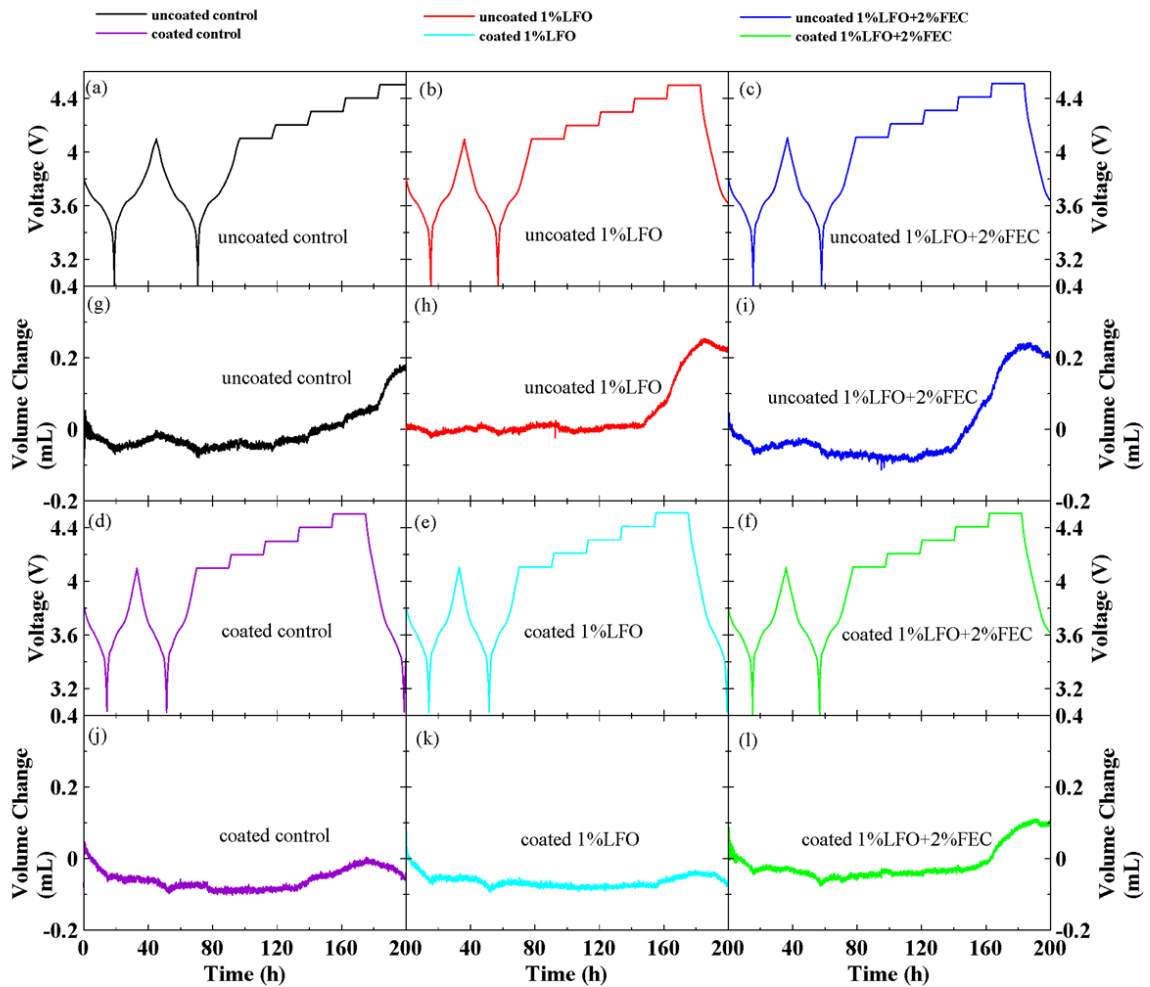


Figure 7.12 The in-situ gas evolution cell voltage as a function of time (a-f), and the gas volume of coated and uncoated SC NMC532/graphite pouch cells with different electrolytes as a function of time (g-l).  $\text{LiPO}_2\text{F}_2$  is called LFO in the Figure legend.

### Summary and observations:

It is clear that the Ti-based coating causes an increase in cell lifetime, a reduction in cell impedance and a reduction in cell gassing in most cases. The most significant exception



to the rule is in the case of cells with coated and uncoated SC NMC532 which contain “PES211”. In that case the cell performance (See Figures 7.5, 7.6 and 7.7) is very similar.

Readers may be tempted to attribute the reason for the effectiveness of the coating to be due to suppression of transition metal dissolution as shown by the XRF measurements reported in the text. The suppression of impedance growth by the coating in positive electrodes stored in pouch bags (Figure 7.2) could perhaps be attributed to less transition metal dissolution in the presence of a coating. The UHPC data in Figure 7.5, showing better results for cells with coated SC NMC532 electrodes (except for “PES211”) could perhaps be explained by the suppression of transition metal dissolution leading to less negative electrode SEI damage, less Li inventory loss and hence better CE. Figures 7.6 and 7.7 show that the presence of the coating on SC NMC532 greatly reduces the rate of impedance growth in cells with control electrolyte, 2% VC and 2% FEC. This, perhaps, could be explained by less transition metal dissolution in the presence of the coating. However, please recall that Ni and Co dissolution did not appear to be suppressed. Therefore, it is our opinion that “suppression of transition metal dissolution” is the “easy” explanation and is probably not the reason for the improved performance of the cells with coated SC NMC532. Some discussion points which address issues with the “easy” explanation are given below:

1. Figure 7.1 shows the voltage drop during storage. A voltage drop of 0.2 V between

4.4 V and 4.2 V corresponds to a loss of about 10% of the cell capacity, which by experience, can mostly be recovered during the next charge [154]. According to the scenarios discussed in Sinha et al., voltage drop in an open circuited cell can only occur if species are oxidized at the positive electrode and  $\text{Li}^+$  ions from the electrolyte are inserted into the positive electrode to balance the charge. This is what causes the voltage drop. In principle, a transition metal, M, can be oxidized to  $\text{M}^{2+}$  and dissolve into the electrolyte, transport to the negative and be reduced there. Since only 0.1 % of the Mn in the positive electrode was found on the negative electrode after 650 cycles and self-discharge during high voltage storage at 60°C corresponds to about 10% of the cell capacity, it seems unlikely that Mn dissolution can play any significant role in self discharge during storage.

2. The experiments on the cells with “PES211” are extremely interesting in that the cells with coated SC NMC532 and uncoated SC NMC532 show almost identical behavior (Figures 7.5, 7.6 and 7.7). Perhaps “PES211” forms a “perfect” interface layer on the uncoated SC 532 and prevents transition metal dissolution, but more likely is that “PES211” stops various electrolyte oxidation reactions. “PES211” has certainly been shown in numerous publications [131,185] to yield NMC442/graphite cells and NMC622/graphite cells with excellent performance even in cases where positive electrodes are uncoated. An extremely important experiment for the future is to compare Mn, Ni and Co levels on the negative electrodes of the cells with “PES211” having

coated and uncoated SC NMC532 electrodes in Figure 7.7. If the Mn levels are significantly different, then it is likely that suppression of Mn dissolution by the coating is simply a fact, but is not important in determining why the coating is successful.

3. The XPS measurements (Figure 7.10) on the negative electrodes extracted from cells after 650 cycles are very important because the SEI chemistry information disclosed here could explain the reason for cell capacity fade. The XPS spectra from negative electrodes extracted from cells with coated or uncoated SC NMC532 are very similar apart from more LiF and less ether-type compounds (287 eV) in the SEI of the electrodes from the cells with coated SC NMC532. Previous XPS work by Joshi et al. [176] more ether-type compounds (287 eV) appeared on graphite electrodes that had a significant amount of transition metal deposition (Figure 6 in Reference 176).

4. Ellis et al. [172] and Xiong et al. [171] demonstrated that the negative electrode in full cells does consume gases produced by the positive electrode. Therefore, the experiments in Figures 7.4 and 7.10 are extremely important. In full cells, the coating reduces the amount of gas generated when additives are present. However, in pouch bags containing only positive electrodes, the coated electrodes produced more gas. There are at least three ways these observations can be explained:

1) The gas product distribution is different in the cells and pouch bags containing either coated SC NMC532 or uncoated SC NMC532. The different gases then would apparently

be consumed more rapidly by the negative electrode in the full cells with coated SC NMC532 electrodes. If the gas product distributions are different, then the coating has affected the electrolyte oxidation at the positive electrode and hence this can certainly affect impedance and lifetime;

2) An increased amount of transition metals in the negative electrode SEI of the cells with uncoated electrodes somehow slows gas consumption. This is counterintuitive because transition metals can be catalytic for many reactions;

3) In Figure 7.4, it might be assumed that the difference between the black bar (gas volume of the pouch bag containing the positive electrode) and the blue bar (gas volume in the full pouch cell), " $\Delta(\text{black} - \text{blue})$ ", represents the amount of gas consumed by the negative electrode. " $\Delta(\text{black-blue})$ " is negative for control electrolyte. This means that there is a lot of gas ( $\text{H}_2$ ) produced by cross-talk in both coated/uncoated pouch cells with control electrolyte [172], which could explain why the voltage drop is large for control cells. " $\Delta(\text{black-blue})$ " is positive for cells with additive-containing electrolytes, which suggests that gas ( $\text{CO}_2$ ) is consumed in these cells. " $\Delta(\text{black} - \text{blue})$ " for cells with coated electrodes having additives is larger " $\Delta(\text{black} - \text{blue})$ " for uncoated electrodes, which suggests that more gas consumption occurs in cells with coated electrodes, either through mechanisms 1) or 2) above. Cells with "PES211" are an exception, for which " $\Delta(\text{black} - \text{blue})$ " for the uncoated electrode is similar to that for the coated electrode. Additionally,

there are other indications that coated cells consume more gas than uncoated cells. In Figure 7.12, uncoated cells produced more gas than coated cells at high voltage. Figure 7.10B shows that cells with coated electrodes have more LiF on the negative than cells with uncoated electrodes. LiF could be formed due to the reaction between  $\text{Li}_2\text{CO}_3$  (from the consumption of  $\text{CO}_2$ ) with  $\text{LiPF}_6$  [186] which also creates  $\text{LiPO}_2\text{F}_2$ , a highly beneficial additive. Based on the previous reports [187,188], the consumption of  $\text{CO}_2$  (creating LiF and  $\text{LiPO}_2\text{F}_2$ ) on the negative electrode could be beneficial to cell performance, which could explain why the performance of coated cells is better than that of uncoated cells.

Based on the discussion in this Summary and Observations section it is clear that further work is required to determine exactly how this Ti-based coating is effective.

### **7.3 Conclusions for Chapter 7**

The work in this chapter focused on studying the effect of a Ti-based surface coating on SC NMC532 using many experiments involving pouch cells, pouch bags and analytical tools. Compared to uncoated SC NMC532 electrode material, the addition of a surface coating did usually suppress parasitic reaction rates between electrodes and electrolytes, extend cell cycle lifetime, control cell impedance and suppress gas evolution at high voltage. The beneficial effect of the coating was most dramatic when simple electrolyte additives like 2% VC and 2% FEC were used. The coating was still beneficial, but less so,

when more modern additive combinations were used, except in the case of “PES211” where the coating provided little or no benefit.

Analysis of the reasons for capacity loss during long-term cycling was performed on 2% VC-containing uncoated SC NMC532/graphite and coated SC NMC532/graphite pouch cells. XRF, XPS, EIS, cross sectional SEM and differential voltage analysis were used to study the cells and positive electrodes. Lithium inventory loss, impedance growth and TM dissolution were found in uncoated SC NMC532/graphite pouch cells after long term cycling. The surface coating on SC NMC532 improved the capacity retention of the 2% VC containing cells by reducing Li inventory loss, suppressing impedance growth and transition metal dissolution. No evidence of micro-cracking leading to capacity loss was observed.

The reasons for the success of the surface coating are not clear as has been pointed out in the Summary and Observations section. Electrolyte additives strongly affect the way that cells with coated and uncoated electrodes behave. It is clear that any attempt to fully understand how this Ti-based coating really works will need to consider cells filled with more than one electrolyte type. Studies that are common in the literature often only study one electrolyte type and therefore are prone to conclusions that cannot be generalized.

## CHAPTER 8 CONCLUSIONS

### 8.1 Conclusions

In this thesis, the goal of increasing cell energy density has been achieved by operating cells at high voltage with an EC-free electrolyte system. The lifetime of SC NMC532/graphite cells has been increased with  $\text{LiPO}_2\text{F}_2$  containing electrolytes. The effect of interactions between SC NMC532 and graphite at high voltage and high temperature on impedance growth and gas evolution was characterized using the pouch bag method [168]. The results can help guide development of Li-ion cells with lower cost, higher energy density and longer lifetime.

In Chapter 4, NMC442/graphite Li-ion pouch cells were operated at 4.4 V by using an EC-free electrolyte system. This system was composed of EMC plus a certain amount of selected electrolyte additives. The main function of the selected electrolyte additives was to passivate graphite. This was characterized by measuring the percentage of EMC trans-esterification using GC-MS. These electrolyte additives had an obvious impact on cell performance from many perspectives: voltage drop during storage testing, cycling lifetime, gas evolution and impedance growth. Among all the electrolyte additives tested, FEC demonstrated the best performance by suppressing gas evolution, stopping impedance growth and extending cell lifetime. The disadvantages of EC-free electrolytes were also disclosed: the issue of gas evolution when Li plating occurred and poor

conductivity when the concentration of  $\text{LiPF}_6$  was lower than 0.4 M.

In Chapter 5, SC NMC532/graphite pouch Li-ion cells showed superior performance when  $\text{LiPO}_2\text{F}_2$  was used as an electrolyte additive. MA was also used as a co-solvent in EC/EMC electrolyte in order to improve cell fast charge rate capability. However, the addition of MA caused a penalty in cell lifetime.

In Chapter 6, the combined effect of  $\text{LiPO}_2\text{F}_2$  and many other electrolyte additives on SC NMC532/graphite pouch cell performance was systematically studied. Some electrolyte additives (e.g. FEC, VC and DiFEC) demonstrated a synergetic effect on SC NMC532/graphite Li-ion pouch cell performance when used with  $\text{LiPO}_2\text{F}_2$ .

In Chapter 7, the effect of a Ti-based surface coating on SC NMC532 was investigated when suitable electrolyte additives or additive combinations were used. The surface coating did further improve SC NMC532/graphite cell performance by extending cycling lifetime, suppressing gas evolution at high voltage, controlling impedance growth and decreasing parasitic reaction rates between the positive electrode and the electrolyte. Failure analysis was applied to 2% VC-containing cells after long term cycling (~ 650 cycles). Compared to uncoated cells, the surface coating improved cell lifetime by controlling impedance growth, suppressing transition metal dissolution and decreasing relative slippage.



## **8.2 Future work**

### **8.2.1 EC-free electrolyte systems**

The use of electrolyte additives is an efficient way to improve cell lifetime as mentioned in Chapter 2. Many theoretical calculations [189–191] have been carried out in order to design more useful electrolyte additives. However, experiments are the only way to determine if novel electrolyte additives are useful.

Chapter 4 showed that the type and the amount of electrolyte additives had an obvious impact on cell performance in the absence of EC. Therefore EC-free electrolyte system can be used to study the characteristics of electrolyte additives and to optimize the amount of electrolyte additives required. Once novel electrolyte additives are synthesized, EC-free electrolyte systems can be used to characterize them from many perspectives: gas evolution, the degree of passivation on graphite (i.e. the percentage of EMC trans-esterification), impedance, cell lifetime in different situations (i.e. during either storage or cycling at different temperatures) and so on. The testing results can give guidance on how to blend electrolyte additives in order to maximize the advantages of several electrolyte additives when used together.

In the future, the combination of EC-free electrolyte systems and positive electrode symmetric cell cycling method [192] may be useful to help screen superior electrode/electrolyte systems for Li-ion cells.

### **8.2.2 SC positive electrode materials**

Chapters 5-7 showed the advantages of SC (grain size is around 3  $\mu\text{m}$ ) positive electrode material (NMC532) from many perspectives (e.g. extend cell lifetime, control impedance growth, suppress gas evolution, etc.) when suitable electrolyte additives were used. Section 1.1 suggested that the development and commercialization of high Ni containing positive electrode materials could be the trend in the Li-ion battery field in order to increase the energy density. This indicates that an incredible amount of exploratory work needs to be done on the development of high Ni containing (NMC622, NMC811, NCA etc.) SC positive electrode materials.

Li et al. [20] and Li et al. [193] recently reported the procedures of synthesizing SC NMC532 and NMC622, respectively, and showed the impact of several factors on the synthesis. Apart from reference [193], few references about synthesizing high Ni-containing SC positive electrode materials can be found in the literature. The synthesis of high Ni-containing SC positive electrode materials must be explored. The reactivity of these charged materials and electrolytes at elevated temperatures needs to be studied by using ARC. Meanwhile, compatible electrolyte systems for high Ni-containing SC positive electrode materials need to be explored.

### **8.2.3 Electrode/electrolyte interactions**

Chapters 7 demonstrated the effect of interactions between SC NMC532 and artificial

graphite during high temperature storage on impedance growth and gas evolution. Chapters 5-7 showed that SC NMC532/artificial graphite pouch cells had superior performance from many perspectives. Based on Section 1.4, natural graphite and Si-containing negative electrode materials will have bright futures because they decrease cost and increase energy density, respectively.

It is valuable to investigate pouch cell performance (e.g. calendar lifetime, cycling lifetime, impedance growth, gas evolution and etc.) when SC materials are used as the positive electrode and natural graphite or Si-containing materials are used as the negative electrode. Fundamental studies of the interaction between SC positive electrodes and natural graphite or Si-containing negative electrodes during high temperature storage need to be explored. This will help elucidate relevant cell failure mechanisms and contribute to the development of novel electrolyte systems for SC NMC/natural graphite or Si-containing material cells.

#### **8.2.4 Coatings on positive electrode materials**

Chapter 7 showed that the Ti-based surface coating on SC NMC532 improved cell performance from many perspectives. Section 2.3 suggested that there were many options for surface coating on positive electrode materials in addition to Ti-based surface coating.

It will be interesting to investigate the effects of different surface coatings on positive electrode materials from many perspectives: impedance, cell lifetime, gas evolution,

compatibility with different electrolyte additives and so on. The amount of coating material is another important parameter that needs to be explored.

### **8.2.5 Differences between SC and polycrystalline materials when Li metal is used as the negative electrode**

Recently the lithium metal anode became a hot topic for increasing cell energy density because of its high theoretical specific capacity (3,860 mAh/g) and low electrochemical potential (-3.04V versus the standard hydrogen electrode) [194]. Zheng et al. [195] showed that the use of electrolyte additives improved NMC442/Li cell performance. Chapters 5-7 demonstrated that SC NMC532/graphite pouch cells performed well with the addition of suitable electrolyte additives.

It is valuable to do comparative studies about the difference between SC NMC/Li cell and traditional polycrystalline NMC/Li cell when electrolyte additives are used. Cell lifetime, impedance, surface chemistry and so on will be characterized systematically.

Miao et al. [196] reported that the choice of electrolyte salt in lithium metal cells affected lithium crystal growth. As a result, this could help suppress the formation of lithium dendrites. It is necessary to investigate the effect of different lithium salts in SC NMC/Li cells and traditional polycrystalline NMC/Li cells, respectively.

### **8.2.6 Failure analysis on coated and uncoated SC NMC532/graphite pouch cells when superior electrolyte additives are used**

In Chapter 7, failure analysis (e.g. EIS testing, differential voltage analysis, transition metal dissolution testing) on coated and uncoated SC NMC532/graphite pouch cells with 2% VC after long term cycling was performed. Since the amount of detected transition metal dissolution is quite small, it is doubtful that transition metal dissolution played an important role in cell capacity fade for the cells tested here.

The coated and uncoated SC NMC532/graphite pouch cells with superior electrolyte additives (e.g. “PES211”, 2%VC+1%DTD, etc.) still have excellent capacity retention and are still testing as of July 25<sup>th</sup>, 2018. It will be very valuable to do failure analysis (e.g. EIS testing, transitional metal dissolution testing, differential voltage analysis, etc.) on those cells when they have a relatively large fraction of capacity loss in the future. This could help explain how the surface coating improves cell performance.

## REFERENCES

- [1] Z. Lu, D.D. MacNeil, J.R. Dahn, Layered  $\text{Li}[\text{Ni}_x\text{Co}_{1-2x}\text{Mnx}]\text{O}_2$  Cathode Materials for Lithium-Ion Batteries, *Electrochem. Solid-State Lett.* 4 (2001) A200–A203.
- [2] T. Ohzuku, Y. Makimura, Layered Lithium Insertion Material of  $\text{LiCo}_{1/3}\text{Ni}_{1/3}\text{Mn}_{1/3}\text{O}_2$  for Lithium-Ion Batteries, *Chem. Lett.* 30 (2001) 642–643.
- [3] C.M. Julien, A. Mauger, K. Zaghib, H. Groult, Comparative Issues of Cathode Materials for Li-Ion Batteries, *Inorganics.* 2 (2014) 132–154.
- [4] Z. Wu, S. Ji, J. Zheng, Z. Hu, S. Xiao, Y. Wei, Z. Zhuo, Y. Lin, W. Yang, K. Xu, K. Amine, F. Pan, Prelithiation Activates  $\text{Li}(\text{Ni}_{0.5}\text{Mn}_{0.3}\text{Co}_{0.2})\text{O}_2$  for High Capacity and Excellent Cycling Stability, *Nano Lett.* 15 (2015) 5590–5596.
- [5] Y. Su, S. Cui, Z. Zhuo, W. Yang, X. Wang, F. Pan, Enhancing the High-Voltage Cycling Performance of  $\text{LiNi}_{0.5}\text{Mn}_{0.3}\text{Co}_{0.2}\text{O}_2$  by Retarding Its Interfacial Reaction with an Electrolyte by Atomic-Layer-Deposited  $\text{Al}_2\text{O}_3$ , *ACS Appl. Mater. Interfaces.* 7 (2015) 25105–25112.
- [6] W. Ahn, S.N. Lim, K. N. Jung, S.-H. Yeon, K.-B. Kim, H.S. Song, K.H. Shin, Combustion-synthesized  $\text{LiNi}_{0.6}\text{Mn}_{0.2}\text{Co}_{0.2}\text{O}_2$  as cathode material for lithium ion batteries, *J. Alloys Compd.* 609 (2014) 143–149.
- [7] J. Choi, J. Lee, Improved electrochemical properties of  $\text{Li}(\text{Ni}_{0.6}\text{Mn}_{0.2}\text{Co}_{0.2})\text{O}_2$  by surface coating with  $\text{Li}_{1.3}\text{Al}_{0.3}\text{Ti}_{1.7}(\text{PO}_4)_3$ , *J. Power Sources.* 307 (2016) 63–68.
- [8] J. Li, L.E. Downie, L. Ma, W. Qiu, J.R. Dahn, Study of the Failure Mechanisms of  $\text{LiNi}_{0.8}\text{Mn}_{0.1}\text{Co}_{0.1}\text{O}_2$  Cathode Material for Lithium Ion Batteries, *J. Electrochem. Soc.* 162 (2015) A1401–A1408.
- [9] R. Petibon, J. Xia, L. Ma, M.K.G. Bauer, K.J. Nelson, J.R. Dahn, Electrolyte System for High Voltage Li-Ion Cells, *J. Electrochem. Soc.* 163 (2016) A2571–A2578.
- [10] K. Xu, Electrolytes and Interphases in Li-Ion Batteries and Beyond, *Chem. Rev.* 114 (2014) 11503–11618.
- [11] J. Xia, R. Petibon, D. Xiong, L. Ma, J.R. Dahn, Enabling linear alkyl carbonate electrolytes for high voltage Li-ion cells, *J. Power Sources.* 328 (2016) 124–135.

- [12] J. Li, A.R. Cameron, H. Li, S. Glazier, D. Xiong, M. Chatzidakis, J. Allen, G.A. Botton, J.R. Dahn, Comparison of Single Crystal and Polycrystalline  $\text{LiNi}_{0.5}\text{Mn}_{0.3}\text{Co}_{0.2}\text{O}_2$  Positive Electrode Materials for High Voltage Li-Ion Cells, *J. Electrochem. Soc.* 164 (2017) A1534–A1544.
- [13] L. Wang, B. Wu, D. Mu, X. Liu, Y. Peng, H. Xu, Q. Liu, L. Gai, F. Wu, Single-crystal  $\text{LiNi}_{0.6}\text{Co}_{0.2}\text{Mn}_{0.2}\text{O}_2$  as high performance cathode materials for Li-ion batteries, *J. Alloys Compd.* 674 (2016) 360–367.
- [14] T. Reddy, *Linden's Handbook of Batteries 4th Edition*, McGraw Hill Professional, 2010.
- [15] M.S. Whittingham, Lithium Batteries and Cathode Materials, *Chem. Rev.* 104 (2004) 4271–4302.
- [16] Y. K. Sun, C.S. Yoon, S.-T. Myung, I. Belharouak, K. Amine, Role of  $\text{AlF}_3$  Coating on  $\text{LiCoO}_2$  Particles during Cycling to Cutoff Voltage above 4.5 V, *J. Electrochem. Soc.* 156 (2009) A1005–A1010.
- [17] J. Jiang, J.R. Dahn, ARC studies of the reaction between  $\text{LiFePO}_4$  and  $\text{LiPF}_6$  or  $\text{LiBOB}$  EC/DEC electrolytes, *Electrochem. Commun.* 6 (2004) 724–728.
- [18] L. X. Yuan, Z. H. Wang, W. X. Zhang, X. L. Hu, J. T. Chen, Y.-H. Huang, J.B. Goodenough, Development and challenges of  $\text{LiFePO}_4$  cathode material for lithium-ion batteries, *Energy Environ. Sci.* 4 (2011) 269–284.
- [19] H. J. Noh, S. Youn, C.S. Yoon, Y. K. Sun, Comparison of the structural and electrochemical properties of layered  $\text{Li}[\text{Ni}_x\text{Co}_y\text{Mn}_z]\text{O}_2$  ( $x = 1/3, 0.5, 0.6, 0.7, 0.8$  and  $0.85$ ) cathode material for lithium-ion batteries, *J. Power Sources.* 233 (2013) 121–130.
- [20] J. Li, H. Li, W. Stone, R. Weber, S. Hy, J.R. Dahn, Synthesis of Single Crystal  $\text{LiNi}_{0.5}\text{Mn}_{0.3}\text{Co}_{0.2}\text{O}_2$  for Lithium Ion Batteries, *J. Electrochem. Soc.* 164 (2017) A3529–A3537.
- [21] Z. Lu, D.D. MacNeil, J.R. Dahn, Layered Cathode Materials  $\text{Li}[\text{Ni}_x\text{Li}_{(1/3-2x/3)}\text{Mn}_{(2/3-x/3)}]\text{O}_2$  for Lithium-Ion Batteries, *Electrochem. Solid-State Lett.* 4 (2001) A191–A194.
- [22] M. Hu, X. Pang, Z. Zhou, Recent progress in high-voltage lithium ion batteries, *J. Power Sources.* 237 (2013) 229–242.

- [23] Z. Lu, L.Y. Beaulieu, R.A. Donaberger, C.L. Thomas, J.R. Dahn, Synthesis, Structure, and Electrochemical Behavior of  $\text{Li}[\text{Ni}_x\text{Li}_{1/3-2x/3}\text{Mn}_{2/3-x/3}]\text{O}_2$ , *J. Electrochem. Soc.* 149 (2002) A778–A791.
- [24] A. van Bommel, L.J. Krause, J.R. Dahn, Investigation of the Irreversible Capacity Loss in the Lithium-Rich Oxide  $\text{Li}[\text{Li}_{1/5}\text{Ni}_{1/5}\text{Mn}_{3/5}]\text{O}_2$ , *J. Electrochem. Soc.* 158 (2011) A731–A735.
- [25] J. Hong, H.D. Lim, M. Lee, S.W. Kim, H. Kim, S.T. Oh, G.C. Chung, K. Kang, Critical Role of Oxygen Evolved from Layered Li-Excess Metal Oxides in Lithium Rechargeable Batteries, *Chem. Mater.* 24 (2012) 2692–2697.
- [26] J. Zheng, M. Gu, A. Genc, J. Xiao, P. Xu, X. Chen, Z. Zhu, W. Zhao, L. Pullan, C. Wang, J.G. Zhang, Mitigating Voltage Fade in Cathode Materials by Improving the Atomic Level Uniformity of Elemental Distribution, *Nano Lett.* 14 (2014) 2628–2635.
- [27] M. Winter, J.O. Besenhard, M.E. Spahr, P. Novák, Insertion Electrode Materials for Rechargeable Lithium Batteries, *Adv. Mater.* 10 (1998) 725–763.
- [28] M. Yoshio, H. Wang, K. Fukuda, T. Umeno, T. Abe, Z. Ogumi, Improvement of natural graphite as a lithium-ion battery anode material, from raw flake to carbon-coated sphere, *J. Mater. Chem.* 14 (2004) 1754–1758.
- [29] H. Zhao, J. Ren, X. He, J. Li, C. Jiang, C. Wan, Modification of natural graphite for lithium ion batteries, *Solid State Sci.* 10 (2008) 612–617.
- [30] X. Guo, C. Wang, M. Chen, J. Wang, J. Zheng, Carbon coating of  $\text{Li}_4\text{Ti}_5\text{O}_{12}$  using amphiphilic carbonaceous material for improvement of lithium-ion battery performance, *J. Power Sources.* 214 (2012) 107–112.
- [31] T. Ohzuku, A. Ueda, N. Yamamoto, Zero-Strain Insertion Material of  $\text{Li}[\text{Li}_{1/3}\text{Ti}_{5/3}]\text{O}_4$  for Rechargeable Lithium Cells, *J. Electrochem. Soc.* 142 (1995) 1431–1435.
- [32] S.D. Beattie, D. Larcher, M. Morcrette, B. Simon, J.-M. Tarascon, Si Electrodes for Li-Ion Batteries—A New Way to Look at an Old Problem, *J. Electrochem. Soc.* 155 (2008) A158–A163.
- [33] M.N. Obrovac, L. Christensen, D.B. Le, J.R. Dahn, Alloy Design for Lithium-Ion Battery Anodes, *J. Electrochem. Soc.* 154 (2007) A849–A855.



- [34] M.N. Obrovac, V.L. Chevrier, Alloy Negative Electrodes for Li-Ion Batteries, *Chem. Rev.* 114 (2014) 11444–11502.
- [35] U. Kasavajjula, C. Wang, A.J. Appleby, Nano- and bulk-silicon-based insertion anodes for lithium-ion secondary cells, *J. Power Sources.* 163 (2007) 1003–1039.
- [36] M. Holzapfel, H. Buqa, L.J. Hardwick, M. Hahn, A. Würsig, W. Scheifele, P. Novák, R. Kötz, C. Veit, F.-M. Petrat, Nano silicon for lithium-ion batteries, *Electrochim. Acta.* 52 (2006) 973–978.
- [37] Z. Du, R.A. Dunlap, M.N. Obrovac, High Energy Density Calendered Si Alloy/Graphite Anodes, *J. Electrochem. Soc.* 161 (2014) A1698–A1705.
- [38] V.L. Chevrier, L. Liu, D.B. Le, J. Lund, B. Molla, K. Reimer, L.J. Krause, L.D. Jensen, E. Figgemeier, K.W. Eberman, Evaluating Si-Based Materials for Li-Ion Batteries in Commercially Relevant Negative Electrodes, *J. Electrochem. Soc.* 161 (2014) A783–A791.
- [39] K. Xu, Nonaqueous Liquid Electrolytes for Lithium-Based Rechargeable Batteries, *Chem. Rev.* 104 (2004) 4303–4418.
- [40] A. Abouimrane, I. Belharouak, K. Amine, Sulfone-based electrolytes for high-voltage Li-ion batteries, *Electrochem. Commun.* 11 (2009) 1073–1076.
- [41] H. Duncan, N. Salem, Y. Abu-Lebdeh, Electrolyte Formulations Based on Dinitrile Solvents for High Voltage Li-Ion Batteries, *J. Electrochem. Soc.* 160 (2013) A838–A848.
- [42] S.S. Zhang, T.R. Jow, Aluminum corrosion in electrolyte of Li-ion battery, *J. Power Sources.* 109 (2002) 458–464.
- [43] S.S. Zhang, K. Xu, T.R. Jow, Study of LiBF<sub>4</sub> as an Electrolyte Salt for a Li-Ion Battery, *J. Electrochem. Soc.* 149 (2002) A586–A590.
- [44] K. Xu, Tailoring Electrolyte Composition for LiBOB, *J. Electrochem. Soc.* 155 (2008) A733–A738.
- [45] J.L. Nowinski, P. Lightfoot, P.G. Bruce, Structure of LiN(CF<sub>3</sub>SO<sub>2</sub>)<sub>2</sub>, a novel salt for electrochemistry, *J. Mater. Chem.* 4 (1994) 1579–1580.

- [46] Y. Yamada, K. Furukawa, K. Sodeyama, K. Kikuchi, M. Yaegashi, Y. Tateyama, A. Yamada, Unusual Stability of Acetonitrile-Based Superconcentrated Electrolytes for Fast-Charging Lithium-Ion Batteries, *J. Am. Chem. Soc.* 136 (2014) 5039–5046.
- [47] R.T. Jow, K. Xu, O. Borodin, *Electrolytes for Lithium and Lithium-ion Batteries*, Springer, New York, 2014.
- [48] L. Li, S. Zhou, H. Han, H. Li, J. Nie, M. Armand, Z. Zhou, X. Huang, Transport and Electrochemical Properties and Spectral Features of Non-Aqueous Electrolytes Containing LiFSI in Linear Carbonate Solvents, *J. Electrochem. Soc.* 158 (2011) A74–A82.
- [49] M. Nie, J. Xia, J.R. Dahn, Development of Pyridine-Boron Trifluoride Electrolyte Additives for Lithium-Ion Batteries, *J. Electrochem. Soc.* 162 (2015) A1186–A1195.
- [50] J. Xia, L. Ma, C.P. Aiken, K.J. Nelson, L.P. Chen, J.R. Dahn, Comparative Study on Prop-1-ene-1,3-sultone and Vinylene Carbonate as Electrolyte Additives for  $\text{Li}(\text{Ni}_{1/3}\text{Mn}_{1/3}\text{Co}_{1/3})\text{O}_2/\text{Graphite}$  Pouch Cells, *J. Electrochem. Soc.* 161 (2014) A1634–A1641.
- [51] E. Peled, The Electrochemical Behavior of Alkali and Alkaline Earth Metals in Nonaqueous Battery Systems—The Solid Electrolyte Interphase Model, *J. Electrochem. Soc.* 126 (1979) 2047–2051.
- [52] M. Winter, The Solid Electrolyte Interphase – The Most Important and the Least Understood Solid Electrolyte in Rechargeable Li Batteries, *Zeitschrift Für Phys. Chemie Int. J. Res. Phys. Chem. Chem. Phys.* 223 (2009) 1395–1406.
- [53] S.S. Zhang, A review on electrolyte additives for lithium-ion batteries, *J. Power Sources.* 162 (2006) 1379–1394.
- [54] A.M. Andersson, K. Edström, Chemical Composition and Morphology of the Elevated Temperature SEI on Graphite, *J. Electrochem. Soc.* 148 (2001) A1100–A1109.
- [55] D. Aurbach, Y. Ein-Eli, B. Markovsky, A. Zaban, S. Luski, Y. Carmeli, H. Yamin, The Study of Electrolyte Solutions Based on Ethylene and Diethyl Carbonates for Rechargeable Li Batteries II . Graphite Electrodes, *J. Electrochem. Soc.* 142 (1995) 2882–2890.

- [56] M. Nie, D. Chalasani, D.P. Abraham, Y. Chen, A. Bose, B.L. Lucht, Lithium Ion Battery Graphite Solid Electrolyte Interphase Revealed by Microscopy and Spectroscopy, *J. Phys. Chem. C*. 117 (2013) 1257–1267.
- [57] S.E. Sloop, J.B. Kerr, K. Kinoshita, The role of Li-ion battery electrolyte reactivity in performance decline and self-discharge, *J. Power Sources*. 119–121 (2003) 330–337.
- [58] S. Mori, H. Asahina, H. Suzuki, A. Yonei, K. Yokoto, Chemical properties of various organic electrolytes for lithium rechargeable batteries, *J. Power Sources*. 68 (1997) 59–64.
- [59] G. V. Zhuang, P.N. Ross, Analysis of the Chemical Composition of the Passive Film on Li-Ion Battery Anodes Using Attenuated Total Reflection Infrared Spectroscopy, *Electrochem. Solid-State Lett.* 6 (2003) A136–A139.
- [60] D. Aurbach, B. Markovsky, I. Weissman, E. Levi, Y. Ein-Eli, On the correlation between surface chemistry and performance of graphite negative electrodes for Li ion batteries, *Electrochim. Acta*. 45 (1999) 67–86.
- [61] S.H. Kang, D.P. Abraham, A. Xiao, B.L. Lucht, Investigating the solid electrolyte interphase using binder-free graphite electrodes, *J. Power Sources*. 175 (2008) 526–532.
- [62] A. Augustsson, M. Herstedt, J.-H. Guo, K. Edström, G. V. Zhuang, J. P. N. Ross, J.E. Rubensson, J. Nordgren, Solid electrolyte interphase on graphite Li-ion battery anodes studied by soft X-ray spectroscopy, 6 (2004) 4185–4189.
- [63] D. Aurbach, M. Moshkovich, A Study of Lithium Deposition-Dissolution Processes in a Few Selected Electrolyte Solutions by Electrochemical Quartz Crystal Microbalance, *J. Electrochem. Soc.* 145 (1998) 2629–2639.
- [64] H. Yoshida, T. Fukunaga, T. Hazama, M. Terasaki, M. Mizutani, M. Yamachi, Degradation mechanism of alkyl carbonate solvents used in lithium-ion cells during initial charging, *J. Power Sources*. 68 (1997) 311–315.
- [65] E. Markevich, K. Fridman, R. Sharabi, R. Elazari, G. Salitra, H.E. Gottlieb, G. Gershinsky, A. Garsuch, G. Semrau, M.A. Schmidt, D. Aurbach, Amorphous Columnar Silicon Anodes for Advanced High Voltage Lithium Ion Full Cells: Dominant Factors Governing Cycling Performance, *J. Electrochem. Soc.* 160 (2013) A1824–A1833.

- [66] A. V. Plakhotnyk, L. Ernst, R. Schmutzler, Hydrolysis in the system  $\text{LiPF}_6$ —propylene carbonate—dimethyl carbonate— $\text{H}_2\text{O}$ , *J. Fluor. Chem.* 126 (2005) 27–31.
- [67] D.J. Xiong, R. Petibon, L. Madec, D.S. Hall, J.R. Dahn, Some Effects of Intentionally Added Water on  $\text{LiCoO}_2$ /Graphite Pouch Cells, *J. Electrochem. Soc.* 163 (2016) A1678–A1685.
- [68] H. Ota, Y. Sakata, A. Inoue, S. Yamaguchi, Analysis of Vinylene Carbonate Derived SEI Layers on Graphite Anode, *J. Electrochem. Soc.* 151 (2004) A1659–A1669.
- [69] L. El Ouatani, R. Dedryvère, C. Siret, P. Biensan, S. Reynaud, P. Iratçabal, D. Gonbeau, The Effect of Vinylene Carbonate Additive on Surface Film Formation on Both Electrodes in Li-Ion Batteries, *J. Electrochem. Soc.* 156 (2009) A103–A113.
- [70] K. Matsumoto, R. Kuzuo, K. Takeya, A. Yamanaka, Effects of  $\text{CO}_2$  in air on Li deintercalation from  $\text{LiNi}_{1-x-y}\text{Co}_x\text{Al}_y\text{O}_2$ , *J. Power Sources.* 81–82 (1999) 558–561.
- [71] R. Amin, D.B. Ravnsbæk, Y. M. Chiang, Characterization of Electronic and Ionic Transport in  $\text{Li}_{1-x}\text{Ni}_{0.8}\text{Co}_{0.15}\text{Al}_{0.05}\text{O}_2$  (NCA), *J. Electrochem. Soc.* 162 (2015) A1163–A1169.
- [72] Z. Wang, X. Huang, L. Chen, Characterization of Spontaneous Reactions of  $\text{LiCoO}_2$  with Electrolyte Solvent for Lithium-Ion Batteries, *J. Electrochem. Soc.* 151 (2004) A1641–A1652.
- [73] Z. Wang, X. Huang, L. Chen, Performance Improvement of Surface-Modified  $\text{LiCoO}_2$  Cathode Materials: An Infrared Absorption and X-Ray Photoelectron Spectroscopic Investigation, *J. Electrochem. Soc.* 150 (2003) A199–A208.
- [74] M. Ménétrier, C. Vaysse, L. Croguennec, C. Delmas, C. Jordy, F. Bonhomme, P. Biensan,  $^7\text{Li}$  and  $^1\text{H}$  MAS NMR Observation of Interphase Layers on Lithium Nickel Oxide Based Positive Electrodes of Lithium-Ion Batteries, *Electrochem. Solid-State Lett.* 7 (2004) A140–A143.
- [75] H. Duncan, D. Duguay, Y. Abu-Lebdeh, I.J. Davidson, Study of the  $\text{LiMn}_{1.5}\text{Ni}_{0.5}\text{O}_4$ /Electrolyte Interface at Room Temperature and  $60^\circ\text{C}$ , *J. Electrochem. Soc.* 158 (2011) A537–A545.

- [76] H. Duncan, Y. Abu-Lebdeh, I.J. Davidson, Study of the Cathode–Electrolyte Interface of  $\text{LiMn}_{1.5}\text{Ni}_{0.5}\text{O}_4$  Synthesized by a Sol–Gel Method for Li-Ion Batteries, *J. Electrochem. Soc.* 157 (2010) A528–A535.
- [77] L. Madec, R. Petibon, J. Xia, J.-P. Sun, I.G. Hill, J.R. Dahn, Understanding the Role of Prop-1-ene-1,3-Sultone and Vinylene Carbonate in  $\text{LiNi}_{1/3}\text{Mn}_{1/3}\text{Co}_{1/3}\text{O}_2$ /Graphite Pouch Cells: Electrochemical, GC-MS and XPS Analysis, *J. Electrochem. Soc.* 162 (2015) A2635–A2645.
- [78] D. Aurbach, K. Gamolsky, B. Markovsky, Y. Gofer, M. Schmidt, U. Heider, On the use of vinylene carbonate (VC) as an additive to electrolyte solutions for Li-ion batteries, *Electrochim. Acta.* 47 (2002) 1423–1439.
- [79] D.Y. Wang, J. Xia, L. Ma, K.J. Nelson, J.E. Harlow, D. Xiong, L.E. Downie, R. Petibon, J.C. Burns, A. Xiao, W.M. Lamanna, J.R. Dahn, A Systematic Study of Electrolyte Additives in  $\text{Li}[\text{Ni}_{1/3}\text{Mn}_{1/3}\text{Co}_{1/3}]\text{O}_2$  (NMC)/Graphite Pouch Cells, *J. Electrochem. Soc.* 161 (2014) A1818–A1827.
- [80] J.C. Burns, N.N. Sinha, D.J. Coyle, G. Jain, C.M. VanElzen, W.M. Lamanna, A. Xiao, E. Scott, J.P. Gardner, J.R. Dahn, The Impact of Varying the Concentration of Vinylene Carbonate Electrolyte Additive in Wound Li-Ion Cells, *J. Electrochem. Soc.* 159 (2011) A85–A90.
- [81] M. Herstedt, H. Rensmo, H. Siegbahn, K. Edström, Electrolyte additives for enhanced thermal stability of the graphite anode interface in a Li-ion battery, *Electrochim. Acta.* 49 (2004) 2351–2359.
- [82] L. Ma, J. Xia, X. Xia, J.R. Dahn, The Impact of Vinylene Carbonate, Fluoroethylene Carbonate and Vinyl Ethylene Carbonate Electrolyte Additives on Electrode/Electrolyte Reactivity Studied Using Accelerating Rate Calorimetry, *J. Electrochem. Soc.* 161 (2014) A1495–A1498.
- [83] C.P. Aiken, J. Xia, D.Y. Wang, D.A. Stevens, S. Trussler, J.R. Dahn, An Apparatus for the Study of In Situ Gas Evolution in Li-Ion Pouch Cells, *J. Electrochem. Soc.* 161 (2014) A1548–A1554.
- [84] J. Self, C.P. Aiken, R. Petibon, J.R. Dahn, Survey of Gas Expansion in Li-Ion NMC Pouch Cells, *J. Electrochem. Soc.* 162 (2015) A796–A802.

- [85] C.P. Aiken, J. Self, R. Petibon, X. Xia, J.M. Paulsen, J.R. Dahn, A Survey of In Situ Gas Evolution during High Voltage Formation in Li-Ion Pouch Cells, *J. Electrochem. Soc.* 162 (2015) A760–A767.
- [86] R. Petibon, N.N. Sinha, J.C. Burns, C.P. Aiken, H. Ye, C.M. VanElzen, G. Jain, S. Trussler, J.R. Dahn, Comparative study of electrolyte additives using electrochemical impedance spectroscopy on symmetric cells, *J. Power Sources.* 251 (2014) 187–194.
- [87] L. Chen, K. Wang, X. Xie, J. Xie, Effect of vinylene carbonate (VC) as electrolyte additive on electrochemical performance of Si film anode for lithium ion batteries, *J. Power Sources.* 174 (2007) 538–543.
- [88] X. Zuo, C. Fan, X. Xiao, J. Liu, J. Nan, High-voltage performance of LiCoO<sub>2</sub>/graphite batteries with methylene methanedisulfonate as electrolyte additive, *J. Power Sources.* 219 (2012) 94–99.
- [89] P. Ridgway, H. Zheng, G. Liu, X. Song, P. Ross, V. Battaglia, Effect of Vinylene Carbonate on Graphite Anode Cycling Efficiency, *ECS Trans.* 19 (2009) 51–57.
- [90] R. Chen, F. Wu, L. Li, Y. Guan, X. Qiu, S. Chen, Y. Li, S. Wu, Butylene sulfite as a film-forming additive to propylene carbonate-based electrolytes for lithium ion batteries, *J. Power Sources.* 172 (2007) 395–403.
- [91] B. Wang, Q.T. Qu, Q. Xia, Y.P. Wu, X. Li, C.L. Gan, T. van Ree, Effects of 3,5-bis(trifluoromethyl)benzeneboronic acid as an additive on electrochemical performance of propylene carbonate-based electrolytes for lithium ion batteries, *Electrochim. Acta.* 54 (2008) 816–820.
- [92] K. Xu, S. Zhang, T.R. Jow, LiBOB as Additive in LiPF<sub>6</sub>-Based Lithium Ion Electrolytes, *Electrochem. Solid-State Lett.* 8 (2005) A365–A368.
- [93] G. Yang, J. Shi, C. Shen, S. Wang, L. Xia, H. Hu, H. Luo, Y. Xia, Z. Liu, Improving the cyclability performance of lithium-ion batteries by introducing lithium difluorophosphate (LiPO<sub>2</sub>F<sub>2</sub>) additive, *RSC Adv.* 7 (2017) 26052–26059.
- [94] B. Yang, H. Zhang, L. Yu, W. Fan, D. Huang, Lithium difluorophosphate as an additive to improve the low temperature performance of LiNi<sub>0.5</sub>Co<sub>0.2</sub>Mn<sub>0.3</sub>O<sub>2</sub>/graphite cells, *Electrochim. Acta.* 221 (2016) 107–114.

- [95] L. Chen, K. Wang, X. Xie, J. Xie, Enhancing Electrochemical Performance of Silicon Film Anode by Vinylene Carbonate Electrolyte Additive, *Electrochem. Solid-State Lett.* 9 (2006) A512–A515.
- [96] M. Q. Li, M. Z. Qu, X. Y. He, Z. L. Yu, Electrochemical Performance of Si/Graphite/Carbon Composite Electrode in Mixed Electrolytes Containing LiBOB and LiPF<sub>6</sub>, *J. Electrochem. Soc.* 156 (2009) A294–A298.
- [97] N. S. Choi, K.H. Yew, H. Kim, S. S. Kim, W. U. Choi, Surface layer formed on silicon thin-film electrode in lithium bis(oxalato) borate-based electrolyte, *J. Power Sources.* 172 (2007) 404–409.
- [98] K. Fridman, R. Sharabi, R. Elazari, G. Gershinsky, E. Markevich, G. Salitra, D. Aurbach, A. Garsuch, J. Lampert, A new advanced lithium ion battery: Combination of high performance amorphous columnar silicon thin film anode, 5 V LiNi<sub>0.5</sub>Mn<sub>1.5</sub>O<sub>4</sub> spinel cathode and fluoroethylene carbonate-based electrolyte solution, *Electrochem. Commun.* 33 (2013) 31–34.
- [99] H. Nakai, T. Kubota, A. Kita, A. Kawashima, Investigation of the Solid Electrolyte Interphase Formed by Fluoroethylene Carbonate on Si Electrodes, *J. Electrochem. Soc.* 158 (2011) A798–A801.
- [100] A.J. Smith, J.C. Burns, D. Xiong, J.R. Dahn, Interpreting High Precision Coulometry Results on Li-ion Cells, *J. Electrochem. Soc.* 158 (2011) A1136–A1142.
- [101] J.C. Burns, A. Kassam, N.N. Sinha, L.E. Downie, L. Solnickova, B.M. Way, J.R. Dahn, Predicting and Extending the Lifetime of Li-Ion Batteries, *J. Electrochem. Soc.* 160 (2013) A1451–A1456.
- [102] J.C. Burns, R. Petibon, K.J. Nelson, N.N. Sinha, A. Kassam, B.M. Way, J.R. Dahn, Studies of the Effect of Varying Vinylene Carbonate (VC) Content in Lithium Ion Cells on Cycling Performance and Cell Impedance, *J. Electrochem. Soc.* 160 (2013) A1668–A1674.
- [103] C. Täubert, M. Fleischhammer, M. Wohlfahrt-Mehrens, U. Wietelmann, T. Buhrmester, LiBOB as Electrolyte Salt or Additive for Lithium-Ion Batteries Based on LiNi<sub>0.8</sub>Co<sub>0.15</sub>Al<sub>0.05</sub>O<sub>2</sub>/Graphite, *J. Electrochem. Soc.* 157 (2010) A721–A728.

- [104] S. Dalavi, M. Xu, B. Knight, B.L. Lucht, Effect of Added LiBOB on High Voltage ( $\text{LiNi}_{0.5}\text{Mn}_{1.5}\text{O}_4$ ) Spinel Cathodes, *Electrochem. Solid-State Lett.* 15 (2011) A28–A31.
- [105] W. Zhao, G. Zheng, M. Lin, W. Zhao, D. Li, X. Guan, Y. Ji, G.F. Ortiz, Y. Yang, Toward a stable solid-electrolyte-interfaces on nickel-rich cathodes:  $\text{LiPO}_2\text{F}_2$  salt-type additive and its working mechanism for  $\text{LiNi}_{0.5}\text{Mn}_{0.25}\text{Co}_{0.25}\text{O}_2$  cathodes, *J. Power Sources.* 380 (2018) 149–157.
- [106] X. Zuo, J. Wu, C. Fan, K. Lai, J. Liu, J. Nan, Improvement of the thermal stability of  $\text{LiMn}_2\text{O}_4$ /graphite cells with methylene methanedisulfonate as electrolyte additive, *Electrochim. Acta.* 130 (2014) 778–784.
- [107] R. Wang, X. Li, Z. Wang, H. Guo, Manganese dissolution from  $\text{LiMn}_2\text{O}_4$  cathodes at elevated temperature: methylene methanedisulfonate as electrolyte additive, *J. Solid State Electrochem.* 20 (2016) 19–28.
- [108] J. Xia, R. Petibon, A. Xiao, W.M. Lamanna, J.R. Dahn, Some Fluorinated Carbonates as Electrolyte Additives for  $\text{Li}(\text{Ni}_{0.4}\text{Mn}_{0.4}\text{Co}_{0.2})\text{O}_2$ /Graphite Pouch Cells, *J. Electrochem. Soc.* 163 (2016) A1637–A1645.
- [109] Y. Han, Synthesis and characterization of difluoroethylene carbonate (DFEC) and lithium difluorophosphate ( $\text{LiPF}_2\text{O}_2$ ) as new additives for lithium-ion batteries, The Hong Kong University of Science and Technology, 2015.
- [110] J. Cho, Y. W. Kim, B. Kim, J. G. Lee, B. Park, A Breakthrough in the Safety of Lithium Secondary Batteries by Coating the Cathode Material with  $\text{AlPO}_4$  Nanoparticles, *Angew. Chemie Int. Ed.* 42 (2003) 1618–1621.
- [111] T. Yang, N. Zhang, Y. Lang, K. Sun, Enhanced rate performance of carbon-coated  $\text{LiNi}_{0.5}\text{Mn}_{1.5}\text{O}_4$  cathode material for lithium ion batteries, *Electrochim. Acta.* 56 (2011) 4058–4064.
- [112] Y. Kim, H.S. Kim, S.W. Martin, Synthesis and electrochemical characteristics of  $\text{Al}_2\text{O}_3$ -coated  $\text{LiNi}_{1/3}\text{Co}_{1/3}\text{Mn}_{1/3}\text{O}_2$  cathode materials for lithium ion batteries, *Electrochim. Acta.* 52 (2006) 1316–1322.
- [113] Y. K. Sun, Y. S. Lee, M. Yoshio, K. Amine, Synthesis and Electrochemical Properties of ZnO-Coated  $\text{LiNi}_{0.5}\text{Mn}_{1.5}\text{O}_4$  Spinel as 5 V Cathode Material for Lithium Secondary Batteries, *Electrochem. Solid-State Lett.* 5 (2002) A99–A102.



- [114] Z. Chen, Y. Qin, K. Amine, Y. K. Sun, Role of surface coating on cathode materials for lithium-ion batteries, *J. Mater. Chem.* 20 (2010) 7606.
- [115] J.C. Badot, A. Mantoux, N. Baffier, O. Dubrunfaut, D. Lincot, Electrical properties of  $V_2O_5$  thin films obtained by atomic layer deposition (ALD), *J. Mater. Chem.* 14 (2004) 3411–3415.
- [116] I. Belharouak, C. Johnson, K. Amine, Synthesis and electrochemical analysis of vapor-deposited carbon-coated  $LiFePO_4$ , *Electrochem. Commun.* 7 (2005) 983–988.
- [117] J. Liu, N. Liu, D. Liu, Y. Bai, L. Shi, Z. Wang, L. Chen, V. Hennige, A. Schuch, Improving the Performances of  $LiCoO_2$  Cathode Materials by Soaking Nano-Alumina in Commercial Electrolyte, *J. Electrochem. Soc.* 154 (2007) A55–A63.
- [118] Z. Chen, J.R. Dahn, Reducing Carbon in  $LiFePO_4/C$  Composite Electrodes to Maximize Specific Energy, Volumetric Energy, and Tap Density, *J. Electrochem. Soc.* 149 (2002) A1184–A1189.
- [119] Z. Chen, J.R. Dahn, Methods to obtain excellent capacity retention in  $LiCoO_2$  cycled to 4.5 V, *Electrochim. Acta.* 49 (2004) 1079–1090.
- [120] Z. Chen, J.R. Dahn, Improving the Capacity Retention of  $LiCoO_2$  Cycled to 4.5 V by Heat-Treatment, *Electrochem. Solid-State Lett.* 7 (2004) A11–A14.
- [121] K.K. Laali, Stable Ion Studies of Protonation and Oxidation of Polycyclic Arenes, *Chem. Rev.* 96 (1996) 1873–1906.
- [122] A.R. Armstrong, M. Holzapfel, P. Novák, C.S. Johnson, S.-H. Kang, M.M. Thackeray, P.G. Bruce, Demonstrating oxygen loss and associated structural reorganization in the lithium battery cathode  $Li[Ni_{0.2}Li_{0.2}Mn_{0.6}]O_2$ , *J. Am. Chem. Soc.* 128 (2006) 8694–8698.
- [123] L.J. Fu, H. Liu, C. Li, Y.P. Wu, E. Rahm, R. Holze, H.Q. Wu, Surface modifications of electrode materials for lithium ion batteries, *Solid State Sci.* 8 (2006) 113–128.

- [124] Y. K. Sun, M. J. Lee, C.S. Yoon, J. Hassoun, K. Amine, B. Scrosati, The Role of  $\text{AlF}_3$  Coatings in Improving Electrochemical Cycling of Li-Enriched Nickel-Manganese Oxide Electrodes for Li-Ion Batteries, *Adv. Mater.* 24 (2012) 1192–1196.
- [125] L. Liu, Z. Wang, H. Li, L. Chen, X. Huang,  $\text{Al}_2\text{O}_3$ -coated  $\text{LiCoO}_2$  as cathode material for lithium ion batteries, *Solid State Ionics.* 152–153 (2002) 341–346.
- [126] D.S. Hall, R. Gauthier, A. Eldesoky and J. R. Dahn, Reactivity of  $\text{LiPF}_6$  with aluminum oxide cathode coating materials. Unpublished data (2018).
- [127] H. Wang, M. Yoshio, Carbon-coated natural graphite prepared by thermal vapor decomposition process, a candidate anode material for lithium-ion battery, *J. Power Sources.* 93 (2001) 123–129.
- [128] M. Yoshio, H. Wang, K. Fukuda, Y. Hara, Y. Adachi, Effect of Carbon Coating on Electrochemical Performance of Treated Natural Graphite as Lithium-Ion Battery Anode Material, *J. Electrochem. Soc.* 147 (2000) 1245–1250.
- [129] M. Yoshio, H. Wang, K. Fukuda, T. Umeno, N. Dimov, Z. Ogumi, Carbon-Coated Si as a Lithium-Ion Battery Anode Material, *J. Electrochem. Soc.* 149 (2002) A1598–A1603.
- [130] Y. He, X. Yu, Y. Wang, H. Li, X. Huang, Alumina-Coated Patterned Amorphous Silicon as the Anode for a Lithium-Ion Battery with High Coulombic Efficiency, *Adv. Mater.* 23 (2011) 4938–4941.
- [131] R.S. Arumugam, L. Ma, J. Li, X. Xia, J.M. Paulsen, J.R. Dahn, Special Synergy between Electrolyte Additives and Positive Electrode Surface Coating to Enhance the Performance of  $\text{Li}[\text{Ni}_{0.6}\text{Mn}_{0.2}\text{Co}_{0.2}]\text{O}_2/\text{Graphite}$  Cells, *J. Electrochem. Soc.* 163 (2016) A2531–A2538.
- [132] Bedri Erdem, Robert A. Hunsicker, Gary W. Simmons, E. David Sudol, and Victoria L. Dimonie, M.S. El-Aasser, XPS and FTIR Surface Characterization of  $\text{TiO}_2$  Particles Used in Polymer Encapsulation, (2001).
- [133] N.N. Sinha, A.J. Smith, J.C. Burns, G. Jain, K.W. Eberman, E. Scott, J.P. Gardner, J.R. Dahn, The Use of Elevated Temperature Storage Experiments to Learn about Parasitic Reactions in Wound  $\text{LiCoO}_2/\text{Graphite}$  Cells, *J. Electrochem. Soc.* 158 (2011) A1194–A1201.

- [134] D.C. Harris, Quantative Chemical Analysis, 8th ed., 2010.
- [135] T.M. Bond, J.C. Burns, D.A. Stevens, H.M. Dahn, J.R. Dahn, Improving Precision and Accuracy in Coulombic Efficiency Measurements of Li-Ion Batteries, *J. Electrochem. Soc.* 160 (2013) A521–A527.
- [136] A.J. Smith, J.C. Burns, S. Trussler, J.R. Dahn, Precision Measurements of the Coulombic Efficiency of Lithium-Ion Batteries and of Electrode Materials for Lithium-Ion Batteries, *J. Electrochem. Soc.* 157 (2010) A196–A202.
- [137] R. Petibon, MSc thesis, Dalhousie University, 2013.
- [138] C. Chen, J. Liu, K. Amine, Symmetric cell approach and impedance spectroscopy of high power lithium-ion batteries, *J. Power Sources.* 96 (2001) 321–328.
- [139] P. Arora, R.E. White, M. Doyle, Capacity Fade Mechanisms and Side Reactions in Lithium-Ion Batteries, *J. Electrochem. Soc.* 145 (1998) 3647.
- [140] M. Broussely, P. Biensan, F. Bonhomme, P. Blanchard, S. Herreyre, K. Nechev, R.J. Staniewicz, Main aging mechanisms in Li ion batteries, *J. Power Sources.* 146 (2005) 90–96.
- [141] I. Bloom, A.N. Jansen, D.P. Abraham, J. Knuth, S.A. Jones, V.S. Battaglia, G.L. Henriksen, Differential voltage analyses of high-power, lithium-ion cells: 1. Technique and application, *J. Power Sources.* 139 (2005) 295–303.
- [142] I. Bloom, J. Christophersen, K. Gering, Differential voltage analyses of high-power lithium-ion cells: 2. Applications, *J. Power Sources.* 139 (2005) 304–313.
- [143] H.M. Dahn, A.J. Smith, J.C. Burns, D.A. Stevens, J.R. Dahn, User-Friendly Differential Voltage Analysis Freeware for the Analysis of Degradation Mechanisms in Li-Ion Batteries, *J. Electrochem. Soc.* 159 (2012) A1405–A1409.
- [144] R. Petibon, L. Rotermund, K.J. Nelson, A.S. Gozdz, J. Xia, J.R. Dahn, Study of Electrolyte Components in Li Ion Cells Using Liquid-Liquid Extraction and Gas Chromatography Coupled with Mass Spectrometry, *J. Electrochem. Soc.* 161 (2014) A1167–A1172.

- [145] J. M. Atebamba, J. Moskon, S. Pejovnik, M. Gaberscek, On the Interpretation of Measured Impedance Spectra of Insertion Cathodes for Lithium-Ion Batteries, *J. Electrochem. Soc.* 157 (2010) A1218–A1228.
- [146] J.C. Burns, X. Xia, J.R. Dahn, The Effect of Trimethoxyboroxine on Carbonaceous Negative Electrodes for Li-Ion Batteries, *J. Electrochem. Soc.* 160 (2012) A383–A386.
- [147] K. Honkura, H. Honbo, Y. Koishikawa, T. Horiba, State Analysis of Lithium-Ion Batteries Using Discharge Curves, *ECS Trans.* 13 (2008) 61–73.
- [148] J. Taylor, *Introduction to Error Analysis, the Study of Uncertainties in Physical Measurements*, 2nd Edition, 1997.
- [149] A. Eftekhari, Lithium-Ion Batteries with High Rate Capabilities, *ACS Sustain. Chem. Eng.* 5 (2017) 2799–2816.
- [150] J. Li, R. Klöpsch, M.C. Stan, S. Nowak, M. Kunze, M. Winter, S. Passerini, Synthesis and electrochemical performance of the high voltage cathode material  $\text{Li}[\text{Li}_{0.2}\text{Mn}_{0.56}\text{Ni}_{0.16}\text{Co}_{0.08}]\text{O}_2$  with improved rate capability, *J. Power Sources.* 196 (2011) 4821–4825.
- [151] H. Yue, X. Huang, D. Lv, Y. Yang, Hydrothermal synthesis of  $\text{LiMn}_2\text{O}_4/\text{C}$  composite as a cathode for rechargeable lithium-ion battery with excellent rate capability, *Electrochim. Acta.* 54 (2009) 5363–5367.
- [152] Q.Q. Liu, D.J. Xiong, R. Petibon, C.Y. Du, J.R. Dahn, Gas Evolution during Unwanted Lithium Plating in Li-Ion Cells with EC-Based or EC-Free Electrolytes, *J. Electrochem. Soc.* 163 (2016) A3010–A3015.
- [153] D.Y. Wang, J.C. Burns, J.R. Dahn, A Systematic Study of the Concentration of Lithium Hexafluorophosphate ( $\text{LiPF}_6$ ) as a Salt for  $\text{LiCoO}_2/\text{Graphite}$  Pouch Cells, *J. Electrochem. Soc.* 161 (2014) A1278–A1283.
- [154] N.N. Sinha, J.C. Burns, J.R. Dahn, Storage Studies on Li/Graphite Cells and the Impact of So-Called SEI-Forming Electrolyte Additives, *J. Electrochem. Soc.* 160 (2013) A709–A714.
- [155] D.J. Xiong, R. Petibon, L. Madec, D.S. Hall, J.R. Dahn, Some Effects of Intentionally Added Water on  $\text{LiCoO}_2/\text{Graphite}$  Pouch Cells, *J. Electrochem. Soc.* 163 (2016) A1678–A1685.

- [156] L. Madec, J. Xia, R. Petibon, K.J. Nelson, J.-P. Sun, I.G. Hill, J.R. Dahn, Effect of Sulfate Electrolyte Additives on  $\text{LiNi}_{1/3}\text{Mn}_{1/3}\text{Co}_{1/3}\text{O}_2$ /Graphite Pouch Cell Lifetime: Correlation between XPS Surface Studies and Electrochemical Test Results, *J. Phys. Chem. C*. 118 (2014) 29608–29622.
- [157] L.J. Krause, L.D. Jensen, J.R. Dahn, Measurement of Parasitic Reactions in Li Ion Cells by Electrochemical Calorimetry, *J. Electrochem. Soc.* 159 (2012) A937–A943.
- [158] K.J. Nelson, G.L. d'Eon, A.T.B. Wright, L. Ma, J. Xia, J.R. Dahn, Studies of the Effect of High Voltage on the Impedance and Cycling Performance of  $\text{Li}[\text{Ni}_{0.4}\text{Mn}_{0.4}\text{Co}_{0.2}]\text{O}_2$ /Graphite Lithium-Ion Pouch Cells, *J. Electrochem. Soc.* 162 (2015) A1046–A1054.
- [159] X. Ma, J. Li, S.L. Glazier, L. Ma, K.L. Gering, J.R. Dahn, A study of highly conductive ester co-solvents in  $\text{Li}[\text{Ni}_{0.5}\text{Mn}_{0.3}\text{Co}_{0.2}]\text{O}_2$ /Graphite pouch cells, *Electrochim. Acta*. 270 (2018) 215–223.
- [160] Q.Q. Liu, L. Ma, C.Y. Du, J.R. Dahn, Effects of the  $\text{LiPO}_2\text{F}_2$  additive on unwanted lithium plating in lithium-ion cells, *Electrochim. Acta*. 263 (2018) 237–248.
- [161] L.E. Downie, J.R. Dahn, Determination of the Voltage Dependence of Parasitic Heat Flow in Lithium Ion Cells Using Isothermal Microcalorimetry, *J. Electrochem. Soc.* 161 (2014) A1782–A1787.
- [162] S.L. Glazier, K.J. Nelson, J.P. Allen, J. Li, J.R. Dahn, The Effect of Different  $\text{Li}(\text{Ni}_{1-x-y}\text{Mn}_x\text{Co}_y)\text{O}_2$  Positive Electrode Materials and Coatings on Parasitic Heat Flow as Measured by Isothermal Microcalorimetry, Ultra-High Precision Coulometry and Long Term Cycling, *J. Electrochem. Soc.* 164 (2017) A1203–A1212.
- [163] J. Xia, M. Nie, L. Ma, J.R. Dahn, Variation of coulombic efficiency versus upper cutoff potential of Li-ion cells tested with aggressive protocols, *J. Power Sources*. 306 (2016) 233–240.
- [164] L. Ma, L. Ellis, S.L. Glazier, X. Ma, Q. Liu, J. Li, J.R. Dahn,  $\text{LiPO}_2\text{F}_2$  as an Electrolyte Additive in  $\text{Li}[\text{Ni}_{0.5}\text{Mn}_{0.3}\text{Co}_{0.2}]\text{O}_2$ /Graphite Pouch Cells, *J. Electrochem. Soc.* 165 (2018) A891–A899.

- [165] Y.X. Lin, Z. Liu, K. Leung, L.Q. Chen, P. Lu, Y. Qi, Connecting the irreversible capacity loss in Li-ion batteries with the electronic insulating properties of solid electrolyte interphase (SEI) components, *J. Power Sources*. 309 (2016) 221–230.
- [166] M. Broussely, S. Herreyre, P. Biensan, P. Kasztejna, K. Nechev, R.J. Staniewicz, Aging mechanism in Li ion cells and calendar life predictions, in: *J. Power Sources*, Elsevier, 2001: pp. 13–21.
- [167] P. Lu, C. Li, E.W. Schneider, S.J. Harris, Chemistry, Impedance, and Morphology Evolution in Solid Electrolyte Interphase Films during Formation in Lithium Ion Batteries, *J. Phys. Chem. C*. 118 (2014) 896–903.
- [168] D.J. Xiong, R. Petibon, M. Nie, L. Ma, J. Xia, J.R. Dahn, Interactions between Positive and Negative Electrodes in Li-Ion Cells Operated at High Temperature and High Voltage, *J. Electrochem. Soc.* 163 (2016) A546–A551.
- [169] L. Ma, M. Nie, J. Xia, J.R. Dahn, A systematic study on the reactivity of different grades of charged  $\text{Li}[\text{Ni}_x\text{Mn}_y\text{Co}_z]\text{O}_2$  with electrolyte at elevated temperatures using accelerating rate calorimetry, *J. Power Sources*. 327 (2016) 145–150.
- [170] J. R. Dahn, S. Trussler, T. D. Hatchard, A. Bonakdarpour, J. R. Mueller-Neuhaus, and K. C. Hewitt, M. Fleischauer, Economical Sputtering System To Produce Large-Size Composition-Spread Libraries Having Linear and Orthogonal Stoichiometry Variations, (2002).
- [171] D.J. Xiong, L.D. Ellis, R. Petibon, T. Hynes, Q.Q. Liu, J.R. Dahn, Studies of Gas Generation, Gas Consumption and Impedance Growth in Li-Ion Cells with Carbonate or Fluorinated Electrolytes Using the Pouch Bag Method, *J. Electrochem. Soc.* 164 (2017) A340–A347.
- [172] L.D. Ellis, J.P. Allen, L.M. Thompson, J.E. Harlow, W.J. Stone, I.G. Hill, J.R. Dahn, Quantifying, Understanding and Evaluating the Effects of Gas Consumption in Lithium-Ion Cells, *J. Electrochem. Soc.* 164 (2017) A3518–A3528.
- [173] I. Bloom, A.N. Jansen, D.P. Abraham, J. Knuth, S.A. Jones, V.S. Battaglia, G.L. Henriksen, Differential voltage analyses of high-power, lithium-ion cells: 1. Technique and application, *J. Power Sources*. 139 (2005) 295–303.
- [174] J.A. Gilbert, I.A. Shkrob, D.P. Abraham, Transition Metal Dissolution, Ion Migration, Electrocatalytic Reduction and Capacity Loss in Lithium-Ion Full Cells, *J. Electrochem. Soc.* 164 (2017) A389–A399.

- [175] J. Wandt, A. Freiberg, R. Thomas, Y. Gorlin, A. Siebel, R. Jung, H.A. Gasteiger, M. Tromp, Transition metal dissolution and deposition in Li-ion batteries investigated by operando X-ray absorption spectroscopy, *J. Mater. Chem. A*. 4 (2016) 18300–18305.
- [176] T. Joshi, K. Eom, G. Yushin, T.F. Fuller, Effects of Dissolved Transition Metals on the Electrochemical Performance and SEI Growth in Lithium-Ion Batteries, *J. Electrochem. Soc.* 161 (2014) A1915–A1921.
- [177] N.P.W. Pieczonka, Z. Liu, P. Lu, K.L. Olson, J. Moote, B.R. Powell, J.H. Kim, Understanding Transition-Metal Dissolution Behavior in  $\text{LiNi}_{0.5}\text{Mn}_{1.5}\text{O}_4$  High-Voltage Spinel for Lithium Ion Batteries, *J. Phys. Chem. C*. 117 (2013) 15947–15957.
- [178] L.M. Thompson, W. Stone, A. Eldesoky, N.K. Smith, C.R.M. McFarlane, J.S. Kim, M.B. Johnson, R. Petibon, J.R. Dahn, Quantifying Changes to the Electrolyte and Negative Electrode in Aged NMC532/Graphite Lithium-Ion Cells, *J. Electrochem. Soc.* 165 (2018) A2732–A2740.
- [179] S. Watanabe, M. Kinoshita, T. Hosokawa, K. Morigaki, K. Nakura, Capacity fade of  $\text{LiAl}_y\text{Ni}_{1-x-y}\text{Co}_x\text{O}_2$  cathode for lithium-ion batteries during accelerated calendar and cycle life tests (surface analysis of  $\text{LiAl}_y\text{Ni}_{1-x-y}\text{Co}_x\text{O}_2$  cathode after cycle tests in restricted depth of discharge ranges), *J. Power Sources*. 258 (2014) 210–217.
- [180] S. Watanabe, M. Kinoshita, T. Hosokawa, K. Morigaki, K. Nakura, Capacity fading of  $\text{LiAl}_y\text{Ni}_{1-x-y}\text{Co}_x\text{O}_2$  cathode for lithium-ion batteries during accelerated calendar and cycle life tests (effect of depth of discharge in charge–discharge cycling on the suppression of the micro-crack generation of  $\text{LiAl}_y\text{Ni}_{1-x-y}\text{Co}_x\text{O}_2$  particle), *J. Power Sources*. 260 (2014) 50–56.
- [181] H. Li, J. Li, X. Ma, J.R. Dahn, Synthesis of Single Crystal  $\text{LiNi}_{0.6}\text{Mn}_{0.2}\text{Co}_{0.2}\text{O}_2$  with Enhanced Electrochemical Performance for Lithium Ion Batteries, *J. Electrochem. Soc.* 165 (2018) A1038–A1045.
- [182] J. Kim, H. Lee, H. Cha, M. Yoon, M. Park, J. Cho, Prospect and Reality of Ni-Rich Cathode for Commercialization, *Adv. Energy Mater.* 8 (2018) 1702028.
- [183] L. Zhang, K. Zhang, Z. Shi, S. Zhang, LiF as an Artificial SEI Layer to Enhance the High-Temperature Cycle Performance of  $\text{Li}_4\text{Ti}_5\text{O}_{12}$ , *Langmuir*. 33 (2017) 11164–11169.

- [184] L.D. Ellis, J.P. Allen, I.G. Hill, J.R. Dahn, High-Precision Coulometry Studies of the Impact of Temperature and Time on SEI Formation in Li-Ion Cells, *J. Electrochem. Soc.* 165 (2018) A1529–A1536.
- [185] K.J. Nelson, G.L. d'Eon, A.T.B. Wright, L. Ma, J. Xia, J.R. Dahn, Studies of the Effect of High Voltage on the Impedance and Cycling Performance of Li[Ni<sub>0.4</sub>Mn<sub>0.4</sub>Co<sub>0.2</sub>]O<sub>2</sub>/Graphite Lithium-Ion Pouch Cells, *J. Electrochem. Soc.* 162 (2015) A1046–A1054.
- [186] B.S. Parimalam, A.D. MacIntosh, R. Kadam, B.L. Lucht, Decomposition Reactions of Anode Solid Electrolyte Interphase (SEI) Components with LiPF<sub>6</sub>, *J. Phys. Chem. C* 121 (2017) 22733–22738.
- [187] L.J. Krause, V.L. Chevrier, L.D. Jensen, T. Brandt, The Effect of Carbon Dioxide on the Cycle Life and Electrolyte Stability of Li-Ion Full Cells Containing Silicon Alloy, *J. Electrochem. Soc.* 164 (2017) A2527–A2533.
- [188] J.O. Besenhard, M.W. Wagner, M. Winter, A.D. Jannakoudakis, P.D. Jannakoudakis, E. Theodoridou, Inorganic film-forming electrolyte additives improving the cycling behaviour of metallic lithium electrodes and the self-discharge of carbon–lithium electrodes, *J. Power Sources* 44 (1993) 413–420.
- [189] Y.W. and, P.B. Balbuena, Theoretical Insights into the Reductive Decompositions of Propylene Carbonate and Vinylene Carbonate: Density Functional Theory Studies, (2002).
- [190] M. Xu, L. Zhou, L. Xing, W. Li, B.L. Lucht, Experimental and theoretical investigations on 4,5-dimethyl-[1,3]dioxol-2-one as solid electrolyte interface forming additive for lithium-ion batteries, *Electrochim. Acta* 55 (2010) 6743–6748.
- [191] E.G. Leggesse, J. C. Jiang, Theoretical Study of the Reductive Decomposition of Ethylene Sulfite: A Film-Forming Electrolyte Additive in Lithium Ion Batteries, *J. Phys. Chem. A* 116 (2012) 11025–11033.
- [192] C. Shen, D. Xiong, L.D. Ellis, K.L. Gering, L. Huang, J.R. Dahn, Using the Charge-Discharge Cycling of Positive Electrode Symmetric Cells to Find Electrolyte/Electrode Combinations with Minimum Reactivity, *J. Electrochem. Soc.* 164 (2017) A3349–A3356.



- [193] H. Li, J. Li, X. Ma, J.R. Dahn, Synthesis of Single Crystal  $\text{LiNi}_{0.6}\text{Mn}_{0.2}\text{Co}_{0.2}\text{O}_2$  with Enhanced Electrochemical Performance for Lithium Ion Batteries, *J. Electrochem. Soc.* 165 (2018) A1038–A1045.
- [194] D. Lin, Y. Liu, Y. Cui, Reviving the lithium metal anode for high-energy batteries, *Nat. Nanotechnol.* 12 (2017) 194–206.
- [195] J. Zheng, M.H. Engelhard, D. Mei, S. Jiao, B.J. Polzin, J. G. Zhang, W. Xu, Electrolyte additive enabled fast charging and stable cycling lithium metal batteries, *Nat. Energy.* 2 (2017) 17012.
- [196] R. Miao, J. Yang, X. Feng, H. Jia, J. Wang, Y. Nuli, Novel dual-salts electrolyte solution for dendrite-free lithium-metal based rechargeable batteries with high cycle reversibility, *J. Power Sources.* 271 (2014) 291–297.

## Appendix A

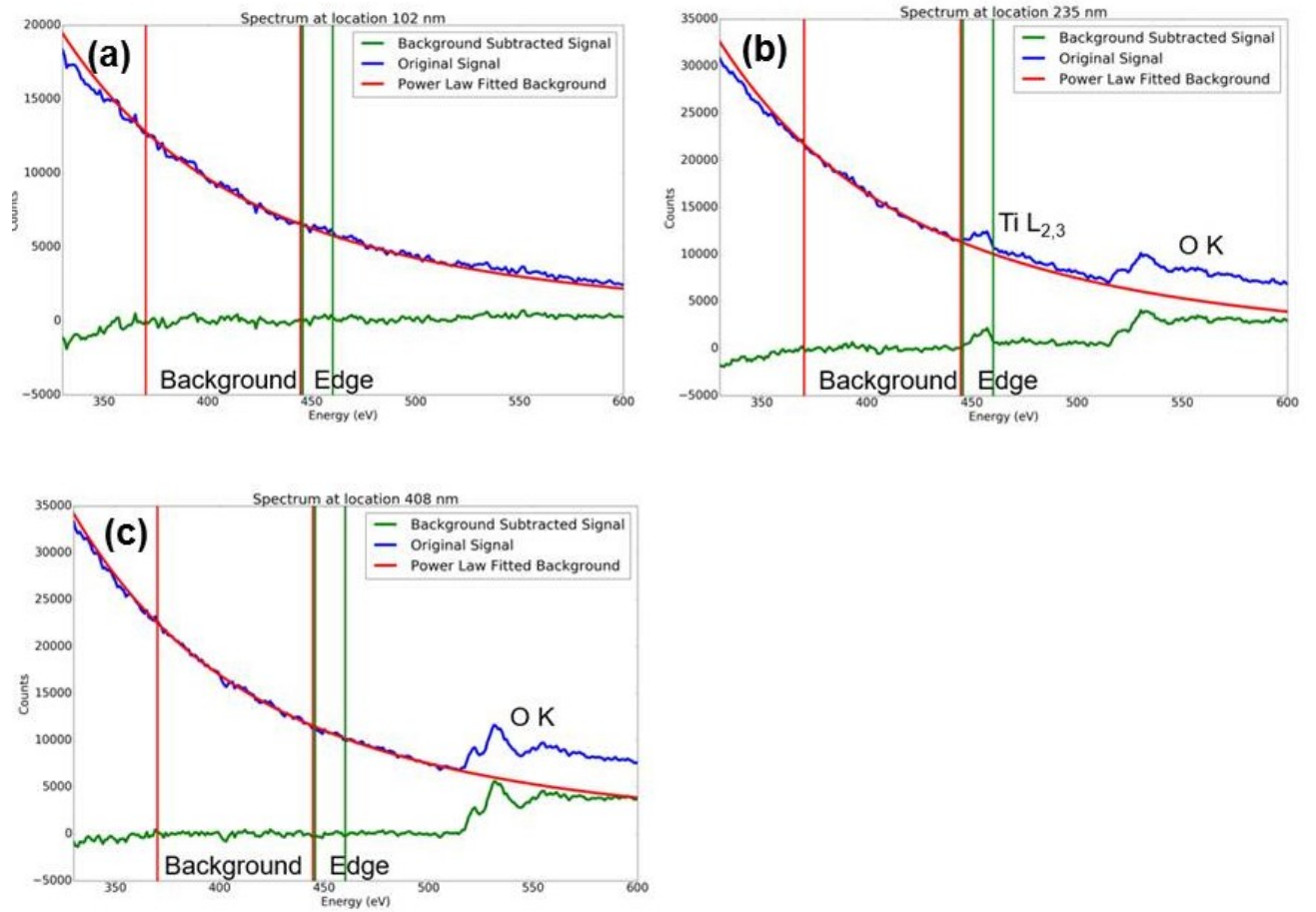


Figure A1 Representative spectra showing the background subtraction procedure in the substrate (a), surface (b) and bulk (c) during EELS line scan testing.

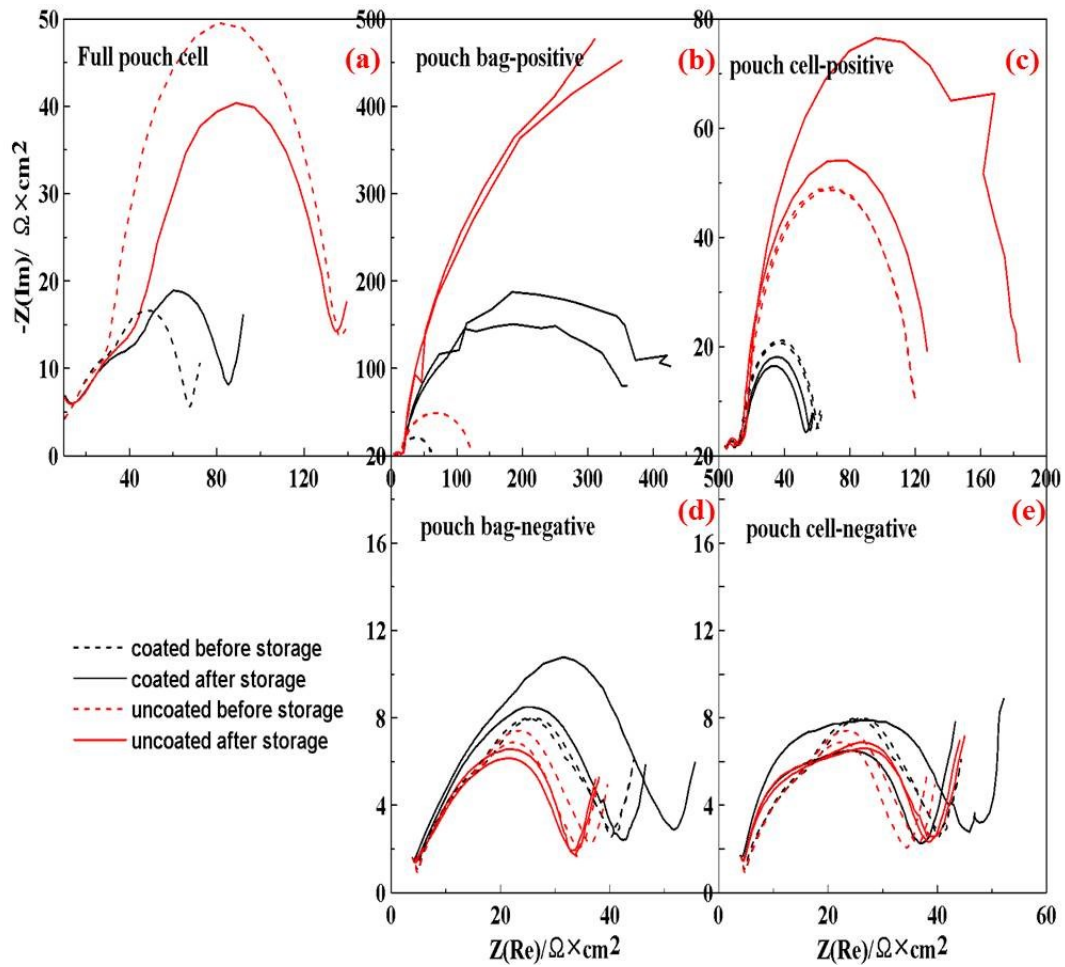


Figure A2 Nyquist plots for coated SC NMC532/graphite and uncoated SC NMC532/graphite pouch full cells (a), delithiated coated or uncoated SC NMC532 taken from pouch bags (b), delithiated coated or uncoated SC NMC532 taken from full pouch cells (c), lithiated graphite taken from pouch bags (d) and lithiated graphite taken from full pouch cells before or after 500h high temperature (60°C) storage (e). The electrolyte used was 1.2M LiPF<sub>6</sub> EC/EMC 3/7. All the data was measured at 10°C.

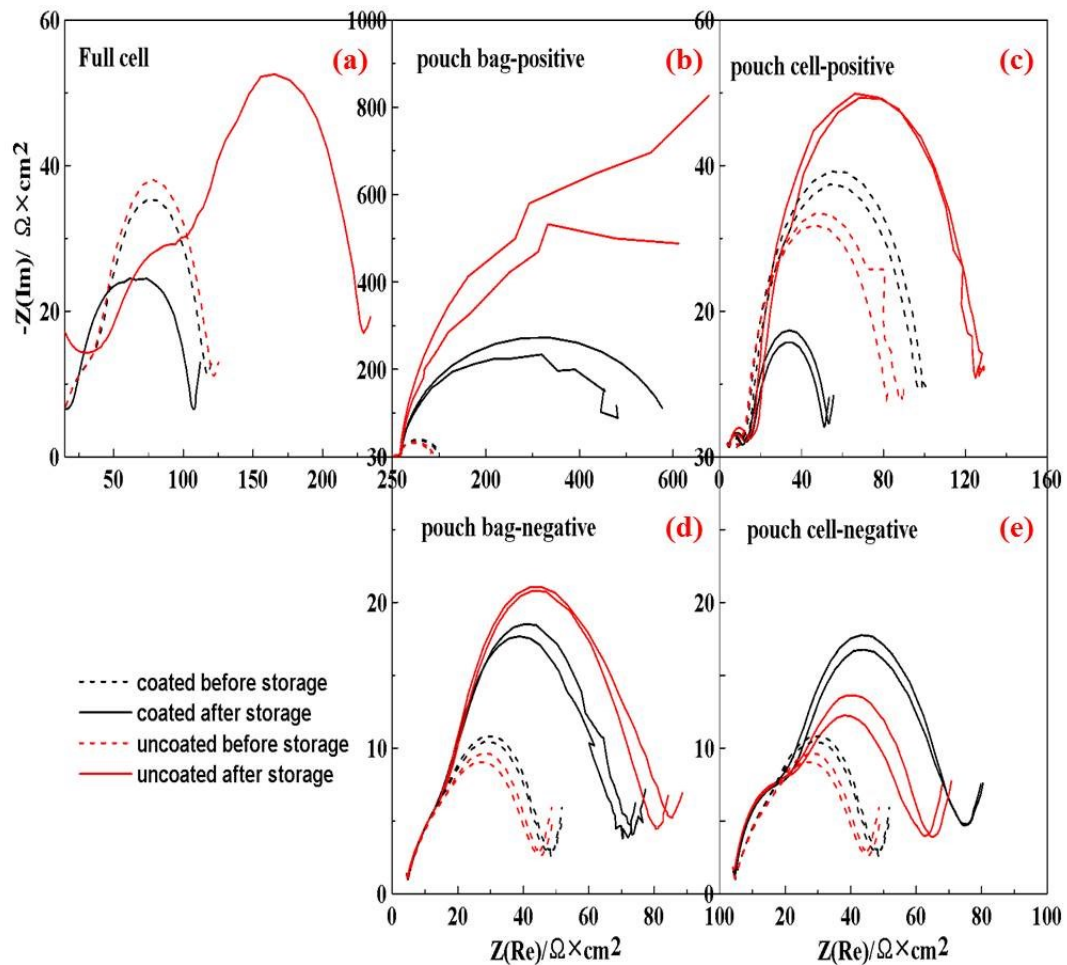


Figure A3 Nyquist plots for coated SC NMC532/graphite and uncoated SC NMC532/graphite pouch full cells (a), delithiated coated or uncoated SC NMC532 taken from pouch bags (b), delithiated coated or uncoated SC NMC532 taken from full pouch cells (c), lithiated graphite taken from pouch bags (d) and lithiated graphite taken from full pouch cells before or after 500h high temperature (60°C) storage (e). The electrolyte used was 1.2M  $\text{LiPF}_6$  EC/EMC 3/7 plus 2% VC + 1% DTD. All the data was measured at 10°C.

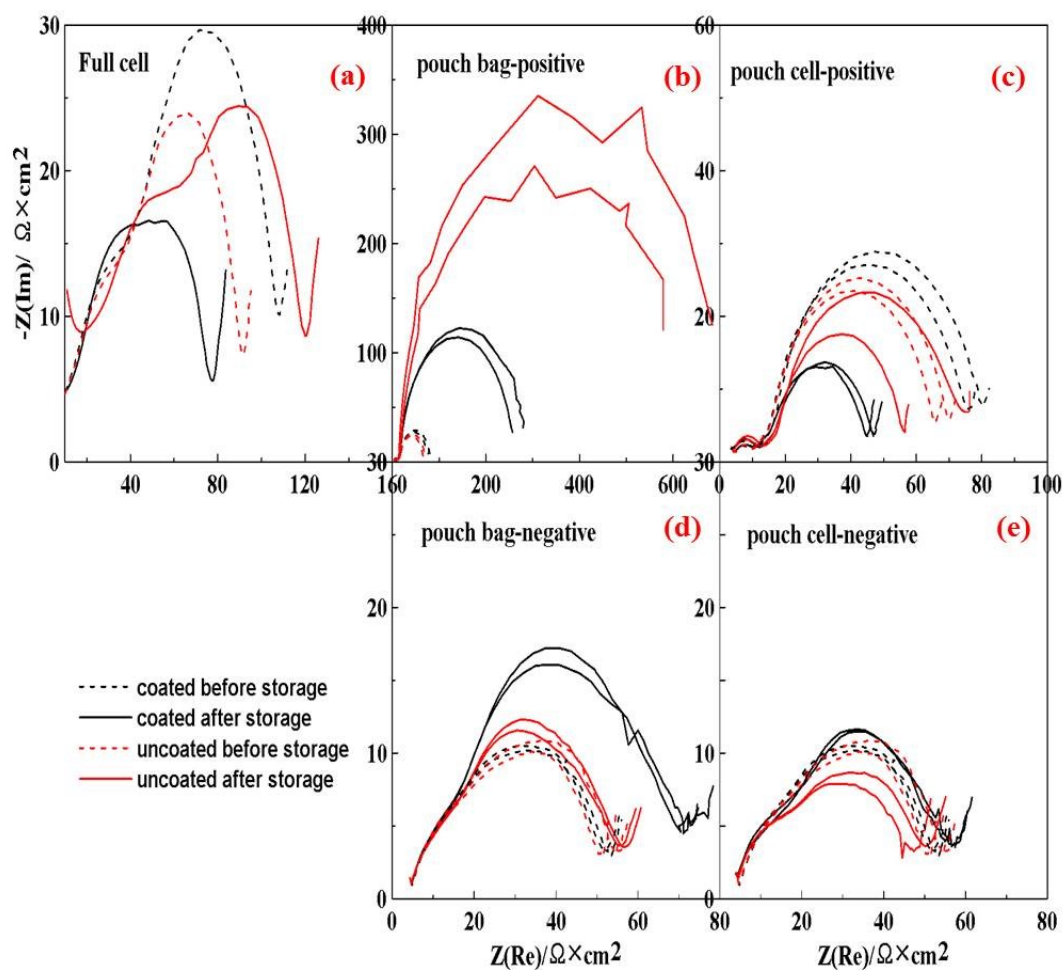


Figure A4 Nyquist plots for coated SC NMC532/graphite and uncoated SC NMC532/graphite pouch full cells (a), delithiated coated or uncoated SC NMC532 taken from pouch bags (b), delithiated coated or uncoated SC NMC532 taken from full pouch cells (c), lithiated graphite taken from pouch bags (d) and lithiated graphite taken from full pouch cells before or after 500h high temperature (60°C) storage (e). The electrolyte used was 1.2M LiPF<sub>6</sub> EC/EMC 3/7 plus 1% LiPO<sub>2</sub>F<sub>2</sub> + 1% VC + 1% FEC. All the data was measured at 10°C.

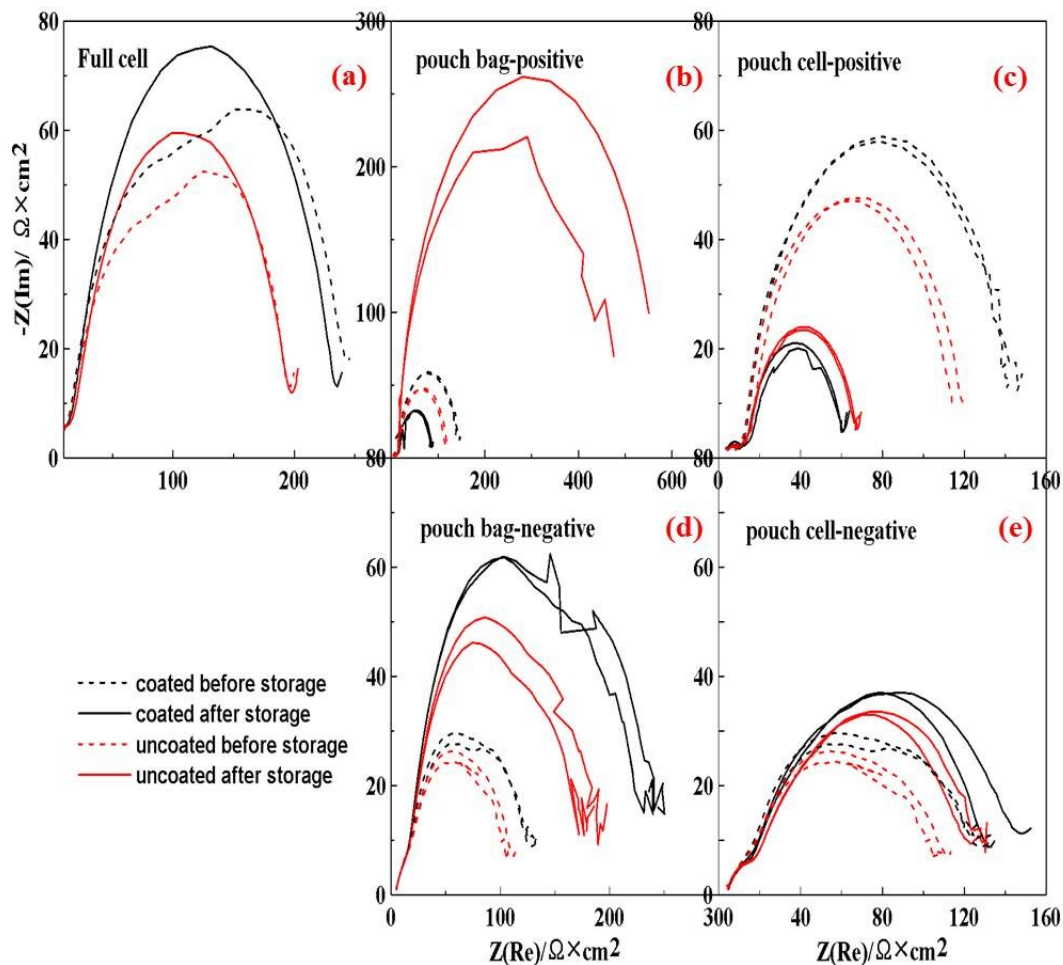


Figure A5 Nyquist plots for coated SC NMC532/graphite and uncoated SC NMC532/graphite pouch full cells (a), delithiated coated or uncoated SC NMC532 taken from pouch bags (b), delithiated coated or uncoated SC NMC532 taken from full pouch cells (c), lithiated graphite taken from pouch bags (d) and lithiated graphite taken from full pouch cells before or after 500h high temperature (60°C) storage (e). The electrolyte used was 1.2M LiPF<sub>6</sub> EC/EMC 3/7 plus 2% PES + 1% DTD + 1% TTSPi (“PES211”). All the data was measured at 10°C.

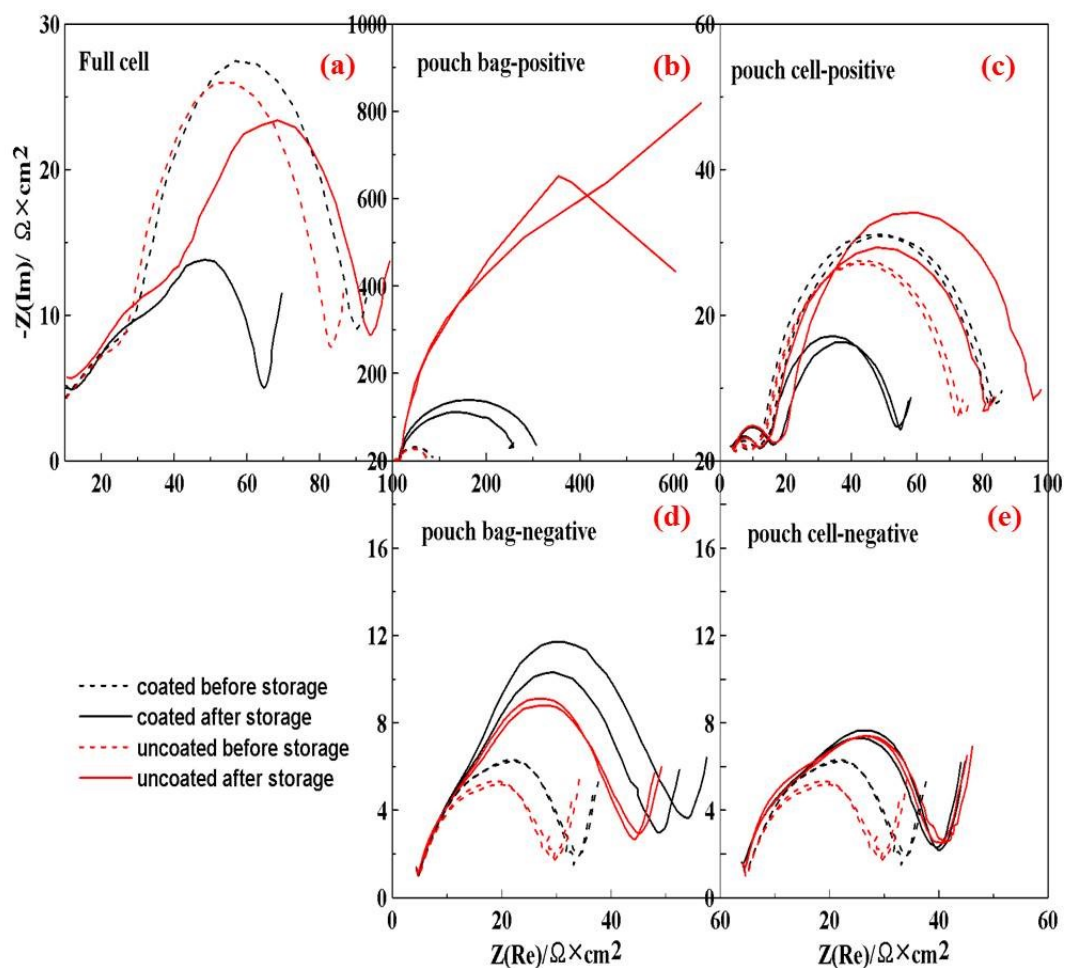


Figure A6 Nyquist plots for coated SC NMC532/graphite and uncoated SC NMC532/graphite pouch full cells (a), delithiated coated or uncoated SC NMC532 taken from pouch bags (b), delithiated coated or uncoated SC NMC532 taken from full pouch cells (c), lithiated graphite taken from pouch bags (d) and lithiated graphite taken from full pouch cells before or after 500h high temperature (60°C) storage (e). The electrolyte used was 1.2M LiPF<sub>6</sub> EC/EMC 3/7 plus 2% FEC + 1% DTD. All the data was measured at 10°C.

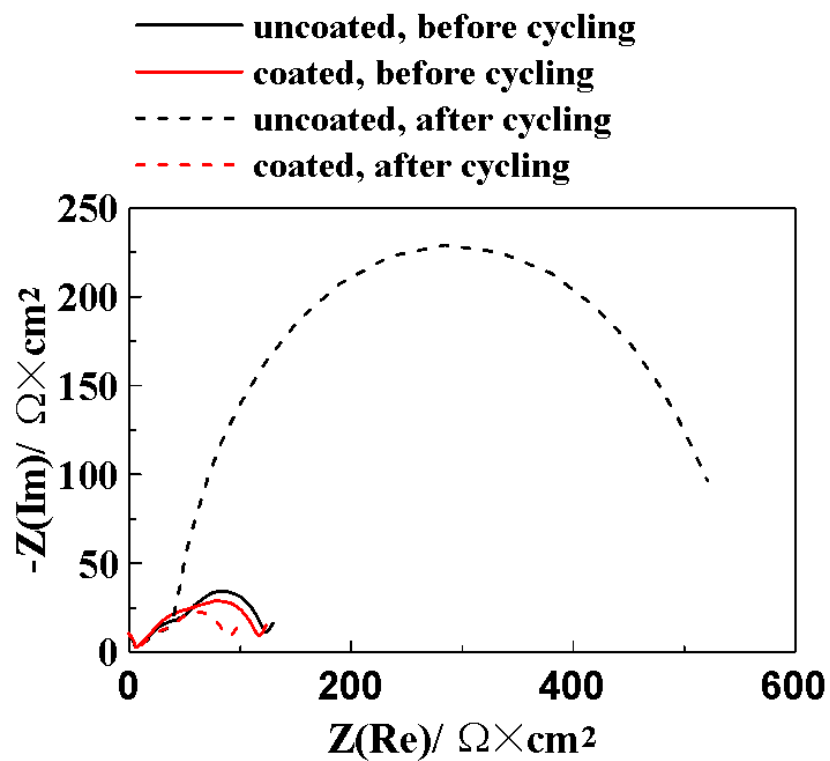


Figure A7 Nyquist plots for coated SC NMC532/graphite and uncoated SC NMC532/graphite pouch cells with 1.2M LiPF<sub>6</sub> EC/EMC 3/7 plus 2% VC before or after long term cycling. The relevant cycling data was shown in Figure 7.9. All the data was measured at 3.8 V and 10°C.



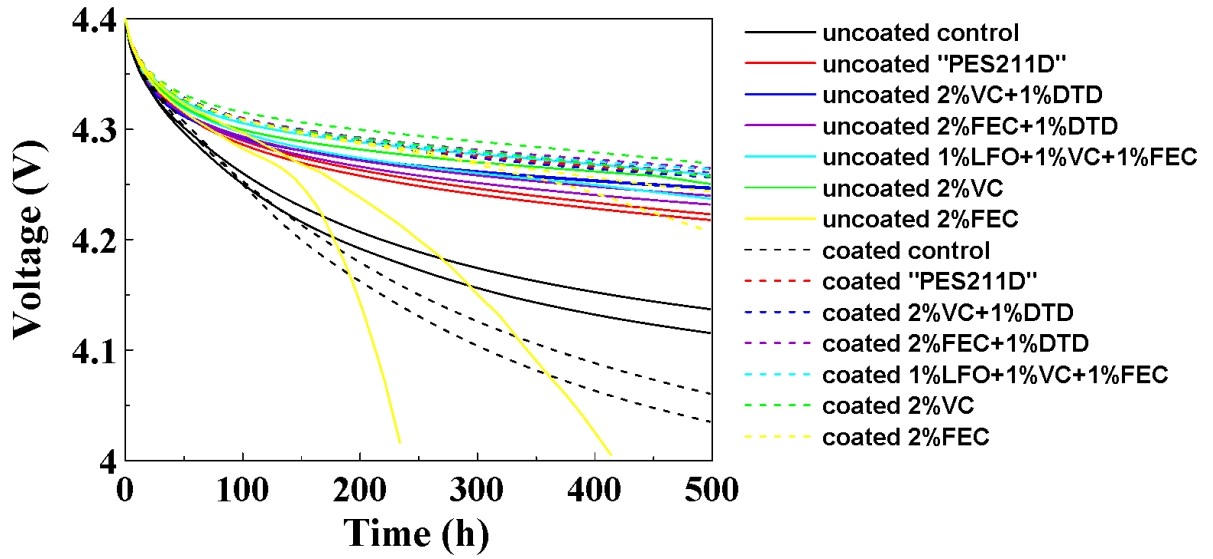


Figure A8 Voltage vs. time for coated and uncoated SC NMC532/graphite pouch cells with different electrolyte additives as indicated during storage testing (60°C, 500h).  $\text{LiPO}_2\text{F}_2$  is called LFO in the Figure legend.

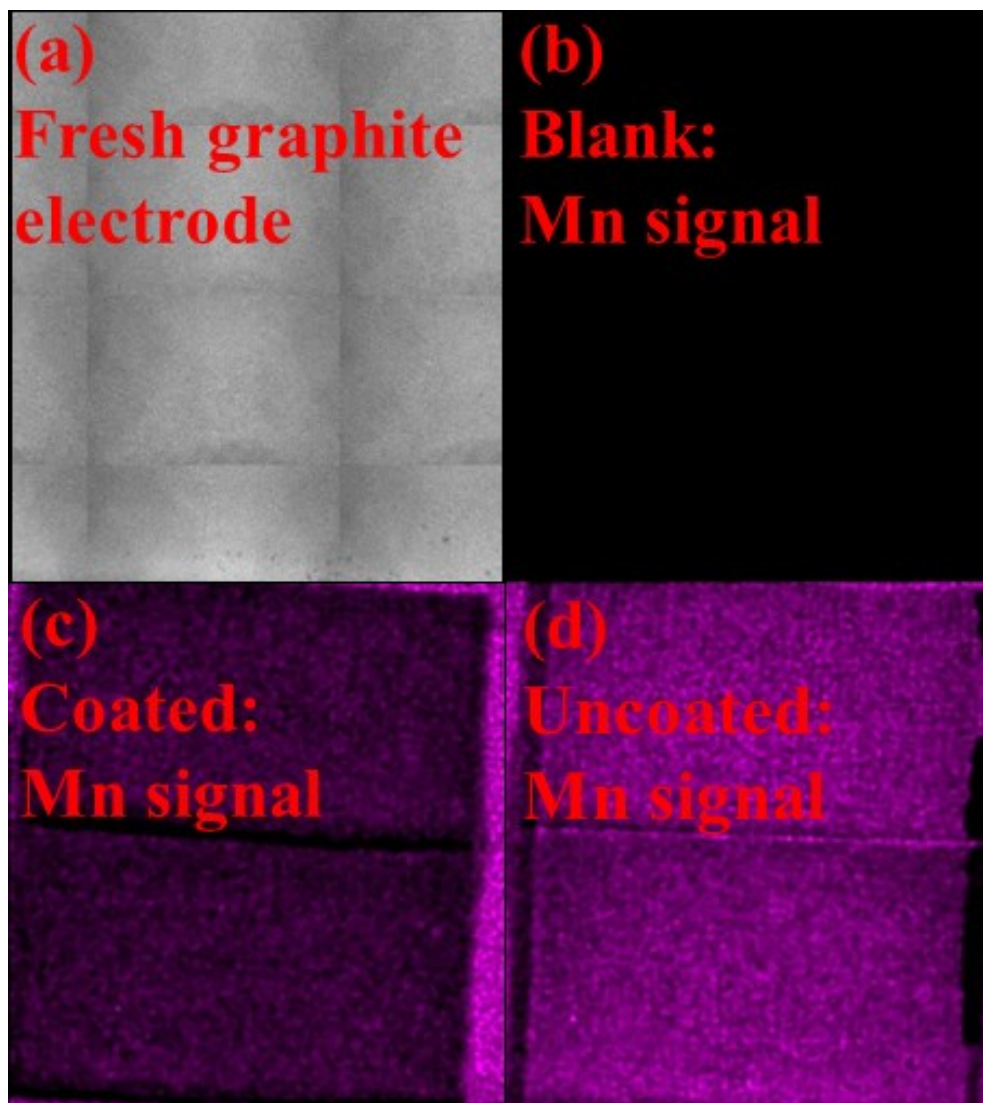


Figure A9 XRF images for (a) fresh graphite electrode, (b) Mn signal for blank sample, (c) Mn signal for graphite electrode taken from coated SC NMC532/graphite cell and (d) Mn signal for graphite electrode taken from uncoated SC NMC532/graphite cell.

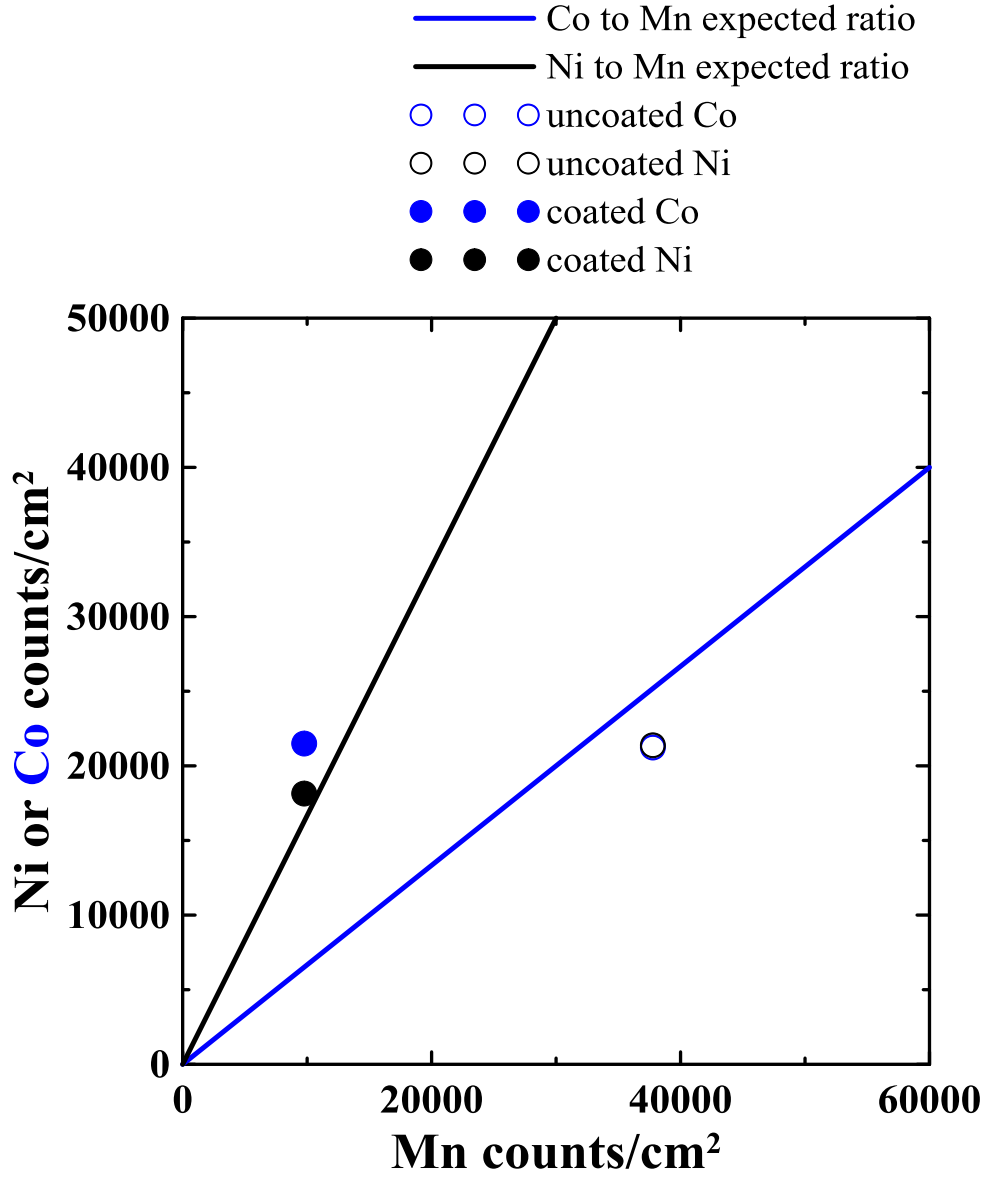


Figure A10 Comparing the Ni (black) and Co (blue)  $\mu$ -XRF signals to the Mn  $\mu$ -XRF signal for the electrodes recovered from the cells described by Figure 7.7. The solid black and solid blue lines represent the expected ratios of all transition metals have equal probability for dissolution from NMC532.

## **Appendix B**

### **Copyright Information**

The copyright information is outlined in this section, with the permission granted for Figures used in this thesis.

**Order detail ID:** 71281857  
**ISSN:** 0013-4651  
**Publication Type:** Journal  
**Volume:**  
**Issue:**  
**Start page:**  
**Publisher:** ELECTROCHEMICAL SOCIETY,  
**Author/Editor:** ELECTROCHEMICAL SOCIETY

**Permission Status:**  **Granted**  
**Permission type:** Republish or display content  
**Type of use:** Republish in a thesis/dissertation  
**Order License Id:** 4383200297433

Hide details

<b>Requestor type</b>	Academic institution
<b>Format</b>	Electronic
<b>Portion</b>	chapter/article
<b>The requesting person/organization</b>	Lin Ma/Dalhousie University
<b>Title or numeric reference of the portion(s)</b>	full article
<b>Title of the article or chapter the portion is from</b>	A Guide to Ethylene Carbonate-Free Electrolyte Making for Li-Ion Cells
<b>Editor of portion(s)</b>	N/A
<b>Author of portion(s)</b>	L. Ma, S.L. Glazier, R. Petibon, J. Xia, J.M. Peters, Q. Liu, J. Allen, R.N.C. Doig, J.R. Dahn
<b>Volume of serial or monograph</b>	164
<b>Page range of portion</b>	
<b>Publication date of portion</b>	2017
<b>Rights for</b>	Main product
<b>Duration of use</b>	Life of current edition
<b>Creation of copies for the disabled</b>	no
<b>With minor editing privileges</b>	no
<b>For distribution to</b>	Worldwide
<b>In the following language(s)</b>	Original language of publication
<b>With incidental promotional use</b>	no
<b>Lifetime unit quantity of new product</b>	Up to 499
<b>Title</b>	DEVELOPMENT OF NOVEL ELECTRODE/ELECTROLYTE SYSTEMS FOR A LI-ION CELL WITH HIGHER ENERGY DENSITY AND LONGER LIFETIME
<b>Instructor name</b>	Dr. Jeff Dahn
<b>Institution name</b>	Dalhousie University
<b>Expected presentation date</b>	Sep 2018

**Order detail ID:** 71281873  
**ISSN:** 0013-4651  
**Publication Type:** Journal  
**Volume:**  
**Issue:**  
**Start page:**  
**Publisher:** ELECTROCHEMICAL SOCIETY,  
**Author/Editor:** ELECTROCHEMICAL SOCIETY

**Permission Status:**  **Granted**  
**Permission type:** Republish or display content  
**Type of use:** Republish in a thesis/dissertation  
**Order License Id:** 4383201268508

Hide details

<b>Requestor type</b>	Academic institution
<b>Format</b>	Electronic
<b>Portion</b>	chapter/article
<b>The requesting person/organization</b>	Lin Ma/Dalhousie University
<b>Title or numeric reference of the portion(s)</b>	full article
<b>Title of the article or chapter the portion is from</b>	Combinations of LiPO 2 F 2 and Other Electrolyte Additives in Li[Ni 0.5 Mn 0.3 Co 0.2 ]O 2 /Graphite Pouch Cells
<b>Editor of portion(s)</b>	N/A
<b>Author of portion(s)</b>	L. Ma, L. Ellis, S.L. Glazier, X. Ma, J.R. Dahn
<b>Volume of serial or monograph</b>	165
<b>Page range of portion</b>	
<b>Publication date of portion</b>	2018
<b>Rights for</b>	Main product
<b>Duration of use</b>	Life of current edition
<b>Creation of copies for the disabled</b>	no
<b>With minor editing privileges</b>	no
<b>For distribution to</b>	Worldwide
<b>In the following language(s)</b>	Original language of publication
<b>With incidental promotional use</b>	no
<b>Lifetime unit quantity of new product</b>	Up to 499
<b>Title</b>	DEVELOPMENT OF NOVEL ELECTRODE/ELECTROLYTE SYSTEMS FOR A LI-ION CELL WITH HIGHER ENERGY DENSITY AND LONGER LIFETIME
<b>Instructor name</b>	Dr. Jeff Dahn
<b>Institution name</b>	Dalhousie University
<b>Expected presentation date</b>	Sep 2018

## Journal of the Electrochemical Society

**Order detail ID:** 71281889  
**Order License Id:** 4383210089910  
**ISSN:** 0013-4651  
**Publication Type:** Journal  
**Volume:**  
**Issue:**  
**Start page:**  
**Publisher:** ELECTROCHEMICAL SOCIETY,  
**Author/Editor:** ELECTROCHEMICAL SOCIETY

**Permission Status:**  **Granted**  
**Permission type:** Republish or display content  
**Type of use:** Republish in a thesis/dissertation

Hide details

<b>Requestor type</b>	Academic institution
<b>Format</b>	Electronic
<b>Portion</b>	chapter/article
<b>The requesting person/organization</b>	Lin Ma/Dalhousie University
<b>Title or numeric reference of the portion(s)</b>	full article
<b>Title of the article or chapter the portion is from</b>	LiPO 2 F 2 as an Electrolyte Additive in Li[Ni 0.5 Mn 0.3 Co 0.2 ]O 2 /Graphite Pouch Cells
<b>Editor of portion(s)</b>	N/A
<b>Author of portion(s)</b>	L. Ma, L. Ellis, S.L. Glazier, X. Ma, Q. Liu, J. Li, J.R. Dahn
<b>Volume of serial or monograph</b>	165
<b>Page range of portion</b>	
<b>Publication date of portion</b>	2018
<b>Rights for</b>	Main product
<b>Duration of use</b>	Life of current edition
<b>Creation of copies for the disabled</b>	no
<b>With minor editing privileges</b>	no
<b>For distribution to</b>	Worldwide
<b>In the following language(s)</b>	Original language of publication
<b>With incidental promotional use</b>	no
<b>Lifetime unit quantity of new product</b>	Up to 499
<b>Title</b>	DEVELOPMENT OF NOVEL ELECTRODE/ELECTROLYTE SYSTEMS FOR A LI-ION CELL WITH HIGHER ENERGY DENSITY AND LONGER LIFETIME
<b>Instructor name</b>	Dr. Jeff Dahn
<b>Institution name</b>	Dalhousie University
<b>Expected presentation date</b>	Sep 2018

---

Journal of the Electrochemical Society

**Order detail ID:** 71281905  
**Order License Id:** 4383210609695  
**ISSN:** 0013-4651  
**Publication Type:** Journal  
**Volume:**  
**Issue:**  
**Start page:**  
**Publisher:** ELECTROCHEMICAL SOCIETY,  
**Author/Editor:** ELECTROCHEMICAL SOCIETY

**Permission Status:**  **Granted**  
**Permission type:** Republish or display content  
**Type of use:** Republish in a thesis/dissertation

Hide details

<b>Requestor type</b>	Academic institution
<b>Format</b>	Electronic
<b>Portion</b>	chapter/article
<b>The requesting person/organization</b>	Lin Ma/Dalhousie University
<b>Title or numeric reference of the portion(s)</b>	Figures 5, 6 and 7
<b>Title of the article or chapter the portion is from</b>	Gas Evolution during Unwanted Lithium Plating in Li-Ion Cells with EC-Based or EC-Free Electrolytes
<b>Editor of portion(s)</b>	N/A
<b>Author of portion(s)</b>	Q.Q. Liu, D.J. Xiong, R. Petibon, C.Y. Du, J.R. Dahn
<b>Volume of serial or monograph</b>	163
<b>Page range of portion</b>	
<b>Publication date of portion</b>	2016
<b>Rights for</b>	Main product
<b>Duration of use</b>	Life of current edition
<b>Creation of copies for the disabled</b>	no
<b>With minor editing privileges</b>	no
<b>For distribution to</b>	Worldwide
<b>In the following language(s)</b>	Original language of publication
<b>With incidental promotional use</b>	no
<b>Lifetime unit quantity of new product</b>	Up to 499
<b>Title</b>	DEVELOPMENT OF NOVEL ELECTRODE/ELECTROLYTE SYSTEMS FOR A LI-ION CELL WITH HIGHER ENERGY DENSITY AND LONGER LIFETIME
<b>Instructor name</b>	Dr. Jeff Dahn
<b>Institution name</b>	Dalhousie University
<b>Expected presentation date</b>	Sep 2018



Journal of the Electrochemical Society

**Order detail ID:** 71281909  
**Order License Id:** 4383210833675  
**ISSN:** 0013-4651  
**Publication Type:** Journal  
**Volume:**  
**Issue:**  
**Start page:**  
**Publisher:** ELECTROCHEMICAL SOCIETY,  
**Author/Editor:** ELECTROCHEMICAL SOCIETY

**Permission Status:**  **Granted**

**Permission type:** Republish or display content  
**Type of use:** Republish in a thesis/dissertation

Hide details

<b>Requestor type</b>	Academic institution
<b>Format</b>	Electronic
<b>Portion</b>	chapter/article
<b>The requesting person/organization</b>	Lin Ma/Dalhousie University
<b>Title or numeric reference of the portion(s)</b>	Figure 6
<b>Title of the article or chapter the portion is from</b>	Dramatic Effects of Low Salt Concentrations on Li-Ion Cells Containing EC-Free Electrolytes
<b>Editor of portion(s)</b>	N/A
<b>Author of portion(s)</b>	D.J. Xiong, T. Hynes, J.R. Dahn
<b>Volume of serial or monograph</b>	164
<b>Page range of portion</b>	
<b>Publication date of portion</b>	2017
<b>Rights for</b>	Main product
<b>Duration of use</b>	Life of current edition
<b>Creation of copies for the disabled</b>	no
<b>With minor editing privileges</b>	no
<b>For distribution to</b>	Worldwide
<b>In the following language(s)</b>	Original language of publication
<b>With incidental promotional use</b>	no
<b>Lifetime unit quantity of new product</b>	Up to 499
<b>Title</b>	DEVELOPMENT OF NOVEL ELECTRODE/ELECTROLYTE SYSTEMS FOR A LI-ION CELL WITH HIGHER ENERGY DENSITY AND LONGER LIFETIME
<b>Instructor name</b>	Dr. Jeff Dahn
<b>Institution name</b>	Dalhousie University
<b>Expected presentation date</b>	Sep 2018